



HAL
open science

Organic and organometallic fluorenyl-porphyrins for optics

Xu Zhang

► **To cite this version:**

Xu Zhang. Organic and organometallic fluorenyl-porphyrins for optics. Cristallography. INSA de Rennes, 2017. English. NNT: 2017ISAR0009 . tel-02141528

HAL Id: tel-02141528

<https://theses.hal.science/tel-02141528v1>

Submitted on 28 May 2019

HAL is a multi-disciplinary open access archive for the deposit and dissemination of scientific research documents, whether they are published or not. The documents may come from teaching and research institutions in France or abroad, or from public or private research centers.

L'archive ouverte pluridisciplinaire **HAL**, est destinée au dépôt et à la diffusion de documents scientifiques de niveau recherche, publiés ou non, émanant des établissements d'enseignement et de recherche français ou étrangers, des laboratoires publics ou privés.

Thèse

UNIVERSITE
BRETAGNE
LOIRE

THESE INSA Rennes
sous le sceau de l'Université Bretagne Loire
pour obtenir le titre de
DOCTEUR DE L'INSA RENNES
Spécialité : CHIMIE

présentée par

Xu ZHANG

ECOLE DOCTORALE : SDLM

LABORATOIRE : UMR6226 / ISCR-INSA de Rennes

Organic and Organometallic Fluorenyl-Porphyrins For Optics

Thèse soutenue le 17. 03. 2017
devant le jury composé de :

Isabelle LEDOUX RAK

Professeur de l'ENS Cachan / Présidente

Duncan CARMICHAEL

Chargé de recherche CNRS à l'Ecole Polytechnique Paris / Rapporteur

Philippe BLANCHARD

Directeur de recherche CNRS à l'Université d'Angers / Rapporteur

Frédéric PAUL

Directeur de Recherche CNRS à l'Univ. de Rennes1 / Examineur

Olivier MONGIN

Maître de Conférences (HDR) à l'Univ. de Rennes1 / Examineur

Christine PAUL-ROTH

Maître de Conférences (HDR) à l'INSA de Rennes / Directrice de thèse

Organic and Organometallic Fluorenyl-Porphyrins for Optics

Xu ZHANG



En partenariat avec



**China Scholarship
Council**
www.csc.edu.cn



UNIVERSITÉ DE
RENNES 1



Durham
University



**Australian
National
University**

Acknowledgments

Three and half years ago, I arrived in Rennes, a very beautiful and peaceful city of France. The mild climate, nice surroundings and kind people favour me very comfortable life here. I gave everything I had on the subjects and now I am going to finish my thesis and prepare my defense. I appreciate everyone who gave me their hands in studies and live.

I should thank China Scholarship Council (CSC) for finance. It provides me the opportunity to get PhD degree and more than three years' life support.

I would like to thank Mrs. Isabelle LEDOUX RAK, Professeur de l'ENS Cachan, Mr. Duncan CARMICHAEL, Chargé de recherche CNRS à l'Ecole Polytechnique Paris, Mr. Philippe BLANCHARD Directeur de Recherche CNRS à l'Université d'Angers, for reviewing this manuscript.

I sincerely thank my supervisor Dr. Christine PAUL-ROTH, who provides me the PhD position on Organic Chemistry in laboratory ISCR-INSA of UMR-6226 in Rennes. Thanks for her patient guidance and professional advises in my work, as well as warmhearted help in my live. Meanwhile, I deeply thank Dr. Frederic PAUL, Dr. Olivier MONGIN who gave me many helps in experiments and measurements, and I have a wonderful experience in this excellent research team. And thanks to Dr. Véronique GUERCHAIS, responsible of the program LIA Rennes-Durham "Molecular Materials and Catalysis (MMC)" for offering me the chance of an oral communication at Durham University (UK).

I also need to thank other scientists: Dr Philippe JÉHAN for mass measurements and Mr. Clément ORIONE for ^{13}C NMR measurements; Mrs. Gwénael COLOMBEL and Nicolas RICHY for technical and equipment help.

I enjoyed my time with the PhD students in lab: Ayam, Amédée, Alphonsine, Dandan, Guille, Limiao, Nicolas, Suzy, Seyfallah, and Xiang. They are dynamic, friendly and always helpful when I was in trouble. I am very grateful for the friendship of them. My gratitude to my friends in INSA de Rennes: Fu Hua, Huang Gang, Ji Hui, Liu Ming, Liu Wei, Liu Shibo, Peng Linning, Wang Duo, Wei Hengyang, Xu Jiali, Yi Xiaohui, and Zhang Jinlin.

At last I would like giving my special appreciation to my family: my dear parents and my elder sister encouraged and supported me to go further on my way!

Contents

Introduction

0.1 Structure of fluorene, porphyrin and dendrimers.....	1
0.1.1 Porphyrin.....	1
0.1.2 Fluorene.....	3
0.1.3 Dendrimers.....	5
0.2 General synthetic methods.....	6
0.2.1 Porphyrin core.....	6
0.2.1.1 Alder Longo's method.....	7
0.2.1.2 Lindsey's method.....	7
0.2.2 Dendrimers.....	9
0.2.3 Sonogashira coupling reaction.....	11
0.3 Properties of porphyrins.....	13
0.3.1 Redox-active properties.....	13
0.3.2 Linear optical properties.....	15
0.3.2.1 Absorption spectrum.....	15
0.3.2.2 Emission spectrum of porphyrin.....	17
0.3.2.3 Energy transfer.....	17
0.3.3 Nonlinear optical properties.....	20
0.3.3.1 The 3 rd order phenomena.....	21
0.3.3.2 Two-photon absorption (TPA).....	21
0.3.3.3 Saturable absorption (SA) and reverse saturable absorption (RSA).....	22
0.3.3.4 Experimental techniques.....	23
0.4 General experiment procedure.....	25
References.....	27

Chapter 1 Syntheses of New Thienyl Porphyrin Dendrimers and Photophysical Properties

1.1 The targets of the project.....	35
1.1.1 Introduction.....	35
1.1.2 Thienyl unit.....	38

1.1.3	Thienyl porphyrins in literature.....	41
1.1.4	Targets of the Chapter.....	43
1.2	Syntheses of the new series of thienyl porphyrins.....	44
1.2.1	Dendrons formation.....	44
1.2.2	Thienyl porphyrin formation.....	46
1.2.3	Target porphyrin dendrimers formation.....	47
1.3	¹ H NMR analyses.....	49
1.3.1	¹ H NMR spectra of Dendrons 2 and 5	49
1.3.2	¹ H NMR spectra of porphyrins 6 , reference TThP , 8 and 9	50
1.4	Optical properties.....	51
1.4.1	Absorption spectra of porphyrins TThP , 8 and 9	51
1.4.2	Emission spectra of porphyrins TThP , 8 and 9	53
1.5	Two-photon absorption.....	55
1.6	Conclusions.....	57
	Experimental Section.....	59
	References.....	73

Chapter 2 Syntheses and Characterization of Ruthenium TFP Cored Porphyrin Complexes

2.1	The targets of the projects.....	79
2.1.1	Background.....	79
2.1.2	Target porphyrins.....	84
2.2	Syntheses of the new Ruthenium metallic Porphyrins.....	88
2.2.1	Organic porphyrins formation.....	88
2.2.2	Ruthenium Porphyrins formation.....	91
2.3	NMR analyses.....	92
2.3.1	¹ H NMR spectra of the organic compounds.....	92
2.3.1.1	Fluorenyl aldehydes 10-12	92
2.3.1.2	Mono-, Bis-, Tri- and Tetra-alkynyl TFP (13-17)	93
2.3.2	NMR spectra of the Ruthenium porphyrins (18-21)	96
2.3.2.1	NMR monitoring.....	96

2.3.2.2 ^1H NMR.....	96
2.3.2.3 ^{31}P NMR.....	98
2.4 Optical properties.....	99
2.5 Conclusions.....	101
Experimental Section.....	103
References.....	119

Chapter 3 Syntheses of New Porphyrin Dendrimers

3.1 Introduction.....	123
3.1.1 Porphyrin dendrimers of our laboratory.....	123
3.1.1.1 Non-conjugated porphyrin dendrimers.....	123
3.1.1.2 Conjugated porphyrin dendrimers.....	125
3.1.2 The target porphyrin dendrimers.....	127
3.2 Syntheses of the new series of porphyrins.....	131
3.2.1 The precursor formations.....	131
3.2.1.1 Conjugated dendron 26 and corresponding Model 1	131
3.2.1.2 Non-conjugated dendron 30 and corresponding Model 2	133
3.2.1.3 Tetra-alkynyl TFP (17) formation.....	135
3.2.2 New porphyrin dendrimers formation.....	136
3.3 ^1H NMR analyses.....	139
3.3.1 The dendrons and the models.....	139
3.3.2 Porphyrins.....	144
3.3.2.1 Tetra-alkynyl TFP precursor.....	144
3.3.2.2 New porphyrin dendrimers.....	145
3.4 Optical properties.....	145
3.4.1 Absorption and emission.....	147
3.4.2 Energy transfer behaviors.....	150
3.5 Two-photon absorption (TPA)	151
3.6 Conclusions.....	153
Experimental Section	155
References.....	170

Chapter 4 Syntheses of *para*-Fluorenone TFP Cored Porphyrins and Photophysical Properties

4.1	The targets of the project.....	173
4.1.1	Meso-fluorenone porphyrin.....	173
4.1.2	Target porphyrin dendrimers.....	174
4.2	Syntheses of the new series of fluorenone porphyrin.....	176
4.2.1	Difluorenyl aldehyde 37 formation.....	176
4.2.2	TFOP 1, 2 and 3 formation.....	179
4.3	¹ H NMR analyses.....	181
4.3.1	Compound 34 , 36 and difluorenyl aldehyde 37	181
4.3.2	Porphyrins: TFOP 1, 2 and 3	184
4.4	Optical properties.....	186
4.4.1	Absorption spectra of TFOP 1, 2 and 3	188
4.4.2	Emission spectra of TFOP 1, 2 and 3	189
4.5	Conclusions.....	193
	Experimental Section.....	195
	References.....	206

Perspectives..... 207

Experimental section..... 219

References..... 224

Appendix

Résumé étendu

Demande de confidentialité de mémoire de thèse

Engagement de confidentialité

Introduction

0.1 Structure of fluorene, porphyrin and dendrimers

0.1.1 Porphyrin

Porphin [$C_{20}H_{14}N_4$] consists of four pyrrole rings bridged by four methine groups to form a highly conjugated planar macrocycle, as shown in Figure 0.1.1. This aromatic system contains 22 π -electrons but only 18 of them (marked in red bonds) are delocalized to form π -electron ring according to Hückel's rule of aromaticity ($4n+2$ delocalized π -electrons, where $n = 4$ not 5). In this macrocycle, the carbon atoms are mainly divided into 3 types: α (alpha), β (beta) and *meso* carbons (Figure 0.1.1), of which the last two can be connected to different external fragments. When substituted in any of these positions, the derivatives are named porphyrins. During this thesis, we only focus on the design and syntheses of the *meso*-porphyrins.

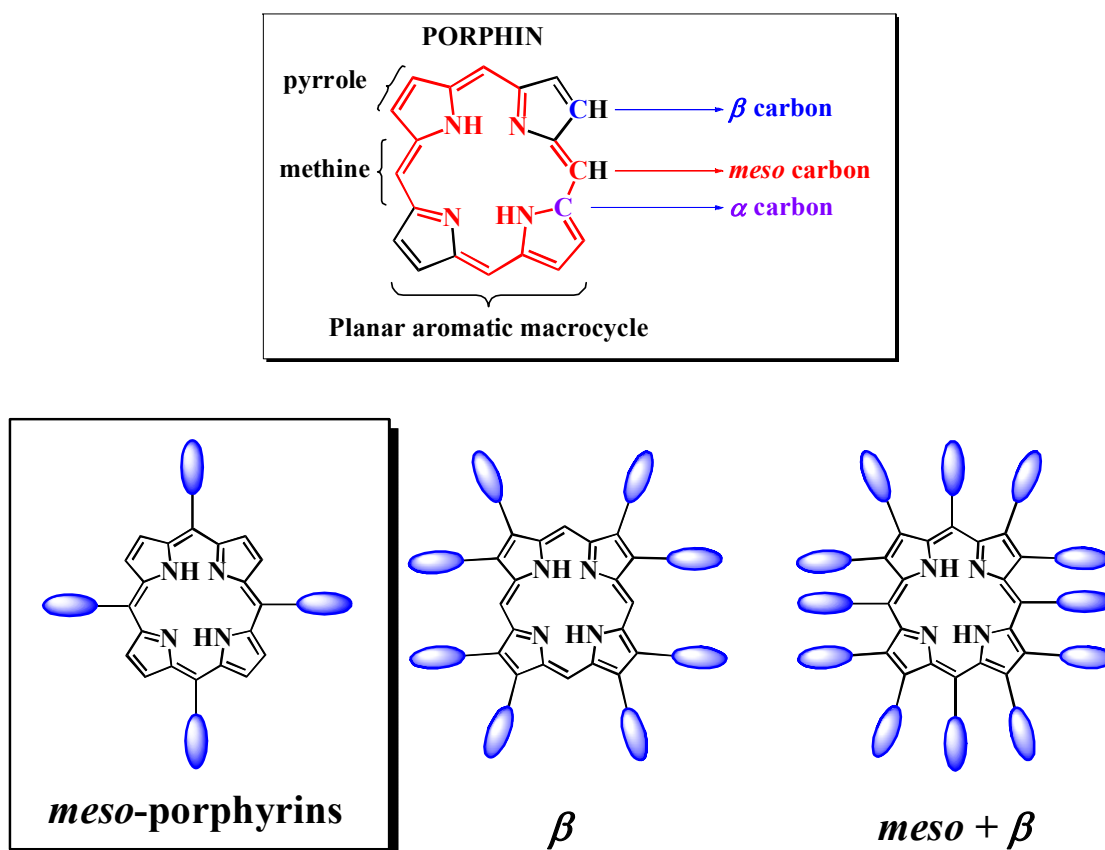


Figure 0.1.1 Porphyrin ring and different porphyrins cored derivatives

Porphyrins are prized as “the pigments of life” because of their extreme importance in nature. Green plants, as the origins of life, use a magnesium porphyrin named Chlorophyll (Figure 0.1.2 a) to transport the energy from sun to support life on earth. On the other hand, animals (including human beings) use an agent in hemoglobin called heme (Figure 0.1.2 b), which is an iron-complexed porphyrin, take in oxygen and to release carbon dioxide^[1]. The role of porphyrins in photosynthetic mechanisms indicates a good capacity of these molecules to mediate visible photon-electron energy transfer processes.

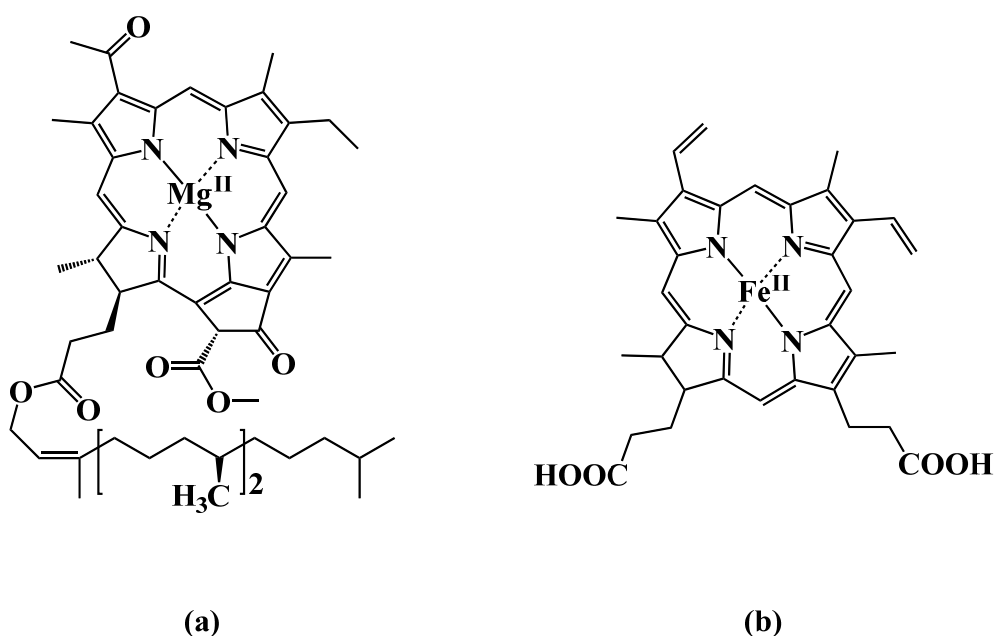


Figure 0.1.2 Porphyrins of Chlorophyll (a) and heme (b)

For these reasons, porphyrins have attracted considerable attention in prospective applications such as mimicking enzymes, catalytic reactions, photodynamic therapy, opto-electronic devices, data storage, and solar cells^[2-7]. Particularly, efforts have been made in the synthesis of numerous porphyrins, for using as basic artificial light-harvesting antennae, with the intention of improving our understanding of the photochemical aspect of natural photosynthesis^[8-10].

0.1.2 Fluorene

Fluorene is a smaller aromatic compound than porphyrins, and has two essentially coplanar aryl groups within rigid structure shown in Figure 0.1.3. In 1954, Brown and Bortner measured the crystal structure of fluorene accurately according to an X-ray analysis of crystalline fluorene done by Iball. The data show that the two six-membered rings in the fluorene molecule are each tilted at about 12° out of the plane of central five-membered ring. The internal angles of the latter are 106° , 109° and 108° , and the bond lengths are: $L(1, 10) = 1.40 \text{ \AA}$, $L(11, 12) = 1.50 \text{ \AA}$ and $L(9, 10) = 1.52 \text{ \AA}$ ^[11,12].

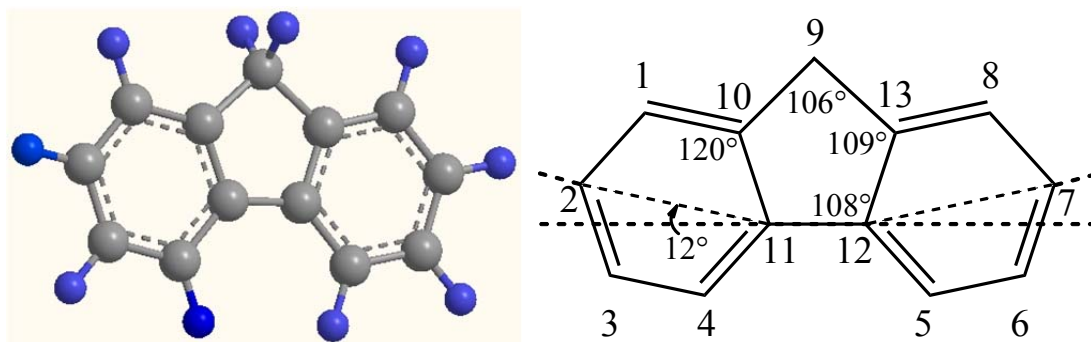


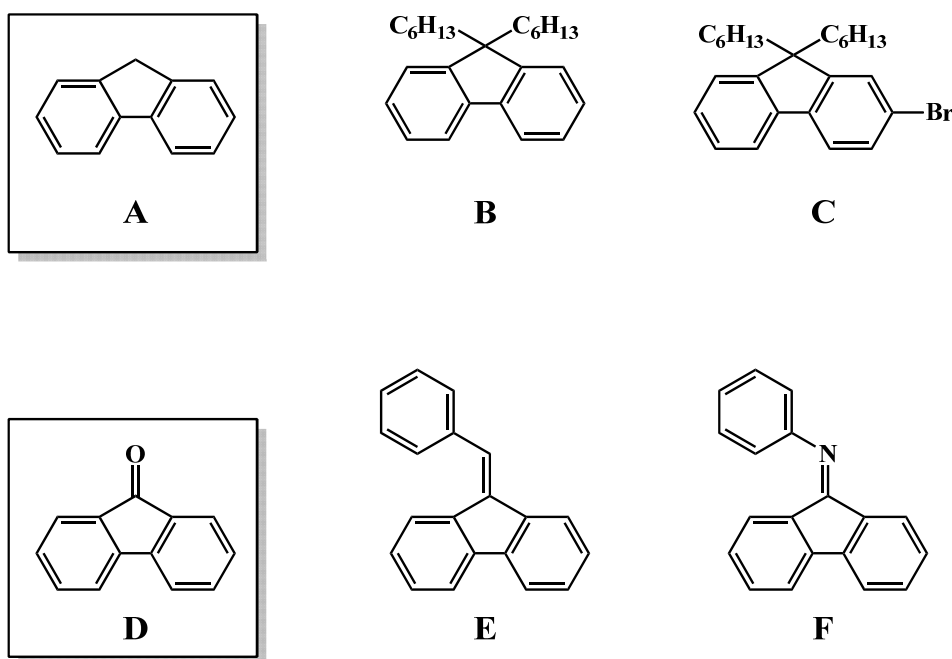
Figure 0.1.3 Fluorene structure and the corresponding crystal data

As one of the conjugated materials used for light-emitting diodes, fluorene presents interesting optical properties because its 9 position can be easily modified. For example, a group of monomers (**B-F**), published in 2010, can be compared to the precursor **A** (see Figure 0.1.4) ^[13]; relevant photophysical data are listed in Table 0.1.1. They all have absorption bands in the UV region. With respect to fluorescence: **A-C** exhibit ultraviolet emission, whilst **D-F** emit in the visible region, especially for **D** which has a keto substituted at 9 position of fluorene and exhibits blue emission (505 nm). The precursor **A** has the highest quantum yield ($\Phi_{fl} = 50\%$), followed by **B**, with alkyl chains ($\Phi_{fl} = 40\%$). Fluorene units **E** and **F** have very low Φ_{fl} but, being synthesized from compound **D**, they serve to show how easily modified fluorenones can be prepared by using this oxygen functionality.

Table 0.1.1 Photophysical properties of compounds A-F ^[13]

Compounds	Abs. / nm ^{a,b}	Em. (fl) / nm ^a	Φ_{fl}^c (in CH ₂ Cl ₂)
precursor A	261	302	0.50
B	267 (304)	319	0.40
C	276	323	0.04
monomer D	258 (377)	505	0.02
E	259 (328)	402	0.00
F	258, 298 (388)	402	0.04

^a Measured in CH₂Cl₂. ^b Values in parentheses denote most bathochromically shifted absorption maximum. ^c Absolute fluorescence quantum yield measured using an integrating sphere.

**Figure 0.1.4 Fluorene derivatives substituted in 9 position**

Throughout this thesis, the modification of the 9 position of fluorene is used to confer specific properties upon a range of porphyrins. Initially, the addition *n*-butyl chains are used to improve the solubility of the product porphyrin. We have also introduced two extra fluorenyl units in this 9 position. Finally by introducing oxygen atoms into fluorene, a new series of conjugated and non-conjugated dendrimers have been synthesized (see **Chapter 3**).

0.1.3 Dendrimers

Nowadays, a number of covalently linked porphyrin dendrimers have been synthesized^[14], many of which involve energy donating positioned dendrons around the porphyrin core that serve as an antenna system to optimize their optical properties. In these cases, phenyl, truxene, and fluorenyl groups are usually chosen as light-harvesting antennae within the energy donating dendron^[15-18].

Many publications have already reported porphyrin dendrimers having fluorenyl or oligo-fluorene units. For example, the group of Bo has synthesized some porphyrin dendrimers bearing linear oligofluorene arms that serve as red light-emitting materials^[19]. They also studied a series of hyperbranched polymers with fluorenyl porphyrins as peripheral or linked groups^[20,21]. Equally, Fréchet demonstrated that the antenna effect was facilitated in dendritic architectures versus the corresponding linear cases and reported the synthesis of porphyrin systems that feature modified fluorenyl units as light-harvesting two-photon absorbing chromophores^[22,23]. Porphyrin derivatives with multi-fluorenyl substituents were also applied in OLEDs as deep red emitters^[24]. Thus, fluorenyl has been chosen as an important light absorber in the syntheses of our porphyrin dendrimers^[25].

We further focus on porphyrin dendrimers containing π -conjugated rigid dendrons, which is a field that has shown great progress in recent years: Takahashi and Samuel reported different methods to synthesize porphyrin dendrimers that have stilbene dendrons and studied their electro-optical or energy transfer properties^[26,27]. In the group of Okada and Kozaki, a series of multi-porphyrins within conjugated networks provided efficient light-harvesting antennae^[28-30].

To construct the dendrimers, the porphyrin ring (as a light-harvesting group) could act as the core, with the junction point and antennae corresponding to: (i) porphyrin cored dendrimers, (ii) porphyrin bridged dendrimers and (iii) porphyrin terminal dendrimers respectively. Porphyrin can as well be used as “core-junction point-antennae” in a huge porphyrin dendrimer (as shown in Figure 0.1.5). During this thesis, we will restrict our studies to *meso*-porphyrin cored dendrimers.

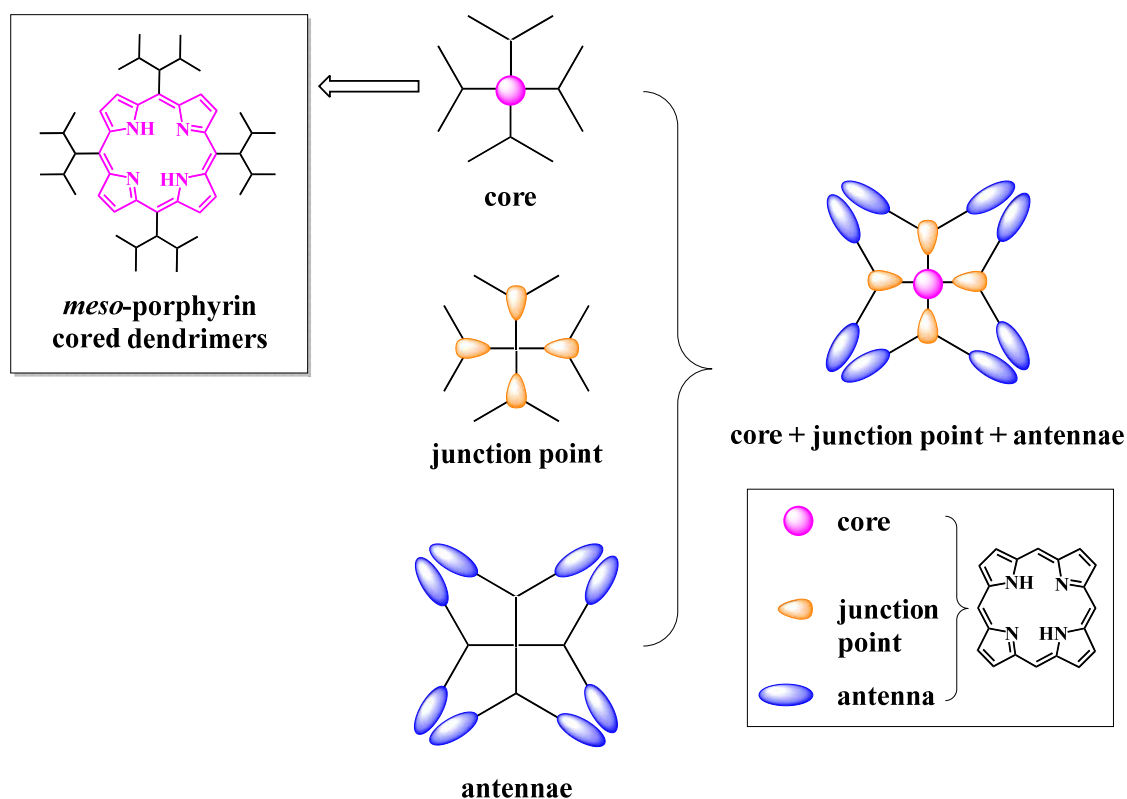


Figure 0.1.5 Porphyrin dendrimers with different structures

0.2 General synthetic methods

0.2.1 Porphyrin core

Rothemund first obtained *tetra*-aryl porphyrins in 1935, through a one step reaction of pyrrole and benzaldehyde in pyridine in a sealed flask at 150 °C for 24h^[31], but the yield was very low and the experimental conditions were severe^[32]. From then on, the syntheses of porphyrins and their derivatives have undergone nearly 80 years of development. Nowadays, the synthesis of porphyrins is mainly done by two methods, under two simple and practical sets of conditions: Adler-Longo's^[33] and Lindsey's^[34] methods.

0.2.1.1 Alder and Longo's method

In 1960, Adler and Longo developed an alternative approach: the reactions were carried out by aromatic aldehyde and pyrrole under acid catalyzed condensation, in open glassware that permits air oxidation. The conditions were optimized with respect to different solvents and reagent concentration range, so that optimized yields of porphyrins are rose to 20-40% (Figure 0.2.1) [35].

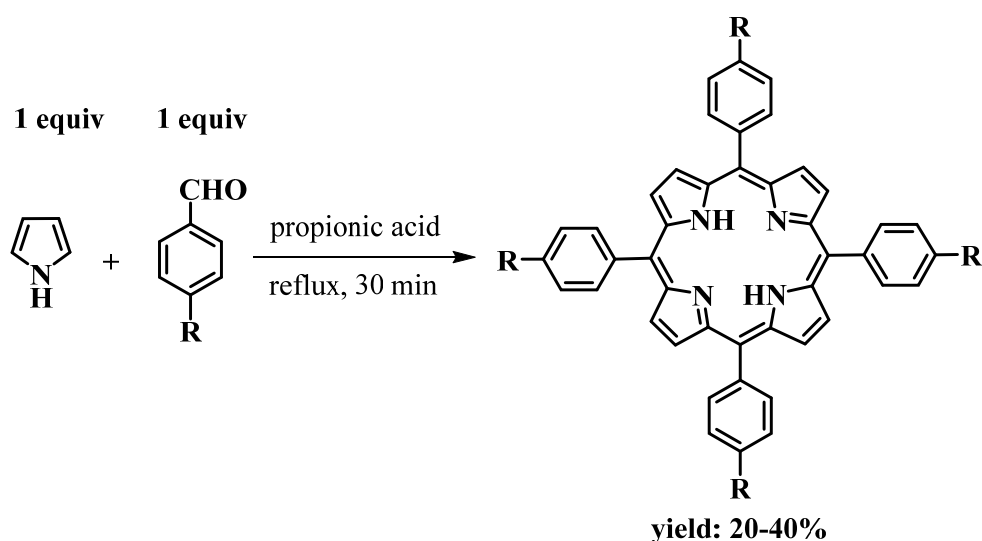


Figure 0.2.1 Adler-Longo's method for *meso*-substituted porphyrins

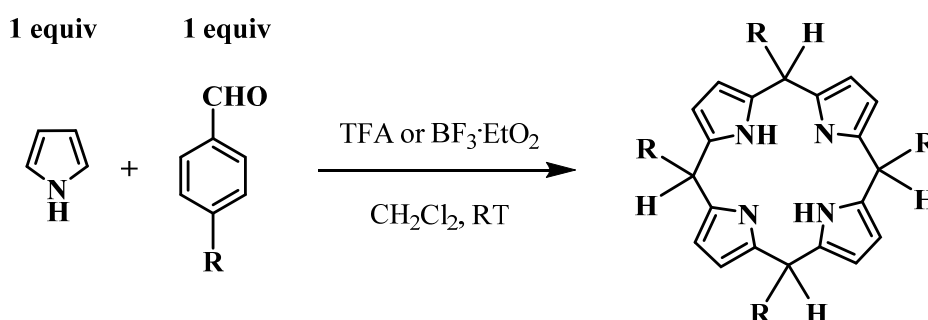
0.2.1.2 Lindsey's method

Over the period of 1979 to 1986, Lindsey's group developed a new two-step synthetic strategy to form substituted porphyrins that employed more gentle conditions for condensation of the aldehyde and pyrrole (Figure 0.2.2): in CH_2Cl_2 with TFA or $\text{BF}_3 \cdot \text{OEt}_2$ as acidic catalyst and *p*-chloranil as oxidant. The Lindsey synthetic approach is more readily adapted to larger scale syntheses and provides much higher yields of substituted tetraphenylporphyrins, always with the addition of salts as template [36,37].

The general method used in our laboratory: one equivalent of pyrrole and one equivalent of aldehyde are dissolved in distilled CHCl_3 under argon, this reaction medium is degassed by argon bubbling for 30 min; then the catalyst $\text{BF}_3 \cdot \text{OEt}_2$ is

injected at R.T. to start the condensation (**step 1**), after covering the system by aluminium foil. This step will last around 3 h. Then, the *p*-chloranil oxidant is added to the mixture to start the oxidation (**step 2**), and the system is refluxed at 60 °C without any protection from air for 1 h. Finally, NEt₃ is injected to neutralize the excess acid. The desired porphyrin is then purified by silica gel chromatography and collected after recrystallization.

Step 1: Condensation: to obtain porphyrinogen



Step 2: Oxidation: to obtain porphyrin

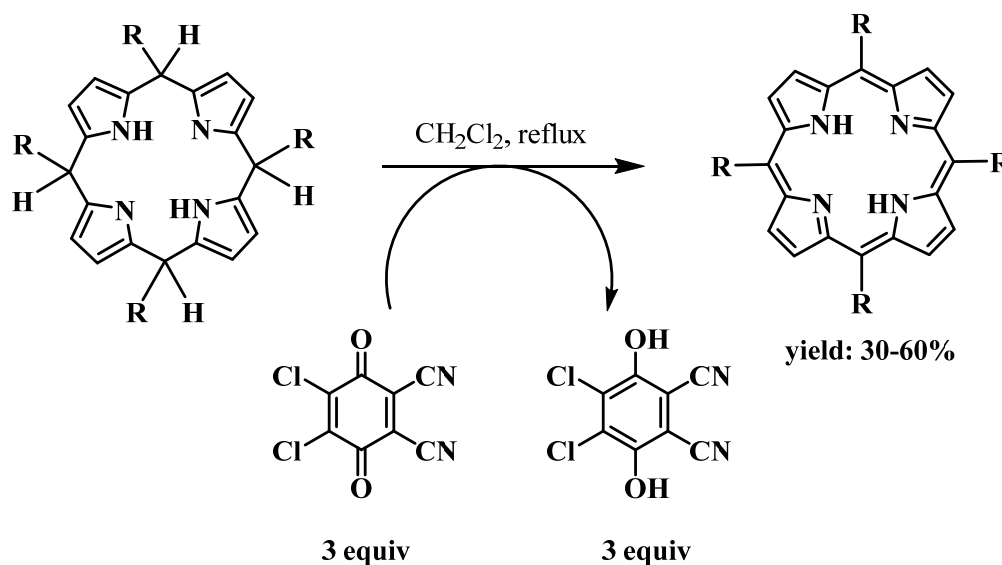


Figure 0.2.2 Two-step synthetic strategy of Lindsey's method for *meso*-substituted porphyrins

0.2.2 Dendrimers

There are two classic routes to form the dendrimers:

(I) **Divergent route**: as shown in Figure 0.2.3, the dendrons are connected to previously prepared porphyrin core gradually to form the new porphyrin dendrimers series. In this thesis, we chose Sonogashira coupling reaction to synthesize the dendrimers, so this route was used to obtain the new series of *meso*-thiophenyl porphyrin dendrimers successfully as generation G0 and G1 in **Chapter 1**.

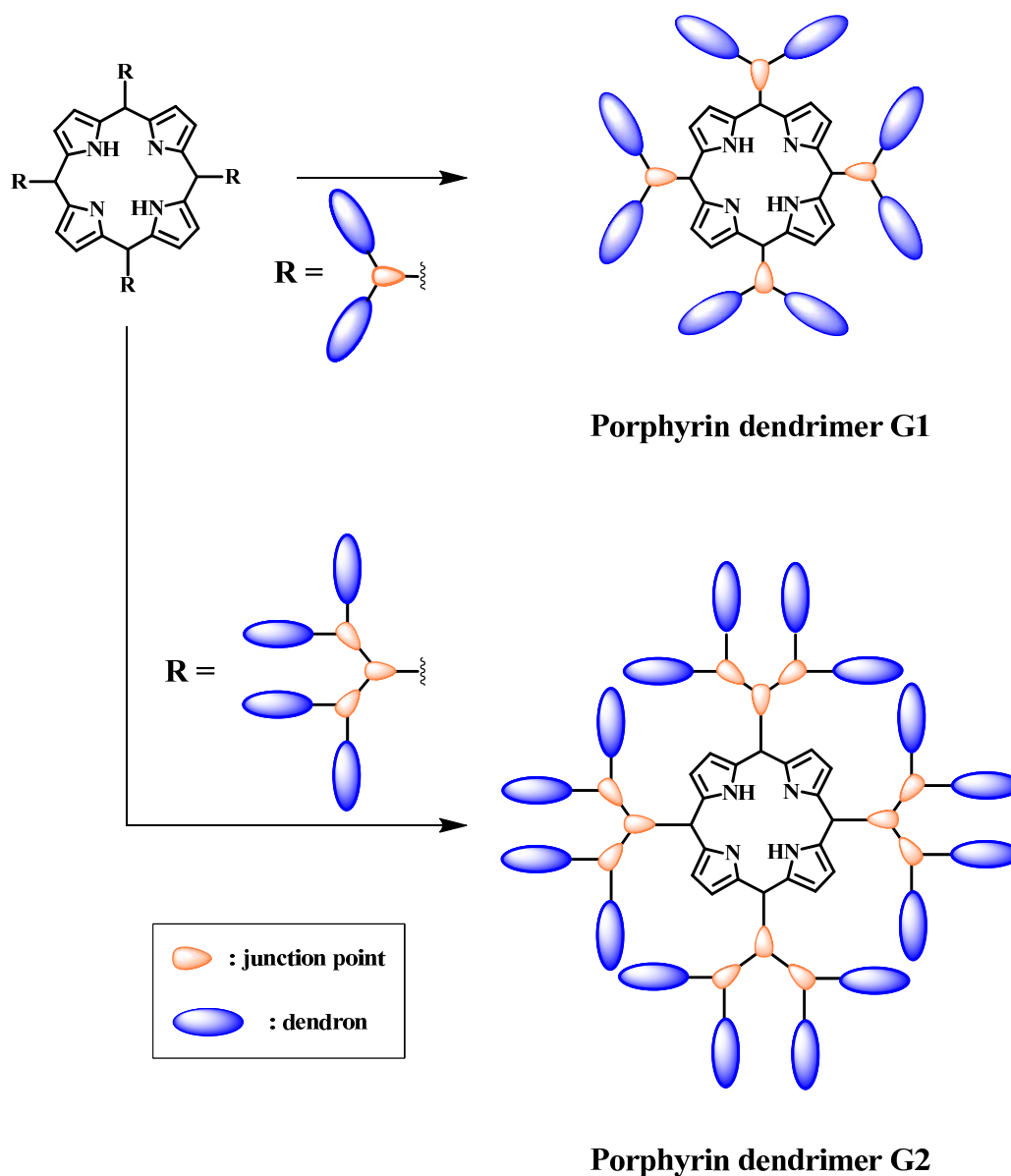


Figure 0.2.3 Semi-divergent route to synthesize the dendrimers (generation G1 and G2)

(II) **Convergent route:** aldehydes functionalized with the desired dendrons are synthesized, and then the porphyrins functionalized with dendrimers are obtained by Lindsey's method. The new series of conjugated and non-conjugated porphyrin dendrimers (**Chapter 3**) were formed by this route, as shown in Figure 0.2.4. Compared to the divergent route, this way might be more appropriate for synthesizing large dendrimers from multi-generation dendrons.

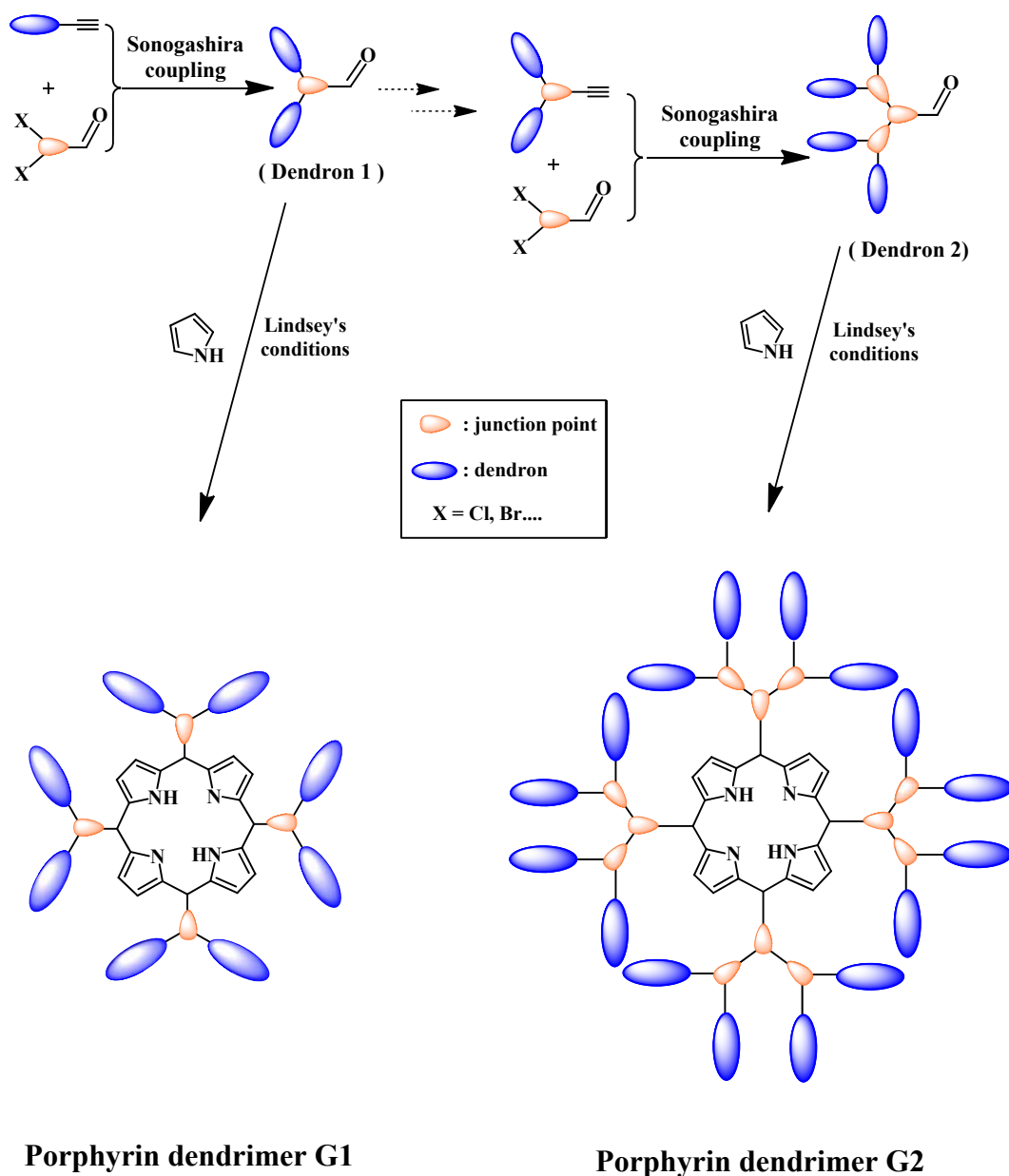
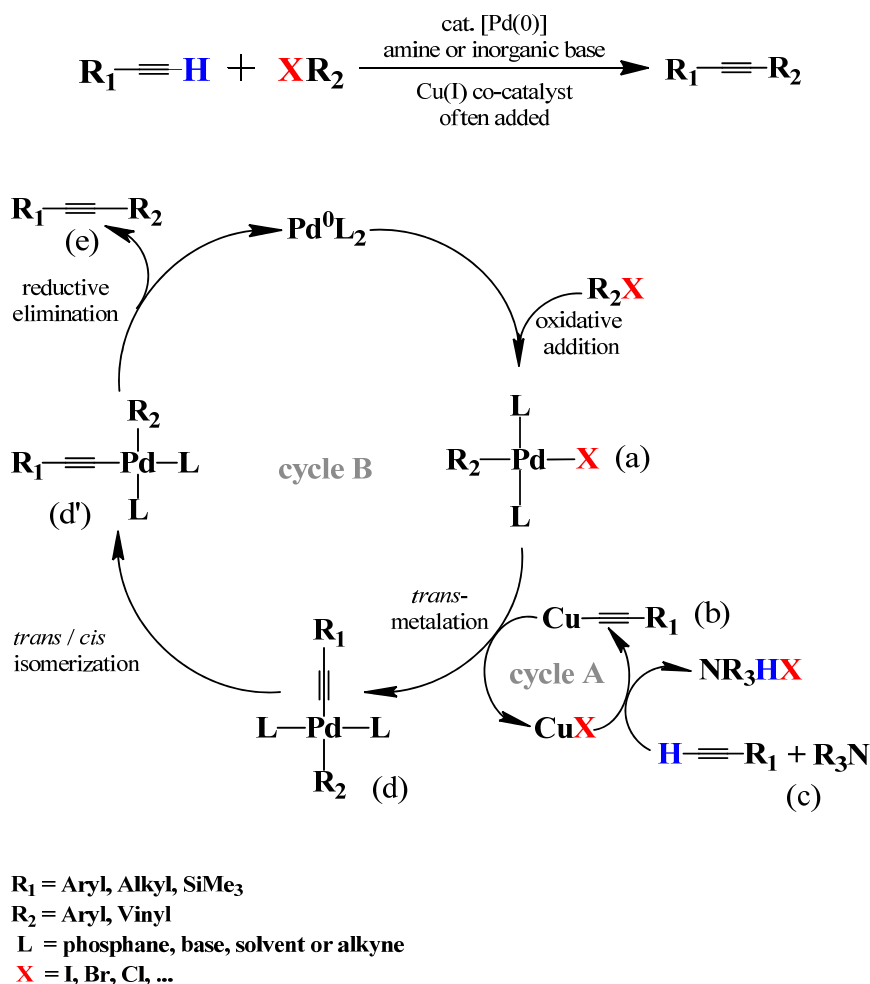


Figure 0.2.4 Convergent route to synthesize the dendrimers (generation G1 and G2)

0.2.3 Sonogashira coupling reaction

The palladium catalyzed C–C bond formation process which is able to couple a terminal sp hybridized carbon from an alkyne with a sp^2 carbon of an aryl or vinyl halide (or triflate) is commonly termed the Sonogashira coupling reaction^[38]. This named reaction arose from the discovery of the process by Sonogashira and his colleagues in 1975^[39]: an alkynyl carbon couples with an sp^2 halo substituted carbon using the catalyst/co-catalyst system [such as $\text{PdCl}_2(\text{PPh}_3)_2/\text{CuI}$] in an amine solvent, shown in Scheme 0.2.1. The exact mechanism of this reaction is still not well understood, because the interaction of the two metal catalysts is hard to analyze^[40]. Generally, two independent catalytic cycles (**A** and **B**) are used to describe the complex reaction process:



Scheme 0.2.1 Sonogashira coupling reaction process and supposed mechanism for the copper-cocatalysed Sonogashira reaction

In **cycle A**, the alkynyl compound (**c**) combines with the co-catalyst **CuX** to form compound (**b**) under protonation of the amine R_3N . In **cycle B** the catalyst Pd^0L_2 and R_2X form the compound (**a**), then the two intermediates (**a**) and (**b**) combine to give the *trans/cis*-metallated compound (**d**) and then (**d'**). Finally, the desired coupled product (**e**) is synthesized through reductive elimination.

Nowadays, thousands of Sonogashira coupling references have been published using different palladium catalysts, such as Pd-phosphorous complexes, Pd-nitrogen complexes or Pd-P, N, O complexes and so on, some examples are shown in Figure 0.2.5 [41-46]. During this thesis, the $PdCl_2(PPh_3)_2$ is chosen as the palladium catalyst, as well as the co-catalyst CuI and a solvent system of DMF/iPr_2NH .

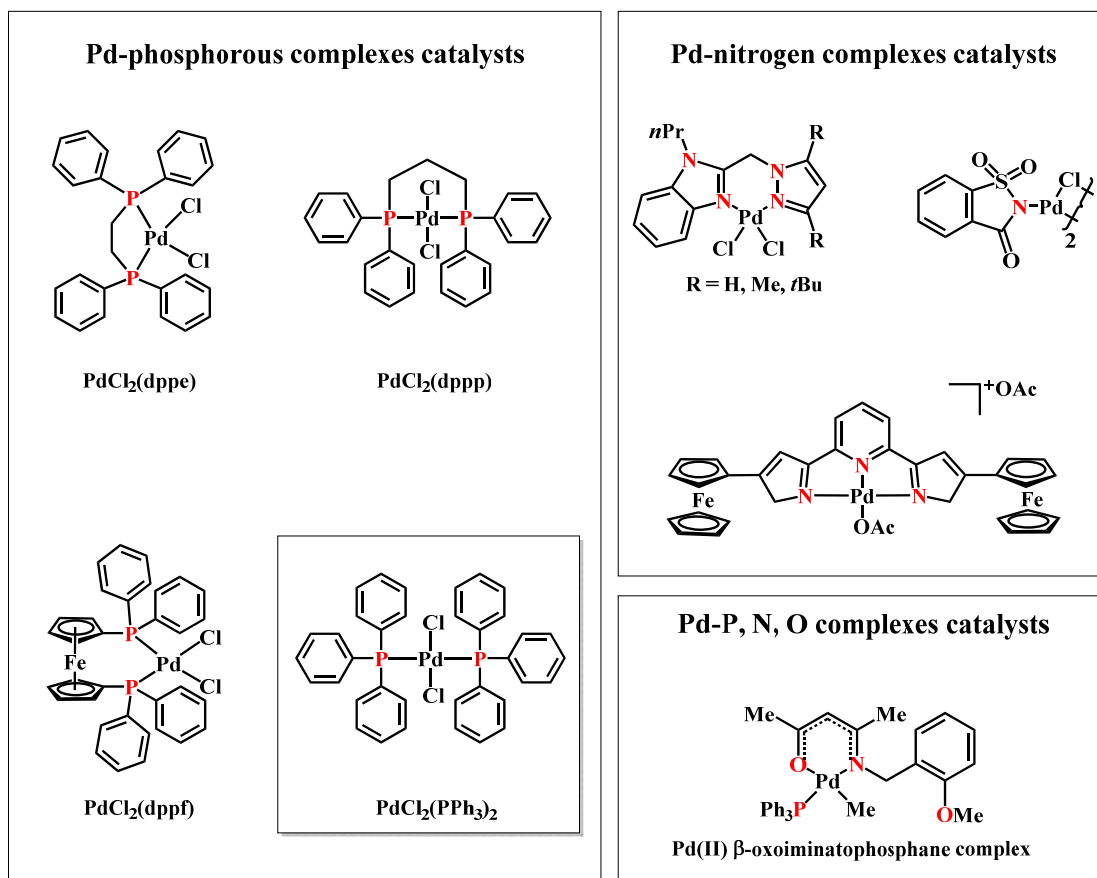


Figure 0.2.5 Catalysts examples of Pd-phosphorous, Pd-nitrogen And Pd-P, N, O complexes

0.3 Properties of porphyrins

0.3.1 Redox-active properties

Cyclic Voltammetry (CV), as the most widely recognized electrochemical technique for studying redox-active properties, is a potential sweep method in which the current giving rise to any redox event is measured and the potential is varied [47-52].

Organometallic porphyrins showing redox-active properties have already been developed for many years. Some iron and ruthenium porphyrin complexes (**G**, **H** and **I**) have been synthesized in our laboratory, their molecular structures are shown in Figure 0.3.1.

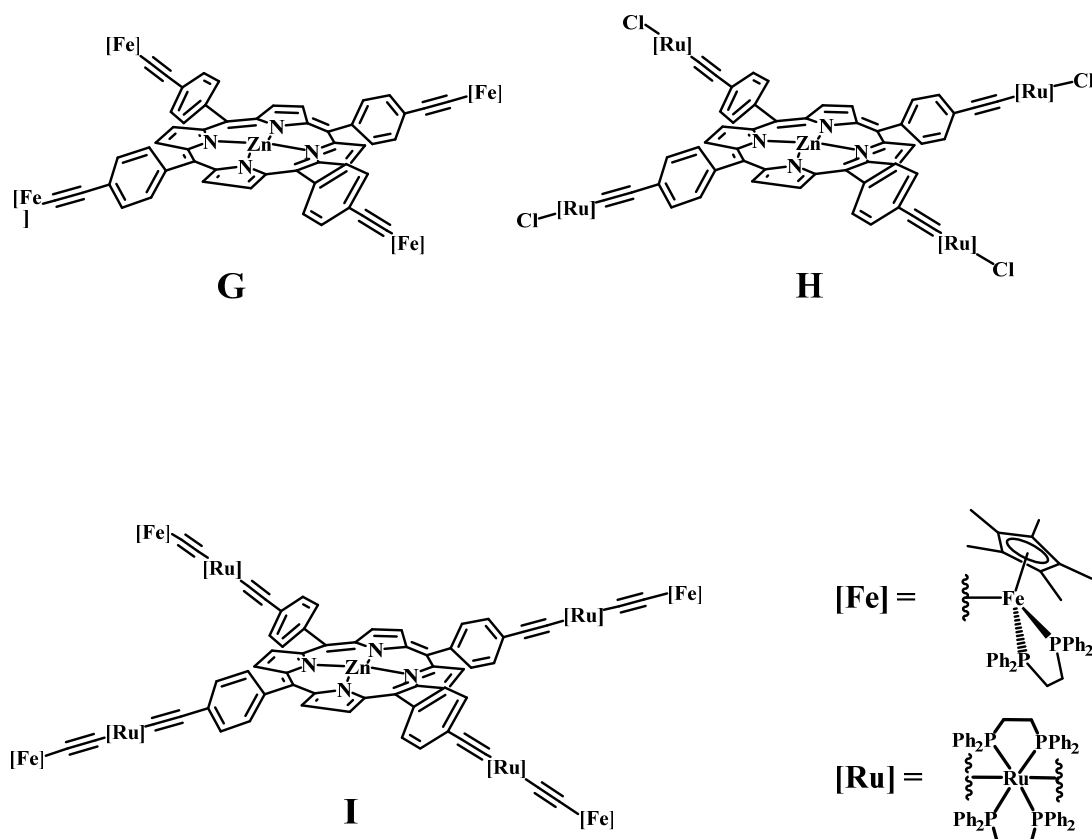


Figure 0.3.1 Ruthenium or Iron porphyrins: compounds **G**, **H** and **I**

Their cyclic voltammograms are shown in Figure 0.3.2. The reversible oxidation processes of Fe(II)/Fe(III) of **G** and **I** are in a lower potential range; the same processes of **H** and **I** corresponding to the oxidation of Ru(II) to Ru(III) occur in a mid-range whilst the oxidation processes concerning the **ZnTPP** cores of these three compounds are found in a higher potential range, for **I**, it seems that the oxidation of Ru(II)/Ru(III) coincides with the first oxidation process of **ZnTPP** core^[53]. So for these organometallic porphyrins **G**, **H** and **I**, each redox-active center (**Fe**, **Ru** or **ZnTPP**) is well identified through the CV potential sweep method.

During this thesis, we will continue to develop organometallic porphyrins with redox-active fragments — ruthenium complexes combined with the highly luminescent core — **TFP**, this work will be detailed in **Chapter 2**.

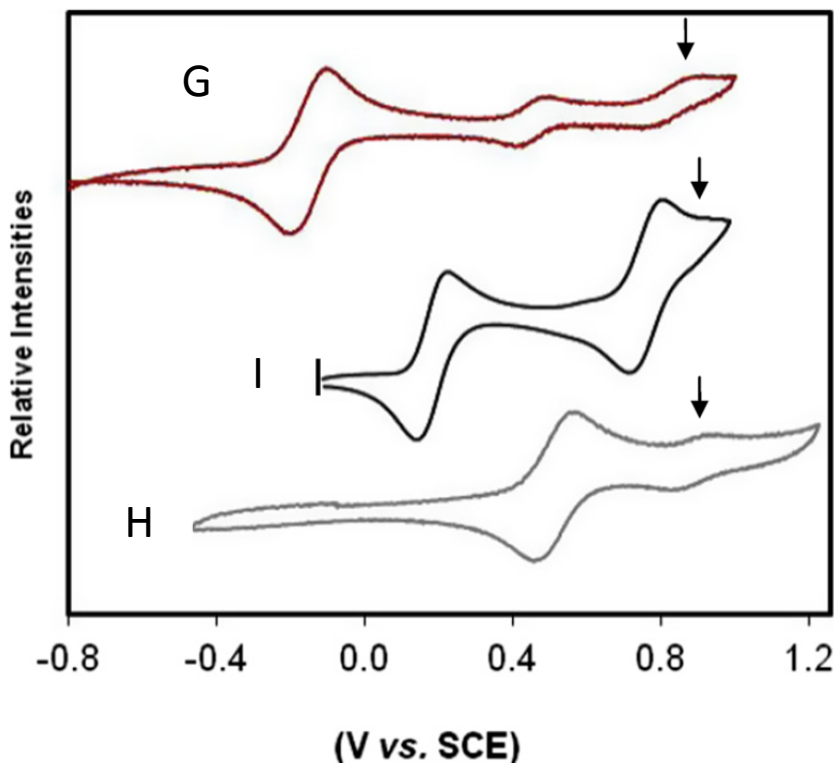


Figure 0.3.2 Cyclic voltammograms of the zinc(II) porphyrins **G–I** in $\text{CH}_2\text{Cl}_2/[\text{n-Bu}_4\text{-N}][\text{PF}_6]$ (0.1 M) at 25 °C at 0.1 V/s between -0.8 and 1.2 V vs. SCE

0.3.2 Linear optical properties

Porphyrins, because of their fascinating features and characteristic UV-visible spectra, have inspired much interest from physicists and chemists for many years, because their spectroscopic characteristics^[54]. All the porphyrins have two distinct absorption regions: near-ultraviolet and visible regions, which mean that these compounds exhibit striking colors.

0.3.2.1 Absorption spectrum

The electronic absorption spectrum of a typical porphyrin consists of two transitions (see Figure 0.3.1 and 0.3.2): (i) a strong transition from ground state to the second excited state ($S_0 \rightarrow S_2$) between 390-480 nm (depending upon whether the porphyrin is β or *meso*-substituted), called the **Soret band** (or B band); and (ii) two to four weak transitions from ground state to the first excited state ($S_0 \rightarrow S_1$) situated between 480-700 nm, called **Q-bands**.

The Soret band and the Q-bands both arise from $\pi\text{-}\pi^*$ transitions, whilst the former is strongly allowed (the extinction molar coefficient ϵ is in order of $10^5 \text{ M}^{-1}\text{cm}^{-1}$) the latter are only weakly allowed (the extinction molar coefficient ϵ is in order of $10^4 \text{ M}^{-1}\text{cm}^{-1}$). Their relative intensities can be explained by considering the Gouterman four orbital model (HOMO and LUMO frontier orbitals)^[55].

Q-bands are due to transitions to the vibrationless S_1 state and other higher vibrational levels in the S_1 state. Their positions and intensities can give powerful clues to the substitution pattern of the porphyrins, and also whether they are metal-coordinated. These properties allow classifications of porphyrins according to their absorption spectra due to the numbers and relative intensities of Q bands: a metal-free porphyrin or metalloporphyrin, a porphyrin with substituents on the pyrrole β or *meso*-positions, or a protonated porphyrin^[56].

All the studied porphyrins found in this thesis present four Q-bands with their intensities decreasing in the order: $Q_{IV} > Q_{III} > Q_I > Q_{II}$, except porphyrin **42** in the “**Perspectives** chapter”.

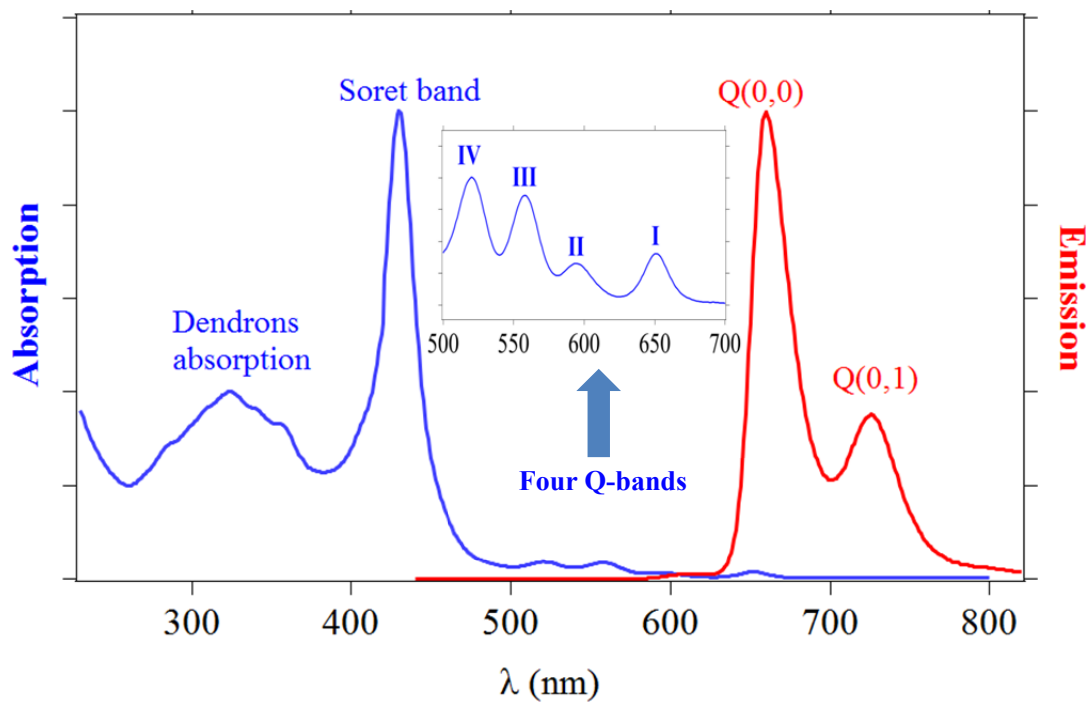
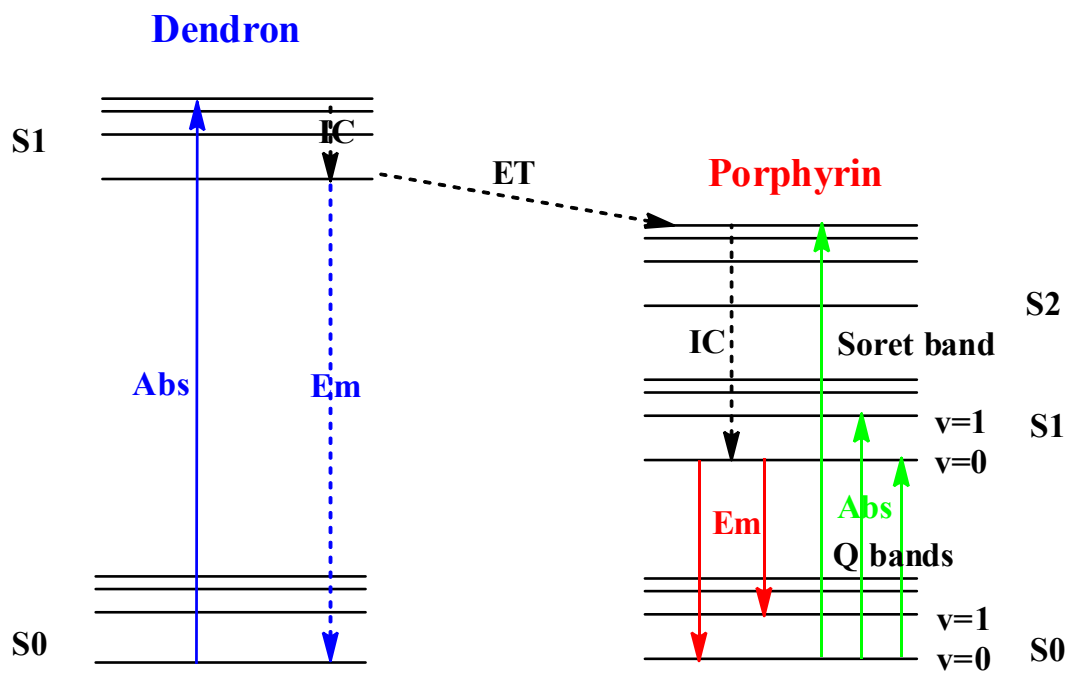

 Figure 0.3.1 Absorption and emission spectra of a free-based *meso*-porphyrin dendrimer


Figure 0.3.2 Jablonski energy-level diagram for a free-base porphyrin dendrimer

0.3.2.2 Emission spectrum of porphyrin

Internal conversion from S₂ to S₁ is rapid, so the emission of the free-based porphyrins is only detected from S₁ to S₀ following Kasha's rule^[57]. Two peaks are shown: one strong peak around 650 nm corresponding to the (0,0) transition, and a weaker peak around 720 nm due to the (0,1) transition (see Figure 0.3.1 and 0.3.2).

0.3.2.3 Energy transfer

An energy transfer process can take place via the interaction between an excited donor group (D*) and a ground-state acceptor group (A), without photon emission during the transition. To allow this kind of energy transfer, the overlap of donor emission and acceptor absorption spectra is necessary (see Figure 0.3.3), so that the energy lost from the excited donor to ground state could be turned to excite the acceptor group. Therefore, when designing a system to enhance energy transfer efficiency, the donor group should firstly have good photon absorption and emission properties, that is, a high extinction coefficient as well as a high quantum yield. Generally, the more spectral overlap of donor emission and acceptor absorption is observed, the more efficient energy transfer will occur from this donor to the acceptor.

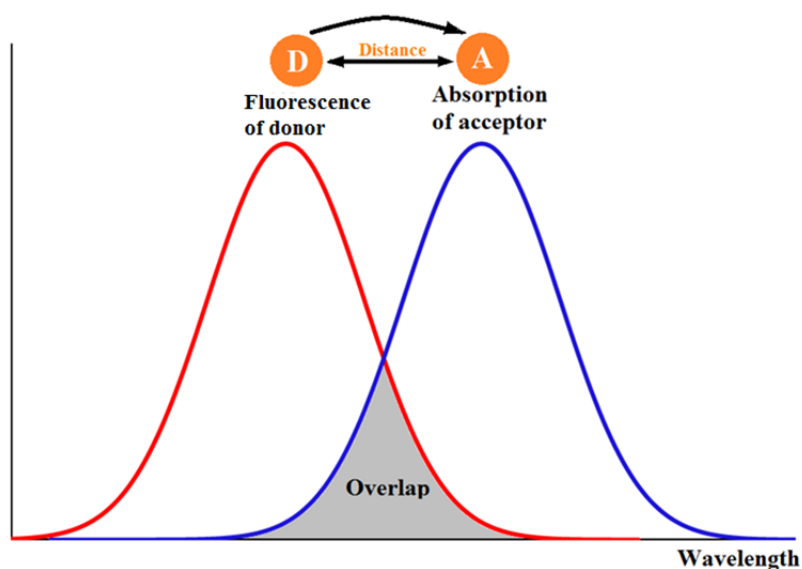


Figure 0.3.3 Spectral overlap between donor emission and acceptor absorption

During photo-induced energy transfer, the distance between donor and acceptor is also an important factor. This gives rise, developing two mechanisms invoked frequently in scientific literature: **Dexter energy transfer** and **Förster resonance energy transfer**, as shown in Figure 0.3.4 and Figure 0.3.5.

(I) Dexter energy transfer (**DET**)

D. L. firstly proposed this mechanism, which theoretically describes the short-range, collisional or exchange energy transfer, as a non-radiative process with electron exchange in 1953 ^[58]. Besides the overlap of Donor emission spectra and Acceptor absorption spectra, an overlap of electron clouds is also necessary for this exchange of energy transfer, meaning this process can only happen over short distances (typically 10 Å). This short distance is almost comparable to the collisional diameter, allowing the energy transfer to occur.

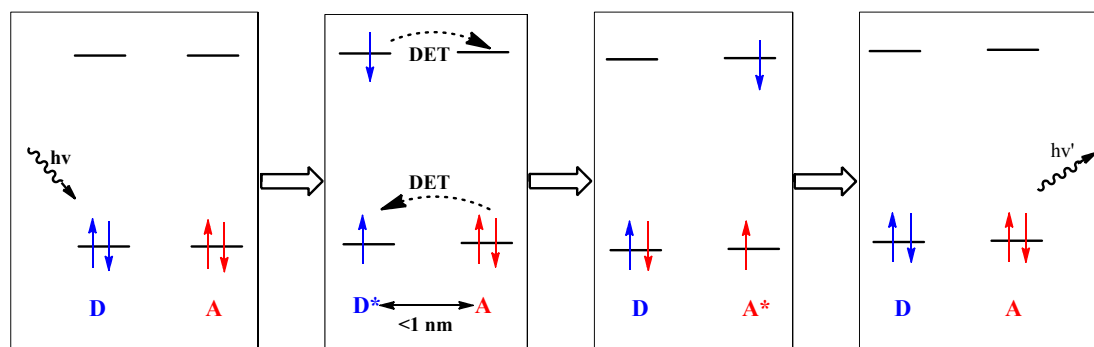


Figure 0.3.4 Schematic diagram for Dexter energy transfer

(II) Förster resonance energy transfer (**FRET**)

The Förster resonance energy transfer is the discovery of a German physical chemist T. Förster ^[59]. The mechanism of FRET was described in terms of an excited donor (D^*) that could transfer energy (not an electron) to excite a ground-state acceptor (A) through a non-radiative dipole-dipole coupling, which results from the

Coulombic interaction between donor and acceptor ^[60]. This process is highly distance-dependent, and it is effective only when the relative distance of Coulombic interaction between D-A pair is longer than the electron exchange energy transfer but smaller than 100 Å. The FRET mechanism is also affected by the relative orientation of the emission transition dipole of D and the absorption dipole of A.

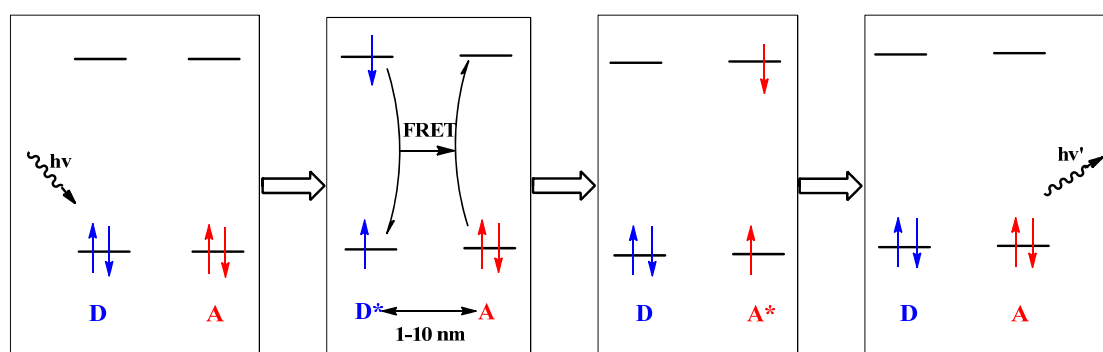


Figure 0.3.5 Schematic diagram for Förster resonance energy transfer

This process can also be expressed in a Jablonski diagram (Figure 0.3.6) ^[61]: A donor group D is excited by a photon and then relaxes to the lowest excited singlet state $S_1(D^*)$. If the distance allows energy transfer, the $S_1(D^*)$ energy is released to the ground state $S_0(D)$, and simultaneously excites the acceptor group A to the lowest excited singlet state $S_1(A^*)$ through non-radiative process. After excitation, the excited acceptor emits a photon and returns to the ground state $S_0(A)$.

Therefore, a suitable dendron, whose emission spectrum overlaps more with porphyrin core absorption, could be benefit to transfer energy from donor (like dendrons) to acceptor (like porphyrin).

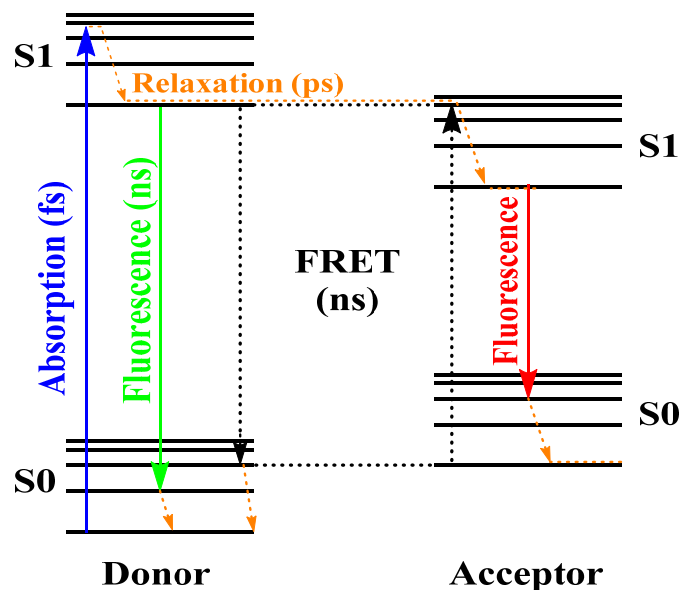


Figure 0.3.6 Jablonski diagram for Förster resonance energy transfer

0.3.3 Nonlinear optical properties

There has been a great interest in the Non-linear Optical (NLO) properties of materials over the last 30 years. Studies of the NLO response of organic molecules have been carried out with many materials being found to have large NLO coefficients and rapid response^[62].

Organic molecules allow for more structural diversity, but many of them pack in a centrosymmetric way, which means that 2nd order NLO properties are limited and commercial applications are compromised. Organometallic complexes were first investigated in the middle of 1980s^[63].

We are interested in one of the branches of NLO: the 3rd order phenomena which will be detailed briefly along with the corresponding Two-Photon Absorption (TPA), Saturable Absorption (SA) and Reverse Saturable Absorption (RSA). These are defined as below.

0.3.3.1 The 3rd order phenomena

At a given wavelength, 3rd order properties are related to the **cubic hyperpolarizability coefficient** γ (or the cubic susceptibility χ^3 on a macroscopic scale). This coefficient γ is a complex number, so γ is divided into real and imaginary parts (Equation 1):

$$\gamma = \sqrt{\gamma_{\text{real}}^2 + \gamma_{\text{imag}}^2} \quad (1)$$

Where: **the real part** (γ_{real}) is called the **refractive part** which is responsible for the modifications of the refractive properties of the molecule or medium. And **the imaginary part** (γ_{imag}) relates to the modifications of the **absorptive properties** [64,65].

As a consequence, the γ_{real} concerns instantaneous electronic effects or frequency tripling, and the γ_{imag} is responsible for absorptive phenomena (two-photon absorption, saturable absorption).

The time scale of these phenomena is the key to differentiate them, due to their different response times. So the time-resolved measurements have to be undertaken for helping us to explain the mechanisms involved in the 3rd order NLO response of certain molecules.

0.3.3.2 Two-photon absorption (TPA)

TPA corresponds to the simultaneous absorption of two photons by the photoactive compound. In 1931, Maria Goeppert-Mayer theoretically predicted this phenomenon which was demonstrated experimentally in the early 1960s [66-68]. Two types of TPA are possible: the degenerate case and the non-degenerate case. Their difference lies in the energy of the two absorbed photons, which is the same for the former case and different for the latter. This NLO effect can be imagined as the stepwise absorption of two photons: firstly, the compound absorbs one photon to reach a virtual state from the ground state; then the second photon (of the same or different energy as the first one) is

absorbed to achieve the real excited state (as shown in Figure 0.3.7 a). Here we need to point out that the virtual state does not exist, and is employed only to simplify the explanation of TPA phenomenon. In fact, the two photons are absorbed simultaneously and a certain density of photons is necessary, so that lasers are the only resource for TPA measurements.

The TPA cross-section (σ_2) is expressed in cm^4/GW or in Goeppert-Mayer units, more conveniently ($1 \text{ GM} = 10^{-50} \text{ cm}^4 \cdot \text{photon}^{-1} \cdot \text{molecule}^{-1}$). In principle, the direct process of two-photon absorption is suitable for optical limiting.

During this thesis, we synthesized several organic porphyrins with large σ_2 , their NLO properties will be detailed in the following chapters.

0.3.3.3 Saturable absorption (SA) and reverse saturable absorption (RSA)

As with TPA, SA and RSA are absorptive phenomena related to the imaginary part (γ_{imag}) of γ . Their difference from TPA is temporal: the two photons are absorbed one after another, in contrast to simultaneous absorption process of TPA.

Due to this stepwise process, a real excited state of the molecule is involved into which the second photon is then absorbed in a process called excited state absorption (ESA). These phenomena (TPA and SA or RSA) are presented in Figure 0.3.7 below.

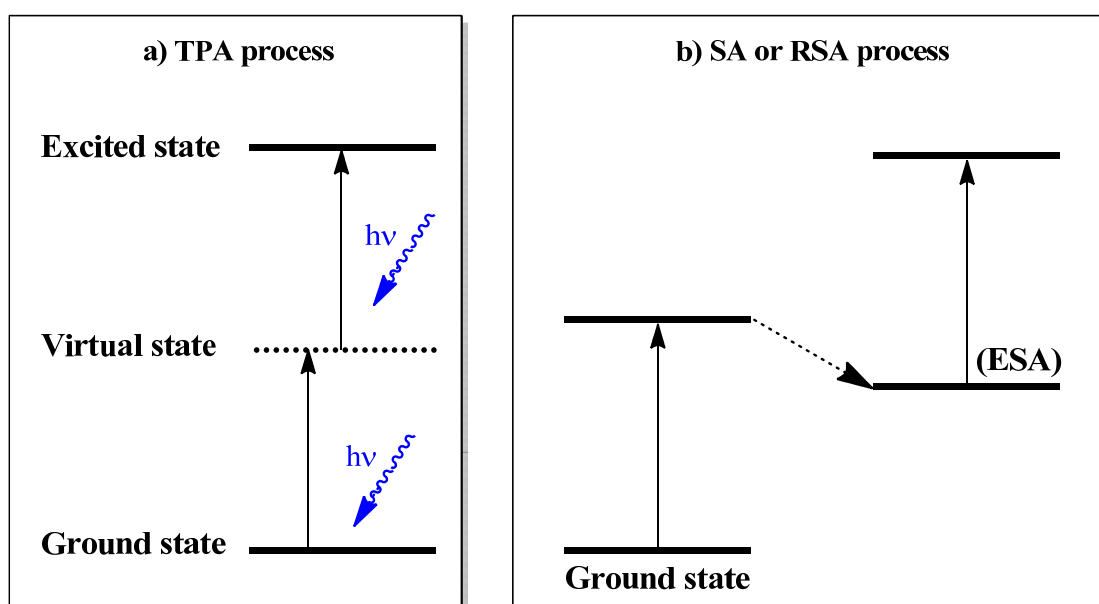


Figure 0.3.7 Presentation of TPA and SA or RSA phenomena

For RSA, a “photo-darkening” effect is observed: the transmission of the medium is decreased. That is the compound in his excited state has higher absorptivity than in the ground state under a certain wavelength.

In contrast, if the excited state has a lower absorptivity than the ground-state, the transmission of the sample will increase, as ground-state molecules are depleted: an absorption bleaching will be observed (**SA**). In other words, if the absorption cross-section of the medium in the excited state is lower than in the ground-state, the transmission of the system increases once the medium is excited.

It should be noted that when $\gamma_{\text{imag}} > 0$, the compound acts as a two-photon absorber or an reverse saturable absorber, whereas when $\gamma_{\text{imag}} < 0$, the compound has saturable absorber properties.

0.3.3.4 Experimental techniques

Many techniques have been used for measurements of 2nd and 3rd order responses of molecules [69,70], such as third-harmonic generation (**THG**), degenerate four-wave mixing (**DFWM**), two-photon excited fluorescence (**TPEF**) and **Z-Scan**. The following will only introduce the **TPEF** briefly, which is the technique we chose for measuring the σ_2 of the porphyrins during this thesis because of the high luminescence of our molecules.

Normally, there are two ways for the compounds returning to their ground-state after absorbing two photons: radiative or non-radiative relaxation. In the former, a fluorescence or phosphorescence emission will be observed, as shown in Figure 0.3.8. In analogy with the linear process, this nonlinear process is termed to **TPEF**.

The whole efficiency of this process is $\sigma_{\text{TPA}} \cdot \Phi_{\text{fl}}$, with the quantum yield (Φ_{fl}) of fluorescence. By measuring the intensity of the emitted fluorescence, σ_{TPA} can be determined through the known Φ_{fl} of fluorescence of the target sample.

This technique requires that the molecule possesses both TPA and fluorescence properties, and so preliminary fluorescence studies have to be carried out in order to determine Φ_{fl} [71].

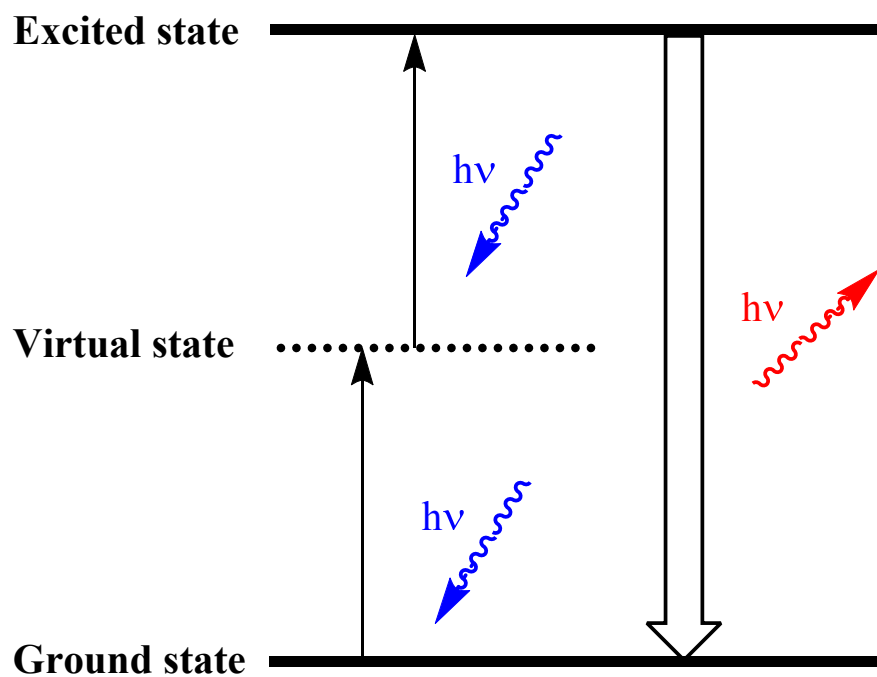


Figure 0.3.8 Principle of TPEF measurement

0.4 Experimental section

¹H NMR spectra were recorded on two spectrometers: BRUKER Ascend 300 and BRUKER Ascend 400 at 298K.

¹³C NMR spectra were recorded on two spectrometers: BRUKER Ascend 400 and BRUKER Ascend 500 at 298K.

High-resolution mass spectra were recorded on two different spectrometers: Bruker MicrOTOF-Q II, and a Thermo Fisher Scientific Q-Exactive in ESI positive mode at CRMPO .

Microanalysis was collected on Microanalyseur Flash EA1112 at CRMPO.

UV-visible absorption and photoluminescence spectroscopy measurements for porphyrin dendrimers and organometallic porphyrins in solvents (HPLC level CH₂Cl₂ and toluene) were performed on BIO-TEK instrument UVIKON XL spectrometer and Edinburg FS920 Fluorimeter (Xe900) at room temperature, respectively.

Quantum yields were measured in CH₂Cl₂ (HPLC level) at room temperature, taking TPP (Φ_{fl} = 11% in HPLC level toluene) as reference.

Fluorescence lifetime in CH₂Cl₂ (HPLC level) was measured on Edimburgh FL920 Fluorescence Lifetime Spectrometer, and time-correlated single-photon counting using pulsed laser excitation at 375 nm was employed.

All the optical measurements were made in solutions of HPLC quality solvents with the same standard conditions: the porphyrin Soret-band maximum absorption intensity was near to 0.1 on UV-visible spectrometer.

Reaction reagents were purchased from commercial suppliers. Some solvents in reactions were distilled using common methods, except for DMF and ¹Pr₂NH that were dried over 3 Å molecular sieves. Some solvents used without further purification unless otherwise stated.

References

- [1] G. McDermott, S. M. Prince, A. A. Free, et al, *Nature*, **1995**, 374, 517.
- [2] S. Severance, I. Hamza, *Chem. Rev.* **2009**, 109, 4596.
- [3] (a) O. Juan, M. B. Helqe, A. Martin, *Chem. Commun.*, **2014**, 50, 3488; (b) T. Ema, Y. Miyazaki, J. Shimonishi, C. Maeda, J. Y. Hasegawa, *J. Am. Chem. Soc.*, **2014**, 136, 15270; (c) Q. Jiang, W. Sheng, M. Tian, J. Tang, C. Guo, *Eur. J. Org. Chem.*, **2013**, 1861.
- [4] (a) M. Ethirajan, Y. Chen, P. Joshi, R. Pandey, *Chem. Soc. Rev.*, **2011**, 40, 340; (b) L. B. Josefsen, R. W. Boyle, *Theranostics*, **2012**, 2, 916; (c) S. K. Pushpan, S. Venkatraman, V. G. Anand, J. D. Sankar, Parmeswaran, S. Ganesan, T. K. Chandrashekar, *Curr. Med. Chem. Anticancer Agents*, **2002**, 2, 187; (d) R. K. Pandey, K. M. Smith, T. J. Dougherty, *J. Med. Chem.*, **1990**, 33, 2032.
- [5] (a) D. Koszelewski, A. Nowak-Król, M. Drobizhev, C. J. Wilson, J. E. Haley, T. M. Cooper, J. Romiszewski, E. Górecka, H. L. Anderson, A. Rebane, D. T. Gryko, *J. Mater. Chem.*, **2013**, 1, 2044; (b) K. R. Graham, Y. Yang, J. R. Sommer, A. H. Shelton, K. S. Schanze, J. Xue, J. R. Reynolds, *Chem. Mater.*, **2011**, 23, 5305; (c) L. G. Zhu, J. Wang, T. G. Reng, C. Y. Li, D. C. Guo, C. C. Guo, *J. Phys. Org. Chem.*, **2010**, 23, 190.
- [6] (a) C. Li, J. Ly, B. Lei, W. Fan, D. Zhang, J. Han, M. Meyyappan, M. Thompson, C. Zhou, *J. Phys. Chem. B*, **2004**, 108, 9646; (b) G. Bussetti, M. Campione, L. Ferraro, L. Raimondo, B. Bonanni, C. Goletti, M. Palummo, C. Hogan, L. Duò, M. Finazzi, A. Sassella, *J. Phys. Chem. C*, **2014**, 118, 15649.
- [7] (a) L. L. Li, E. W. G. Diau, *Chem. Soc. Rev.*, **2013**, 42, 291; (b) X. Huang, C. Zhu, S. Zhang, W. Li, Y. Guo, X. Zhan, Y. Liu, Z. Bo, *Macromolecules*, **2008**, 41, 6895.
- [8] (a) M. Kozaki, A. Uetomo, S. Suzuki, K. Okada, *Org. Lett.*, **2008**, 10, 4477; (b) A. Uetomo, M. Kozaki, S. Suzuki, K. I. Yamanaka, O. Ito, K. Okada, *J. Am. Chem. Soc.*, **2011**, 133, 13276.

- [9] (a) A. Harriman, M. Hissler, O. Trompette, R. Ziessel, *J. Am. Chem. Soc.*, **1999**, *121*, 2516; (b) J. Fortage, J. Boixel, E. Blart, H. C. Becker, F. Odobel, *Inorg. Chem.*, **2008**, *48*, 518.
- [10] (a) O. Mongin, C. Papamicaël, N. Hoyler, A. Gossauer, *J. Org. Chem.*, **1998**, *63*, 5568; (b) A. Nakano, Y. Yasuda, T. Yamazaki, S. Akimoto, I. Yamazaki, H. Miyasaka, A. Itaya, M. Murakami, A. Osuka, *J. Phys. Chem. A*, **2001**, *105*, 4822.
- [11] D. M. Burns, J. Iball, *Nature*, **1954**, *173*, 635.
- [12] G. M. Brown, M. H. Bortner, *Acta Cryst.*, **1954**, *7*, 139.
- [13] S. Dufresne, I. U. Roche, T. Skalski, W. G. Skene, *J. Phys. Chem. C.*, **2010**, *114*, 13106.
- [14] (a) B. P. Singh, R. Vigava, S. J. Shetty, K. Kandasamy, P. N. Puntambekar, T. S. Srivastava, *J. Porphyrins Phthalocyanines*, **2000**, *4*, 659; (b) V. Rozhkov, D. Wilson, S. Vinogradov, *Macromolecules*, **2002**, *35*, 1991; (c) D. L. Jiang, T. Aida, *J. Am. Chem. Soc.*, **1998**, *120*, 10895.
- [15] (a) B. Li, Y. Fu, Y. Han, Z. Bo, *Macromol. Rapid Commun.*, **2006**, *27*, 1355; (b) Z. Fei, Y. Han, Z. Bo, *J. Polym. Sci., Part A: Polym. Chem.*, **2008**, *46*, 4037.
- [16] (a) M. Kozaki, K. Akita, S. Suzuki, K. Okada, *Org. Lett.*, **2007**, *9*, 3315; (b) M. Kimura, T. Shiba, M. Yamazaki, K. Hanabusa, H. Shirai, N. Kobayashi, *J. Am. Chem. Soc.*, **2001**, *123*, 5636.
- [17] (a) L. Wang, Y. Jiang, J. Luo, Y. Zhou, J. H. Zhou, J. Wang, J. Pei, Y. Cao, *Adv. Mater.*, **2009**, *47*, 4854; (b) X. F. Duan, J. L. Wang, J. Pei, *Org. Lett.*, **2005**, *7*, 4071.
- [18] (a) M. Kreyenschmidt, G. Klaerner, T. Fuhrer, J. Aschenhurst, S. Karg, W. D. Chen, V. Y. Lee, J. C. Scott, R. D. Miller, *Macromolecules*, **1998**, *31*, 1099; (b) N. A. Montgomery, J. C. Denis, S. Schumacher, A. Ruseckas, P. J. Skabara, A. Kanibolotsky, M. J. Paterson, I. Galbraith, G. A. Turnbull, I. D. W. Samuel, *J. Phys. Chem. A.*, **2011**, *115*, 2913.
- [19] (a) B. Li, X. Xu, M. Sun, Y. Fu, G. Yu, Y. Liu, Z. Bo, *Macromolecules*, **2005**, *39*, 456; (b) B. Li, J. Li, Y. Fu, Z. Bo, *J. Am. Chem. Soc.*, **2004**, *126*, 3430.
- [20] Z. Fei, B. Li, Z. Bo, R. Lu, *Org. Lett.*, **2004**, *6*, 4703.
- [21] M. Sun, Z. Bo, *J. Polym. Sci., Part A: Polym. Chem.*, **2007**, *45*, 111.

- [22] E. M. Harth, S. Hecht, B. Helms, E. E. Malmstrom, J. M. J. Fréchet, C. J. Hawker, *J. Am. Chem. Soc.*, **2002**, *124*, 3926.
- [23] (a) M. A. Oar, W. R. Dichtel, J. M. Serin, J. M. J. Fréchet, J. E. Rogers, J. E. Slagle, P. A. Fleitz, L. S. Tan, T. Y. Ohulchansky, P. N. Prasad, *Chem. Mater.* **2006**, *18*, 3682; (b) W. R. Dichtel, J. M. Serin, C. Edder, J. M. J. Fréchet, M. Matuszewski, L. S. Tan, T. Y. Ohulchansky, P. N. Prasad, *J. Am. Chem. Soc.*, **2004**, *126*, 5380.
- [24]. (a) M. Tavasli, S. Bettington, M. R. Bryce, H. Al-Attar, F. B. Dias, S. King, A. P. Monkman, *J. Mater. Chem.*, **2005**, *15*, 4963; (b) H. Al-Attar, A. P. Monkman, M. Tavasli, S. Bettington, M. R. Bryce, *Appl. Phys. Lett.*, **2005**, *86*, 121101.
- [25] U. Scherf, E. J. W. List, *Adv. Mater.*, **2002**, *14*, 477.
- [26] (a) K. Onitsuka, H. Kitajima, M. Fujimoto, A. Iuchi, F. Takei, S. Takahashi, *Chem. Commun.*, **2002**, 2576; (b) B. Du, D. Fortin, P. D. Harvey, *Inorg. Chem.*, **2011**, *50*, 11493.
- [27] (a) M. J. Frampton, R. Beavington, J. M. Lupton, I. D. W. Samuel, P. L. Burn, *Synth. Met.*, **2001**, *121*, 1671; (b) M. J. Frampton, S. W. Magennis, J. N. G. Pillow, P. L. Burn, I. D. W. Samuel, *J. Mater. Chem.*, **2003**, *13*, 235; (c) J. N. G. Pillow, M. Halim, J. M. Lupton, P. L. Burn, I. D. W. Samuel, *Macromolecules*, **1999**, *32*, 5985.
- [28] M. Kozaki, S. Morita, S. Suzuki, K. Okada, *J. Org. Chem.*, **2012**, *77*, 9447.
- [29] (a) M. Kozaki, A. Uetomo, S. Suzuki, K. Okada, *Org. Lett.*, **2008**, *10*, 4477. (b) A. Uetomo, M. Kozaki, S. Suzuki, K. I. Yamanaka, O. Ito, K. Okada, *J. Am. Chem. Soc.*, **2011**, *133*, 13276.
- [30] M. Kozaki, K. Akita, S. Suzuki, K. Okada, *Org. Lett.*, **2007**, *9*, 3315.
- [31] P. Rothmund, *J. Am. Chem. Soc.*, **1935**, *57*, 2010.
- [32] (a) P. Rothmund, *J. Am. Chem. Soc.*, **1936**, *58*, 625; (b) P. Rothmund, A. R. Menotti, *J. Am. Chem. Soc.*, **1941**, *63*, 267.
- [33] (a) A. D. Adler, F. R. Longo, J. D. Finarelli, J. Assour, L. Korsakoff, *J. Org. Chem.*, **1967**, *32*, 476; (b) A. D. Adler, F. R. Longo, W. Shergalis, *J. Am. Chem. Soc.*, **1964**, *86*, 3145.

- [34] (a) J. S. Lindsey, H. C. Hsu, I. C. Schreiman, *Tetrahedron Lett.*, **1986**, 27, 4969;
(b) J. S. Lindsey, I. C. Schreiman, H. C. Hsu, P. C. Kearney, A. M. Marguerettaz, *J. Org. Chem.*, **1987**, 52, 827.
- [35] A. D. Adler, F. R. Longo, J. D. Finarelli, J. Goldmacher, J. Assour, L. Korsakoff, *J. Org. Chem.*, **1967**, 32, 476.
- [36] (a) C. H. Lee, J. S. Lindsey, *Tetrahedron*, **1994**, 50, 11427. (b) J. S. Lindsey, K. A. MacCrum, J. S. Tyhonas, Y. Y. Chuang, *J. Org. Chem.*, **1994**, 59, 579.
- [37] F. R. Li, K. X. Yang, J. S. Tyhonas, K. A. MacCrum, J. S. Lindsey, *Tetrahedron*, **1997**, 53, 12339.
- [38] R. Chinchilla, C. Nájera, *Chem. Soc. Rev.*, **2011**, 40, 5084.
- [39] K. Sonogashira, Y. Tohda, N. Hagihara, *Tetrahedron Lett.*, **1975**, 50, 4467.
- [40] C. He, J. Ke, H. Xu, A. Lei, *Angew. Chem. Int. Ed.*, **2013**, 52, 1527.
- [41] R. Chinchilla, C. Nájera, *Chem. Rev.*, **2014**, 114, 1783.
- [42] C. R. Hopkins, N. Collar, *Tetrahedron Lett.*, **2004**, 43, 8087.
- [43] F. Li, T. S. A. Hor, *Adv. Synth. Catal.*, **2008**, 350, 2391.
- [44] Z. Feng, S. Yu, Y. Shang, *Appl. Organomet. Chem.*, **2008**, 22, 577.
- [45] N. S. C. Ramesh Kumar, I. V. P. Raj, A. Sudalai, *J. Mol. Catal. A: Chem.*, **2007**, 269, 218.
- [46] D. H. Lee, H. Qiu, M. H. Cho, I. M. Lee, M. J. Jin, *Synlett*, **2008**, 1657.
- [47] A. J. Bard, Faulkner, R. Larry, *Electrochemical Methods: Fundamentals and Applications*, 2nd ed., John Wiley & Sons, Inc., New York, **2001**.
- [48] S. L. Queiroz, M. P. De Araujo, A. A. Batista, K. S. MacFarlane, B. R. James, *J. Chem. Ed.*, **2001**, 78, 89.
- [49] D. H. Evans, K. M. O'Connell, R. A. Petersen, M. J. Kelly, *J. Chem. Ed.*, **1983**, 60, 290.
- [50] P. T. Kissinger, W. R. Heineman, *J. Chem. Ed.*, **1983**, 60, 702.
- [51] J. J. V. Benschoten, J. Y. Lewis, W. R. Heineman, D. A. Roston, P. T. Kissinger, *J. Chem. Ed.*, **1983**, 60, 772.
- [52] A. L. Eckermann, D. J. Feld, J. A. Shaw, T. J. Meade, *Coord. Chem. Rev.*, **2010**, 254, 1769.

- [53] A. Merhi, C. Grelaud, N. Ripoche, A. Barlow, M. P. Cifuentes, M. G. Humphrey, F. Paul, C. O. Paul-Roth, *Polyhedron*, **2015**, *86*, 64.
- [54] (a) D. J. Quimby, F. R. Longo, *J. Am. Chem. Soc.*, **1975**, *97*, 5111; (b) M. Uttamlal, A. Sheila Holmes-Smith, *Chem. Phys. Lett.*, **2008**, *454*, 223; (c) J. L. Retsek, C. J. Medforth, D. J. Nurco, S. Gentemann, V. S. Chirvony, K. M. Smith, D. Holten, *J. Phys. Chem. B*, **2001**, *105*, 6396.
- [55] (a) M. Gouterman, *J. Mol. Spectroscopy*, **1961**, *6*, 138; (b) M. Gouterman, *J. Chem. Phys.*, **1959**, *30*, 1139.
- [56] L. R. Milgrom, “*The colours of Life: An Introduction to the Chemistry of Porphyrins and Related Compounds*”, Oxford Univ. Press: Oxford **1997**.
- [57] M. Kasha, *Discussions of the Faraday Society*, **1950**, *9*, 14.
- [58] D. L. Dexter, *J. Chem. Phys.*, **1953**, *21*, 836.
- [59] T. Förster, *Annalen der Physik (in German)*, **1948**, *437*, 55.
- [60] V. Helms, *Principles of Computational Cell Biology*, **2008**, Wiley-VCH, Weinheim.
- [61] D. L. Andrews, *Chemical Physics*, **1989**, *135*, 195.
- [62] B. Kirtman, B. Champagne, *Int. Rev. Phys. Chem*, **1997**, *16*, 389.
- [63] H. S. Nalwa, *Appl. Organomet. Chem*, **1991**, *5*, 349.
- [64] N. J. Long, *Angew. Chem. Int. Ed.*, **1995**, *34*, 21.
- [65] I. R. Whittall, A. M. McDonagh, M. G. Humphrey, M. Samoc, *Adv. Organomet. Chem.*, **1998**, *42*, 291.
- [66] M. Goepfert-Mayer, *Ann. Phys.*, **1931**, *9*, 273.
- [67] W. Kaiser, C. G. B. Garrett, *Phys. Rev. Lett.*, **1961**, *7*, 229.
- [68] I. D. Abella, *Phys. Rev. Lett.*, **1962**, *9*, 453.
- [69] R. L. Sutherland, “*Handbook of Nonlinear Optics*”, Marcel Dekker: New York **1996**.
- [70] P. N. Butcher, D. Cotter, in “*The Elements of Nonlinear Optics*”, Cambridge Univ. Press: New York **1990**.
- [71] O. Mongin, L. Porrès, M. Charlot, C. Katan, M. Blanchard-Desce, *Chem. Eur. J.*, **2007**, *13*, 1481.

Chapter 1

**Syntheses of
New Thieryl Porphyrin Dendrimers and
Photophysical Properties**

1.1 The targets of the project

1.1.1 Introduction

Materials having third-order nonlinear optical (3rd NLO) properties are used in a wide range of applications, such as optical communication, data storage, dynamic holography, optical switching, harmonic generators, frequency mixing and optical computing^[1-4].

As described in the introduction, classic 3rd NLO processes mainly include two parts: Two-photon absorption (TPA) and Saturable absorption (SA).

Conjugated organic molecules reveal some interesting features with respect to TPA. They present intrinsically fast absorption (femtosecond) and can satisfy an essential requirement for efficient TPA: a large two-photon absorption cross-section (σ_2).

Some molecules that have been synthesized are presented in Figure 1.1.1. They show different degrees of conjugation and have electron donor (D) or electron acceptor (A) which are intended to provide higher σ_2 ^[5-9]. Table 1.1.1 lists their TPA properties at specific wavelengths.

Figure 1.1.2 shows a comparison of the σ_2 values of these compounds. The σ_2 of **H (d)** (blue bar), having 12 phenyls, is 1360 GM. This σ_2 [**H(d)**] is broadly double the value found for **H (b)** with 9 phenyls, σ_2 [**H(b)**] = 740 GM, so that the additional 3 phenyls significantly enlarge the two-photon absorption cross-section. This effect is reproduced for the couples **A** and **C**, as well as **B** and **D**, **F (a)** and **G (a)**. We also can see that **E**, containing two thienyl linkers, has high value of σ_2 (1340 GM).

The importance of designing and synthesizing organic molecules having highly conjugated systems is therefore clear. Most particularly, it is noteworthy that the two thienyl groups (marked blue in Figure 1.1.1) of compound **E** enlarge the σ_2 relative to the homologue **C** having two phenyls (marked in red). The other factors, like symmetrical structure and D- π -D or A- π -A quadrupole, also enhance the TPA effect^[10].

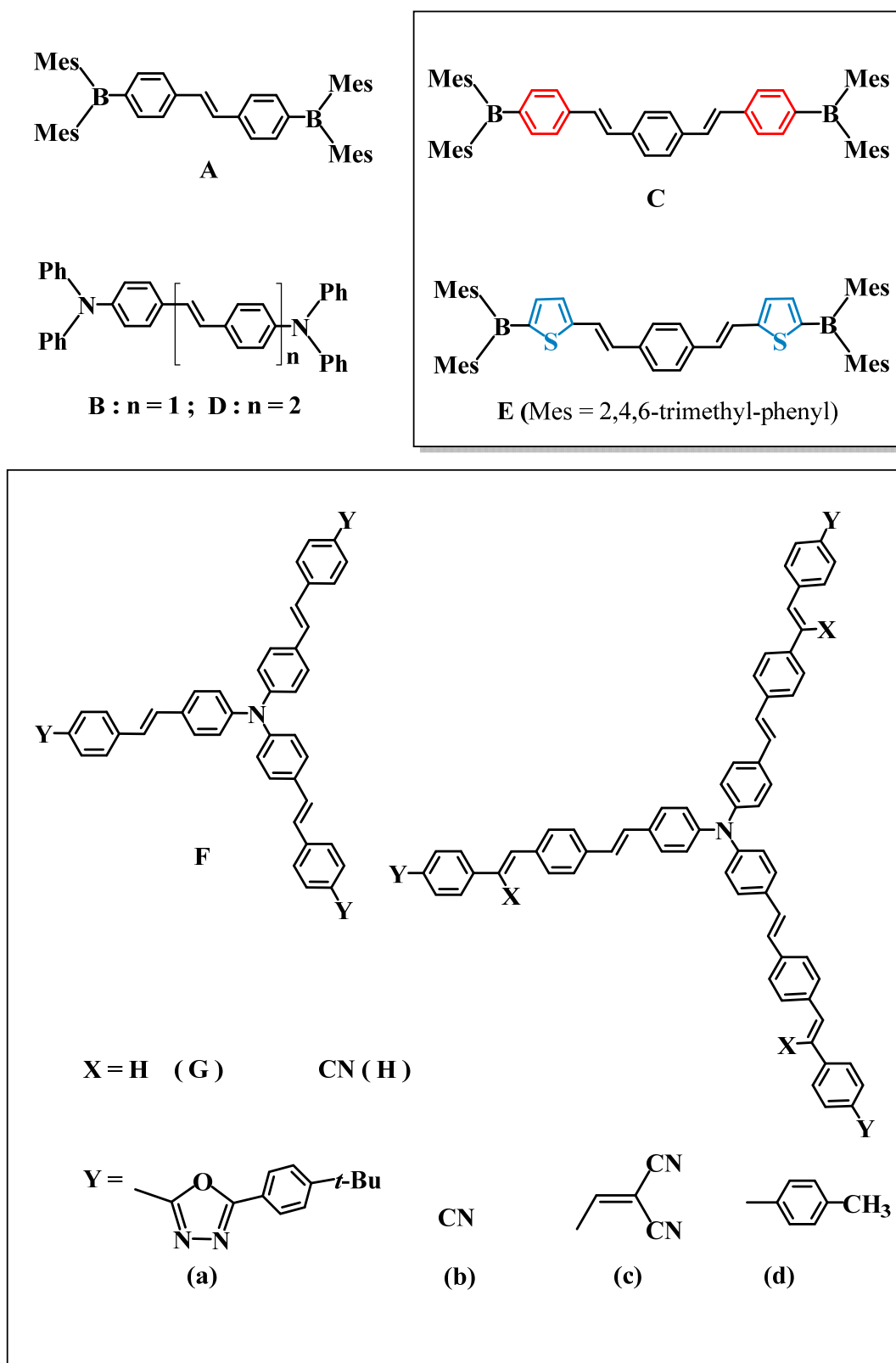


Figure 1.1.1 Conjugated molecules A, B, C, D, and E in linear structure and symmetrical molecules F, G and H

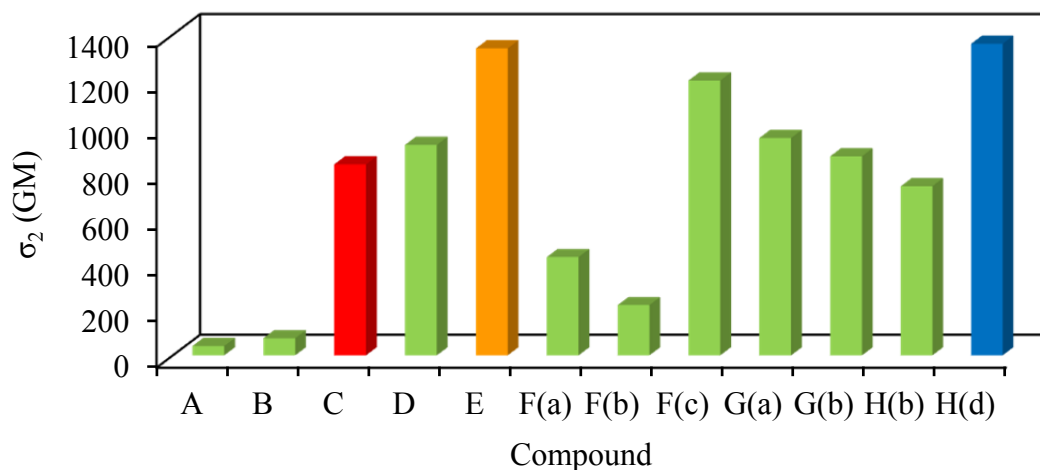
Figure 1.1.2 Comparison of cross-sections (σ_2) of the different conjugated compounds (A-H)

Table 1.1.1 TPA properties of the conjugated molecules: A-H

Compound	Two-photon excited fluorescence (TPEF)		
	N° of Phenyl	λ_{\max} (nm)	σ_2 (GM)
A^a	6	431	41 (720 nm) ^b
B^a	6	436, 455	75 (720 nm) ^b
C^a	7	445, 468	835 (730 nm) ^b
D^a	7	466, 488	920 (745 nm) ^b
E^a	5	491, 514	1340 (775 nm)^b
F(a)^c	9	760	430 (760 nm) ^b
F(b)^c	6	760	220 (760 nm) ^b
F(c)^c	6	890	1200 (890 nm) ^b
G(a)^c	12	780	950 (780 nm) ^b
G(b)^c	9	780	870 (780 nm) ^b
H(b)^c	9	890	740 (890 nm) ^b
H(d)^c	12	800	1360 (800 nm)^b

^a TPA properties were measured at 5.0×10^{-4} mol/L in THF.

^b TPA cross-section determined using fluorescein as the standard, the data in parentheses are the excitation wavelengths of the laser.

^c Measurements in Toluene.

1.1.2 Thienyl unit

In 1883, Victor Meyer isolated thiophene as a contaminant of benzene ^[11]. This heterocyclic compound is shown in Figure 1.1.3.

In the planar ring of thiophene, the bond angle at sulfur ($\angle C_1SC_4$) is around 93° ; the two angles: $\angle C_3C_4S$ and $\angle C_2C_1S$ are around 109° ; and the other two carbon bond angles: $\angle C_1C_2C_3$ and $\angle C_4C_3C_2$ are close to 114° . The C_1-C_2 and C_3-C_4 bonds are about 1.34 \AA ; the C_3-C_4 bond is about 1.41 \AA ; and the two bonds length: C_1-S and C_4-S are around 1.70 \AA (from the Cambridge Structural Database). The presence of the sulfur atom allows the thienyl center to be used as a polar bridge.

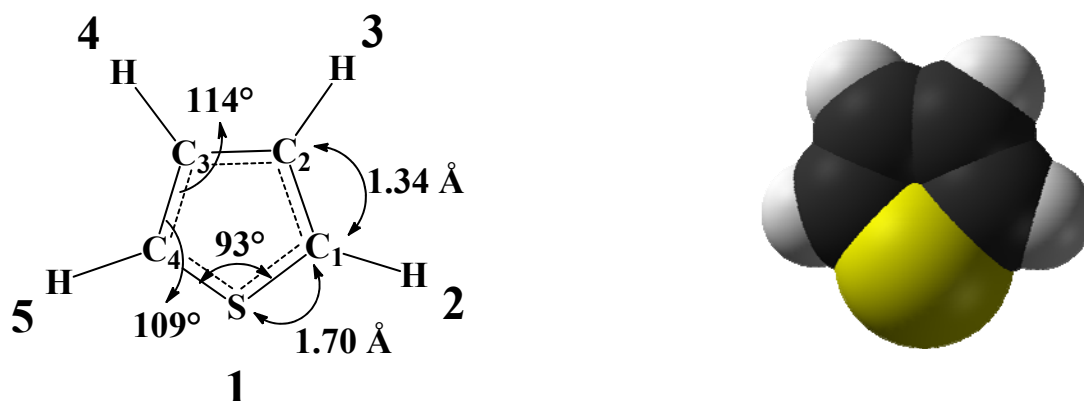
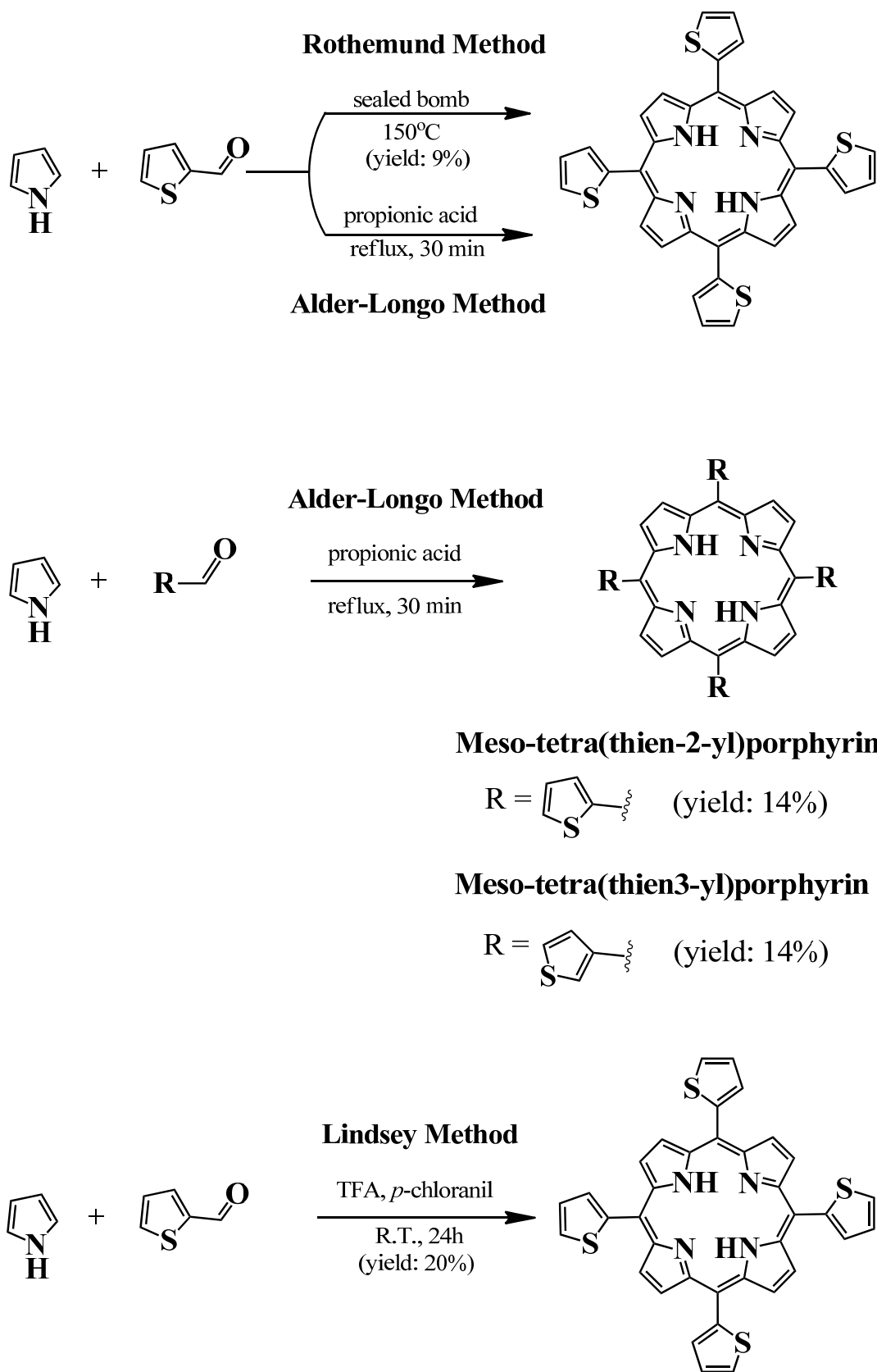


Figure 1.1.3 The structure of thiophene

The first porphyrin core embellished with a thienyl group was synthesized in 1968 by Triebs et al. via an adapted Rothmund method in 9% yield ^[12]. In 1972, the Alder-Longo method was used by Torr ns et al. who did not report a yield ^[13]. By 2001, Bhyrappa and Bhavana had prepared *meso*-tetra(thien-2-yl)porphyrin and *meso*-tetra(thien-3-yl)porphyrin using the Alder-Longo method in 14% yield for both compounds ^[14]. In 1998, Ono et al. synthesized a series of *meso*- and β -dodeca substituted thienyl porphyrins through Lindsey's method, giving a maximum yield of 20% (shown in Scheme 1.1.4) ^[15].



**Scheme 1.1.4 Comparison among the Rothmund, Alder-Longo and Lindsey methods
On synthesizing the *meso*-tetra(thien-2-yl)porphyrin**

In recent years, TPA materials have attracted much interest from chemists, who have set out to investigate the efficiency of different TPA substituents. As seen previously, thienyl based compounds (shown in Figure 1.1.1) gave interesting TPA cross-sections σ_2 .

The importance of thienyl as a TPA substituent arises from the strong polarizability of the sulfur atom, which improves the TPA cross-section [16-18]. Carbon disulfide, being the archetypal sulfur-rich compound, has been used as a standard in 3rd NLO research for several decades [17,19]. In 2006, Brückner et al. calculated the energy of the porphyrin as a function of the rotation of a single *meso* aryl group to partially investigate the origin of the bathochromic shifts in the absorption spectra of thienyl porphyrins by employing the density functional theory (DFT). Compared to the *meso*-phenylporphyrin, the reduced steric hindrance was found for the smaller *meso*-tetra-thienyl porphyrin. Besides, the thien-2-yl substituent lacks one *o*-phenyl proton to β -pyrrolic proton interaction (shown in Figure 1.1.5) [20, 21].

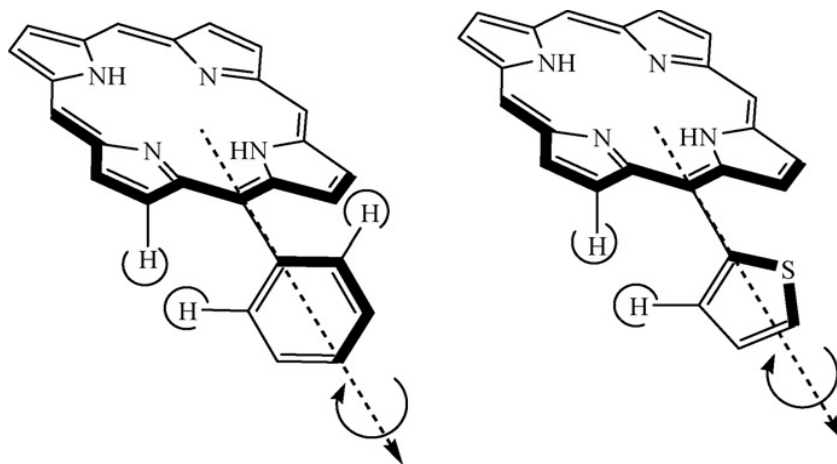


Figure 1.1.5 Schemata of rotation for phenyl and thienyl substituents at the *meso* position of the porphyrin ring

1.1.3 Thienyl porphyrins in literatures

During the past decade, various porphyrins possessing thienyl arms in *meso* positions have been reported. For example, Rochford et al. reported a group of porphyrins (**I1-I7**) with mono-, di-, tri- and tetra-(thien-2-yl) groups in their *meso* positions in 2008 (Figure 1.1.6). These zinc complexes present interesting photophysical and electrochemical properties.

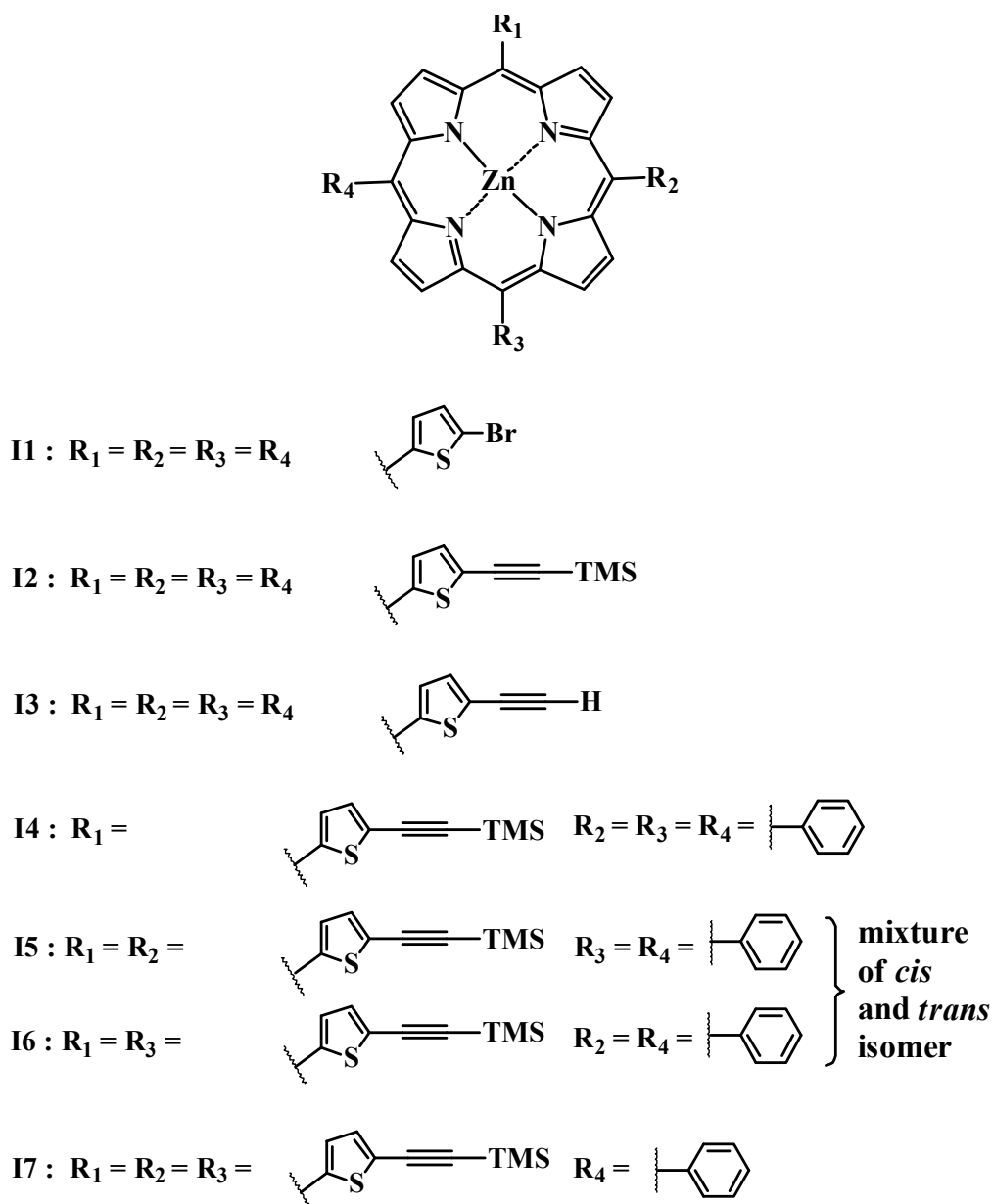
Figure 1.1.6 The entire structure of the Zn thienyl porphyrins **I1-I7**

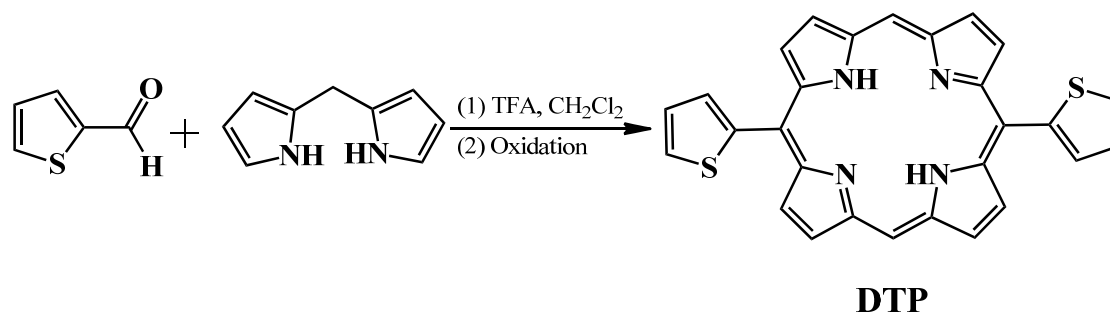
Table 1.1.2 lists selected photophysical properties of compounds **I1-I7**. For Zn porphyrins, the Soret band absorptions appear around 430 nm, and because of the presence of the zinc centre within the porphyrin ring, they only present two Q bands [Q(0,1) and Q(0,0)]. Compounds **I1-I7** all exhibit red emission, and all their quantum yields (Φ_f) are low, the best being observed in porphyrin **I4** ($\Phi_f = 4.6\%$). The lifetime (τ) of the zinc complex of thien-2-yl porphyrins derivatives was also measured, with the longest lifetime ($\tau_{\max} = 1.94$ ns) also being observed for compound **I4**. The cyclic voltammetry of these thien-2-yl porphyrins were studied as well [22].

Table 1.1.2 Photophysical data of *meso*-thien-2-yl porphyrins (I1-I7) recorded in toluene

	UV-visible absorption			Fluorescence			τ/ns
	$\lambda_{\max}^{\text{Soret}}/\text{nm}$ ($\epsilon \times 10^5 \text{ M}^{-1} \text{ cm}^{-1}$)	$\lambda_{\max}^{\text{Q(0,1)}}/\text{nm}$ ($\epsilon \times 10^3 \text{ M}^{-1} \text{ cm}^{-1}$)	$\lambda_{\max}^{\text{Q(0,0)}}/\text{nm}$ ($\epsilon \times 10^3 \text{ M}^{-1} \text{ cm}^{-1}$)	Q(0,0)* / nm	Q(0,1)* / nm	Φ_f / %	
I1	434 (2.82)	558 (8.57)	600 (2.20)	-	636	0.6	0.52
I2	438 (2.21)	560 (11.80)	606 (3.48)	629	650	1.8	0.76
I3	436 (2.42)	560 (10.32)	600 (2.64)	639	650	1.4	0.74
I4	426 (2.18)	522 (9.62)	594 (2.01)	607	651	4.6	1.94
I5				615	647	4.2	1.48
I6	430 (2.37)	554 (9.64)	598 (2.78)				
I7	434 (2.23)	552 (9.81)	594 (1.87)	614	644	2.8	1.92

In the same year, *meso*-5,15-bis-(2-thienyl)-porphyrin (**DTP**) was reported by our group, as shown in Scheme 1.1.5. Its Soret band absorption appears at 411 nm in the UV-visible absorption spectrum. Upon excitation at this wavelength, **DTP** exhibits the strong red luminescence at 642 nm followed by a weak shoulder at 707 nm [23].

Thus far, using thienyl as a linker between the porphyrin core and dendrons has been rarely studied. There has also been relatively little exploration on two-photon absorption relating to *meso*-tetra-thienyl porphyrin (**TThP**) and its corresponding dendrimers.

Scheme 1.1.5 Synthesis of *meso*-5,15-(2-thienyl)-porphyrin (DTP)

1.1.4 Targets of the Chapter

Porphyrins show rich promise as potential π -systems for several applications. The planar porphyrin ring constitutes a highly conjugated 18 π -electrons aromatic macrocycle. This meets the needs of organic molecules that are required to have a large two-photon absorption cross-section^[24-27].

In this chapter, we connect the thienyl group to the *meso* position of porphyrin to form a quadrupolar structure. The thienyl groups are used as a strong polar bridge between the porphyrin ring and the dendrons.

Dendrons in this chapter are built from fluorenyl and phenyl components. Their rigid structures are propitious to light-harvesting in the UV region.

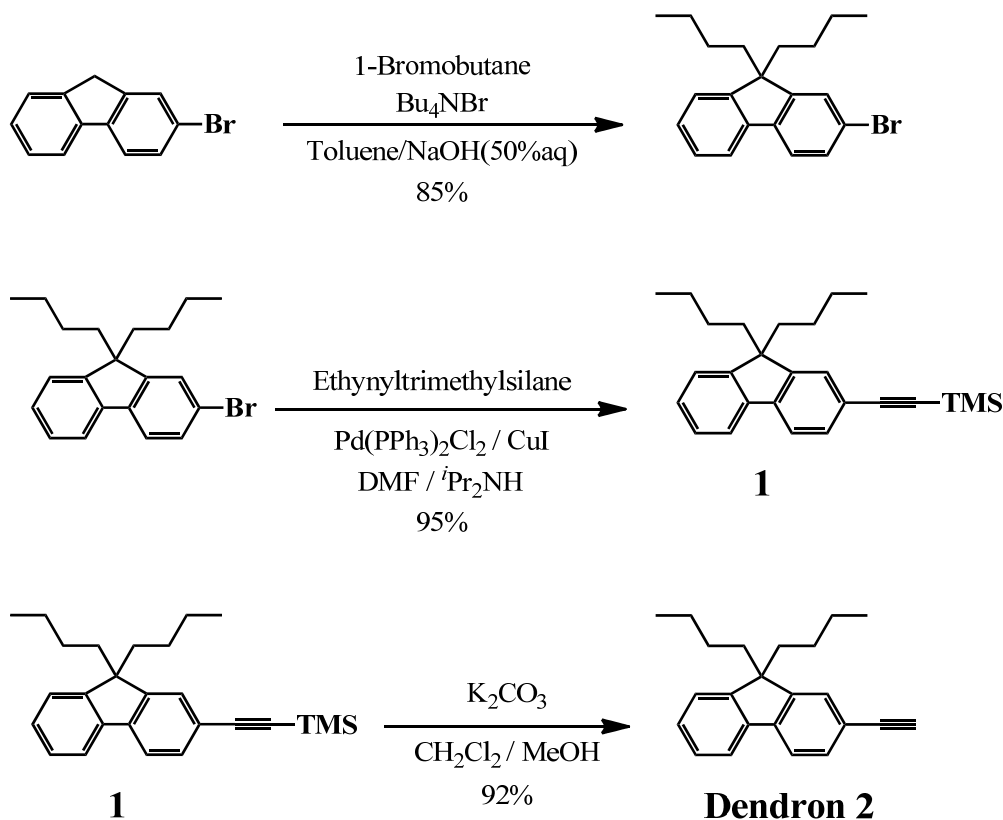
Porphyrins with large metalated π -architectures are already well known as efficient TPA materials for various applications^[28,29]. The *meso*-positioned electron-releasing substituents on the macrocyclic core improve their TPA cross-sections^[30]. In 2015, a series of ruthenium-metallated porphyrins with interesting TPA properties were successfully synthesized in our laboratory. We had chosen a less polarizable substituent: phenyl to bridge the dendron to porphyrin core, and these compounds showed interesting TPA cross-sections^[31]. It therefore seemed promising to introduce a stronger polarizable thienyl between the organic dendrons and porphyrin core, aiming to form a group of pure organic porphyrin dendrimers with large TPA cross-sections.

For these reasons the following compounds: *meso-tetra-thienyl porphyrin* (TThP (7) as the reference), *meso-(2-((9,9-dibutyl-fluoren-2-yl)ethynyl)-thienyl)-porphyrin* (8) and *meso-(2-((3,5-bis((9,9-dibutyl-fluoren-2-yl)ethynyl)phenyl)ethynyl)thiophenyl)porphyrin* (9) have been prepared (as shown in Scheme 1.2.4) and will be described in this chapter. Firstly, these molecules were well characterized by ^1H NMR, ^{13}C NMR, MASS and microanalysis. Then their photophysical properties were measured: Linear optical properties and Two-photon absorption (TPA) properties. These revealed satisfactory results.

1.2 Syntheses of the new series of thienyl porphyrins

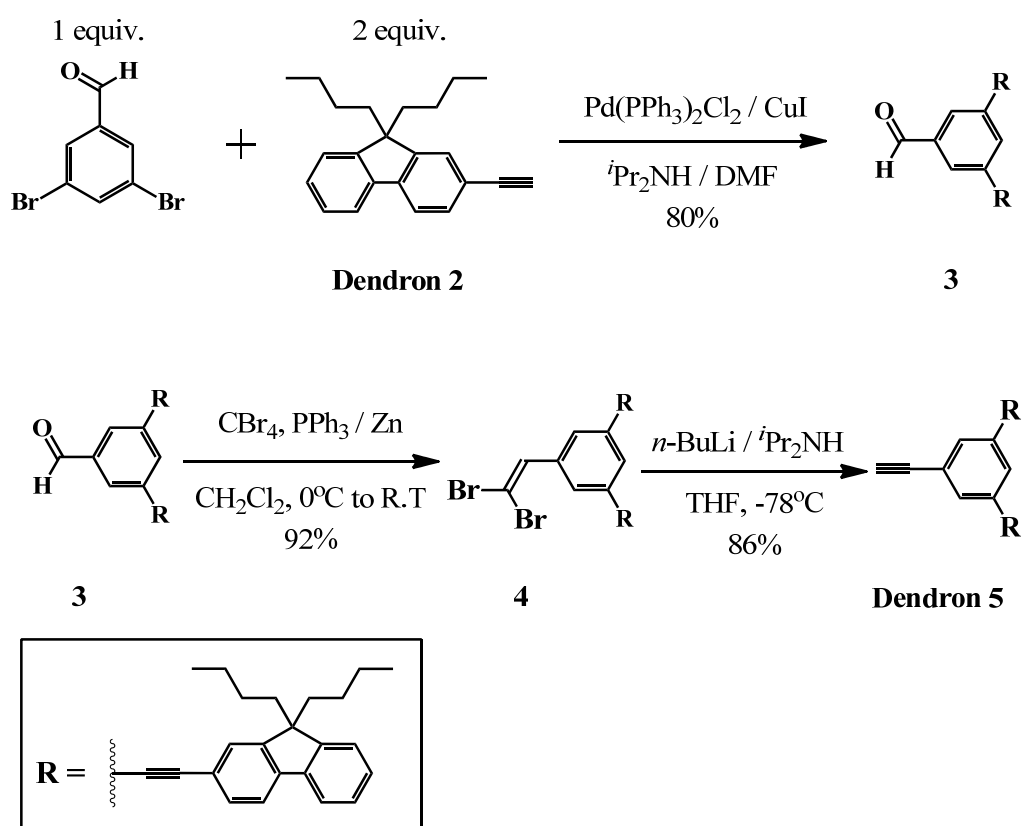
To prepare this new family of organic porphyrin dendrimers, the Lindsey Method [32,33], Sonogashira coupling [34] and Corey-Fuchs reaction [35] were used successively to provide the target molecules: TThP (7), 8 and 9.

1.2.1 Dendrons formation



Scheme 1.2.1 Synthesis of Dendron 2

For dendron **2**, *n*-butyl chains were firstly fixed in 9 position of 2-bromofluorene, to improve the solubility properties of the targets, in a yield of 85%. Then the triple bond was introduced through exchanging the Br of fluorene with ethynyltrimethylsilane by Sonogashira coupling^[34]. The corresponding trimethylsilyl substituted product was isolated. Following treatment with by K_2CO_3 (in a solution of methanol/ CH_2Cl_2 (1:3)) to achieve deprotection, the **9, 9-dibutyl-2-ethynyl-fluorene** (**dendron 2**) was obtained, in a yield of 87% over the two steps (shown in Scheme 1.2.1).



Scheme 1.2.2 Synthesis of Dendrons 5

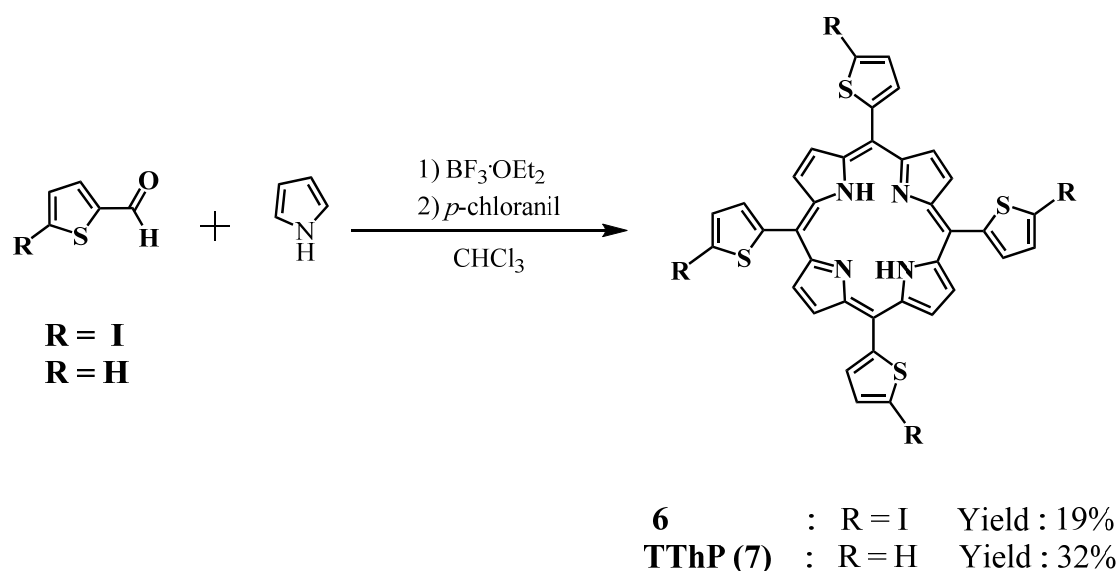
As shown in Scheme 1.2.2, one equivalent of 3,5-dibromobenzaldehyde and two equivalents of dendron **2** were used to synthesize the doubly triple-bond substituted compound **3** under Sonogashira coupling conditions, in 80% yield. Next, the desired dendron **5** was prepared by the two-step Corey-Fuchs reaction (92% yield for the first step, 86% yield for the second step).

1.2.2 Thienyl porphyrins formation

In our studies, we exploited the thienyl units in *meso*-positions of porphyrin, as shown in Scheme 1.2.3. Lindsey's conditions were chosen for synthesizing these thienyl porphyrins.

To synthesize the reference **TThP (7)**, $\text{BF}_3 \cdot \text{OEt}_2$ was injected into a degassed solution of 2-thienylcarboxaldehyde and pyrrole in distilled chloroform under argon. The flask was covered with aluminum foil, because the reaction is light sensitive at this stage, and the mixture was then stirred at room temperature for 2 h. Then *p*-chloranil was added, the reaction was refluxed for 1 h, and the $\text{BF}_3 \cdot \text{OEt}_2$ was then neutralized by NEt_3 . After evaporation of volatiles, the residue was adsorbed onto a small quantity of silica, applied to the top of a silica column and purified by chromatography using a CH_2Cl_2 /heptane (1:5) mixture as eluent. The desired porphyrin **TThP (7)** was isolated as a dark violet powder with a yield of 32%.

The related porphyrin: **tetra-(5-iodo-thienyl)porphyrin (6)** was synthesized using the same methods in a yield of 19%.



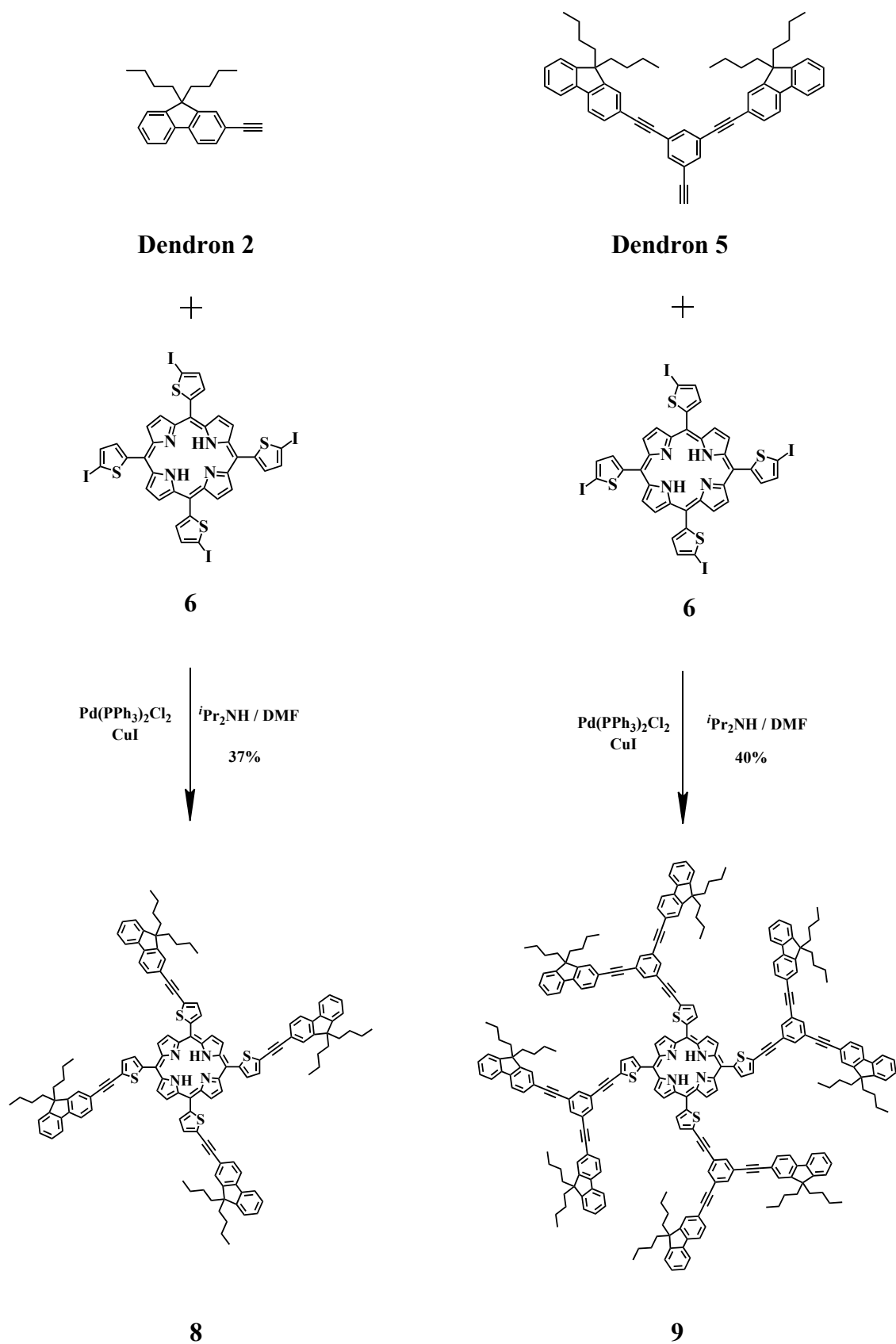
Scheme 1.2.3 Syntheses of the reference *tetra*-thienylporphyrin (**TThP**; **7**) and the *tetra*-(5-iodo-thienyl)porphyrin (**6**)

1.2.3 Target porphyrin dendrimers formation

Having prepared dendrons **2**, **5** and porphyrin **6**, the target porphyrin dendrimers **8** and **9** were synthesized by Sonogashira coupling reactions ^[34].

As an example, the dendron **2** and porphyrin **6** were mixed with Pd(PPh₃)₂Cl₂ and CuI in doubly freeze-pump-thaw cycled DMF/*i*Pr₂NH and then heated for 48 h at 95 °C in a Schenk tube under argon. After evaporation of volatiles, the residue was purified by chromatography on silica using a CH₂Cl₂/heptane (1:5) mixture as eluent. The desired dendrimer **8** was isolated in a yield of 37%.

Porphyrin dendrimer **9** was obtained by the same method from coupling dendron **5** with porphyrin **6**, in a yield of 40%, as shown in Scheme 1.2.4.



Scheme 1.2.4 Syntheses of the target porphyrin 8 and dendrimer 9

1.3 ^1H NMR analyses

The product: dendrons **2**, **5**, porphyrin **6**, **TThP** and porphyrin dendrimers **8**, **9** were characterized by ^1H NMR in CDCl_3 (400 MHz).

1.3.1 ^1H NMR spectra of Dendrons **2** and **5**

The peaks of protons of dendrons can be divided into two parts:

- Aromatic protons from phenyl linkers and fluorenyl arms;
- Terminal alkynyl proton and methyl/ methylene protons in *n*-butyl chains.

^1H NMR full spectra of dendrons **2** and **5** are shown in Figure 1.3.1. Peaks of protons around 7.3-8.0 ppm match with the aromatic moieties: fluorenyl and phenyl. The peaks of protons from *n*-butyl chains (H_a , H_b , H_c and H_d) are presented at 0.5-2.0 ppm, and the singlet around 3.0 ppm arises from the ethynyl proton.

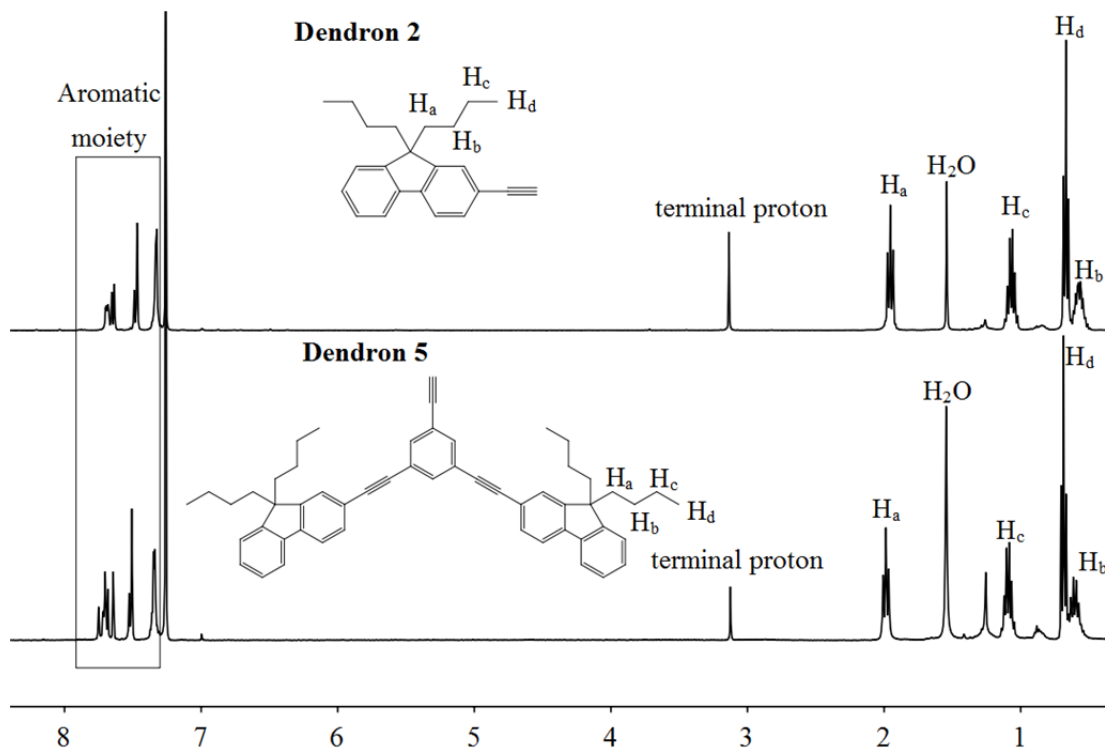


Figure 1.3.1 Detailed complete ^1H NMR spectra of dendrons **2** and **5**

1.3.2 ^1H NMR spectra of porphyrins **6**, reference **TThP**, **8** and **9**

The protons of porphyrin **6**, reference **TThP** and dendrimers **8**, **9** have four components:

- Eight β -pyrrolic H;
- Aromatic H arising from thienyl bridges, phenyl linkers and fluorenyl arms;
- Methyl and methylene H of *n*-butyl chains;
- Two NH protons.

The Figure 1.3.2 presents the partial ^1H NMR of the porphyrins. The singlets at around 9.2 ppm are characteristic of porphyrin macrocycles, and are assigned to eight β -pyrrolic H ($\text{H}_{\beta\text{-pyrrolic}}$). These $\text{H}_{\beta\text{-pyrrolic}}$ signals of **8** and **9** present a slight shift to low field relative to the reference **TThP**. The multiplets in region of 7.3-8.0 ppm arise from the aromatic thienyl, fluorenyl and phenyl protons. The methyl and methylene protons of the *n*-butyl chains in the porphyrin dendrimers **8** and **9** are clearly visible between 0.5 ppm to 2.1 ppm and are well separated. In addition, the two NH protons of **TThP**, **8** and **9** are characterized by a high field singlet at around -2.6 ppm due to the shielding cone of the porphyrin ring.

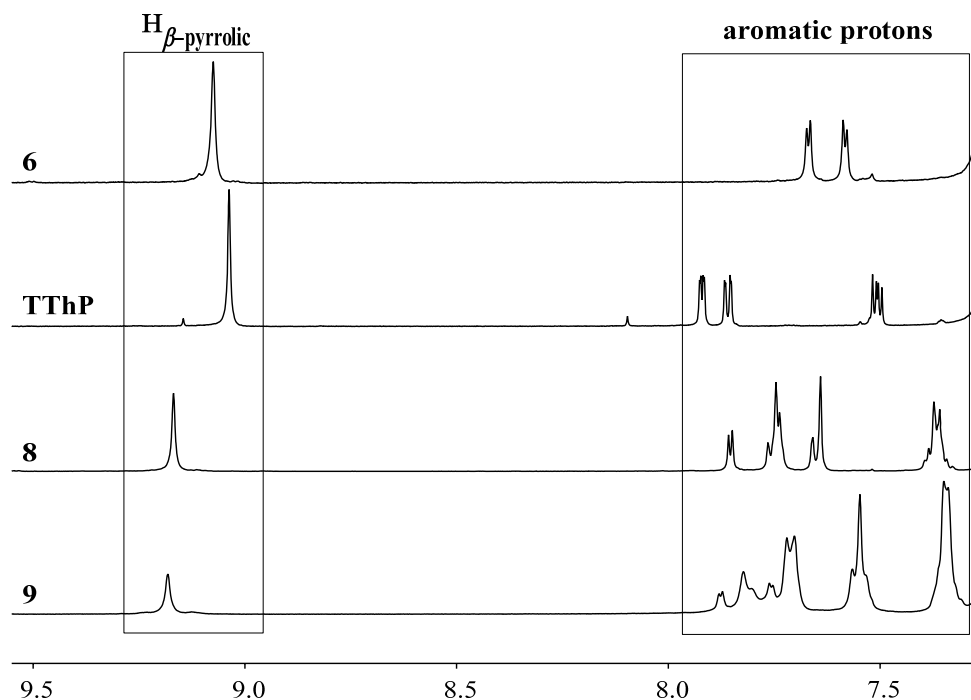


Figure 1.3.2 Partial ^1H NMR spectra of porphyrins **6**, **TThP** and dendrimers **8** and **9**

1.4 Optical properties

TThP was chosen as the reference for the photophysical studies of the new dendrimers **8** and **9**. The molecular structures of these three porphyrins are given in Figure 1.4.1 and their optical properties data are listed in Table 1.4.1.

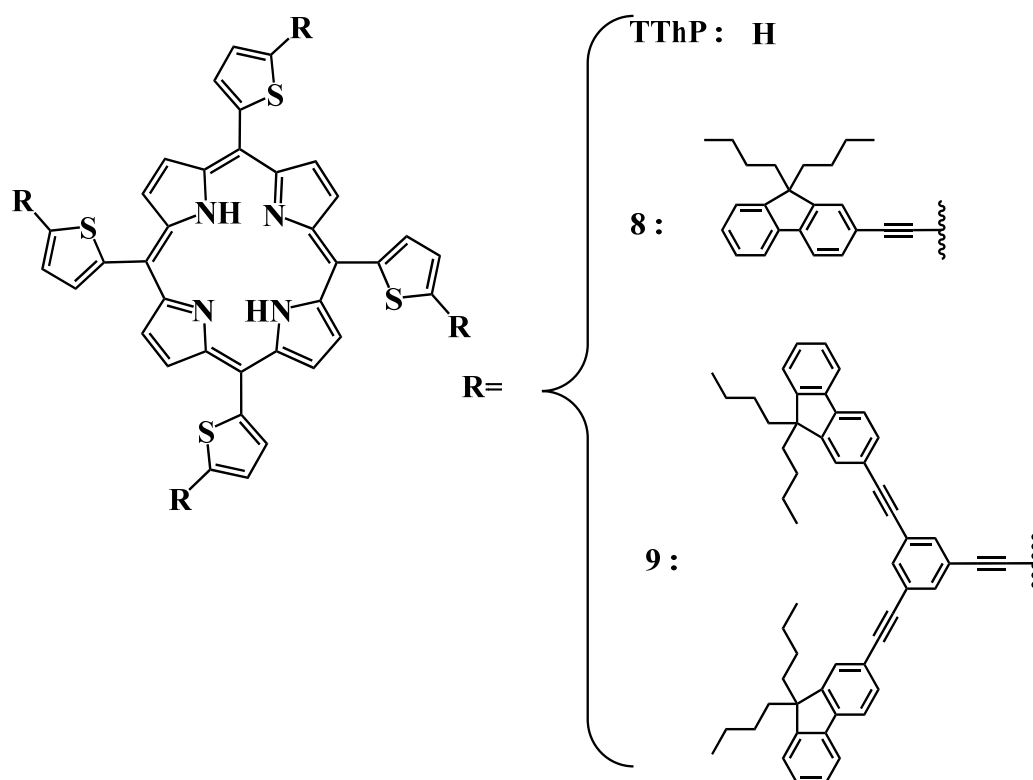


Figure 1.4.1 Molecular structures of reference TThP and new dendrimers **8**, **9**

1.4.1 Absorption spectra of porphyrins TThP, **8** and **9**

Dendrimers **8** and **9** present two distinct components in their UV-visible absorption spectra shown in Figure 1.4.2:

- An intense Soret-band absorption around 435 nm and four Q-bands from 500-700 nm. These are typical of free base porphyrin absorptions;
- A dendron absorption that appears between 250-400 nm. This region is clear

for the porphyrin core possessing only four thienyl groups (**TThP**), which suggests that thienyl-cored porphyrin does make no contribution to the dendron absorption.

Table 1.4.1 Optical properties of molecules: TThP and dendrimers 8, 9 in CH₂Cl₂ at 298 K

	$\lambda_{\text{Dendron}}^{\text{abs}}$ / nm	$\lambda_{\text{Soret}}^{\text{abs}}$ /nm	$\epsilon_{\text{Soret}}^{\text{max}}$ / M ⁻¹ cm ⁻¹	$\lambda_{\text{Q-bands}}^{\text{abs}}$ / nm	λ_{em} / nm	Φ_{fl}^a /%
TThP	-	425	362000	522, 560, 596, 659	670, 729	5
8	330	442	276400	528, 572, ≈ 590, 663	680, ≈725	4
9	329	438	354000	529, 558, ≈ 585, 661	690	3

^a Fluorescence quantum yield determined relative to TPP in toluene.

Figure 1.4.2 shows that the Soret bands in **8** and **9** present a slight red shift when compared with the reference **TThP**. The Soret band absorption of the porphyrin dendrimer **9** is slightly blue-shifted relative to **8** and appears at 438 nm; this is probably because the dendron **5** having two fluorenyl units in position 3 and 5 of phenyl is less conjugated than dendron **2** with one in position 4.

In the Q-bands region, **TThP** shows four standard porphyrin Q band absorptions, where $Q_y(1,0) > Q_y(0,0) > Q_x(1,0) > Q_x(0,0)$.

For the porphyrin dendrimer **8**, $Q_y(1,0)$, $Q_y(0,0)$ and $Q_x(0,0)$ are clearly separated, whilst $Q_y(0,0)$ overlaps with $Q_x(1,0)$ and appears as a small shoulder.

For the Q-bands in **9**, $Q_y(1,0)$, $Q_y(0,0)$ and $Q_x(1,0)$ could be distinguished despite serious overlaps, and $Q_x(0,0)$ appears clearly.

The thienyl bridged dendrons in the *meso* positions mean that the porphyrin dendrimers present dendron absorptions in the anticipated region of 250–380 nm. The dendron absorption of **8** appears as a broad band whose λ_{max} is at 330 nm.

Dendrimer **9** features eight fluorenyl arms, and these give rise to dendron absorption that is stronger than that of **8** (at 330 nm). This dendron absorption in **9** is so intense that it is even stronger than the Soret band.

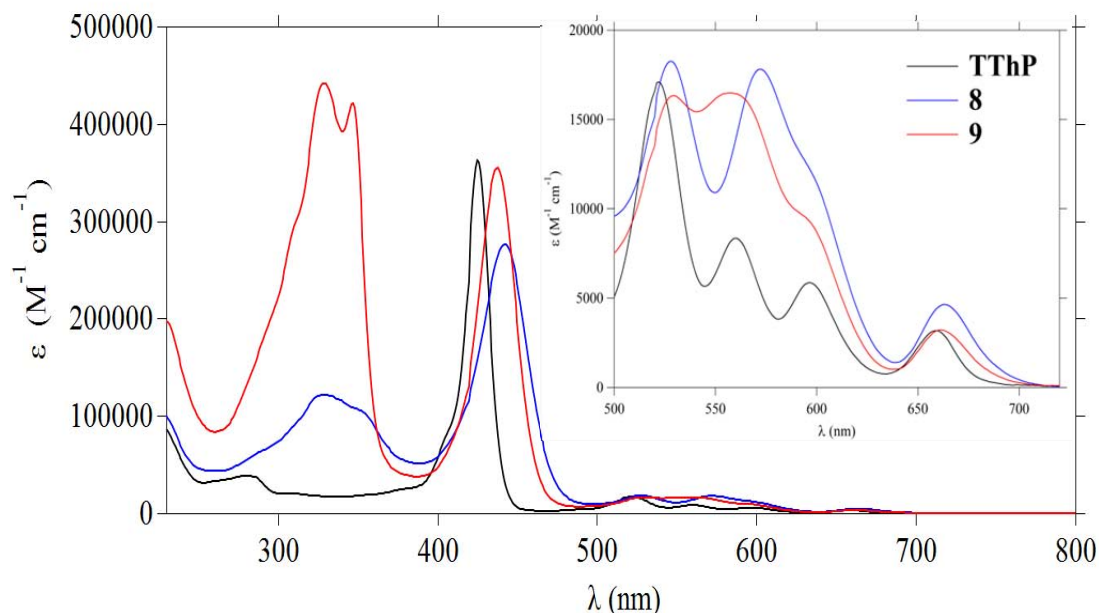


Figure 1.4.2 UV-visible absorption spectra of TThP, **8** and **9**

1.4.2 Emission spectra of porphyrins TThP, **8** and **9**

After being excited at Soret band, the normalized emission spectra of TThP, **8** and **9** were measured in dichloromethane (HPLC grade), and the spectra are shown in Figure 1.4.3. These porphyrins all exhibit red emission between 650-820 nm.

As shown in Figure 1.4.3, after excitation at Soret band (425 nm), TThP presents the typical emission bands: Q(0,0) and Q(0,1). These two bands are dependent on the relative orbital energy of the excited state of the porphyrins^[35-37].

For porphyrin **8**, one broad emission band is found that presents an obvious red shift relative to TThP. For **9**, we can see two large overlapping Q-bands which show small red shifts compared to TThP. The emission bands of porphyrin **9** are slightly blue shifted relative to those in **8**.

To study the **Energy Transfer (ET)** between dendrons and porphyrin core, **8** and **9** were excited at the wavelength corresponding to absorption within the dendrons

(320 nm). The resulting emission spectra are shown in Figure 1.4.4. The compound **8** displays exclusively red emission, which reveals a very efficient ET from former dendron **2** to porphyrin core. Dendrimer **9** also shows a strong red emission, but a quite weak and broad band at around 375 nm is now observed, which suggests that the ET from the dendrons to the porphyrin core is less efficient in **9** than in the more compact compound **8**. This suggests that moving towards higher generation dendrons is unlikely to improve performance. We can also notice that the quantum yields of TThP, **8** and **9** are very similar, 5%, 4% and 3% respectively.

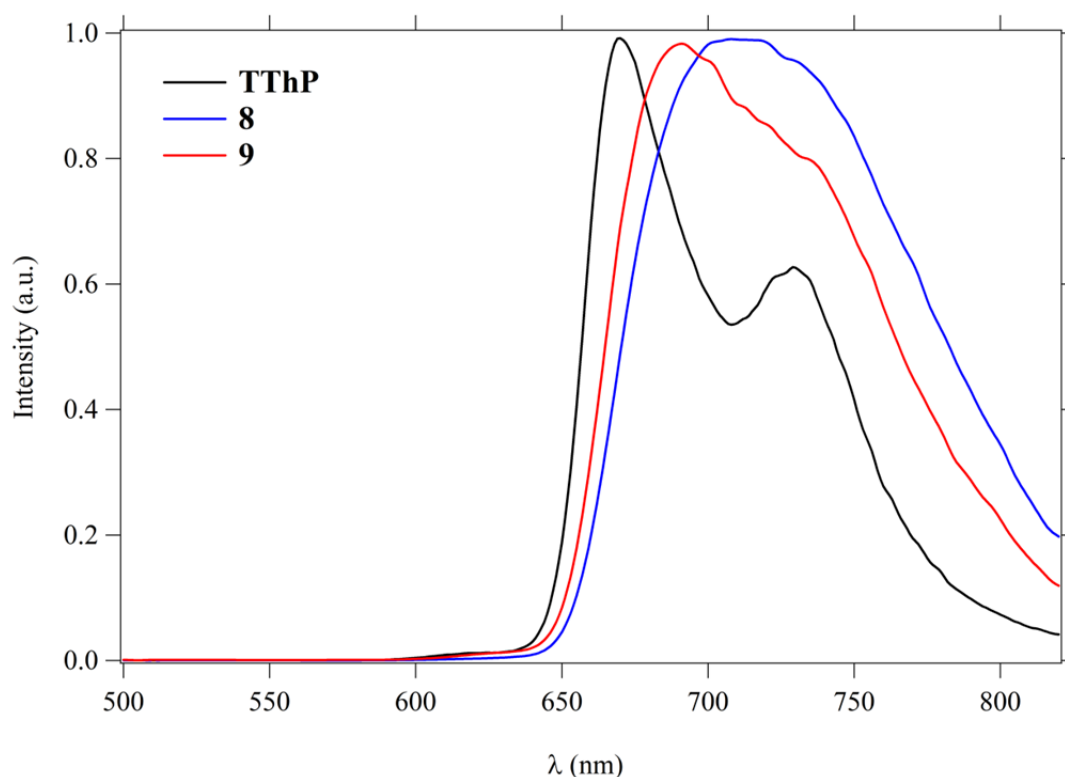


Figure 1.4.3 Emission spectra of TThP, **8** and **9** excited by λ_{abs} of Soret band in dichloromethane (HPLC), R.T.

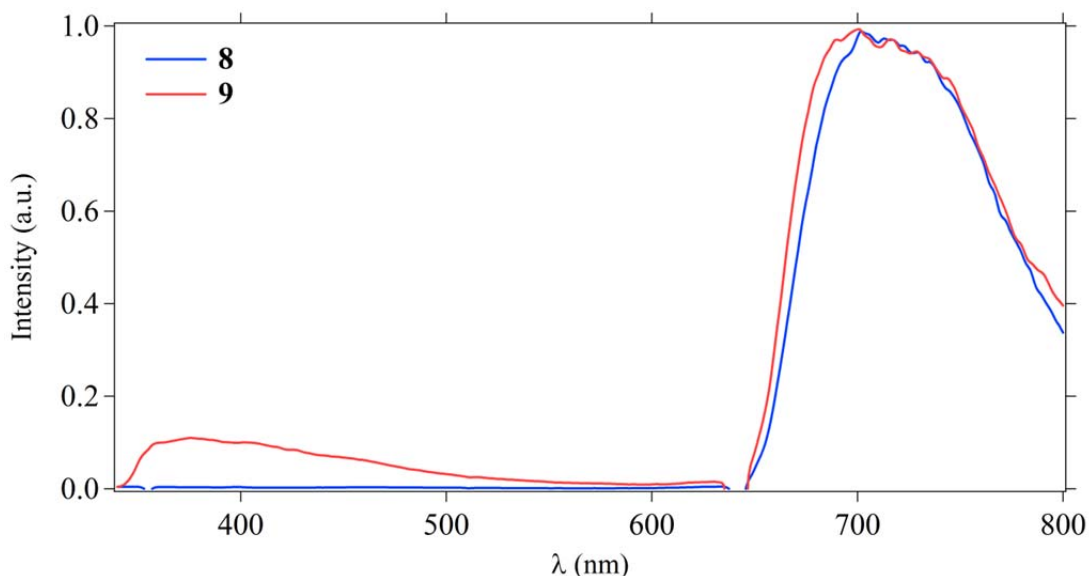


Figure 1.4.4 Emission spectra of **8** and **9** excited by λ_{abs} of dendron absorption in UV region in dichloromethane (HPLC), R.T.

1.5 Two-photon absorption

The two-photon absorption (TPA) cross-sections (σ_2) of **TThP**, **8** and **9** were determined by investigating their two-photon excited fluorescence (TPEF) in dichloromethane, using the experimental protocol described by Xu and Webb^[38]. A fully quadratic dependence of the fluorescence intensity on the excitation power was observed for each sample at all the wavelengths of the spectra shown in Figure 1.5.1, indicating that the cross-sections determined are only due to TPA.

Compared to σ_2 of **TThP** (12 GM at 790 nm), an obviously increased σ_2 was observed for both new thienyl porphyrin dendrimers: **8** and **9**. Comparison among these three porphyrins reveals that the combination with former conjugated dendrons (**2** and **5**) leads to a clear improvement of the TPA properties: as an impact factor, the cross-sections are strongly enlarged when these two dendrons were fixed in 5 position of the thienyl units.

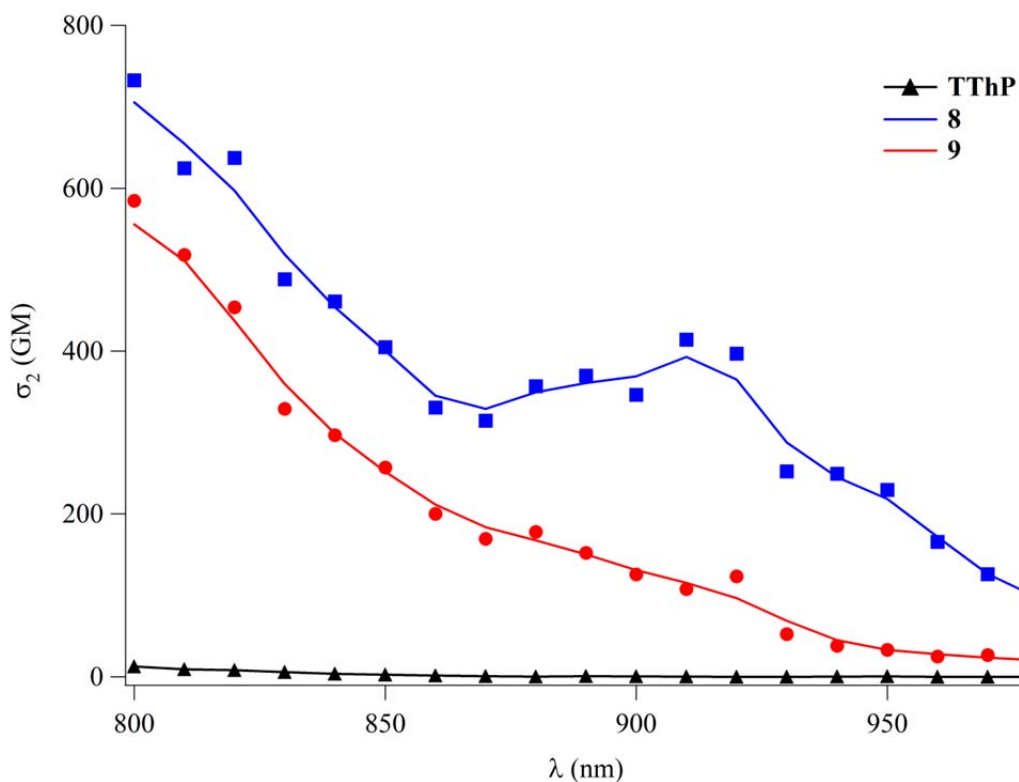
Finally, the combination of *meso*-thienyl porphyrin core and four fluorenyl alkynyl groups is much more efficient for TPA than that with dendron **5**, confirming that conjugation is rather restricted through the 1,3,5-trisubstituted benzene connectors. As a result, dendrimer **9** exhibits smaller two-photon absorptivity.

Table 1.5.1 Two-Photon Absorption and Brightness Properties for TPP, TThP and for the new porphyrin dendrimers 8 and 9

	$\lambda_{\text{TPA}}^{\text{max}}/\text{nm}$	$\sigma_2^{\text{max}}/\text{GM}^b$
TPP	790	12 ^a
TThP	790	12
8	790	730
9	790	580

^a Data from lit.[35];

^b Intrinsic TPA cross-sections measured in 10^{-4}M dichloromethane solutions by TPEF in the femtosecond regime;

**Figure 1.5.1 Two-photon absorption cross-section spectra of TThP, 8 and 9**

1.6 Conclusions

1. A group of new thienyl porphyrin dendrimers (**8** and **9**) were designed and successfully synthesized, as well as the reference **TThP** compound. The two new dendrimers both have conjugated dendrons with bridged phenyl-alkynyl and terminal fluorenyl arms.

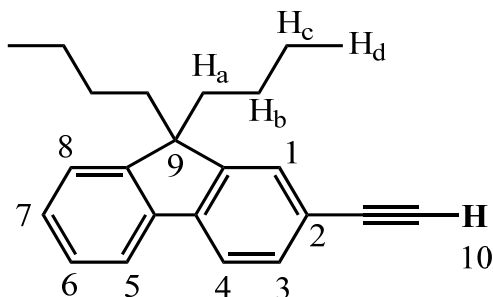
2. Alkynyl dendrons **2**, **5** and corresponding new dendrimers **8**, **9** were all well characterized and analysed by ^1H NMR spectra.

3. Linear optical properties of **8** and **9** were studied by UV-visible absorption and emission spectra:

- (i) Their dendron absorptions were observed in UV region and the UV absorption of dendrimer **9** is significantly improved compared to **8**;
- (ii) Their Soret band presents red shift compared to reference **TThP**, due to the stronger conjugation of dendrons **2** and **5**;
- (iii) They present red luminescence after being excited at Soret band, similar to this observed for the **TThP** reference;
- (iv) The energy transfer from dendrons to thienyl porphyrin core is efficient particularly for smaller dendrimer **8**.

4. The two-photon absorption cross-sections (σ_2) of **8** and **9** were measured by TPEF method, their σ_2 were strongly enlarged compared to reference tetra-thienyl porphyrin **TThP**.

Experimental Section

9, 9-dibutyl-2-ethynyl-fluorene (2)

In a two-neck bottle, a mixture of commercial 2-bromofluorene (10.0 g, 40.8 mmol, 1 equiv.), 1-bromobutane (13.2 mL, 122.4 mmol, 3 equiv.), Bu₄NBr (658 mg, 40.8 mmol, 5% equiv.) were stirred in a mixture of toluene (40 mL) / NaOH (24 mL, 50%aq.) and heated for 40 h at 85 °C. Then the mixture was extracted with water and ethyl acetate for three times. After evaporation of the volatiles, residue was further purified by silica chromatography using heptane. The **2-bromo-9, 9-dibutyl-fluorene** was isolated as colorless solid (12.4 g, 85% yield).

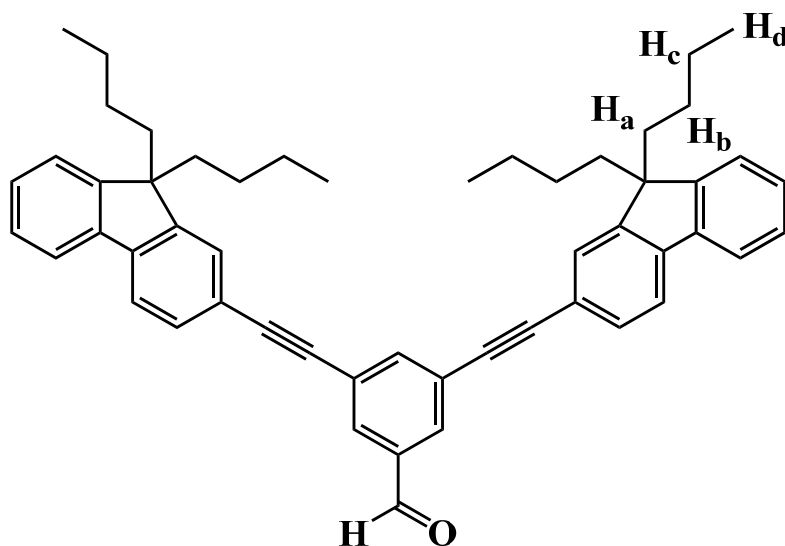
¹H NMR (400 MHz, CDCl₃, ppm): δ = 7.68-7.65 (m, 1H), 7.56 (d, 1H, *J* = 6.0Hz), 7.46-7.43 (m, 2H), 7.35-7.32 (m, 3H), 2.00-1.88 (m, 4H), 1.12-1.03 (m, 4H), 0.68 (t, 6H, *J* = 8.0 Hz), 0.64-0.50 (m, 4H).

(2) In a Schlenk tube, a mixture of **2-bromo-9,9-dibutyl-fluorene** (3.0 g, 8.4 mmol, 1 equiv), ethynyltrimethylsilane (1.44 mL, 10.1 mmol, 1.2 equiv), Pd (PPh₃)₂Cl₂ (35.0 mg, 0.05 mmol, 0.6% equiv) and CuI (4.8 mg, 0.025 mmol, 0.3% equiv) were dissolved in DMF (4.5 mL) and ^tPr₂NH (7.5 mL) was added under argon. The reaction medium was degassed by freeze-pump-thaw twice and heated for 48h at 95 °C. After evaporation of the volatiles, residue was further purified by silica chromatography using heptane as eluent; the yellow crude powder of **1** (3.0 g, 95% yield) was obtained.

¹H NMR (400 MHz, CDCl₃, ppm): δ = 7.69-7.66 (m, 1H), 7.62 (d, J = 8.0 Hz, 1H), 7.46 (d, J = 7.8 Hz, 1H), 7.43 (s, 1H), 7.33-7.31 (m, 3H), 1.95 (t, J = 8.6 Hz, 4H), 1.11-1.02 (m, 4H), 0.66 (t, J = 7.2 Hz, 6H), 0.62-0.48 (m, 4H), 0.29 (s, 9H).

(3) Crude product was dissolved in a mixture of CH₂Cl₂ (120 mL), THF (40 mL) and MeOH (40 mL), together with K₂CO₃ (3.3 g, 24.0 mmol, 3 equiv). Then this mixture was stirred overnight at room temperature. After evaporation of the volatiles, residue was purified by silica chromatography using heptane as eluent, **9,9-dibutyl-2-ethynyl-fluorene (2)** was isolated as white powder (2.3 g, 92% yield).

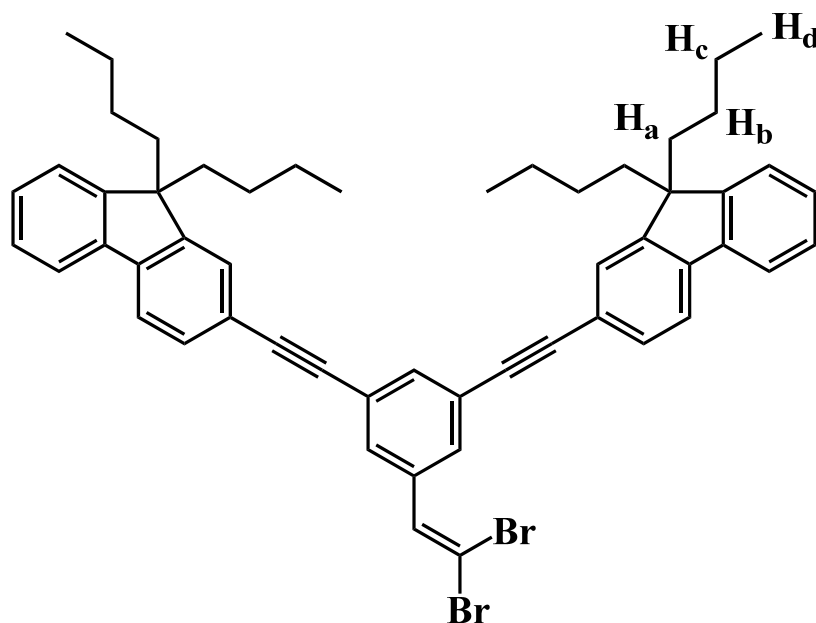
¹H NMR (400 MHz, CDCl₃, ppm): δ = 7.70-7.68 (m, 1H, H₅), 7.64 (d, J = 7.6 Hz, 1H, H₄), 7.49-7.47 (m, 2H, H_{1,8}), 7.36-7.33 (m, 3H, H_{3,6,7}), 3.14 (s, 1H, H₁₀), 1.96 (t, J = 8.4 Hz, 4H, H_a), 1.12-1.03 (m, 4H, H_c), 0.67 (t, J = 7.4 Hz, 6H, H_d), 0.63-0.49 (m, 4H, H_b).

3, 5-bis ((9, 9-dibutyl-fluoren-2-yl)ethynyl)benzaldehyde (3)

In a Schlenk tube, a mixture of commercial 3, 5-dibromobenzaldehyde (569 mg, 2.2 mmol, 1 equiv.), **9, 9-dibutyl-2-ethynyl-fluorene (2)** (1.63 g, 5.4 mmol, 2.5 equiv.), Pd (PPh₃)₂Cl₂ (18 mg, 0.1 mmol, 1.2% equiv.) and CuI (3.0 mg, 0.1 mmol, 0.6% equiv.) was stirred in DMF (5 mL) and ^tPr₂NH (5 mL) was added under argon. The reaction medium was degassed by freeze-pump-thaw twice and heated for 48 h at 95 °C. After evaporation of the volatiles, residue was purified by silica chromatography using heptane/CH₂Cl₂ (5:1) mixture as eluent. **3,5-bis ((9, 9-dibutyl-fluoren-2-yl)ethynyl)-benzaldehyde (3)** was isolated as a white powder (1.2 g, 80% yield).

¹H NMR (400 MHz, CDCl₃, ppm): δ = 10.04 (s, 1H, H_{CHO}), 8.01 (s, 3H, H_{fluorenyl}), 7.73-7.70 (m, 4H, H_{fluorenyl}), 7.54 (d, *J* = 7.6 Hz, 4H, H_{fluorenyl}), 7.38-7.32 (m, 6H, H_{fluorenyl}, H_{phenyl}), 2.00 (t, *J* = 8.2 Hz, 8H, H_a), 1.15-1.05 (m, 8H, H_c), 0.69 (t, *J* = 7.4 Hz, 12H, H_d), 0.66-0.55 (m, 8H, H_b).

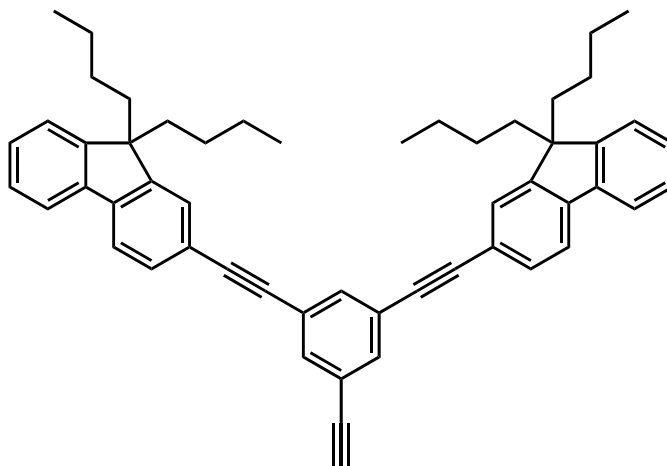
2,2'-(5-(2,2-dibromovinyl)-1,3-phenylene)bis(ethyne-2,1-diyl)bis(9,9-dibutyl-fluorene) (4)



In a Schlenk tube, a mixture of PPh_3 (2.5 g, 9.34 mmol, 2 equiv.) and Zn powder (0.61 g, 9.34 mmol, 2 equiv.) was stirred in dried CH_2Cl_2 (45 mL). The reaction medium was degassed by freeze-pump-thaw twice and cooled to 0°C . Secondly, CBr_4 was added into the Schlenk tube under argon. The mixture was kept stirring at low temperature for 2 min. Then removing the bath, the mixture was stirred overnight at room temperature. At last the mixture was cooled to 0°C again and **3, 5-bis ((9,9-dibutyl-fluorene-2-yl)ethynyl)benzaldehyde (3)** (3.3 g, 4.67 mmol, 1 equiv.) was dissolved in dried CH_2Cl_2 (20 mL) in another Schlenk tube under argon, following be transferred into the former Schlenk tube at 0°C and stirred the system in dark at room temperature for 4 h. After evaporation of the volatiles, residue was adsorbed on silica and purified by silica chromatography using a heptane/ CH_2Cl_2 (100: 5), **2, 2'-(5-(2, 2-dibromovinyl)-1,3-p-**

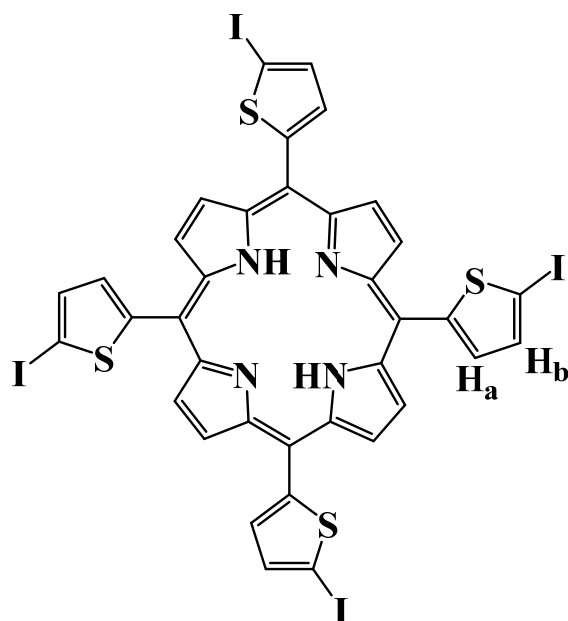
henylene)bis(ethyne-2,1-diyl)bis(9,9-dibutyl-fluorene) (4) was isolated as a white powder (3.7 g, 92% yield).

¹H NMR (400 MHz, CDCl₃, ppm): δ = 7.75 (s, 1H, H_{CHBr2}), 7.72-7.70 (m, 3H, H_{fluorenyl}), 7.69 (s, 1H, H_{fluorenyl}), 7.67 (s, 2H, H_{fluorenyl}), 7.54 (s, 1H, H_{fluorenyl}), 7.51 (s, 3H, H_{fluorenyl}), 7.47 (s, 1H, H_{fluorenyl}), 7.37-7.31 (m, 6H, H_{fluorenyl}, H_{phenyl}), 1.99 (t, J = 8.4 Hz, 8H, H_a), 1.14-1.05 (m, 8H, H_c), 0.69 (t, J = 7.2 Hz, 12H, H_d), 0.65-0.52 (m, 8H, H_b).

2, 2'-(5-ethynyl-1, 3-phenylene)bis(ethyne-2,1-diyl)bis(9,9-dibutyl-fluorene) (5)

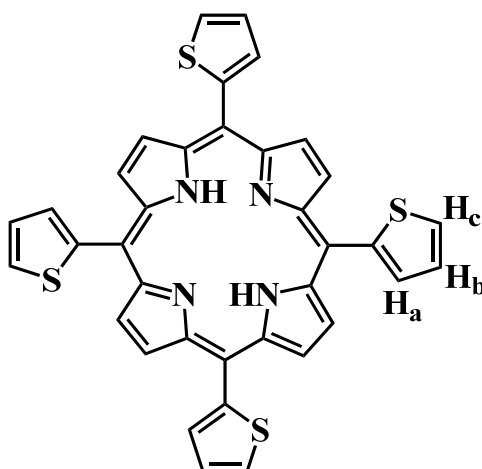
In a Schlenk tube, *n*-BuLi (3.2 mL, 5.2 mmol, 3 equiv.) was injected dropwise into a solution of ⁱPr₂NH (0.7 mL, 5.2 mmol, 3 equiv.) and dried THF (13 mL) at -78 °C. In the same time, **2,2'-(5-(2,2-dibromovinyl)-1,3-phenylene)bis(ethyne-2,1-diyl)bis(9,9-dibutyl-fluorene) (4)** (1.5 g, 1.7 mmol, 1 equiv.) was dissolved in dried THF (32 mL) in another Schlenk tube and cooled to -78 °C. Then the solution of **4** was transferred dropwise to the former Schlenk tube. The reaction was stirred after removing the bath until the temperature was up to room temperature. At last the reaction was quenched by saturated NH₄Cl (5 mL) and extracted with ethyl acetate and water. After evaporation of volatiles, residue was adsorbed in silica and purified by silica chromatography using a mixture of heptane/CH₂Cl₂ (20:1) as eluent, the desired compound **5** was isolated as a white powder (1.1 g, 86% yield).

¹H NMR (400 MHz, CDCl₃, ppm): δ = 7.78(s, 1H, H_{fluorenyl}), 7.74-7.67 (m, 6H, H_{fluorenyl}), 7.55-7.54 (m, 4H, H_{fluorenyl}, H_{phenyl}), 7.39-7.33 (m, 6H, H_{fluorenyl}, H_{phenyl}), 3.14 (s, 1H, H_{alkynyl}), 2.01 (t, *J* = 8.0 Hz, 8H, H_a), 1.16-1.07 (m, 8H, H_c), 0.71 (t, *J* = 7.2 Hz, 12H, H_d), 0.66-0.55 (m, 8H, H_b).

5-iodo-tetrathienylporphyrin (6)

In a two-neck bottle, a mixture of 5-iodo-2-thienylcarboxaldehyde (500 mg, 2.1 mmol, 1 equiv.), pyrrole (0.2 mL, 2.1 mmol, 1 equiv.) were dissolved in dried chloroform (125 mL) under argon. The reaction medium was degassed by argon bubbling for 30 min. Then $\text{BF}_3 \cdot \text{OEt}_2$ (0.1 mL) was injected into the system. The reaction was stirred in dark for 3 h under argon at room temperature. At last *p*-chloranil (388 mg, 1.58 mmol, 0.75 equiv.) was added and the reaction was heated at 60 °C for another 1 h without argon protection. The $\text{BF}_3 \cdot \text{OEt}_2$ was neutralized by NEt_3 (2 mL). After evaporation of volatiles, residue was adsorbed on silica and purified by silica chromatography using a CH_2Cl_2 /heptane (1:6) mixture as eluent, the desired porphyrin **6** was isolated as a dark violet powder (100 mg, 19% yield).

$^1\text{H NMR}$ (400 MHz, CDCl_3 , ppm): $\delta = 9.07$ (s, 8H, $\text{H}_{\beta\text{-pyrrolic}}$), 7.67 (d, 4H, $J^4 = 3.2$ Hz, H_a), 7.58 (d, 4H, $J = 3.6$ Hz, H_b), -2.74 (s, 2H, NH).

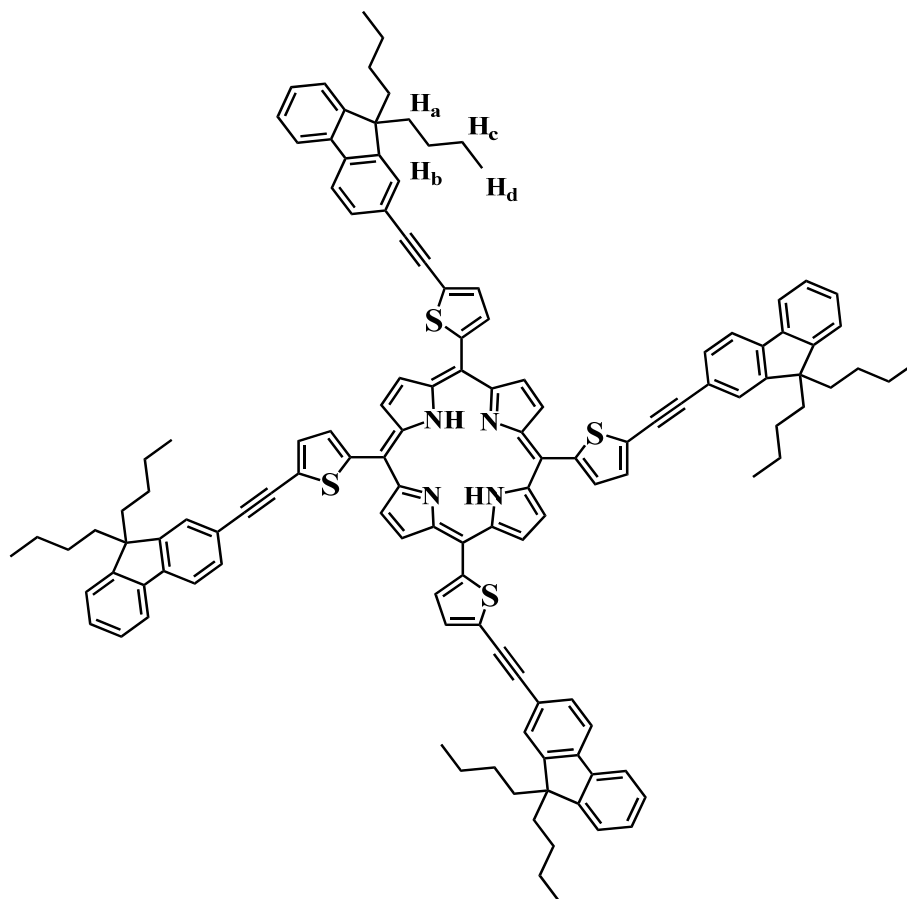
Meso-thienyl porphyrin (TThP, 7)

In a two-neck bottle, a mixture of 2-thienylcarboxaldehyde (1 mL, 1.1 mmol, 1 equiv), pyrrole (0.1 mL, 1.1 mmol, 1 equiv.) were dissolved in dried chloroform (100 mL) under argon. The reaction medium was degassed by argon bubbling for 30 min. Then $\text{BF}_3 \cdot \text{OEt}_2$ (0.1 mL, 0.25 mmol, 0.25 equiv.) was injected into the system. The reaction was stirred in dark for 2 h under argon at room temperature. At last *p*-chloranil (300 mg) was added and the reaction was heated at 60 °C for another 1 h without argon protection. The $\text{BF}_3 \cdot \text{OEt}_2$ was neutralized by NEt_3 (2 mL). After evaporation of volatiles, residue was adsorbed on silica and purified by silica chromatography using a CH_2Cl_2 /heptane (1:5) mixture as eluent, the desired porphyrin **TThP** (**7**) was isolated as a dark violet powder (55 mg, 32% yield).

$^1\text{H NMR}$ (400 MHz, CDCl_3 , ppm): $\delta = 9.04$ (s, 8H, $\text{H}_{\beta\text{-pyrrolic}}$), 7.92 (d, $J = 4.0$ Hz, 4H, H_a), 7.86 (d, $J = 6.4$ Hz, 4H, H_c), 7.52-7.51 (m, 4H, H_b), -2.64 (s, 2H, NH).

$^{13}\text{C NMR}$ (100 MHz, CDCl_3 , ppm): $\delta = 146.0, 142.6, 133.9, 127.9, 126.0, 112.4, 59.5, 54.0, 38.2, 31.2, 29.7, 14.1, 1.0$.

UV-vis [λ_{max} , CH_2Cl_2 , nm]: 425 (3.62), 522, 560, 597, 659.

Meso-(2-((9,9-dibutyl-fluoren-2-yl)ethynyl)-thienyl)porphyrin (8)

In Schlenk tube, a mixture of **5-iodo-tetrathienylporphyrin (6)** (117 mg, 0.1 mmol, 1 equiv.), **9,9-dibutyl-2-ethynyl-fluorene (2)** (139 mg, 0.5 mmol, 4.5 equiv.), Pd(PPh₃)₂Cl₂ (1.9 mg, 0.45 mmol, 0.6% equiv.) and CuI (1 mg, 0.5 mmol, 0.3% equiv.) were stirred in DMF (4 mL) and ^tPr₂NH (4 mL) was added under argon. The system was degassed by freeze-pump-thaw twice and heated for 48 h at 95 °C. After evaporation of volatiles, the residue was purified by silica chromatography (heptane /CH₂Cl₂ = 5:1), providing dark violet powder (72 mg, 37% yield).

¹H NMR (400 MHz, CDCl₃, ppm) : δ = 9.17 (s, 8H, H_{β-pyrrolic}), 7.85 (d, 4H, *J* = 3.6 Hz, H_{thienyl}), 7.76-7.74 (m, 12H, H_{fluorenyl}), 7.65 (d, 8H, *J* = 7.6 Hz, H_{thienyl}, H_{fluorenyl}),

7.40-7.33 (m, 12H, H_{fluorenyl}), 2.09-1.98 (m, 16H, H_a), 1.17-1.08 (m, 16H, H_c), 0.72 (t, 24H, *J* = 7.2 Hz, H_d), 0.68-0.54 (m, 16H, H_b), -2.58 (s, 2H, NH).

¹³C NMR (100 MHz, CDCl₃, ppm) : δ = 151.1, 150.9, 144.0, 141.9, 140.4, 134.1, 131.1, 130.6, 127.6, 126.9, 126.5, 126.0, 122.9, 120.9, 120.1, 119.8, 111.9, 95.7, 82.5, 55.2, 40.2, 31.2, 29.7, 25.9, 23.1, 14.1, 13.8, 1.0.

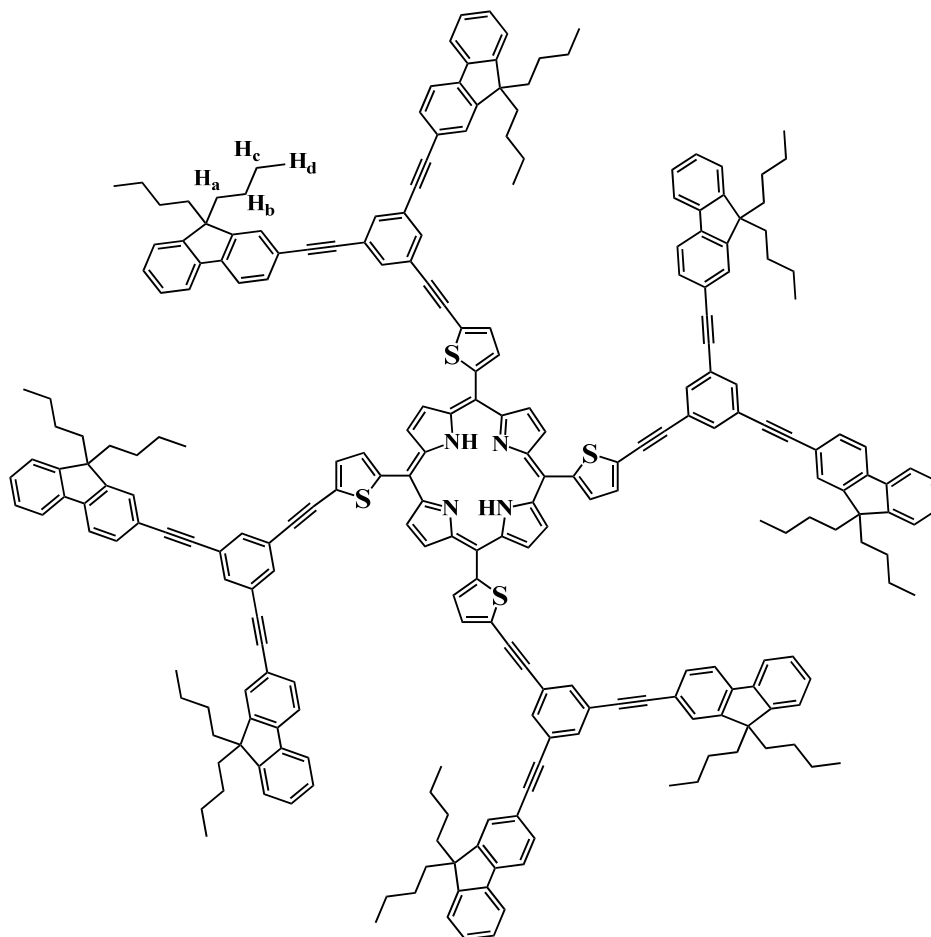
UV-vis [λ_{\max} , CH₂Cl₂, nm]: 442 (2.76), 529, 570, 595, 662.

HRMS-ESI for C₁₂₈H₁₁₈N₄S₄: *m/z* = 1839.8266 [M+H]⁺ (calcd: 1839.8312);

m/z = 920.4184 [M+2H]²⁺ (calcd: 920.4192).

Anal. Calcd (%) for C₁₂₈H₁₁₈N₄S₄·2THF: C 82.30; H 6.81; N 2.82; S 6.46.

Found: C 82.46; H 7.00; N 2.34; S 5.78.

Meso-(2-((3,5-bis((9,9-dibutyl-fluorene-2-yl)ethynyl)phenyl)ethynyl)thienyl)porphyrin (9)

In Schlenk tube, a mixture of **5-iodo-tetrathienylporphyrin (6)** (36 mg, 0.1 mmol, 1equiv.), **2, 2'-(5-ethynyl-1,3-phenylene)bis(ethyne-2,1-diy)bis(9,9-dibutyl-fluorene) (5)** (100 mg, 0.1 mmol, 4.5 equiv.), Pd(PPh₃)₂Cl₂ (1 mg, 0.1 mmol, 0.6% equiv.) and CuI (0.1 mg, 0.1 mmol, 0.3% equiv.) were added DMF (3 mL) and ^tPr₂NH (3 mL) under argon. The system was degassed by freeze-pump-thaw twice and heated for 48 h at 95 °C. After evaporation of volatiles, the residue was purified by silica chromatography (heptane /THF = 8:1), providing dark violet powder (41 mg, 40% yield).

¹H NMR (400 MHz, CDCl₃, ppm): δ = 9.18 (s, 8H, H_{β-pyrrolic}), 7.87 (d, 4H, *J* = 3.2 Hz, H_{thienyl}), 7.82 (d, 8H, *J* = 7.6 Hz, H_{thienyl}), 7.76 (d, 4H, *J* = 3.2 Hz, H_{thienyl}), 7.71 (d, 17H, *J* = 7.2 Hz, H_{fluorenyl}), 7.56-7.53 (m, 17H, H_{fluorenyl}), 7.35-7.34 (m, 26H, H_{fluorenyl}), 2.00 (t, 32H, H_a), 1.14-1.06 (m, 32H, H_c), 0.69 (t, 48H, *J* = 7.2 Hz, H_d), 0.65-0.54 (m, 32H, H_b), -2.59 (s, 2H, NH).

¹³C NMR (100 MHz, CDCl₃, ppm): δ = 226.0, 210.3, 202.5, 179.0, 163.3, 155.4, 147.6, 139.7, 116.2, 100.5, 92.7, 53.5, 45.6, 30.0, 14.3.

UV-vis [λ_{\max} , CH₂Cl₂, nm]: 438, 530, 560, 594, 660.

MS (Maldi-TOF) for C₂₅₂H₂₃₀N₄S₄: *m/z* = 3440.852 [M+H]⁺ (calcd: 3440.7076).

Anal.Calcd (%) for C₂₅₂H₂₃₀N₄S₄: C 87.91; H 6.73; N 1.63; S 6.46. **Found:** C 87.77; H 6.73; N 1.63; S 3.73.

References

- [1] S. R. Marder, *Chem. Commun.*, **2006**, 131.
- [2] K. J. Thorley, J. M. Hales, H. L. Anderson, J. W. Perry, *Angew. Chem. Int. Ed.*, **2008**, *47*, 7095.
- [3] S. Tao, T. Miyagoe, A. Maeda, H. Matsuzaki, H. Ohtsu, M. Hasegawa, S. Takaishi, M. Yamashita, H. Okamoto, *Adv. Mater.*, **2007**, *19*, 2707.
- [4] G. J. Zhou, W. Y. Wong, C. Ye, Z. Y. Lin, *Adv. Funct. Mater.* **2007**, *17*, 963.
- [5] Z. Q. Liu, Q. Fang, D. X. Cao, D. Wang, G. B. Xu, *Org. Lett.*, **2004**, *6*, 2933.
- [6] W. J. Yang, D. Y. Kim, C. H. Kim, M. Y. Jeong, S. K. Lee, S. J. Jeon, B. R. Cho, *Org. Lett.*, **2004**, *6*, 1389.
- [7] C. W. Spangler, *J. Mater. Chem.*, **1999**, *9*, 2013.
- [8] X. M. Wang, D. Wang, G. Y. Zhou, W. T. Yu, Y. F. Zhou, Q. Fang, M. H. Jiang, *J. Mater. Chem.*, **2001**, *11*, 1600.
- [9] C. W. Spangler, E. H. Elandaloussi, B. Ozer, K. Ashworth, L. Madrigal, B. Reeves, *Mater. Res. Soc. Symp. Proc.*, **2000**, *597*, 369.
- [10] (a) M. Albota, D. Beljonne, J. L. Brédas, J. E. Ehrlich, J. Y. Fu, A. A. Heikal, S. E. Hess, T. Kogej, M. D. Levin, S. R. Marder, D. McCord-Maughon, J. W. Perry, H. Röckel, M. Rumi, G. Subramaniam, W. W. Webb, X. L. Wu, C. Xu, *Science*, **1998**, *281*, 1653; (b) M. Rumi, J. E. Ehrlich, A. A. Heikal, J. W. Perry, S. Barlow, Z. Hu, D. McCord-Maughon, T. C. Parker, H. Röckel, S. Thayumanavan, S. R. Marder, D. Beljonne, J. L. Brédas, *J. Am. Chem. Soc.*, **2000**, *122*, 9500; (c) S. J. K. Pond, M. Rumi, M. D. Levin, T. C. Parker, D. Beljonne, M. W. Day, J. L. Brédas, S. R. Marder, J. W. Perry, *J. Phys. Chem. A*, **2002**, *106*, 11470.
- [11] M. Viktor, *Ber. Dtsch. Chem. Ges.*, **1883**, *16*, 1465.
- [12] A. Treibs, N. Haeberle, J. Liebigs, *Ann. Chem.*, **1968**, *718*, 183.
- [13] M. A. Torrén, T. K. Straub, L. M. Epstein, *J. Am. Chem. Soc.*, **1972**, *94*, 4160.
- [14] P. Bhyrappa, P. Bhavana, *Chem. Phys. Lett.*, **2001**, *349*, 399.
- [15] N. Ono, H. Miyagawa, T. Ueta, T. Ogawa, H. Tani, *J. Chem. Soc., Perkin Trans.*, **1998**, *1*, 1595.
- [16] H. S. Nalwa, *Adv. Mater.*, **1993**, *5*, 341.

- [17] J. G. Breitzer, D. D. Dlott, L. K. Iwaki, S. M. Kirkpatrick, T. B. Rauchfuss, *J. Phys. Chem. A.*, **1999**, *103*, 6930.
- [18] A. Mishira, C. Q. Ma, P. Bäuerle, *Chem. Rev.*, **2009**, *109*, 1141.
- [19] Z. H. Chen, X. Y. Zhou, Z. Y. Li, L. H. Niu, J. X. Yi, F. S. Zhang, *J. Photochemistry and Photobiology A: Chem.*, **2011**, *64*, 218.
- [20] C. Brückner, P. C. D. Foss, J. O. Sullivan, R. Pelto, M. Zeller, R. R. Birge, G. Crundwell, *Phys. Chem.*, **2006**, *8*, 2402.
- [21] N. M. Boylea, J. Rochfordb, M. T. Prycea, *Coord. Chem. Rev.*, **2010**, *254*, 77.
- [22] J. Rochford, S. Botchway, J. J. McGarvey, A. D. Rooney, M. T. Pryce, *J. Phys. Chem.*, **2008**, *112*, 11611.
- [23] C. O. Paul-Roth, J. Letessier, S. Juillard, G. Simonneaux, T. Roisnel, J. Rault-Berthelot, *J. Mol. Struct.*, **2008**, *872*, 105.
- [24] E. Zojer, D. Beljonne, P. Pacher, J. L. Brédas, *Chem. Eur. J.*, **2004**, *10*, 2668.
- [25] S. Kato, T. Matsumoto, T. Ishi, T. Thiemann, M. Shigeiwa, H. Gorohmaru, S. Maeda, Y. Yamashita, S. Mataka, *Chem. Commun.*, **2004**, 2342.
- [26] A. Abboto, L. Beverina, R. Bozio, A. Facchetti, C. Ferrante, G. A. Pagani, D. Pedron, R. Signorini, *Chem. Commun.*, **2003**, 2144.
- [27] M. Calvete, G. Y. Yang, M. Hanack, *Synth. Met.*, **2004**, *141*, 231.
- [28] M. Ravikanth, K. G. Ravindra, *Curr. Sci.*, **1995**, *68*, 1010.
- [29] M. Pawlicki, H. A. Collins, R. G. Denning, H. L. Anderson, *Angew. Chem., Int. Ed.*, **2009**, *48*, 3244.
- [30] S. V. Rao, N. K. M. N. Srinivas, D. N. Rao, L. Giribabu, B. G. Mayia, R. Philip, G. R. Kumar, *Opt. Commun.*, **2000**, *182*, 255.
- [31] A. Merhi, G. Grelaud, K. A. Green, N. H. Minh, M. Reynolds, I. Ledoux, A. Barlow, G. Wang, M. P. Cifuentes, M. G. Humphrey, F. Paul, C. O. Paul-Roth, *Dalton Trans.*, **2015**, *44*, 7748.
- [32] J. S. Lindsey, K. A. Maccrum, J. S. Tyhonas, Y. Y. Chuang, *J. Org. Chem.*, **1994**, *59*, 579.
- [33] F. R. Li, K. X. Yang, J. S. Tyhonas, K. A. Maccrum, J. S. Lindsey, *Tetrahedron*, **1997**, *53*, 12339.
- [34] K. Sonogashira, Y. Tohda, N. Hagihara, *Tetrahedron Lett.*, **1975**, *50*, 4467.

- [35] M. J. Frampton, R. Beavington, J. M. Lupton, I. D. W. Samuel, P. L. Burn, *Synth. Met.*, **2001**, *121*, 1671.
- [36] M. J. Frampton, S. W. Magennis, J. N. G. Pillow, P. L. Burn, I. D. W. Samuel, J. *Mater. Chem.*, **2003**, *13*, 235.
- [37] J. N. G. Pillow, M. Halim, J. M. Lupton, P. L. Burn, I. D. W. Samuel, *Macromolecules*, **1999**, *32*, 5985.
- [38] C. Xu, W. W. Webb, *J. Opt. Soc. Am. B*, **1996**, *13*, 481.

Chapter 2

Syntheses and Characterization Of Ruthenium TFP Cored Porphyrin Complexes

2.1 The targets of the projects

2.1.1 Background

In the literature, we can find two types of porphyrin metal complexes: **coordination type** which have the metal in the center of the macrocyclic cavity and another **organometallic type** with external metals that decorate the porphyrin core (Figure 2.1.1).

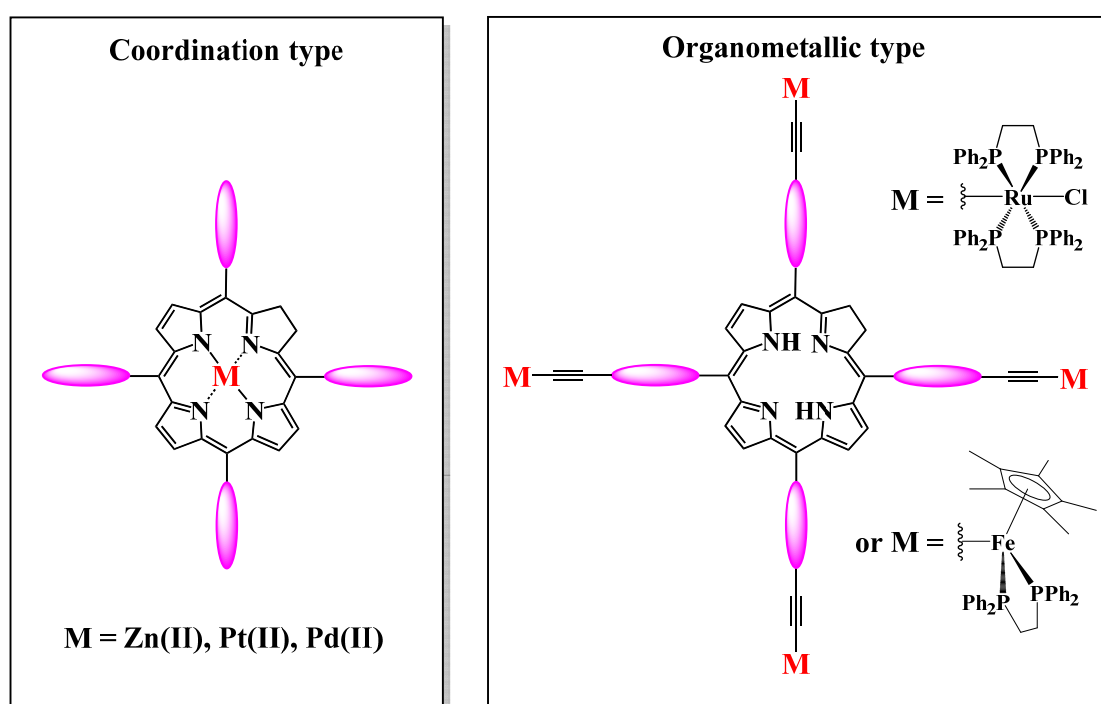


Figure 2.1.1 Porphyrin metal complexes: coordination type and organometallic type

We will rapidly describe selected examples of **coordination type** here. In 1998, the **Octa-alkylporphyrin** (Figure 2.1.2) was reported as the first red-emitting platinum complex used in OLEDs (organic light-emitting diodes) ^[1]. For this type of compound, the advantages, such as their narrow bands of emission and high red color purity, partly compensated the disadvantages of long lifetime (τ), and continued to attract interest.

Recently, we prepared the zinc and platinum complexes of **tetra-aryl porphyrins**

(**TPP** and **TFP** as shown in Figure 2.1.3) with the latter being specially designed as red emitters for OLEDs. Their photophysical data are listed in Table 2.1.1, and as expected, these porphyrins all exhibit red emission. When compared with the **PtTPP**, the Soret band of **PtTFP** presents a slight red shift in the UV-visible absorption spectrum and an even smaller red shift of the Q bands. These coordination compounds are efficient red emitters in OLEDs ^[2].

COORDINATION TYPE EXAMPLES: METALLIC PORPHYRINS

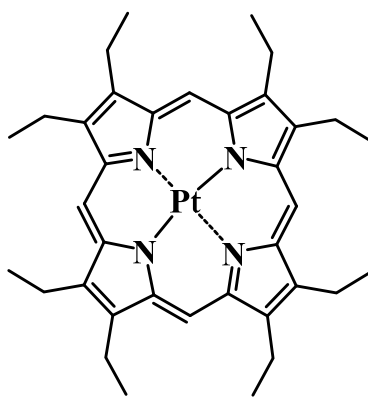


Figure 2.1.2 The first platinum Octa-alkylporphyrin

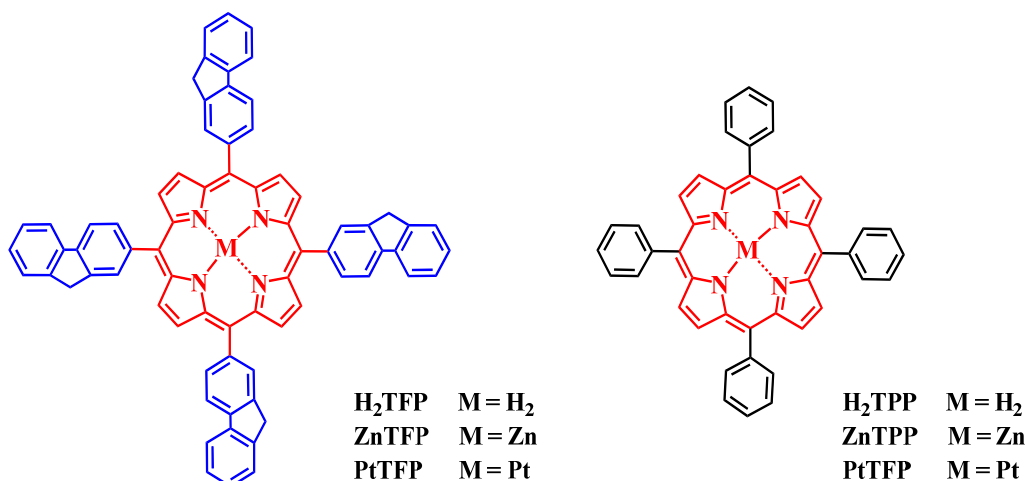


Figure 2.1.3 Two series of metallated TFP and TPP derivatives

Table 2.1.1 Absorption and emission data of the TPP and TFP complexes at 298 K

	λ_{abs}^a /nm	λ_{em}^a	τ	$\Phi^b \times 10^2$
	Soret ; Q bands	/nm	/ μs	/%
ZnTFP	428 ; 555, 601	608, 657	-	8.5
ZnTPP	421 ; 556, 603	603, 650	0.15 ^c	3.3
PtTFP	400 ; 508, 538	668, 734	22	2.0
PtTPP	409 ; 512, 540	679, 741	59	4.6

^a The wavelength of the Soret band is given first, followed by the wavelengths of the two observed Q bands (Extinction coefficients, including those in the high-energy region, are given in the Experimental Section).

^b Quantum yields were measured using free tetra-phenyl porphyrin in toluene as the standard.

^c From [3]

On another hand, **organometallic** porphyrins, which are large metallated π -compounds with external metals, are considered to be efficient 3rd order NLO-phores [4-6]. In this chapter, we will develop this type of porphyrin metal complexes.

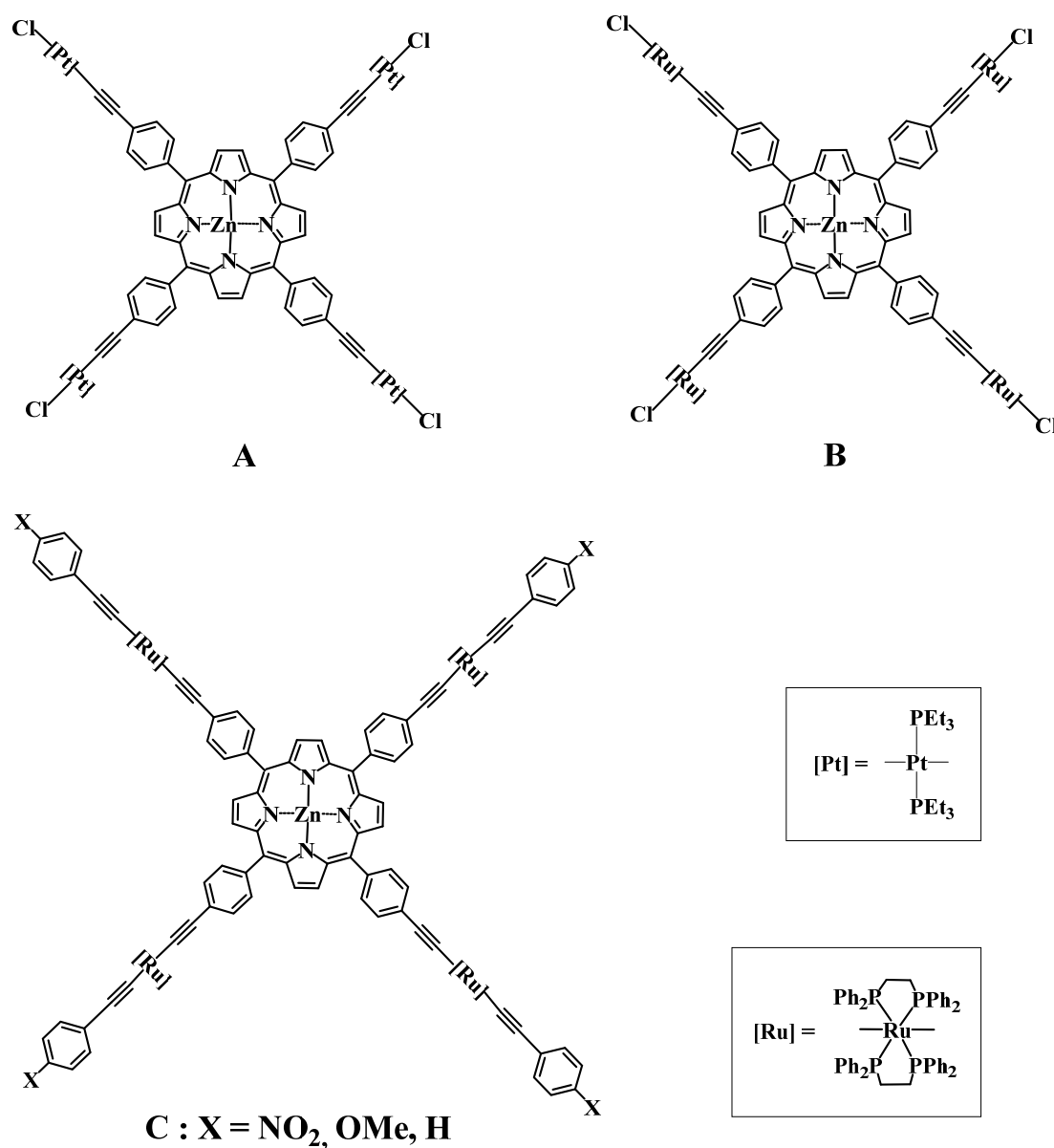
Earlier, our group (Christine PAUL-ROTH and coll.) reported the syntheses and photophysical properties of some pure organic tetrafluorenyl porphyrin derivatives (**TFP**) and demonstrated a very significant effect of the *meso*-substituents on the photophysical properties of porphyrins [6-9,17-20]. To the best of our knowledge, few metal complexes substituted porphyrins that contain peripheral alkynyl groups have been published to date [10,11], even fewer of which have been used to assemble metals around a TPP-core, such as compound **A** (Figure 2.1.4).

Their 3rd order NLO properties have also been rarely studied. With this background, in 2012, our group reported the synthesis and characterization of three new extended **ZnTPP** derivatives **C** derived from the *tetra*-chloro precursor **B**, their 3rd order nonlinear absorption properties were measured by Z-scan. The data obtained which are listed in Table 2.1.2, revealed that organometallic porphyrins **C** behave as strong two-photon absorbers at ca. 700 and 1100 nm. Also their effective TPA cross-sections are significantly larger than those reported for related monomeric **ZnTPP** derivatives [12-14]. The TPA with single zinc porphyrins was rarely studied except by Anderson and colleagues. We also notice that the potentials of these redox-active compounds are with respect to electro-switching their optical properties.

Table 2.1.2 Comparison of extremal values of the effective $\sigma_{2\text{eff}}$ between 700-1300 nm for the substituted C complexes

Compound	$\sigma_{2\text{eff}}$	λ	$\sigma_{2\text{eff}}$	λ
	(1 st max.) [GM]	(1 st max.) [nm]	(2 nd max.) [GM]	(2 nd max.) [nm]
X = NO ₂ ^a	6000 ± 3000	770	1500 ± 500	1000
C X = H	4800 ± 500	710	1400 ± 500	1300
X = OMe ^a	4200 ± 500	710	1300 ± 100	1000

^a An additional maximum is apparent at $\lambda < 530$ nm with $\sigma_{2\text{eff}} = 6400$ GM.

**Figure 2.1.4 Selected ZnTPP-based porphyrins substituted by terminal alkynyl complexes**

Our group has previously published the syntheses and Z-scan measurements of compounds **E1** and **E2**, which were investigated to understand the 3rd order NLO properties of the peripheral metallated **ZnTPP**, taking simple iron complex **D** as reference (Figure 2.1.5). Compounds **E1** and **E2** possess a first crown of ruthenium *bis*-acetylides, each of which has a terminal iron group. Their two-photon absorption cross-sections ($\sigma_{2\text{eff}}$) were measured by Z-scan. Table 2.1.3 lists the $\sigma_{2\text{eff}}$ of reference **D** and organometallic porphyrins **E1** and **E2** [15,16]. It can clearly be seen that a significant σ_2 increase is observed for these complexes.

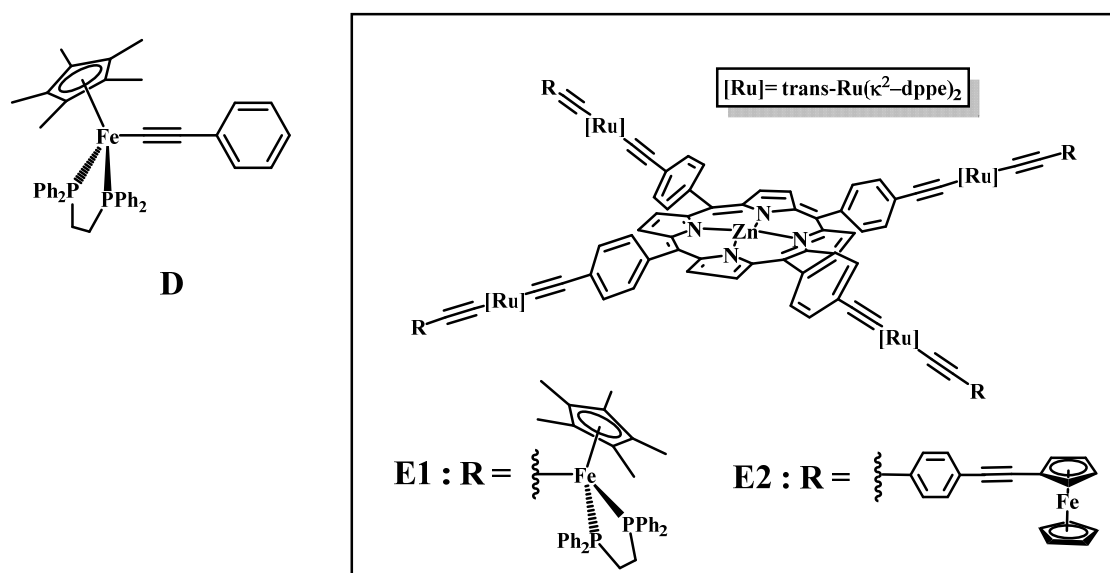


Figure 2.1.5 Structures of compounds **D**, **E1** and **E2**

Table 2.1.3 The comparative two-photon absorption cross-sections ($\sigma_{2\text{eff}}$) of **D**, **E1** and **E2**

	σ_2 (1 st max.) [GM]	λ (1 st max.) [nm]	σ_2 (2 nd max.) [GM]	λ (2 nd max.) [nm]
D	6 ± 3	695	-	-
E1	18400 ± 8200	560	2240 ± 650	630
E2	8900 ± 1500	550	8000 ± 500	740

2.1.2 Target porphyrins

In 2004, our group synthesized a purely organic *tetra*-fluorenylporphyrin (**TFP**) that possesses four fluorenyl arms. **TFP** exhibits a high quantum yield (Φ_{fl}) of 24%^[17]. The corresponding Zn porphyrin complex, **ZnTFP** was also prepared (Figure 2.1.2), and it was found that the fluorescence of free base **H₂TFP** and **ZnTFP** are much more intense than the corresponding analogues where fluorenyl is replaced by phenyl (e.g. **H₂TTP** and **ZnTTP**, Figure 2.1.3)^[18-20]. These fluorenyl cored porphyrins can be used as efficient red luminophores.

In 2013, Akita synthesized a mono-ruthenium acetylide functionalized porphyrin complex (shown in Figure 2.1.6), whose fluorescence could be redox-switched upon cycling the ruthenium between its Ru(II) and Ru(III) oxidation levels. The presence of only two phenyl groups means that quantum yield of this organometallic porphyrin is inherently low: $\Phi_{off} = 0.18\%$, but it could be raised to 1.4% (Φ_{on}) when the fluorescence of the molecule was switched on by oxidation^[21].

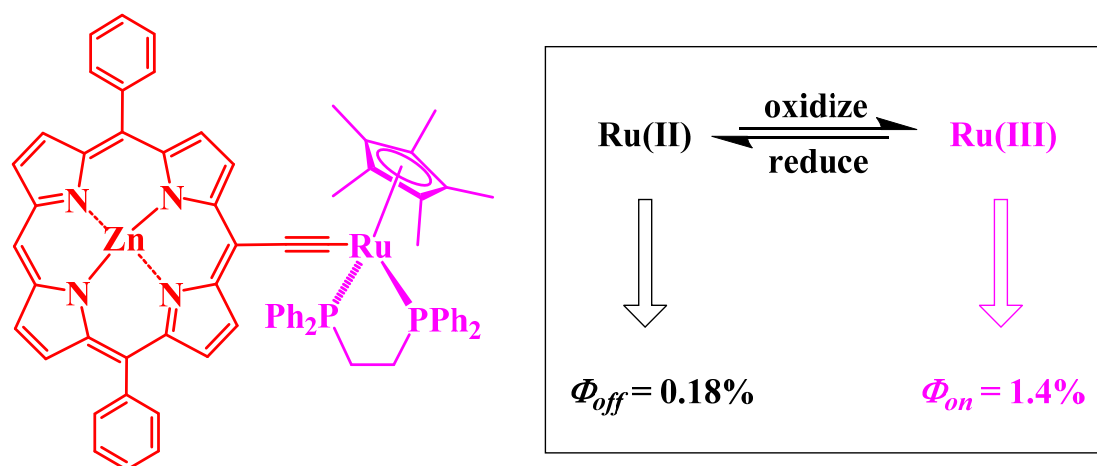


Figure 2.1.6 Zinc porphyrin cored mono-ruthenium compound

In 2015, two new mono-ruthenium acetylide porphyrins **H** and **I**, both one phenyl and three fluorenyl arms, were synthesized in our laboratory; Porphyrin **I** also has a zinc ion center (Figure 2.1.7). We were interested in their redox-active properties. Generally cyclic voltammetry (CV) of porphyrins shows two oxidation and two reduction waves corresponding to oxidation and reduction at the porphyrin core. These four waves, which are presented in the CV shown in Figure 2.1.8 for **F** and **G**, are reversible. For the organometallic porphyrins **H** and **I**, we observe only two waves for the porphyrin core, but an extra wave corresponding to the Ru(II) to Ru(III) redox couple is also clearly visible. So, in these new organometallic porphyrins **H** and **I**, the potential that defines ruthenium redox-activity part is well delineated for switching [22].

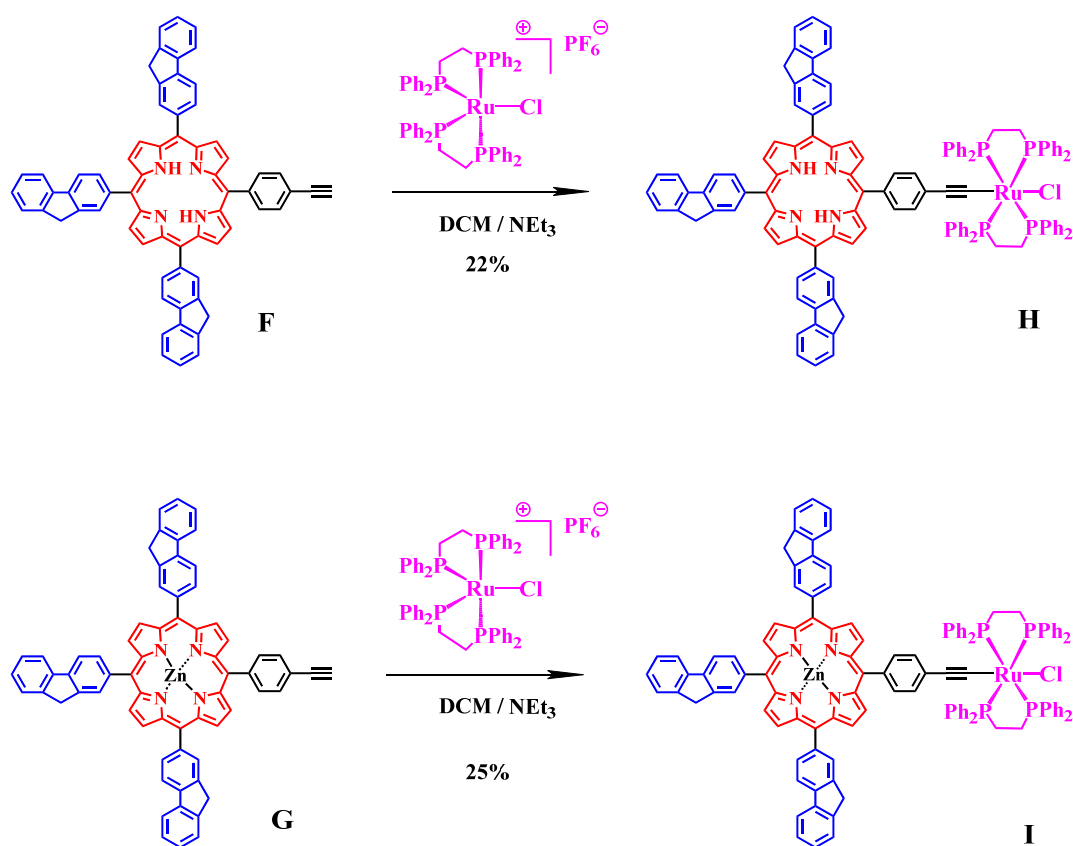


Figure 2.1.7 Organometallic porphyrin **H** and corresponding Zn derivative **I** and their parents porphyrins **F** and **G**

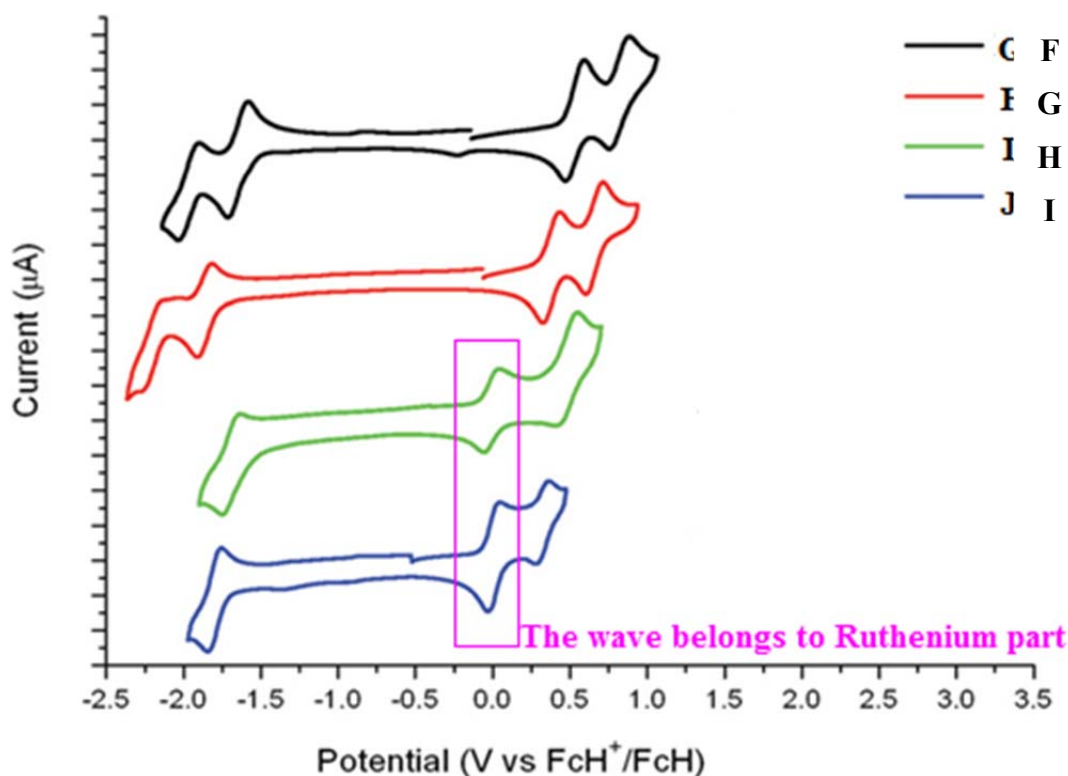


Figure 2.1.8 Redox-active properties of the [Ru] porphyrins H and I Compared to parent porphyrins F and G

The work here represents an attempt to develop new organometallic porphyrin that combines the efficient **TFP** luminophore with the redox-active ruthenium switch. This new family of organometallic compounds advantageously retains the benefits of luminescence that arise from the four fluorenyl arms.

Our aim was to obtain and characterize the mono, bis, tri and tetra-ruthenium complexes derived from the free TFP core porphyrin. Their detailed structures are shown in Figure 2.1.9. These four organometallic porphyrins feature the high luminescence core **TFP-Bu**, which contains *n*-butyl chains for enhancing solubility. A classical ruthenium(II) complex salt is used to assemble the corresponding organometallic compounds. The four Ru porphyrin products feature one to four redox-active ruthenium centers respectively. Their syntheses, characterization and optical properties will be described in this chapter.

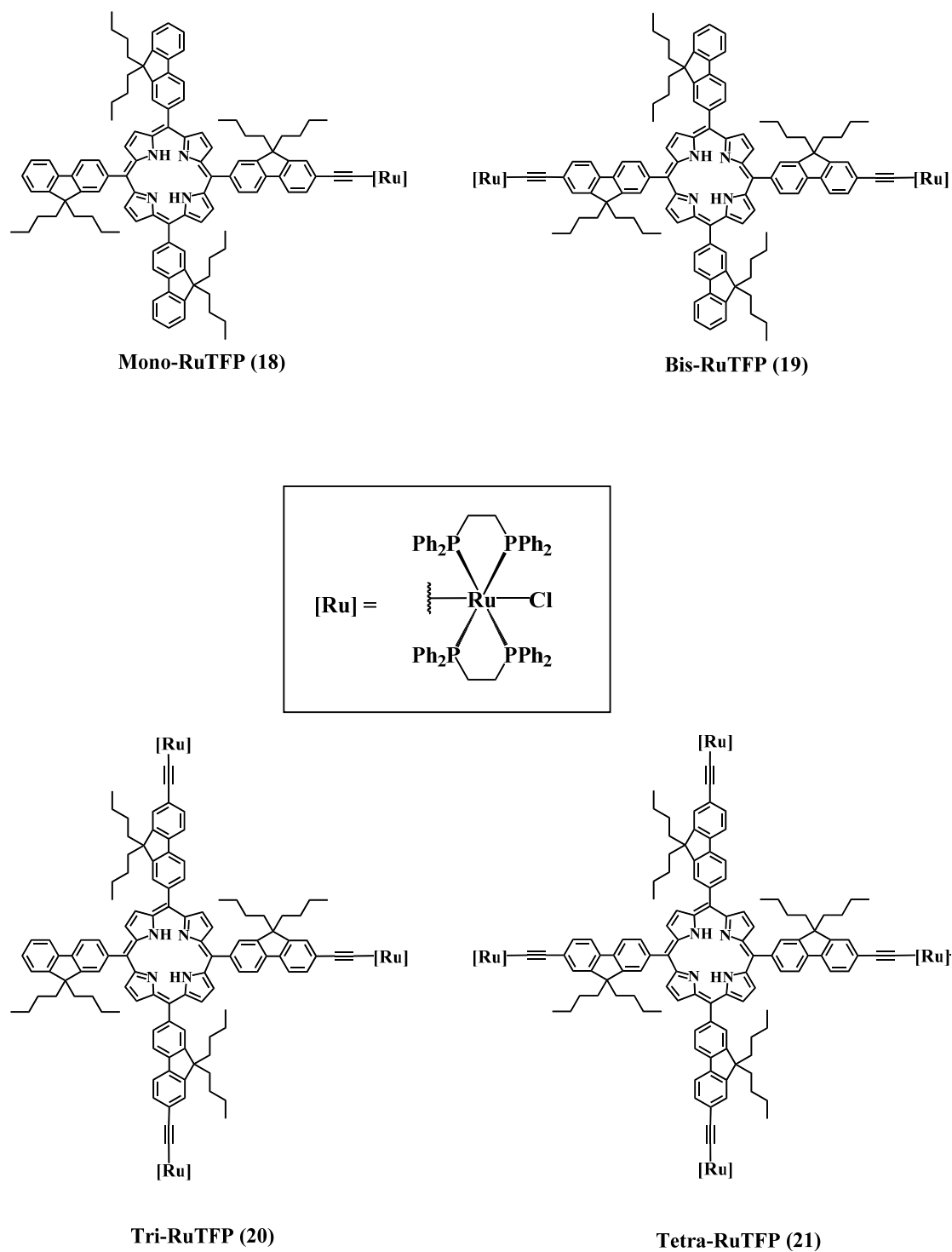
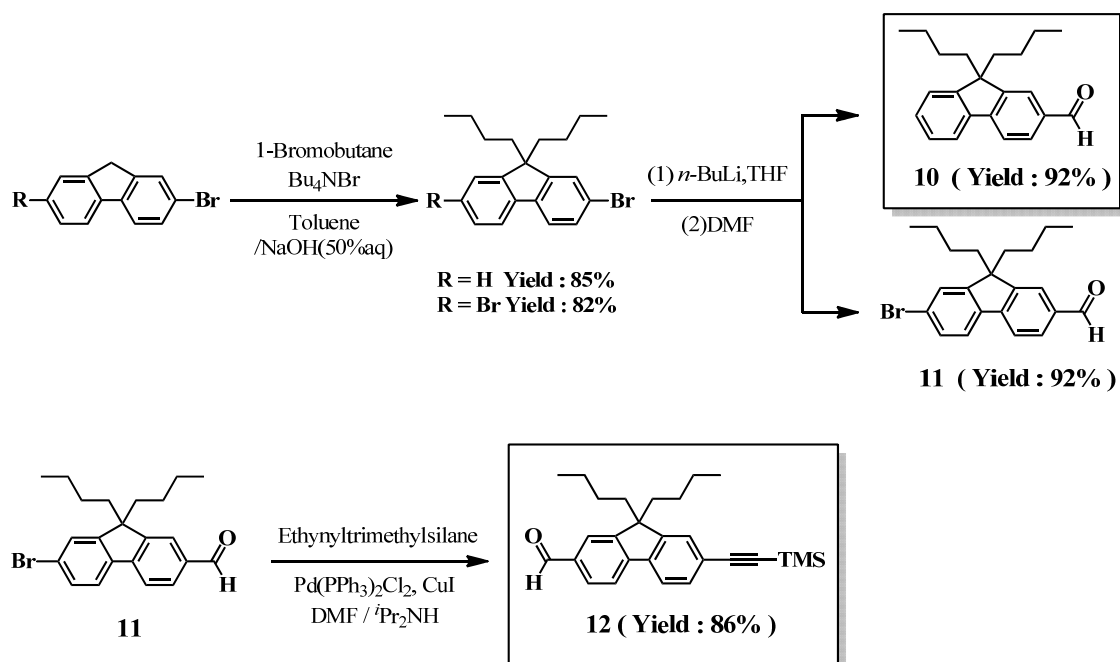


Figure 2.1.9 Mono-, Bis-, Tri- and Tetra-ruthenium tetrafluorenyl porphyrins (18-21)

2.2 Syntheses of the new Ruthenium metallic Porphyrins

2.2.1 Organic porphyrins formation

2-bromofluorene and 2,7-dibromofluorene are used as the starting materials. To improve solubility, *n*-butyl chains were added at the 9 position, with yields of 85% and 82% respectively. One of the bromine atoms was then transformed into the corresponding aldehyde with yields of 92% and 86% respectively. Finally, the triple-bond was introduced into compound by Sonogashira coupling ^[23] using ethynyltrimethylsilane, which allowed the product: **9,9-dibutyl-7-((trimethylsilyl)ethynyl)-fluorene-2-carbaldehyde (12)**, to be isolated in a yield of 65% (shown in Scheme 2.2.1).



Scheme 2.2.1 Synthesis of compounds 10, 11 and 12

The detailed syntheses of **Mono-**, **Bis-**, **Tri-** and **Tetra-TMS** fluorenyl cored porphyrins are given in Scheme 2.2.2.

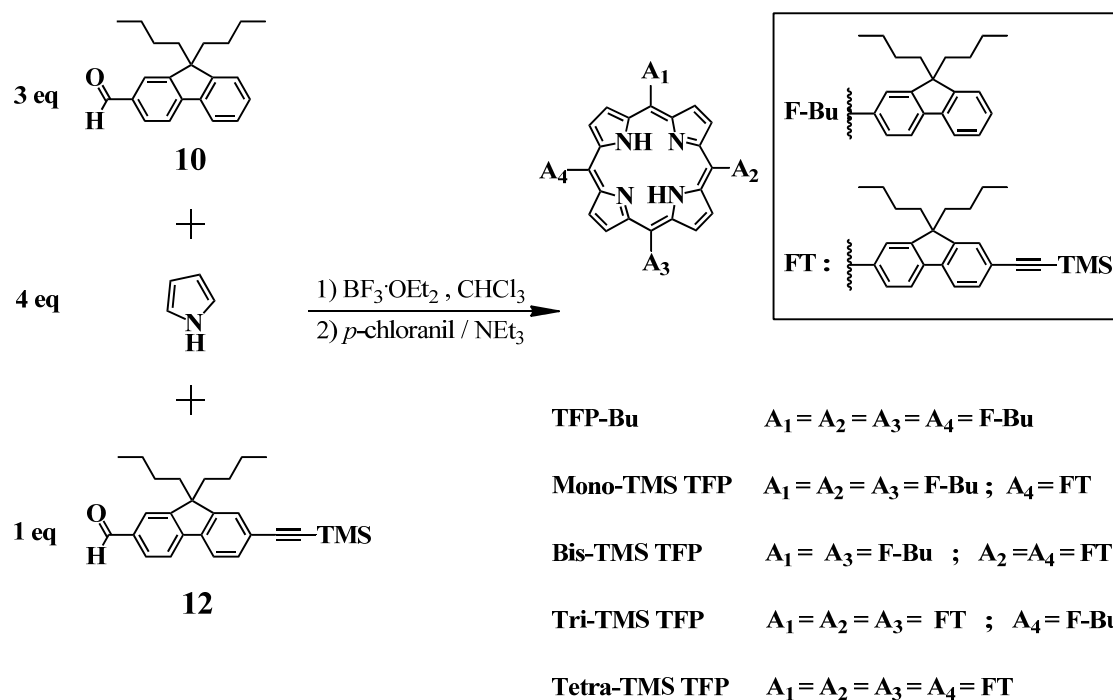
We adopted the following Lindsey conditions to form the series of TFP cored

porphyrin protected by TMS ^[24,25]:

(1) Firstly, starting materials aldehydes **10**, **12** and pyrrole (in a 3:1:4 ratio) were dissolved in distilled CHCl_3 in a two-necked flask under argon. After degassing the system with an argon purge for 30 min, the Lewis acid $\text{BF}_3 \cdot \text{OEt}_2$ was injected to start the reaction. The mixture was then stirred in dark for 3 h under a protective argon blanket;

(2) In a second step, *p*-chloranil was added to quench the cyclization and effect the oxidation of the porphyrinogen product. Dehydrogenation began upon refluxing at 60 °C for another 1 h, without argon protection;

(3) For the last step, the system was cooled to room temperature, and a controlled amount of NEt_3 was injected to neutralize the protonated porphyrin. Purification was effected by chromatography on silica, but unfortunately, the porphyrins were collected as a mixture because of their similar polarities. They were obtained as an inseparable dark red powder, which was therefore used directly for deprotection of the alkynyl groups.



Scheme 2.2.2 Multi-substituted porphyrin mixtures

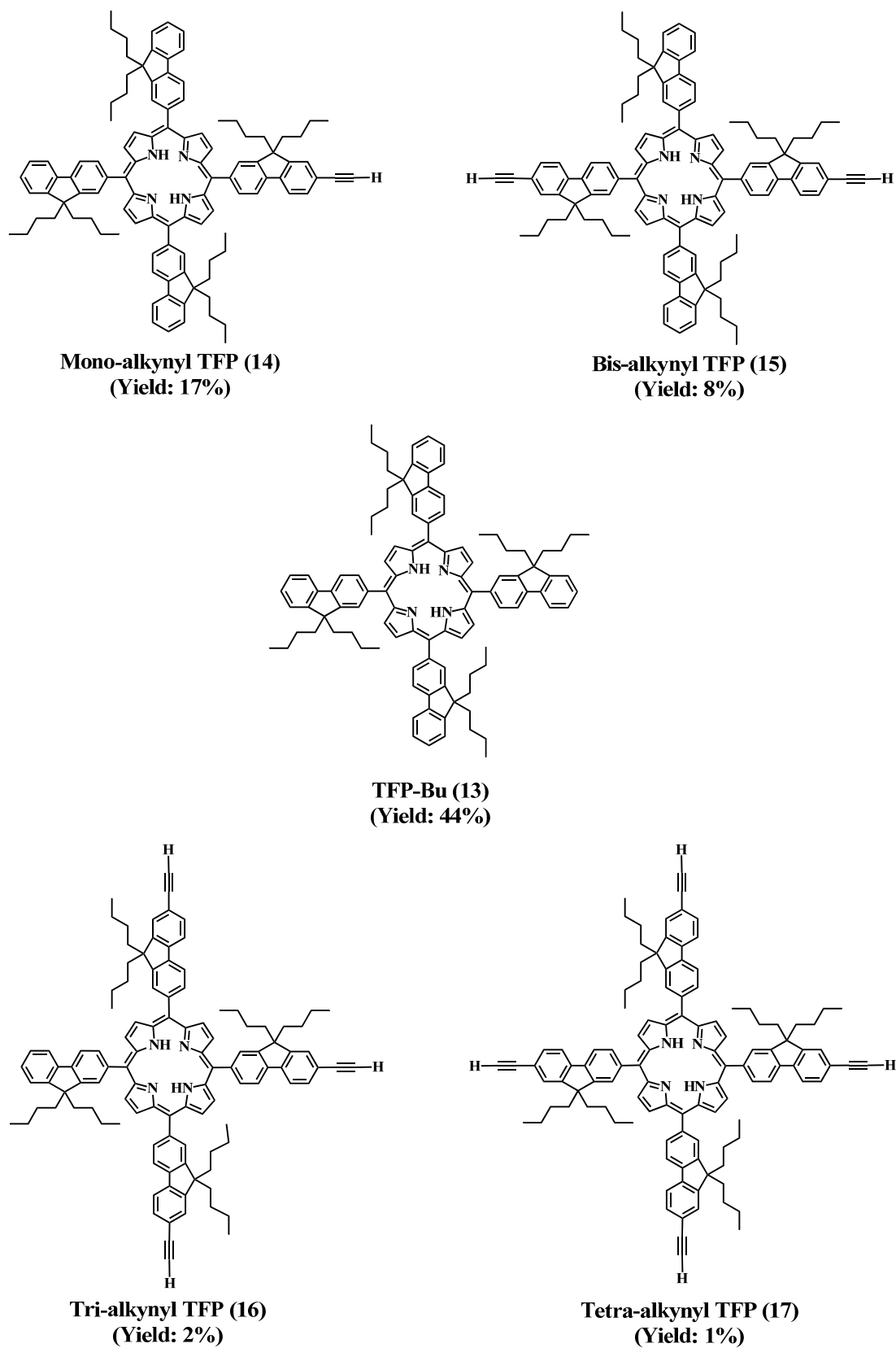


Figure 2.2.1 Mono-, Bis-, Tri- and Tetra-alkynyl TFP and TFP-Bu (13-17)

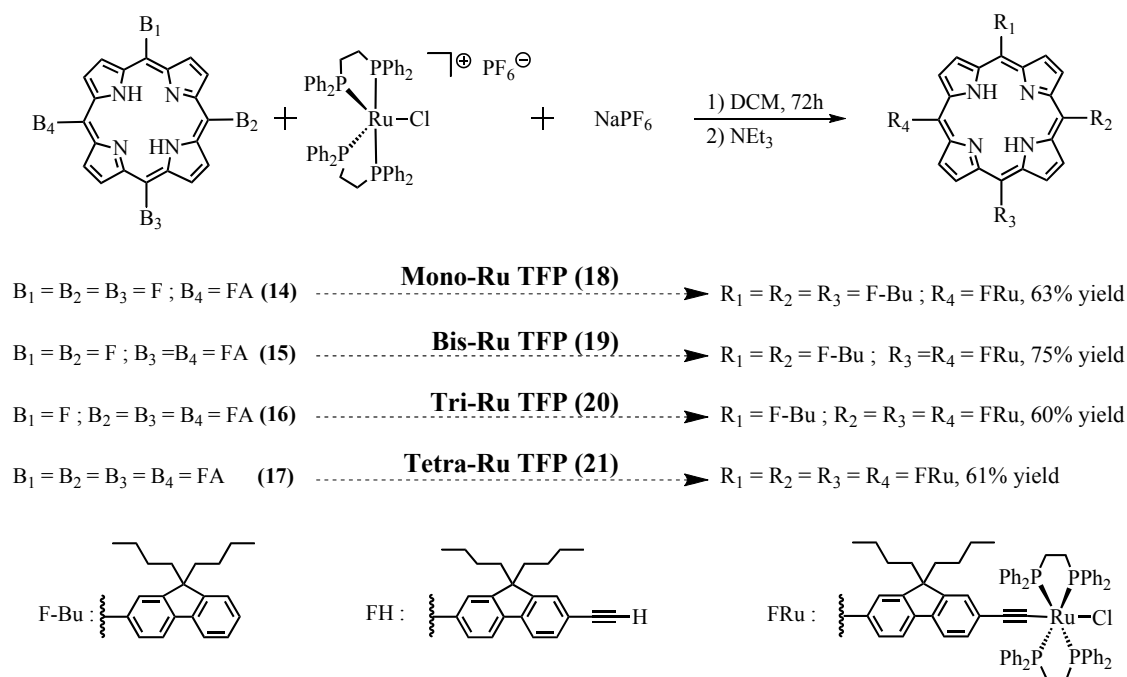
This subsequent deprotection of TMS was achieved directly in a $\text{CH}_2\text{Cl}_2/\text{MeOH}$ solvents mixture by using excess K_2CO_3 , and a controlled amount of THF, which was added to help dissolving all the porphyrin components. The reaction was heated at 45 °C for 10 h. Then silica chromatography was used to isolate compounds: different eluents were tested, and heptane/THF (4:1) was found to separate each component on TLC. However a large scale separation could not be effected, even when adding a little CH_2Cl_2 . Finally, a less polar eluent (heptane:THF = 10:1) was adopted successfully for chromatography on silica. The desired organic **Mono-**, **Bis-**, **Tri-**, **Tetra-alkynyl TFP** cored porphyrins (**14-17**) were collected selectively (shown in Figure 2.2.1), with the reference **TFP-Bu (13)** also being recovered from the first band in the column. Yields were 17%, 8%, 2%, 1% and 44% respectively.

2.2.2 Ruthenium Porphyrins formation

The four organic porphyrins: **Mono-alkynyl TFP (14)**, **Bis-alkynyl TFP (15)**, **Tri-alkynyl TFP (16)** and **Tetra-alkynyl TFP (17)** can be metallated in one final step. This employs organometallic *cis*-ruthenium(II) which was prepared as reported in the literature [26]. As shown in Scheme 2.2.3, the desired organometallic compounds can be synthesized in two steps with good yields.

Taking the **Mono-ruthenium TFP (18)** synthesis as an example, the organic **mono-alkynyl TFP (14)**, ruthenium(II) complex salt and NaPF_6 were mixed in a Schlenk tube under argon. Degassed and distilled DCM was injected into the system, which was then stirred at room temperature. The reaction finished after 72h according to ^1H NMR and ^{31}P NMR monitoring.

Subsequently, NEt_3 was added dropwise under argon, and the mixture was stirred further for a few minutes. Once the desired product was obtained, the mixture was filtered through basic alumina to remove ruthenium starting material.



Scheme 2.2.3 Syntheses of Mono-, Bis-, Tri-, Tetra-ruthenium TFP cored porphyrins (18-21)

2.3 NMR analyses

The organic porphyrins (**14-17**) and the corresponding organometallic porphyrins (**18-21**) were well characterized by 1H and ^{31}P NMR in $CDCl_3$ (400 MHz).

2.3.1 1H NMR spectra of the organic compounds

2.3.1.1 Fluorenyl aldehydes **10-12**

The complete 1H NMR for the aldehydes **10-12** are shown in Figure 2.3.1. The characteristic aldehyde singlet appeared around 10.0 ppm. The fluorenyl protons are well defined and lie within the classical aromatic zone, within 7.0-8.0 ppm. The *n*-butyl chains are identified by the multiplets between 0.3 and 2.2 ppm as H_a , H_b , H_c and H_d . The TMS group presents an intense singlet close to 0 ppm, which disappears after deprotection, in favor of another singlet emerging at around 3.2 ppm due to the terminal alkynyl H in the various porphyrins (**Mono-alkynyl TFP** to **Tetra-alkynyl TFP**).

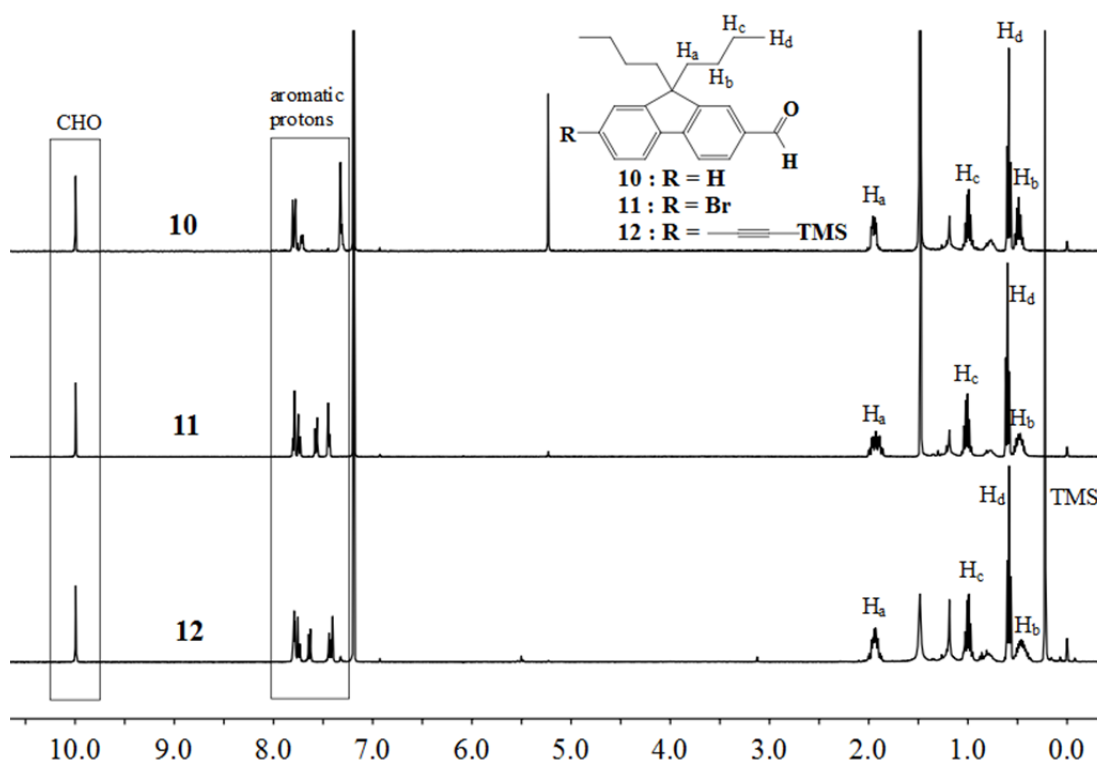


Figure 2.3.1 Complete ^1H NMR of fluorenyl aldehydes 10, 11 and 12

2.3.1.2 TFP-Bu and Mono-, Bis-, Tri-, Tetra-alkynyl TFP (13-17)

The proton peaks of **Mono-**, **Bis-**, **Tri-** and **Tetra-alkynyl TFP (14-17)** and **TFP-Bu (13)** have four components:

- (1) Eight β -pyrrolic H and two NH protons;
- (2) Fluorenyl protons in the aromatic zone;
- (3) H of the terminal alkynyl groups;
- (4) H of *n*-butyl chains in alkyls.

Comparisons of the partial ^1H NMR spectra of the organic porphyrins are shown in Figure 2.3.2. The peaks laying in the region of 8.9 ppm correspond to the typical

β -pyrrolic protons. They shift slightly to high field with increasing alkynyl substitution in the fluorenyl 7 position (Figure 2.3.2 (a)). These shifts, from 8.93 to 8.90 ppm, suggest that the density of outer electrons of $H_{\beta\text{-pyrrolic}}$ becomes increasingly delocalized, so that introducing of the alkynyl groups causes the conjugation of porphyrin macrocycle to be enhanced. In another words, the π -electrons of the macrocycle are more delocalized within a larger system. Especially, the symmetrical doublet of porphyrin **15** suggests that the two alkynyl units are in *trans* position in this porphyrin.

In the aromatic zone, between 7.3 and 8.3 ppm, the doublets and the multiplets characterize the fluorenyl protons. The multiplet found around 8.2 ppm corresponds to H_1 and H_3 , which lie near to the shielding cone of the porphyrin core, and H_4 appears as a doublet at 8.1 ppm. These peaks are not shifted by alkynyl substitution. In contrast, the H_5 doublet shows very regular stepwise shifts to higher field, going from an initial value of 7.96 to a final value of 7.91 ppm for the tetra-alkynyl porphyrin, in the same way as the β -pyrrolic peaks. For non-substituted **TFP-Bu (13)**, the peaks of H_6 , H_7 and H_8 overlap and appear as a broad multiplet (marked in the red box). In **Mono-alkynyl TFP**, when H_7 of one of the fluorenyl arms is exchanged for an alkynyl group, the peaks of H_6' and H_8' start to appear to lower field at 7.63 ppm (marked in blue frame). Increasing substitution by alkynyl groups causes the overlapped doublet of H_6' and singlet of H_8' to increase stepwise in intensity whereas the multiplet comprising $H_{6,7,8}$ decreases correspondingly, until the four H_7 are completely substituted. For **Tetra-alkynyl TFP (14)**, only H_6' and H_8' peaks are seen.

The terminal alkynyl protons are identified by a singlet at 3.2 ppm, the protons of *n*-butyl chains are easily recognized in the zone of 0.5-2.5 ppm, and the NH protons are presented by peaks at -2.5 ppm.

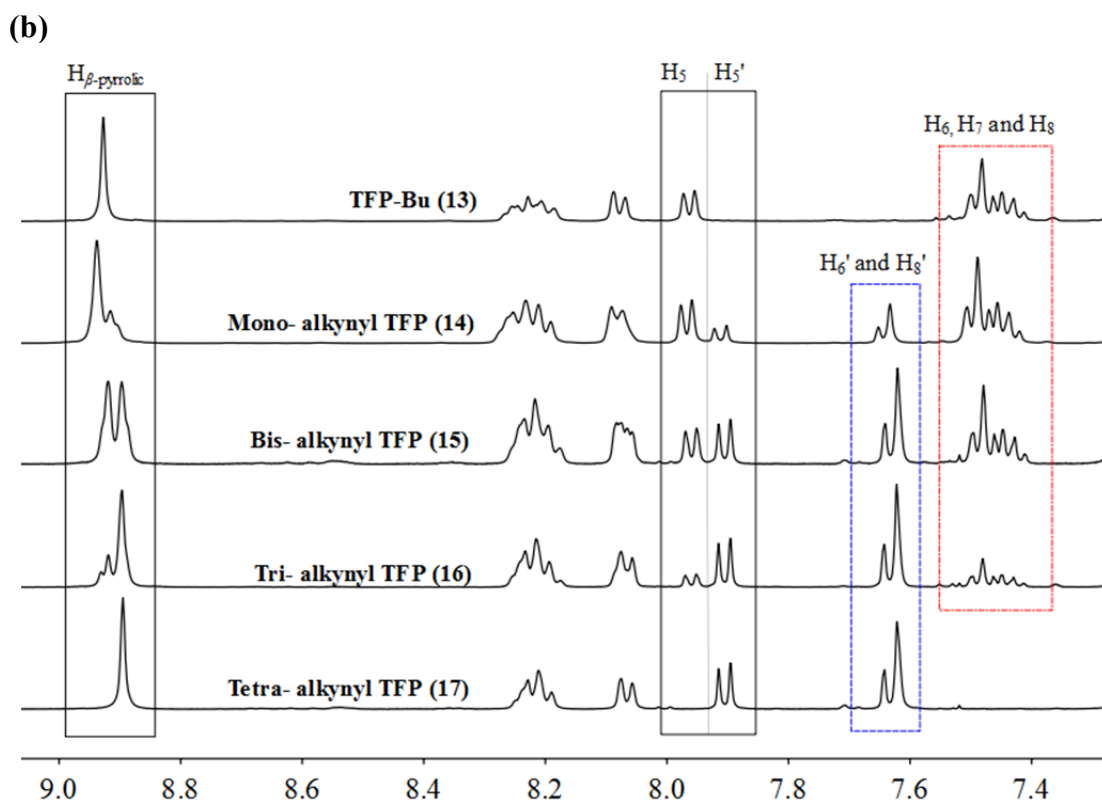
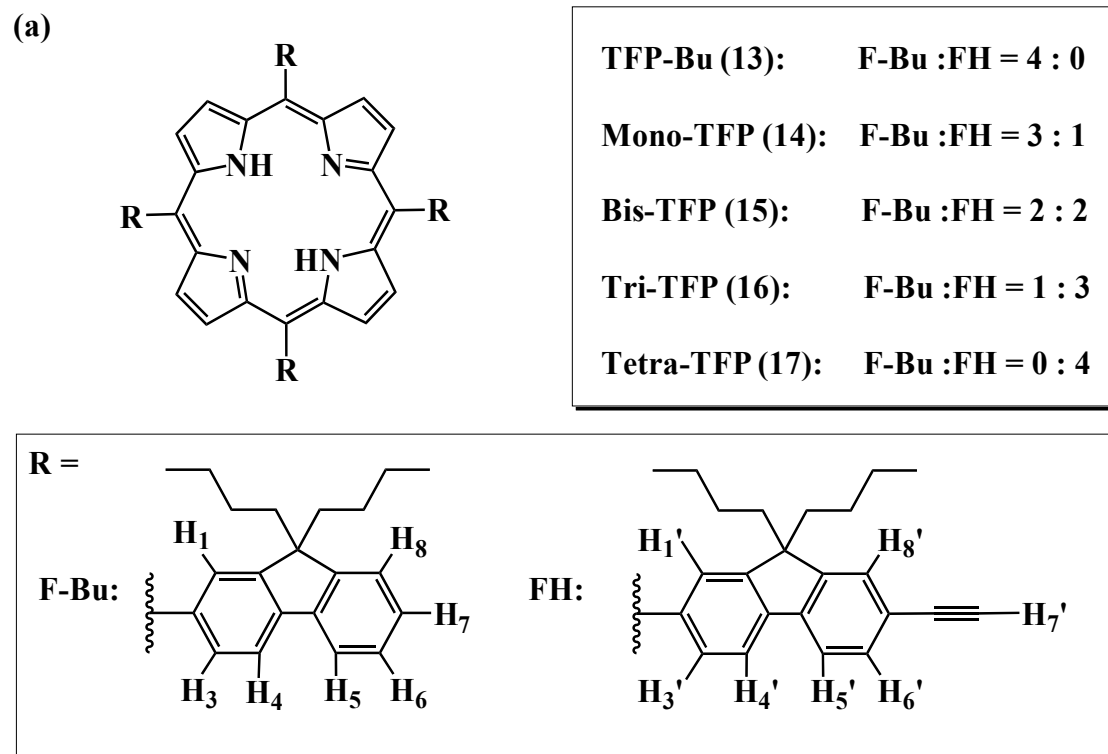


Figure 2.3.2 Partial comparative ^1H NMR of TFP-Bu And Mono-, Bis-, Tri-, Tetra-alkynyl TFP (13-17)

2.3.2 NMR spectra of the Ruthenium porphyrins (18–21)

2.3.2.1 NMR monitoring

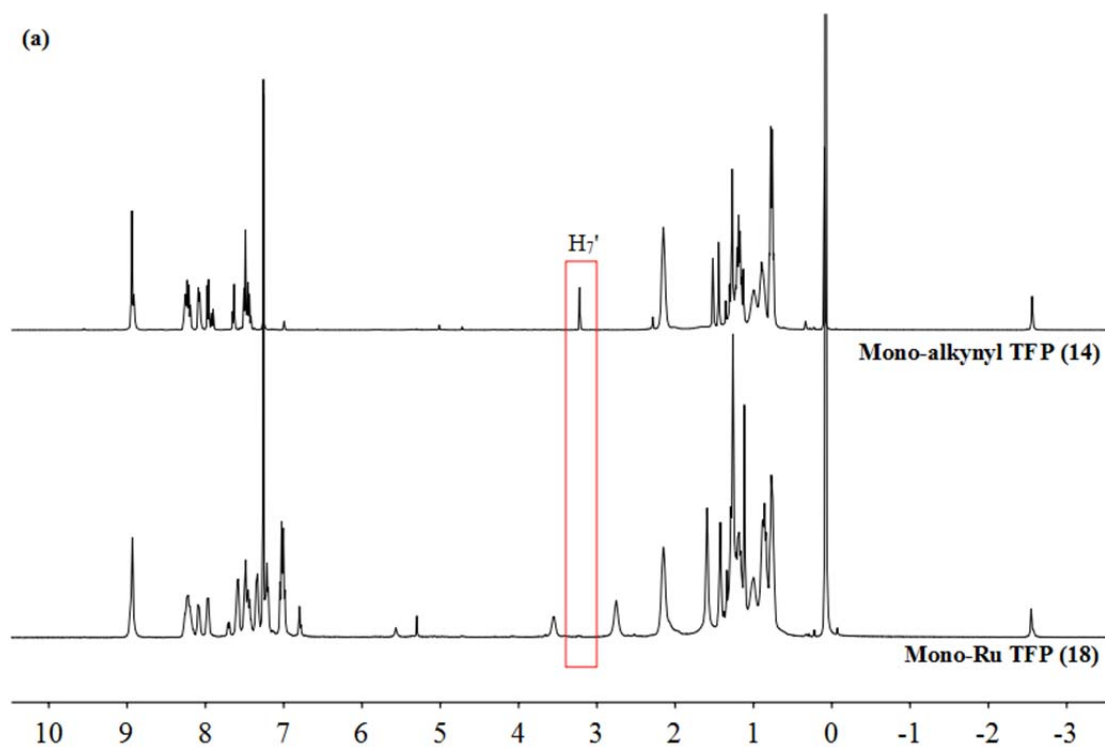
During the formation of organometallic porphyrins, the reaction progress was followed by ^1H NMR monitoring, with the disappearance of the singlet at 3.2 ppm corresponding to terminal alkynyl proton $\text{H}_{7'}$, revealing the degree of completion. The replacement of proton $\text{H}_{7'}$ in **Mono-alkynyl TFP (14)** to give the ruthenium(II) complex salt in **Mono-Ru TFP (18)** is clearly shown in Figure 2.3.3(a).

It is also possible to follow the reaction by ^{31}P NMR. Due to the *cis*-structure, the four phosphoruses in ruthenium(II) complex salt present two triplets in ^{31}P NMR, which coalesce to singlet after the formation of the organometallic compounds. This process is shown for **Mono-Ru TFP (18)** as an example in Figure 2.3.3(b).

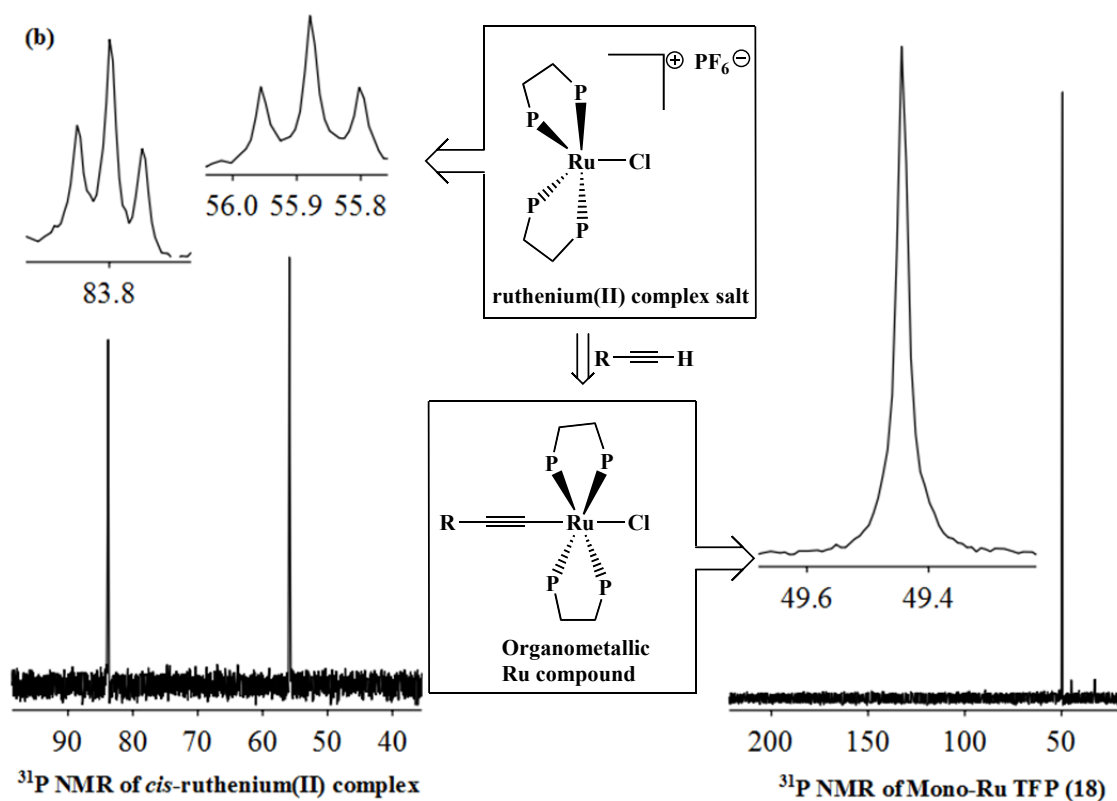
2.3.2.2 ^1H NMR

In Figure 2.3.4, the eight β -pyrrolic protons are visible at around 9.0 ppm in the partial ^1H NMR spectra of the organometallic porphyrins. When compared to **Mono-Ru TFP (18)**, the three other ruthenium porphyrins show weak shifts of the β -pyrrolic peaks to lower field, which is the opposite trend to the case alkynyl substitution.

When comparing the partial ^1H NMR spectra of the ruthenium complexes in Figure 2.3.4 with the pure organic precursors, we notice that each peak can be easily recognized except the new peaks appearing at 7.5–7.4 ppm, where the peaks of protons H_6 , H_7 and H_8 of fluorenyl units overlap with several protons of dppe ligands. Between 6.5 ppm and 8.5 ppm, the multiplets arise from the protons of fluorenyl arms and the phenyl groups of the dppe in the ruthenium complex. The peaks from 2.4 to 3.8 ppm arise from the methylene protons of the dppe ligands. Classically, the protons of *n*-butyl chains are found in the 0.4 to 2.4 ppm region, and the NH protons are identified at -2.6 ppm.



- Complete ^1H NMR monitoring of Mono-alkynyl TFP (14) and Mono-Ru TFP (18)



- ^{31}P NMR monitoring of ruthenium(II) complex salt and Mono-Ru TFP (18)

Figure 2.3.3 Complete ^1H NMR of Mono-alkynyl TFP (14) and Mono-Ru TFP (18)
And ^{31}P NMR of ruthenium(II) complex salt and Mono-Ru TFP (18)

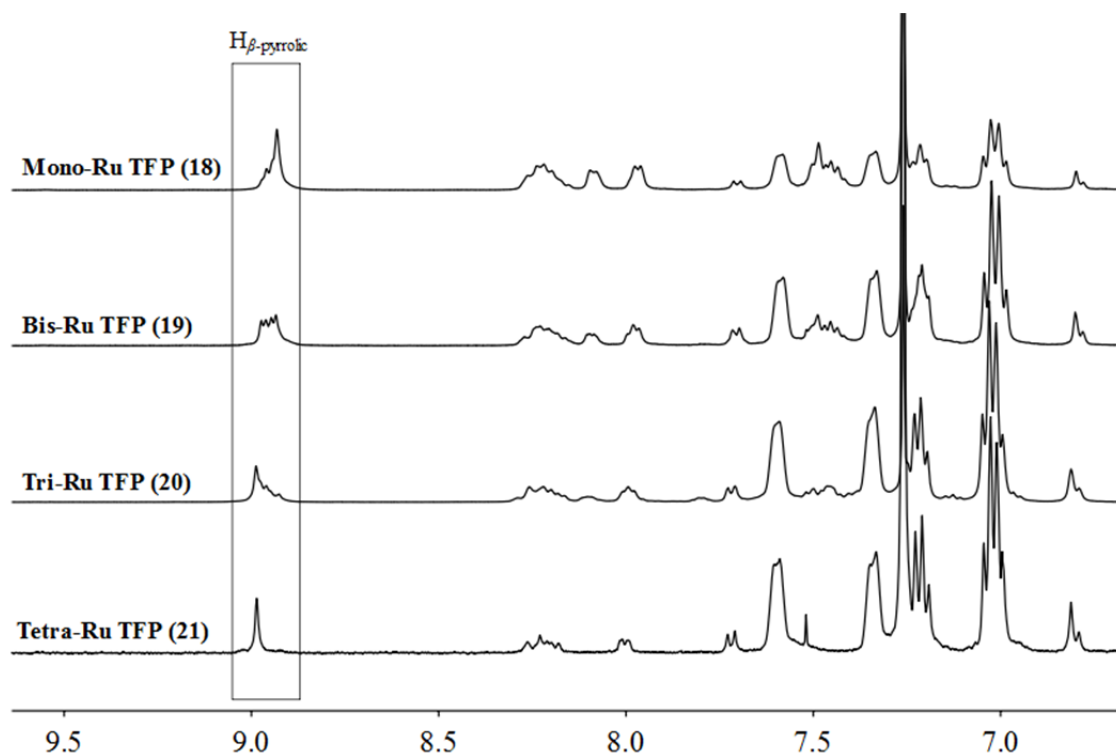


Figure 2.3.4 Partial ^1H NMR of Mono-, Bis-, Tri- and Tetra-Ru TFP (18-21)

2.3.2.3 ^{31}P NMR

Additionally, these new organometallic porphyrins were all also characterized by ^{31}P NMR. They present singlets around 49 ppm, corresponding to the 4, 8, 12, 16 equivalents phosphorus atoms of the dppe ligands of *cis*-ruthenium complexes in **Mono**, **Bis**, **Tri** and **Tetra-Ru porphyrins (18-21)** respectively.

These ^{31}P NMR spectra are all very similar to the example of **Mono-Ru TFP (18)** shown in Figure 2.3.3(b).

2.4 Optical properties

Porphyrins have attracted much interest from both physicists and chemists over many years because of their unusual spectroscopic features ^[24-29]. All porphyrins have two distinct absorption regions in the near-ultraviolet and visible regions, and their striking colors mean that UV-Visible spectra can be used to characterize the porphyrins compounds well.

The UV-Visible spectra were measured for two groups of compounds: the purely **organic TFP (14-17)** (shown in Figure 2.4.1) and the **organometallic ruthenium TFP (18-21)** class (shown in Figure 2.4.2). These two groups of compounds both exhibit intense Soret bands and four Q-bands absorption in visible region, and there are no obvious shifts for each group with respect to reference **TFP-Bu (13)**. By comparing the UV-visible spectra shown in Figure 2.4.1 and Figure 2.4.2, we observe that the Metal Ligand Charge Transfer (**MLCT**) absorptions of the ruthenium porphyrins appear between 350 and 400 nm. As expected, this **MLCT** absorption is enhanced with increasing number of ruthenium fragments in the molecule.

Table 2.4.1 UV-visible absorption data of organic porphyrin 13-17 and organometallic porphyrin 18-21 in CH₂Cl₂ at 298 K

	MLCT /nm	Soret band /nm	Q-bands /nm
13	-	427	519, 555, 592, 652
14	-	426	520, 558, 595, 650
15	-	428	518, 557, 602, 649
16	-	428	519, 556, 589, 680
17	-	428	519, 556, 595, 650
18	374	426	520, 560, 591, 653
19	374	426	520, 565, 588, 653
20	374	425	515, 573, 657
21	375	426	522, 567, 658

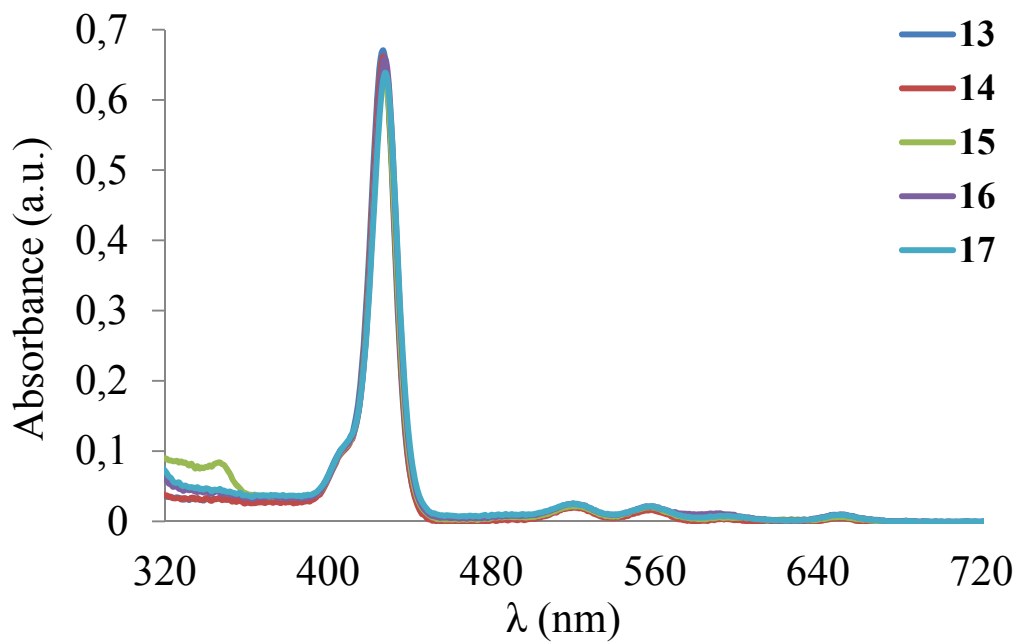


Figure 2.4.1 UV-Visible spectra of organic alkynyl porphyrins 13-17

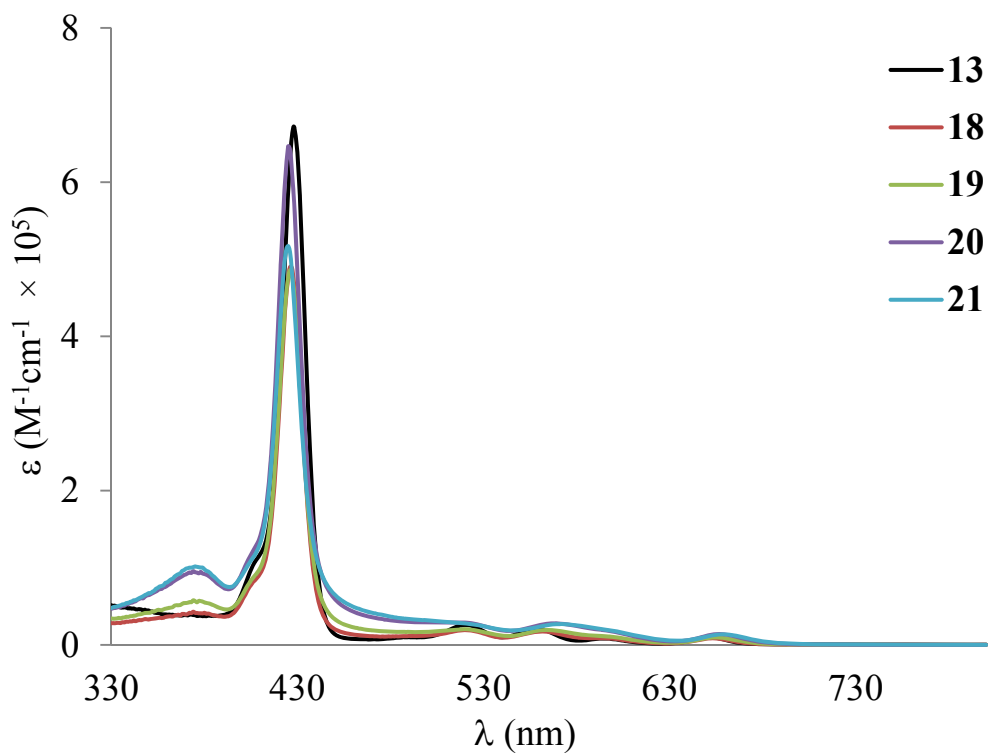


Figure 2.4.2 UV-Visible spectra of organometallic Ru porphyrins 18-21 and reference 13

2.5 Conclusions

1. A group of new organometallic porphyrins (**18-21**), combining the high luminescence core TFP with the ruthenium fragment, were synthesized successfully. They feature one to four ruthenium complexes parts in their architectures.

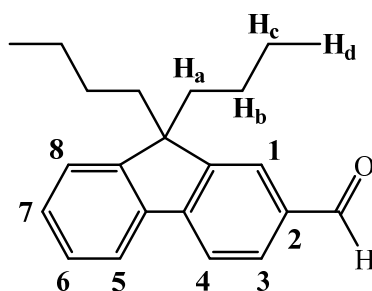
2. Aiming to the target porphyrins (**18-21**), the pure organic mono, bis, tri and tetra-alkynyl TFP cored porphyrins (**14-17**) were firstly isolated, as well as the reference **TFP-Bu (13)**.

3. These new organometallic ruthenium porphyrins (**18-21**) and the corresponding organic porphyrin precursors (**14-17**) were all characterized and analyzed by ^1H NMR, and the phosphorus atoms in ruthenium fragments of **18-21** were identified by each singlet presented in their ^{31}P NMR.

4. The UV-visible absorption spectra of the two series porphyrins: organic group (**14-17**) and organometallic group (**18-21**), as well as the reference TFP-Bu (**13**), were measured in CH_2Cl_2 at 298 K. Their typical intense Soret band and four Q-bands are all showing that they are center free porphyrins. Due to the connection to organometallic ruthenium fragment, the MLCT absorption band appear in 350-400 nm region, and following the increasing number of Ru parts surrounding the TFP core, this absorption band are much intense compared to **TFP-Bu**.

5. The redox-active properties and the NLO properties of the new organometallic Ru porphyrins **18-21** will be studied.

Experimental Section

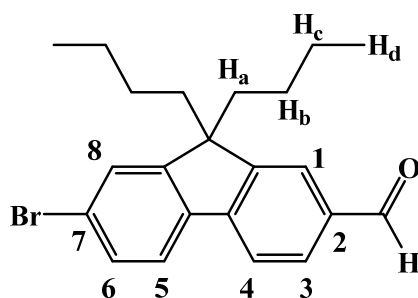
9, 9-dibutyl-fluorene-2-carbaldehyde (10)

(1) A mixture of commercial 2-bromofluorene (10.0 g, 40.8 mmol, 1 equiv), 1-bromobutane (13.2 mL, 122.4 mmol, 3 equiv) and Bu_4NBr (658.0 mg, 2.0 mmol, 5% equiv) were stirred in toluene (40 mL) and 50% NaOH (aq.) (24 mL) was added. The reaction medium was stirred at 85 °C for 40 h. Then the mixture was extracted with water and ethyl acetate. After the evaporation of volatiles, residue was purified by silica chromatography using heptane as eluent, the **2-bromo-9,9-dibutyl-fluorene** was isolated as colorless crystal (12.4 g, 85% yield).

$^1\text{H NMR}$ (400 MHz, CDCl_3 , ppm): $\delta = 7.68\text{-}7.65$ (m, 1H), 7.56 (d, 1H, $J = 6.0$ Hz), 7.46-7.43 (m, 2H), 7.35-7.32 (m, 3H), 2.00-1.88 (m, 4H), 1.12-1.03 (m, 4H), 0.68 (t, 6H, $J = 8.0$ Hz), 0.64-0.50 (m, 4H).

(2) In a Schlenk tube, a mixture of **2-bromo-9,9-dibutyl-fluorene** (3 g, 8.40 mmol, 1 equiv) was dissolved in dry THF (25 mL). The reaction medium was cooled to -78 °C in liquid nitrogen-acetone bath. Under low temperature, *n*-BuLi (5.77 mL, 9.24 mmol, 1 equiv) was injected dropwise to the mixture for 30 min. The system was kept stirring at -78 °C for 1.5 h. Then dried DMF (1.3 mL) was injected and the reaction was kept stirring at -78 °C for another 1.5 h. The reaction was stirred overnight at room temperature. At last saturated NH_4Cl (aq.) was injected for quenching the reaction. The mixture was extracted with ethyl acetate. After evaporation of the volatiles, residue was purified by silica chromatography using heptane/ CH_2Cl_2 (7:1) as eluent, aldehyde **10** was isolated as white powder (2.37 g, 92% yield).

$^1\text{H NMR}$ (400 MHz, CDCl_3 , ppm): $\delta = 10.06$ (s, 1H, H_{CHO}), 7.88 (s, 1H, H_1), 7.85-7.83 (m, 2H, $\text{H}_{3,4}$), 7.80-7.77 (m, 1H, H_5), 7.42-7.35 (m, 3H, $\text{H}_{6,7,8}$), 2.08-1.96 (m, 4H, H_a), 1.11-1.02 (m, 4H, H_c), 0.66 (t, $J = 7.4$ Hz, 6H, H_d), 0.59-0.51 (m, 4H, H_b).

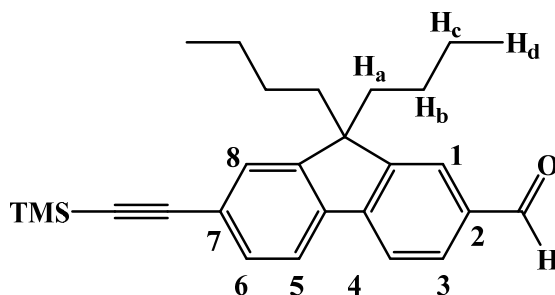
2,7-dibromo-9,9-dibutyl-fluorene-2-carbaldehyde (11)

(1) A mixture of commercial 2,7-dibromofluorene (5.0 g, 15.4 mmol, 1 equiv), 1-bromobutane (5 mL, 46.3 mmol, 3 equiv) and Bu₄NBr (249 mg, 0.77 mmol, 5% equiv) were stirred in toluene (20 mL) and 50% NaOH (aq.) (12 mL) was added. The reaction medium was stirred at 85 °C for 40 h. Then the mixture was extracted with water and ethyl acetate. After the evaporation of volatiles, residue was purified by silica chromatography using heptane as eluent, the **2,7-dibromo-9,9-dibutyl-fluorene** was isolated as colorless crystal (5.5 g, 82% yield).

¹H NMR (400 MHz, CDCl₃, ppm): δ 7.53-7.51 (m, 2H), 7.46-7.47 (m, 4H), 1.94-1.90 (m, 4H), 1.14-1.04 (m, 4H), 0.69 (t, *J* = 7.6 Hz, 6H), 0.61-0.53 (m, 4H).

(2) In a Schlenk tube, a mixture of **2,7-dibromo-9,9-dibutyl-fluorene** (4.018 g, 9.21 mmol, 1 equiv) was dissolved in dry THF (40 mL). The reaction medium was cooled to -78 °C in liquid nitrogen-acetone bath. Under low temperature, *n*-BuLi (5.756 mL, 9.21 mmol, 1 equiv) was injected dropwise to the mixture over 30 min. The system was kept stirring at -78 °C for 1.5 h. Then dried DMF (1.42 mL) was injected and the reaction was kept stirring at -78 °C for another 1.5 h. Finally, the mixture was stirred overnight at room temperature. At last, saturated NH₄Cl (aq.) was injected for quenching the reaction. The mixture was extracted with ethyl acetate/water. After evaporation of the volatiles, residue was purified by silica chromatography using heptane/CH₂Cl₂ (7:1) mixture as eluent, **7-bromo-9,9-dibutyl-fluorene-2-carboxaldehyde (11)** was isolated as white powder (3.27 g, 92% yield).

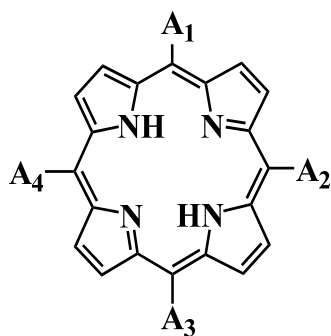
¹H NMR (400 MHz, CDCl₃, ppm): δ 10.06 (s, 1H, H_{CHO}), 7.87-7.86 (m, 2H, H_{1,4}), 7.81 (d, *J* = 8.4 Hz, 1H, H₃), 7.64 (d, *J* = 8.8 Hz, 1H, H₅), 7.52-7.50 (m, 2H, H_{6,8}), 2.07-1.93 (m, 4H, H_a), 1.13-1.04 (m, 4H, H_c), 0.67 (t, *J* = 7.2 Hz, 6H, H_d), 0.62-0.47 (m, 4H, H_b).

9, 9-dibutyl-7-((trimethylsilyl)ethynyl)-fluorene-2-carbaldehyde (12)

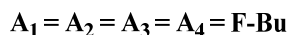
In a Schlenk tube, a mixture of **7-bromo-9,9-dibutyl-fluorene-2-carbaldehyde (11)** (2.1 g, 5.4 mmol, 1 equiv), commercial ethynyltrimethylsilane (1.2 mL, 8.1 mmol, 1.5 equiv), Pd(PPh₃)₂Cl₂ (23 mg, 0.1 mmol, 0.6% equiv) and CuI (3 mg, 0.1 mmol, 0.3% equiv) was stirred in DMF (5 mL) and iPr₂NH (5 mL) was added under argon. The reaction medium was degassed by freeze-pump-thaw twice and heated for 48 h at 95 °C. After evaporation of the volatiles, residue was purified by silica chromatography using heptane as eluent. Aldehyde **12** was isolated as a white powder (1.86 g, 86% yield).

¹H NMR (400 MHz, CDCl₃, ppm): δ 10.06 (s, 1H, H_{CHO}), 7.87-7.85 (m, 2H, H_{1,4}), 7.82-7.80 (m, 1H, H₃), 7.71 (d, *J* = 8.0 Hz, 1H, H₅), 7.50 (d, *J* = 8.0 Hz, 1H, H₆), 7.47 (s, 1H, H₈), 2.07-1.94 (m, 4H, H_a), 1.10-1.04 (m, 4H, H_c), 0.65 (t, *J* = 8.0 Hz, 6H, H_d), 0.60-0.44 (m, 4H, H_b), 0.29 (s, 9H, H_{TMS}).

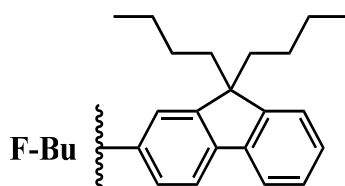
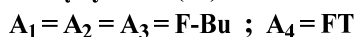
Organic porphyrins: Mono-, Bis-, Tri- and Tetra-alkynyl TFP (13-17)



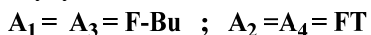
TFP-Bu (13)



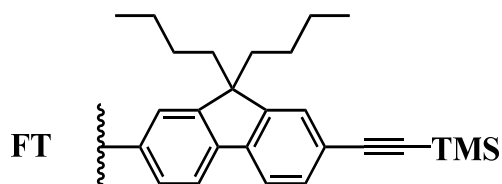
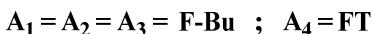
Mono-alkynyl TFP (14)



Bis-alkynyl TFP (15)



Tri-alkynyl TFP (16)

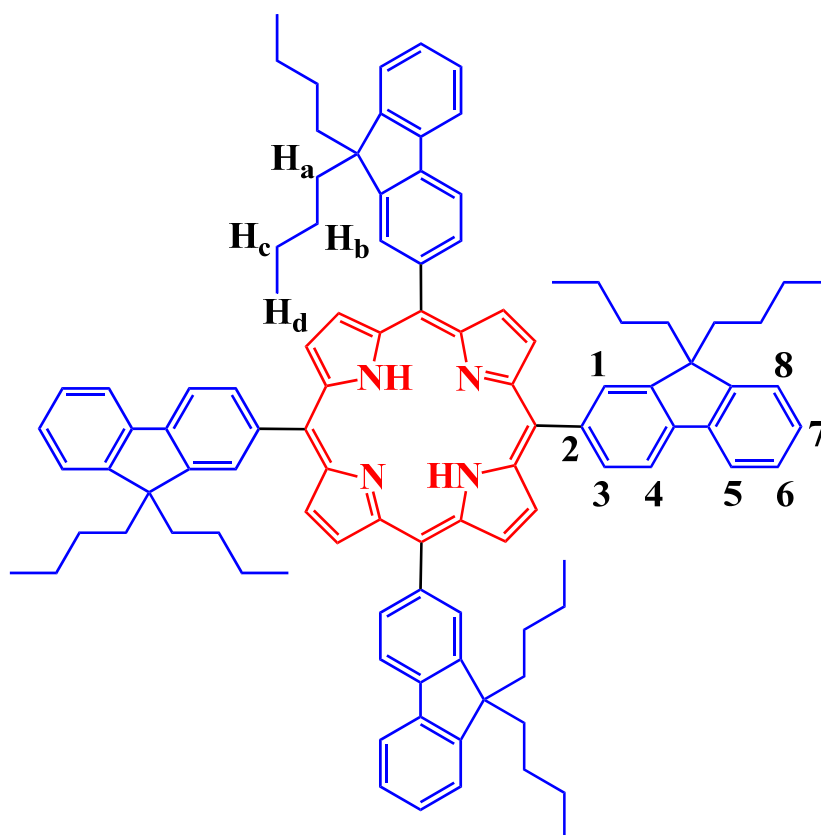


Tetra-alkynyl TFP (17)

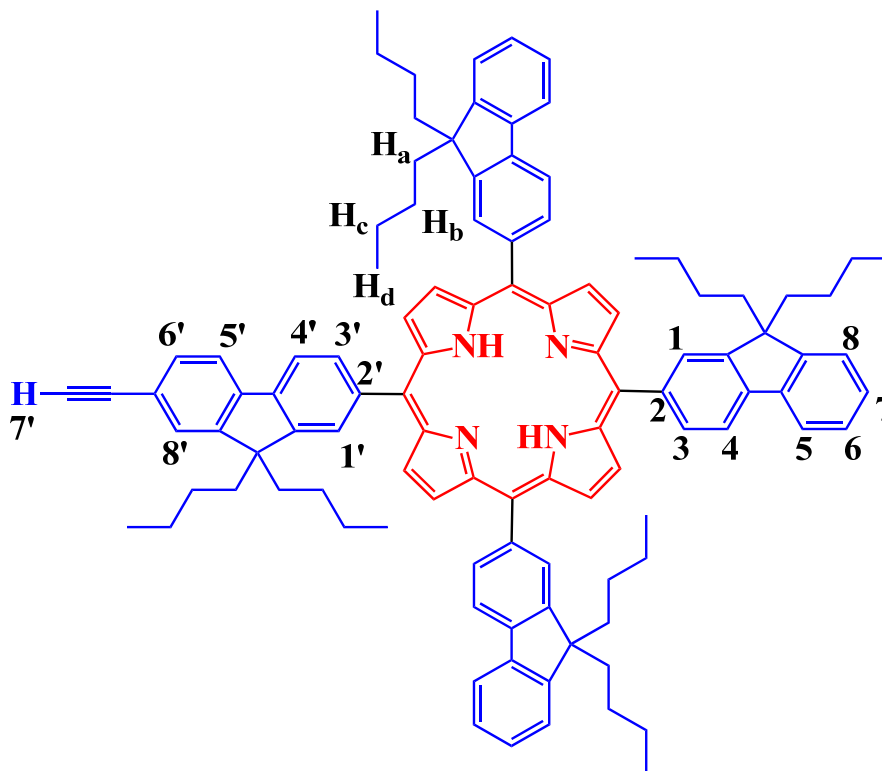


In a two-neck flask, a mixture of **10** (2.1 g, 6.7 mmol, 3 equiv), **12** (900 mg, 2.2 mmol, 1 equiv) and pyrrole (0.6 mL, 8.9 mmol, 4 equiv) was dissolved in dry chloroform (550 mL) under argon. After degassing the mixture with argon bubbling for 30 min, $\text{BF}_3 \cdot \text{OEt}_2$ (0.2 mL) was injected and the reaction was stirred in dark for 3 h under argon at room temperature. Then oxidant *p*-chloranil (1.5 g, 6.1 mmol) was added, and the reaction was heated at 60 °C for another 2 h without argon protection. After cooling the reaction to room temperature, NEt_3 (2 mL) was injected, and the medium was kept stirring for 10 min. After evaporation of the volatiles, purification was done by silica chromatography using a CH_2Cl_2 /heptane (1:3) mixture as eluent, the porphyrin mixture was collected as red powder. This mixture could not be separated into the pure components, the mixture was firstly deprotected by K_2CO_3 (2.0 g, 14.47 mmol) in solvents of CH_2Cl_2 /THF/MeOH (3:1:1) at 60°C, overnight. At last, the **TFP-Bu**, **Mono-**, **Bis-**, **Tri-** and **Tetra-alkynyl TFP (13-17)** were isolated by silica chromatography using a THF/pentane (1:30) mixture as eluent, the yield are 44%, 17%, 8%, 2% and 1%, respectively.

Reference TFP-Bu (13)



$^1\text{H NMR}$ (400 MHz, CDCl_3 , ppm): δ = 8.92 (s, 8H, $\text{H}_{\beta\text{-pyrrolic}}$), 8.26-8.18 (m, 8H, $\text{H}_{1,3}$), 8.07 (d, 4H, $J=7.5$ Hz, H_4), 7.96 (d, 4H, $J=7.3$ Hz, H_4), 7.52-7.41 (m, 12H, $\text{H}_{6,7,8}$), 2.14 (t, $J=7.2$ Hz, 16H, H_a), 1.21-1.14 (m, 16H, H_c), 1.02-0.87 (m, 16H, H_b), 0.78-0.72 (m, 24H, H_d), -2.57 (s, 2H, NH).

Mono-alkynyl TFP (14)

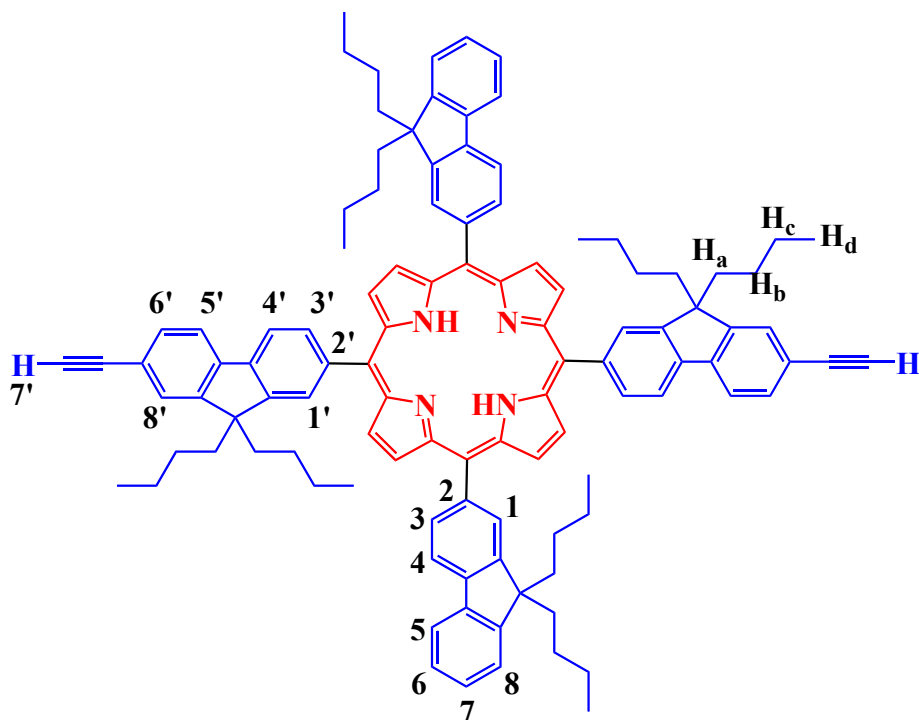
$^1\text{H NMR}$ (400 MHz, CDCl_3 , ppm): δ = 8.92-8.89 (m, 8H, $\text{H}_{\beta\text{-pyrrolic}}$), 8.27-8.17 (m, 8H, $\text{H}_{1,3}$, $\text{H}_{1'}$, $\text{H}_{3'}$), 8.08-8.06 (m, 4H, J = 7.3 Hz, H_4 , $\text{H}_{4'}$), 7.96 (d, 3H, J = 7.3 Hz, H_5), 7.91 (d, 1H, J = 7.7 Hz, $\text{H}_{5'}$), 7.63 (d, 2H, J = 8.0 Hz, $\text{H}_{6'}$, $\text{H}_{8'}$), 7.52-7.41 (m, 9H, $\text{H}_{6,7,8}$), 3.21 (s, 1H, $\text{H}_{7'}$), 2.14 (s, 16H, H_a), 1.21-1.14 (m, 16H, H_c), 1.02-0.84 (m, 16H, H_b), 0.78-0.72 (m, 24H, H_d), -2.58 (s, 2H, NH).

$^{13}\text{C NMR}$ (100 MHz, CDCl_3 , ppm): δ = 151.4, 149.3, 142.0, 141.8, 141.1, 141.0, 140.9, 140.0, 133.9, 133.8, 131.6, 129.5, 127.6, 127.2, 126.9, 123.2, 121.1, 121.0, 120.7, 120.6, 120.2, 120.1, 118.4, 118.0, 84.9, 77.4, 55.5, 55.4, 40.4, 38.3, 31.4, 26.5, 23.3, 23.2, 14.1, 14.0.

UV-vis (λ_{max} , CH_2Cl_2 , nm) : 426, 520, 558, 591, 650.

MS (Maldi-DCTB) for $\text{C}_{106}\text{H}_{110}\text{N}_4$: m/z = 1438.877 [M^{+}] (calcd: 1438.8725).

Anal. Calcd. (%) for $\text{C}_{106}\text{H}_{110}\text{N}_4 \cdot \text{EtOH}$: C, 87.29; H, 7.87; N, 3.77. **Found:** C, 87.18; H, 7.87; N, 3.59.

Bis-alkynyl TFP (15)

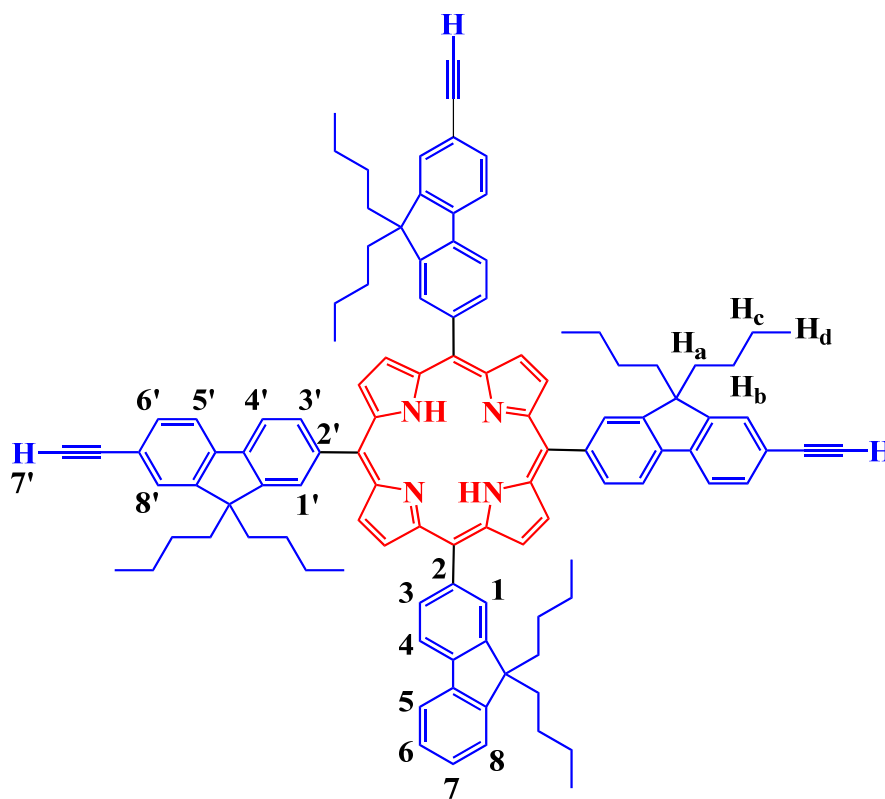
$^1\text{H NMR}$ (400 MHz, CDCl_3 , ppm): δ = 8.91 (d, 8H, J = 9.1 Hz, $\text{H}_{\beta\text{-pyrrolic}}$), 8.23-8.18 (m, 8H, $\text{H}_{1,3}$, $\text{H}_{1'}$, $\text{H}_{3'}$), 8.08-8.06 (m, 4H, H_4 , $\text{H}_{4'}$), 7.96 (d, 2H, J = 7.2 Hz, H_5), 7.91 (d, 2H, J = 7.7 Hz, $\text{H}_{5'}$), 7.63 (d, 4H, J = 8.0 Hz, $\text{H}_{6'}$, $\text{H}_{8'}$), 7.52-7.41 (m, 6H, $\text{H}_{6,7,8}$), 3.21 (s, 2H, $\text{H}_{7'}$), 2.14 (s, 16H, H_a), 1.21-1.14 (m, 16H, H_c), 0.99-0.85 (m, 16H, H_b), 0.78-0.73 (m, 24H, H_d), -2.58 (s, 2H, NH).

$^{13}\text{C NMR}$ (100 MHz, CDCl_3 , ppm): δ = 151.4, 149.7, 149.3, 141.9, 141.8, 141.1, 141.0, 140.9, 140.0, 133.9, 133.8, 131.6, 129.5, 129.4, 127.6, 127.2, 126.9, 123.2, 121.1, 121.0, 120.8, 120.7, 120.6, 120.2, 120.1, 118.4, 118.0, 84.9, 77.4, 59.7, 55.5, 55.4, 40.4, 40.3, 40.2, 38.3, 31.4, 29.9, 26.5, 23.2, 14.3, 14.2, 14.1, 14.0.

UV-vis (λ_{max} , CH_2Cl_2 , nm) : 427, 520, 558, 604, 650.

MS (Maldi-DCTB) for $\text{C}_{108}\text{H}_{110}\text{N}_4$: m/z = 1462.895 [M^{++}] (calcd: 1462.8725).

Anal. Calcd. (%) for $\text{C}_{108}\text{H}_{110}\text{N}_4 \cdot \text{EtOH}$: C, 87.49; H, 7.74; N, 3.71. **Found:** C, 87.58; H, 7.76; N, 3.48.

Tri-alkynyl TFP (16)

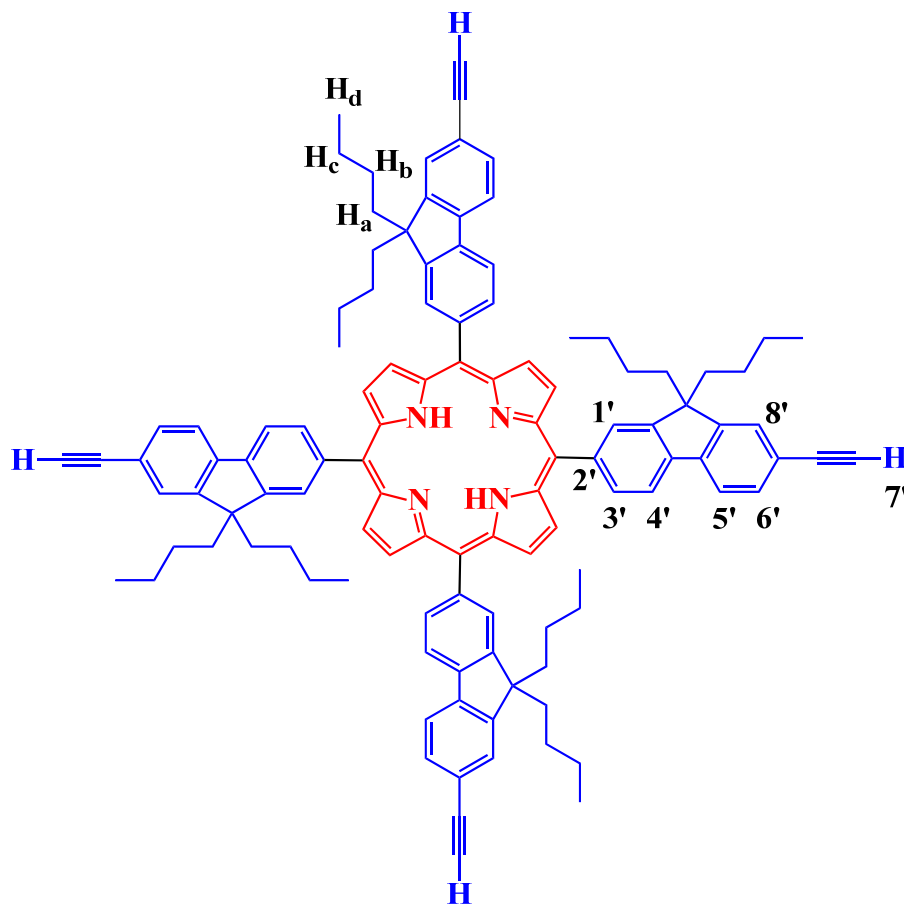
¹H NMR (400 MHz, CDCl₃, ppm): δ = 8.93-8.90 (m, 8H, H _{β} -pyrrolic), 8.25-8.18 (m, 8H, H_{1,3}, H_{1'}, H_{3'}), 8.07 (d, 4H, J = 7.2 Hz, H₄, H_{4'}), 7.96 (d, 1H, J = 7.2 Hz, H₅), 7.91 (d, 3H, J = 7.6 Hz, H_{5'}), 7.63 (d, 3H, J = 8.0 Hz, H_{6'}, H_{8'}), 7.51-7.41 (m, 3H, H_{6,7,8}), 3.21 (s, 3H, H_{7'}), 2.13 (s, 16H, H_a), 1.22-1.14 (m, 16H, H_c), 0.91-0.84 (m, 16H, H_b), 0.79-0.73 (m, 24H, H_d), -2.59 (s, 2H, NH).

¹³C NMR (100 MHz, CDCl₃, ppm): δ = 151.2, 149.6, 141.8, 141.6, 139.9, 133.8, 131.5, 129.4, 129.3, 129.2, 126.7, 120.6, 120.5, 120.1, 120.0, 118.3, 117.9, 84.7, 77.2, 59.5, 55.4, 55.3, 40.3, 40.2, 38.2, 33.7, 32.0, 31.9, 31.3, 29.7, 29.4, 26.7, 26.3, 23.1, 23.0, 22.7, 22.6, 14.1, 13.9, 14.0, 13.9.

UV-vis (λ_{\max} , CH₂Cl₂, nm) : 428, 520, 556, 592, 653.

Anal. Calcd. (%) for C₁₀₈H₁₁₀N₄·EtOH: C, 87.49; H, 7.74; N, 3.71. **Found:** C, 87.58; H, 7.76; N, 3.48.

Tetra-alkynyl TFP (17)



$^1\text{H NMR}$ (400 MHz, CDCl_3 , ppm): $\delta = 8.90$ (s, 8H, $\text{H}_{\beta\text{-pyrrolic}}$), 8.25-8.19 (m, 8H, $\text{H}_{1'}$, $\text{H}_{3'}$), 8.07 (d, 4H, $J = 7.3$ Hz, $\text{H}_{4'}$), 7.91 (d, 4H, $J = 7.8$ Hz, $\text{H}_{5'}$), 7.63 (d, 8H, $J = 8.0$ Hz, $\text{H}_{6'}$, $\text{H}_{7'}$, $\text{H}_{8'}$), 3.21 (s, 4H, $\text{H}_{7'}$), 2.13 (t, 16H, $J = 6.9$ Hz, H_a), 1.21-1.14 (m, 16H, H_c), 0.92-0.83 (m, 16H, H_b), 0.79-0.73 (m, 24H, H_d), -2.60 (s, 2H, NH).

$^{13}\text{C NMR}$ (100 MHz, CDCl_3 , ppm): $\delta = 151.4, 149.7, 141.9, 141.7, 140.1, 133.9, 131.6, 129.5, 126.9, 120.8, 120.2, 118.4, 88.6, 84.9, 77.4, 59.7, 55.5, 40.4, 38.3, 31.4, 29.7, 26.5, 23.3, 14.1, 14.0$.

UV-vis (λ_{max} , CH_2Cl_2 , nm): 428, 520, 558, 592, 650.

MS (Maldi-DCTB) for $\text{C}_{112}\text{H}_{110}\text{N}_4$: $m/z = 1510.869$ [M^+] (calcd: 1510.8725).

Anal. Calcd. (%) for $\text{C}_{112}\text{H}_{110}\text{N}_4 \cdot \text{EtOH}$: C, 87.87; H, 7.50; N, 3.60. Found: C, 87.89; H, 7.59; N, 3.49.

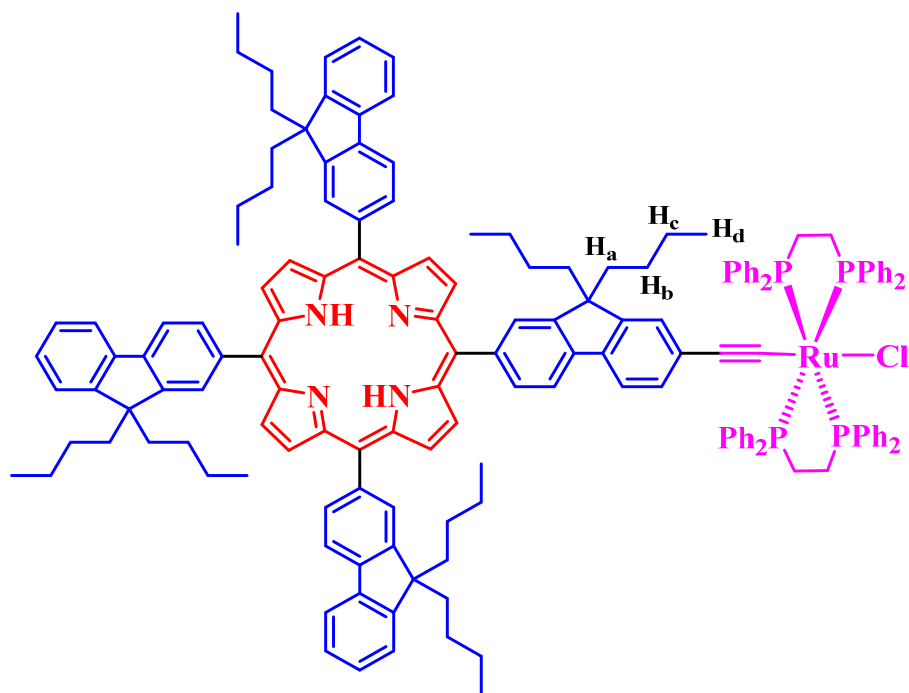
Organometallic porphyrins: Mono-, Bis-, Tri- and Tetra-Ru TFP (18-21)

Taking the **Mono-Ru TFP (18)** as example, in a Schlenk tube, a mixture of **Mono-alkynyl TFP (14)** (40 mg, 0.03 mmol, 1 equiv), ruthenium(II) complex (33 mg, 0.03 mmol, 1.1 equiv) and NaPF₆ (5.0 mg, 0.1 mmol, 1 equiv) were stirred in distilled dichloromethane under argon at room temperature. The reaction medium was degassed by argon bubbling for 10 min. Then the system was kept stirring for 96 h at room temperature in dark. At last, NEt₃ was injected to complete the reaction. After evaporation of the volatiles, the residue was purified by basic Al₂O₃ chromatography using CH₂Cl₂/Net₃ (100:1) as eluent; the dark violet powder was isolated (42 mg, 63% yield).

In more details, ruthenium(II) complex salt was used in excess to avoid a mixture of the starting material and the desired product. This is because the separation will be difficult since **Mono-alkynyl TFP (14)** decomposes on Al₂O₃ support. In addition, **Mono-alkynyl TFP (14)** and **Mono-Ru TFP (18)** have the nearly same solubility, so purification by precipitation cannot be used. The reaction mixture was stirred at room temperature and followed by ³¹P and ¹H NMR. The ruthenium precursor is characterized by two triplets at 55.8 and 83.7 ppm for ³¹P NMR, whereas the ruthenium part formed on porphyrin is expected to have a singlet at around 49 ppm.

Besides, ³¹P NMR can be used to monitor the reaction but not to completion since the ruthenium species is used in excess, so the total disappearance of the two triplets will not be observed. On the contrary, the ¹H NMR provides significant signals in this case. **Mono-alkynyl TFP (14)** must be totally consumed, so the singlet of the terminal alkyne at 3.2 ppm must disappear.

The **Bis-, Tri- and Tetra-Ru TFP (19-21)** were obtained in the same way as the former described synthesis of **Mono-Ru TFP (18)**.

Mono-Ru TFP (18)

$^1\text{H NMR}$ (400 MHz, CDCl_3 , ppm): $\delta = 8.96\text{--}8.93$ (m, 8H, $\text{H}_{\beta\text{-pyrrolic}}$), 8.26–8.15 (m, 8H, $\text{H}_{\text{fluorenyl}}$), 8.10–8.08 (m, 4H, $\text{H}_{\text{fluorenyl}}$), 7.97 (d, 4H, $J = 6.0$ Hz, $\text{H}_{\text{fluorenyl}}$), 7.70 (d, 1H, $J = 7.6$ Hz, $\text{H}_{\text{fluorenyl}}$), 7.59–7.58 (m, 7H, $\text{H}_{\text{fluorenyl}}$, $\text{H}_{\text{Ph-dppe}}$), 7.50–7.42 (m, 11H, $\text{H}_{\text{fluorenyl}}$, $\text{H}_{\text{Ph-dppe}}$), 7.35–7.33 (m, 8H, $\text{H}_{\text{fluorenyl}}$, $\text{H}_{\text{Ph-dppe}}$), 7.21 (t, $J = 7.0$ Hz, 8H, $\text{H}_{\text{Ph-dppe}}$), 7.05–6.99 (m, 14H, $\text{H}_{\text{Ph-dppe}}$), 6.79 (d, 2H, $J = 7.6$ Hz, $\text{H}_{\text{Ph-dppe}}$), 3.55 (s, 2H, $\text{H}_{\text{CH}_2\text{-dppe}}$), 2.75 (s, 6H, $\text{H}_{\text{CH}_2\text{-dppe}}$), 2.15 (s, 16H, H_a), 1.22–1.15 (m, 16H, H_c), 0.90–0.84 (m, 16H, H_b), 0.82–0.70 (m, 24H, H_d), $-2.55\text{--}2.57$ (m, 2H, NH).

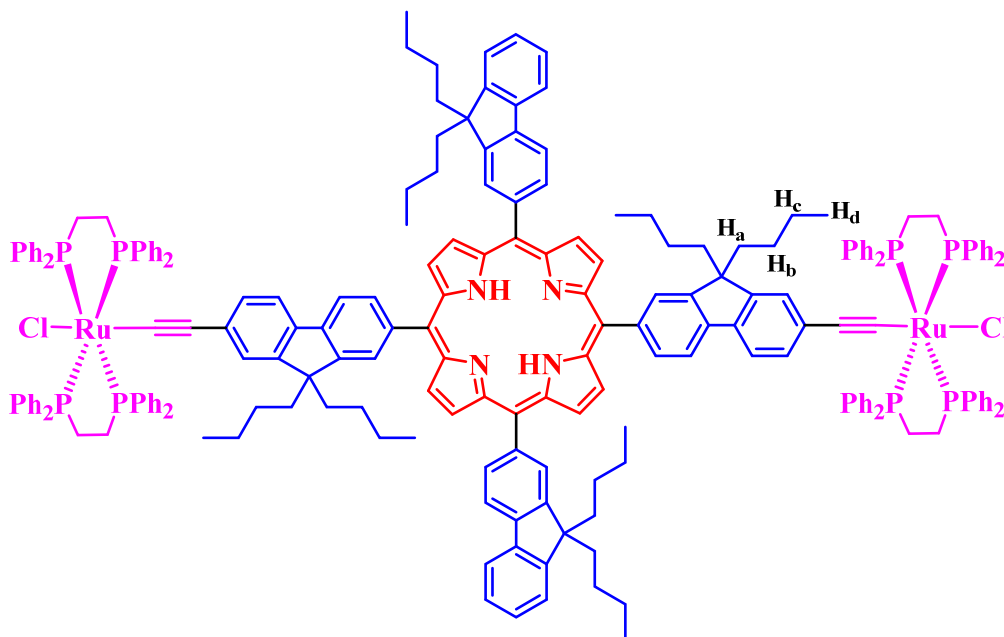
$^{13}\text{C NMR}$ (100 MHz, CDCl_3 , ppm): $\delta = 144.5, 141.0, 134.4, 128.8, 127.2, 127.1, 127.0, 126.9, 123.1, 120.1, 117.9, 115.7, 113.2, 110.5, 107.2, 103.1, 98.0, 81.4, 77.4, 55.3, 38.2, 31.3, 29.7, 26.4, 23.2, 22.7, 14.2, 14.0, 14.0, 8.1$.

$^{31}\text{P NMR}$ (100 MHz, CDCl_3 , ppm): $\delta = 49.4$ (s, 4P, $(\text{dppe})_2$).

UV-vis (λ_{max} , CH_2Cl_2 , nm): 280, 426, 520, 560, 591, 653.

HRMS-ESI for $\text{C}_{158}\text{H}_{157}\text{N}_4\text{P}_4\text{RuCl}$: $m/z = 2371.0070$ [M^{+}] (calcd: 2371.0085).

Anal. Calcd. (%) for $\text{C}_{158}\text{H}_{157}\text{N}_4\text{P}_4\text{RuCl}$: C 79.99; H 6.67; N 2.36. Found: C 74.55; H 8.03; N 1.83.

Bis-Ru TFP (19)

$^1\text{H NMR}$ (400 MHz, CDCl_3 , ppm): $\delta = 8.97\text{--}8.93$ (m, 8H, $\text{H}_{\beta\text{-pyrrolic}}$), $8.27\text{--}8.16$ (m, 8H, $\text{H}_{\text{fluorenyl}}$), $8.10\text{--}8.09$ (m, 2H, $\text{H}_{\text{fluorenyl}}$), $7.99\text{--}7.97$ (m, 4H, $\text{H}_{\text{fluorenyl}}$), $7.72\text{--}7.71$ (m, 3H, $\text{H}_{\text{Ph-dppe}}$), $7.59\text{--}7.58$ (m, 14H, $\text{H}_{\text{fluorenyl}}$, $\text{H}_{\text{Ph-dppe}}$), $7.52\text{--}7.42$ (m, 9H, $\text{H}_{\text{fluorenyl}}$, $\text{H}_{\text{Ph-dppe}}$), $7.35\text{--}7.33$ (m, 15H, $\text{H}_{\text{fluorenyl}}$, $\text{H}_{\text{Ph-dppe}}$), $7.24\text{--}7.19$ (m, 15H, $\text{H}_{\text{Ph-dppe}}$), $7.04\text{--}6.98$ (m, 28H, $\text{H}_{\text{Ph-dppe}}$), 6.79 (d, 4H, $J = 7.8$ Hz, $\text{H}_{\text{Ph-dppe}}$), 5.59 (s, 4H, $\text{H}_{\text{Ph-dppe}}$), 2.76 (s, 12H, $\text{H}_{\text{CH}_2\text{-dppe}}$), $2.58\text{--}2.52$ (m, 4H, $\text{H}_{\text{CH}_2\text{-dppe}}$), $2.23\text{--}2.03$ (m, 16H, H_a), $1.06\text{--}0.96$ (m, 16H, H_c), $0.90\text{--}0.71$ (m, 40H, H_b , H_d), $-2.49\text{--}2.61$ (m, 2H, NH).

$^{13}\text{C NMR}$ (100 MHz, CDCl_3 , ppm): $\delta = 134.4$, 130.8 , 128.8 , 127.2 , 127.0 , 77.2 , 67.6 , 53.0 , 40.4 , 38.2 , 31.3 , 29.7 , 26.4 , 23.4 , 23.2 , 18.8 , 14.3 , 14.2 , 14.0 , 13.9 , 8.1 .

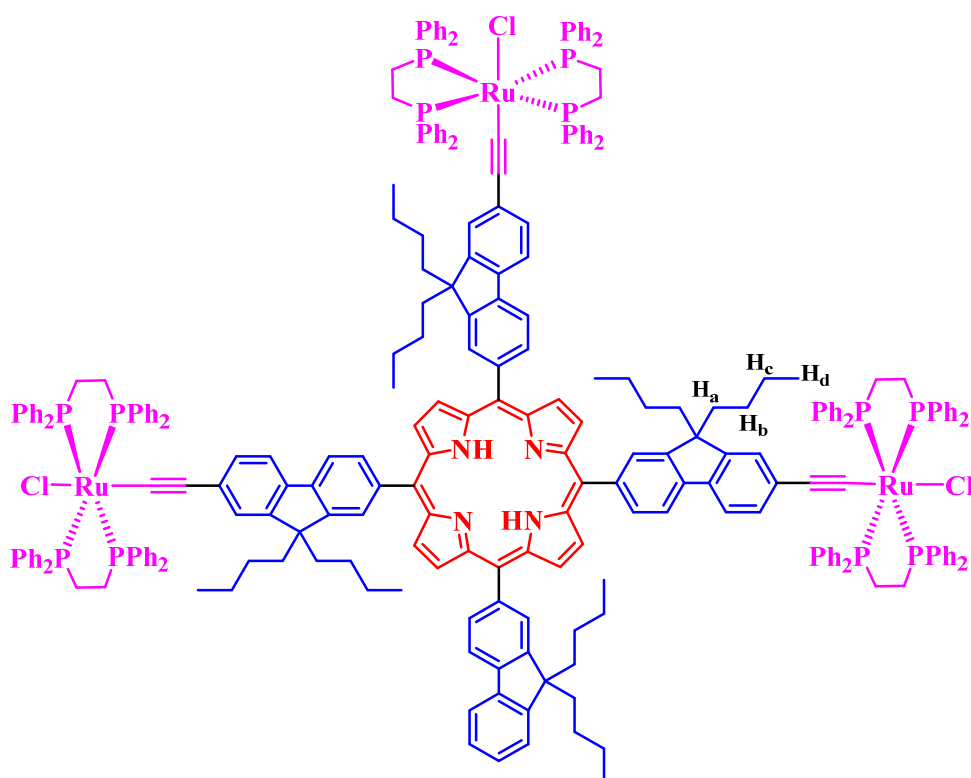
$^{31}\text{P NMR}$ (100 MHz, CDCl_3 , ppm): $\delta = 49.4$ (s, 8P, $(\text{dppe})_2$).

UV-vis (λ_{max} , CH_2Cl_2 , nm): 280, 426, 520, 565, 588, 653 .

HRMS-ESI for $\text{C}_{212}\text{H}_{204}\text{N}_4\text{P}_8\text{Ru}_2\text{Cl}_2$: $m/z = 1663.5735$ [M^{2+}] (calcd: 1663.5720);

$m/z = 3327.1438$ [M^+] (calcd: 3327.1446).

Anal. Calcd. (%) for $\text{C}_{212}\text{H}_{204}\text{N}_4\text{P}_8\text{Ru}_2\text{Cl}_2$: C 76.49; H 6.18; N 1.68. **Found:** C 69.04; H 7.10; N 1.73.

Tri-Ru TFP (20)

$^1\text{H NMR}$ (400 MHz, CDCl_3 , ppm): $\delta = 8.99\text{--}8.93$ (m, 8H, $\text{H}_{\beta\text{-pyrrolic}}$), $8.29\text{--}8.16$ (m, 8H, $\text{H}_{\text{fluorenyl}}$), $8.11\text{--}8.07$ (m, 1H, $\text{H}_{\text{fluorenyl}}$), $8.01\text{--}7.96$ (m, 4H, $\text{H}_{\text{fluorenyl}}$), $7.82\text{--}7.78$ (m, 1H, $\text{H}_{\text{fluorenyl}}$), 7.72 (d, 3H, $J = 7.5$ Hz, $\text{H}_{\text{Ph-dppe}}$), $7.67\text{--}7.55$ (m, 21H, $\text{H}_{\text{fluorenyl}}$, $\text{H}_{\text{Ph-dppe}}$), $7.52\text{--}7.38$ (m, 10H, $\text{H}_{\text{fluorenyl}}$, $\text{H}_{\text{Ph-dppe}}$), $7.37\text{--}7.30$ (m, 24H, $\text{H}_{\text{fluorenyl}}$, $\text{H}_{\text{Ph-dppe}}$), $7.25\text{--}7.20$ (m, 21H, $\text{H}_{\text{Ph-dppe}}$), $7.05\text{--}6.99$ (m, 46H, $\text{H}_{\text{Ph-dppe}}$), 6.80 (d, 5H, $J = 8.3$ Hz, $\text{H}_{\text{Ph-dppe}}$), 5.85 (t, 1H, $J = 8.3$ Hz, $\text{H}_{\text{Ph-dppe}}$), $3.55\text{--}3.51$ (m, 2H, $\text{H}_{\text{CH}_2\text{-dppe}}$), 2.76 (s, 22H, $\text{H}_{\text{CH}_2\text{-dppe}}$), $2.29\text{--}2.06$ (m, 16H, H_a), $1.08\text{--}1.05$ (m, 16H, H_c), $0.91\text{--}0.72$ (m, 40H, H_b , H_d), $-2.49\text{--}-2.57$ (m, 2H, NH).

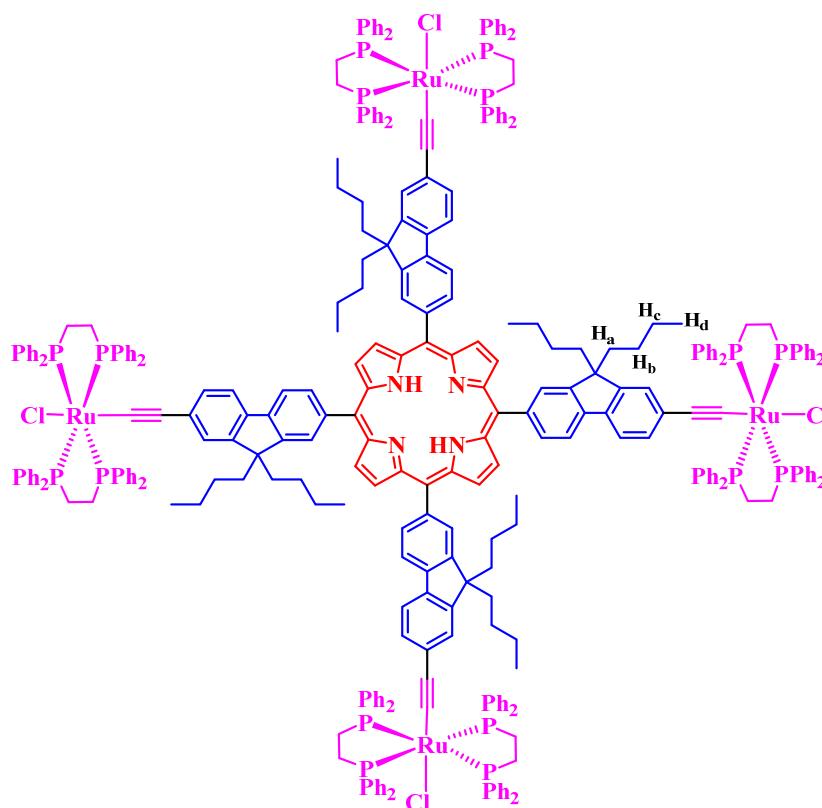
$^{13}\text{C NMR}$ (100 MHz, CDCl_3 , ppm): $\delta = 224.9, 219.7, 134.5, 134.4, 129.8, 128.8, 128.7, 127.2, 127.1, 127.0, 122.9, 110.0, 109.3, 103.2, 99.7, 77.2, 59.6, 38.2, 31.4, 29.7, 29.6, 14.2, 14.1, 11.1$.

$^{31}\text{P NMR}$ (100 MHz, CDCl_3 , ppm): $\delta = 49.5$ (s, 12P, $(\text{dppe})_2$).

UV-vis (λ_{max} , CH_2Cl_2 , nm): 280, 425, 515, 573, 657.

HRMS-ESI for $\text{C}_{266}\text{H}_{251}\text{N}_4\text{P}_{12}\text{Ru}_3\text{Cl}_3$: $m/z = 1427.7616$ [M^{3+}] (calcd: 1427.7598);
 $m/z = 2141.6372$ [M^{2+}] (calcd: 2141.6400).

Anal. Calcd. (%) for $\text{C}_{266}\text{H}_{251}\text{N}_4\text{P}_{12}\text{Ru}_2\text{Cl}_3$: C 74.56; H 5.90; N 1.31. **Found:** C 67.17; H 8.25; N 1.03.

Tetra-Ru TFP (21)

^1H NMR (400 MHz, CDCl_3 , ppm): δ = 8.99 (s, 8H, $\text{H}_{\beta\text{-pyrrolic}}$), 8.26-8.18 (m, 8H, $\text{H}_{\text{fluorenyl}}$), 8.02-7.99 (m, 4H, $\text{H}_{\text{fluorenyl}}$), 7.72 (d, 4H, J = 7.6 Hz, $\text{H}_{\text{fluorenyl}}$), 7.61-7.59 (m, 31H, $\text{H}_{\text{fluorenyl}}$, $\text{H}_{\text{Ph-dppe}}$), 7.35-7.33 (m, 31H, $\text{H}_{\text{fluorenyl}}$, $\text{H}_{\text{Ph-dppe}}$), 7.24-7.19 (m, 32H, $\text{H}_{\text{Ph-dppe}}$), 7.04-7.00 (m, 70H, $\text{H}_{\text{Ph-dppe}}$), 6.80 (d, 8H, J = 8.5 Hz, $\text{H}_{\text{Ph-dppe}}$), 2.76 (s, 32H, $\text{H}_{\text{CH}_2\text{-dppe}}$), 2.20-2.09 (m, 16H, H_a), 1.08-0.99 (m, 16H, H_c), 0.89-0.83 (m, 40H, H_b , H_d), -2.47 (m, 2H, NH).

^{13}C NMR (100 MHz, CDCl_3 , ppm): δ = 141.3, 139.8, 136.5, 135.7, 134.4, 132.1, 130.9, 130.8, 130.7, 129.1, 128.8, 127.2, 127.0, 77.2, 59.5, 55.0, 40.8, 38.2, 31.3, 30.8, 30.7, 30.6, 29.7, 26.5, 23.4, 14.2, 14.1.

^{31}P NMR (100 MHz, CDCl_3 , ppm): δ = 49.5 (s, 16P, $(\text{dppe})_2$).

UV-vis (λ_{max} , CH_2Cl_2 , nm): 280, 426, 522, 567, 658.

HRMS-ESI for $\text{C}_{320}\text{H}_{298}\text{N}_4\text{P}_{16}\text{Ru}_4\text{Cl}_4$: m/z = 1309.8595 [M^{4+}] (calcd: 1309.8337);
 m/z = 1746.4761 [M^{3+}] (calcd: 1746.4755).

Anal. Calcd. (%) for $\text{C}_{321}\text{H}_{298}\text{N}_4\text{P}_{16}\text{Ru}_4\text{Cl}_4$: C 73.33; H 5.73; N 1.07. Found: C 70.63; H 6.38; N 0.87.

References

- [1] M. A. Baldo, D. F. O'Brien, Y. You, A. Shoustikov, S. Sibley, M. E. Thompson, S. R. Forrest, *Nature*, **1998**, *395*, 151.
- [2] S. Drouet, C. O. Paul-Roth, V. Fattori, M. Cocchi, J. A. G. Williams, *New J. Chem.*, **2011**, *35*, 438.
- [3] N. Armaroli, F. Diederich, L. Echegoyen, T. Habicher, L. Flamigni, G. Marconi, J. F. Nierengarten, *New J. Chem.*, **1999**, *23*, 77.
- [4] M. Pawlicki, H. A. Collins, R. G. Denning, H. L. Anderson, *Angew. Chem., Int. Ed.*, **2009**, *48*, 3244.
- [5] M. Ravikanth, K. G. Ravindra, *Curr. Sci.*, **1995**, *68*, 1010.
- [6] G. de la Torre, P. Vazquez, F. Agullo-Lopez, T. Torres, *Chem. Rev.*, **2004**, *104*, 3723.
- [7] C. O. Paul-Roth, J. Rault-Berthelot, J. Letessier, G. Simonneaux, J. F. Bergamini, *J. Electroanal. Chem.*, **2007**, *606*, 103.
- [8] S. Drouet, C. O. Paul-Roth, *Tetrahedron*, **2009**, *65*, 10693.
- [9] S. Drouet, A. Merhi, D. D. Yao, M. P. Cifuentes, M. G. Humphrey, M. Wielgus, J. Olesiak-Banska, K. Matczyszyn, M. Samoc, F. Paul, C. O. Paul-Roth. *Tetrahedron*, **2012**, *68*, 10351.
- [10] D. Bellows, S. M. Ali, C. P. Gros, M. E. Ojaimi, J. M. Barbe, R. Guillard, P. D. Harvey, *Inorg. Chem.*, **2009**, *48*, 7613.
- [11] Y. J. Chen, S. S. Chen, S. S. Lo, T. H. Huang, C. C. Wu, G. H. Lee, S. M. Peng, C. Y. Yeh, *Chem. Commun.*, **2006**, 1015.
- [12] S. A. Odom, S. Webster, L. A. Padilha, D. Peceli, H. Hu, G. Nootz, S.J. Chung, S. Ohira, J. D. Matichak, O. V. Przhonska, A. D. Kachkovski, S. Barlow, J.L. Brédas, H. L. Anderson, D. J. Hagan, E. W. Van Stryland. S. R. Marder, *J. Am. Chem. Soc.*, **2009**, *131*, 7510.
- [13] M. Drobizhev, Y. Stepanenko, Y. Dzenis, A. Karotki, A. Rebane, P. N. Taylor, H. L. Anderson, *J. Am. Chem. Soc.*, **2004**, *126*, 15352.
- [14] S. Drouet, A. Merhi, G. Grelaud, M. P. Cifuentes, M. G. Humphrey, K. Matczyszyn, M. Samoc, L. Toupet, C. O. Paul-Roth, F. Paul, *New J. Chem.*, **2012**, *36*, 2192.
- [15] M. P. Cifuentes, M. G. Humphrey, J. P. Morrall, M. Samoc, F. Paul, T. Roisnel, C. Lapinte, *Organometallics*, **2005**, *24*, 4280.

- [16] A. Merhi, G. Grelaud, N. Ripoché, A. Barlow, M. P. Cifuentes, M. G. Humphrey, F. Paul, C. O. Paul-Roth, *Polyhedron*, **2015**, *86*, 64.
- [17] C. O. Paul-Roth, J. Rault-Berthelot, G. Simonneaux, *Tetrahedron*, **2004**, *60*, 12169.
- [18] C. O. Paul-Roth, J. A. G. Williams, J. Lestessier, G. Simonneaux, *Tetrahedron Lett.*, **2007**, *48*, 4317.
- [19] C. O. Paul-Roth, G. Simonneaux, *Tetrahedron Lett.*, **2006**, *47*, 3275.
- [20] C. O. Paul-Roth, G. Simonneaux, *C.R. Acad. Sci., Ser. IIC: Chim.*, **2006**, *9*, 1277.
- [21] M. Murai, M. Sugimoto, M. Akita, *Dalton Trans.*, **2013**, *42*, 16108.
- [22] A. Merhi, X. Zhang, D. Yao, S. Drouet, O. Mongin, F. Paul, J. A. G. Williams, M. A. Fox, C. O. Paul-Roth, *Dalton Trans.*, **2015**, *10*, 1039.
- [23] K. Sonogashira, Y. Tohda, N. Hagihara, *Tetrahedron Lett.*, **1975**, *50*, 4467.
- [24] J. S. Lindsey, K. A. Maccrum, J. S. Tyhonas, Y. Y. Chuang, *J. Org. Chem.*, **1994**, *59*, 579.
- [25] F. R. Li, K. X. Yang, J. S. Tyhonas, K. A. Maccrum, J. S. Lindsey, *Tetrahedron*, **1997**, *53*, 12339.
- [26] B. Chaudret, G. Commenges, R. Poilblanc, *J. Chem. Soc.*, **1984**, 1635.
- [27] D. J. Quimby, F. R. Longo, *J. Am. Chem. Soc.*, **1975**, *97*, 5111.
- [28] M. Uttamlal, S. Holmes-Smith, *A. Chem. Phys. Lett.*, **2008**, *454*, 223.
- [29] J. L. Retsek, C. J. Medforth, D. J. Nurco, S. Gentemann, V. S. Chirvony, K. M. Smith, D. Holten, *J. Phys. Chem. B*, **2001**, *105*, 6396.

Chapter 3

Syntheses and characterization of New Porphyrin Dendrimers and Photophysical Properties

3.1 Introduction

3.1.1 Porphyrin dendrimers of our laboratory

In recent years, we have reported several porphyrin dendrimers from both non-conjugated and conjugated classes. They all presented interesting linear optical properties (**LO**) and some of them, like the non-conjugated dendrimers **OOFP**, **SOFP** as well as conjugated dendrimers (**TPP2**, **TPP3**, **TPP5** and **TPP6**), also presented interesting nonlinear optical properties (**NLO**).

3.1.1.1 Non-conjugated porphyrin dendrimers

The structures of the entire series of non-conjugated porphyrin dendrimers that were known in 2009 are shown in Figure 3.1.1. As described below, **OOFP** and **SOFP** possess eight and sixteen peripheral fluorenyl arms respectively, whose fluorenyl units are connected to the phenyl linkers by 2-hydroxyl-methyl chains ^[1-4].

Table 3.1.1 lists the photophysical data of these non-conjugated porphyrin dendrimers and those of **TPP**, which is taken as a reference. The Soret bands of **OOFP** and **SOFP** are slightly red shifted compared to this of **TPP** (417 nm), as are their Q-bands. The π - π^* absorptions appear in a UV range that is characteristic of the peripheral fluorenyl units. The intensity of dendrons absorption is enhanced as the number of peripheral arms increases, upon passing from eight to sixteen fluorenyl units: the UV absorption of **SOFP** (at 270 nm) becomes as intense as its Soret band.

The intrinsic **TPA** cross-sections σ_2 of **OOFP** and **SOFP** were measured by Two-Photon-Excited Fluorescence (**TPEF**) in the femtosecond regime. The σ_2 of the **TPP** cored porphyrin dendrimers are enhanced by increasing the numbers of fluorenyl units. Compared to the reference value of $\sigma_{2,TPP} = 12$ GM, the $\sigma_{2,OOFP}$, and $\sigma_{2,SOFP}$ are improved very significantly: by 45 GM and 75 GM respectively (listed in Table 3.1.1).

In conclusion, this series of dendrimers already present slightly improved LO properties and also interesting NLO properties relative to **TPP**. In an attempt to improve these systems further, we have developed a new series featuring conjugated linker **I**.

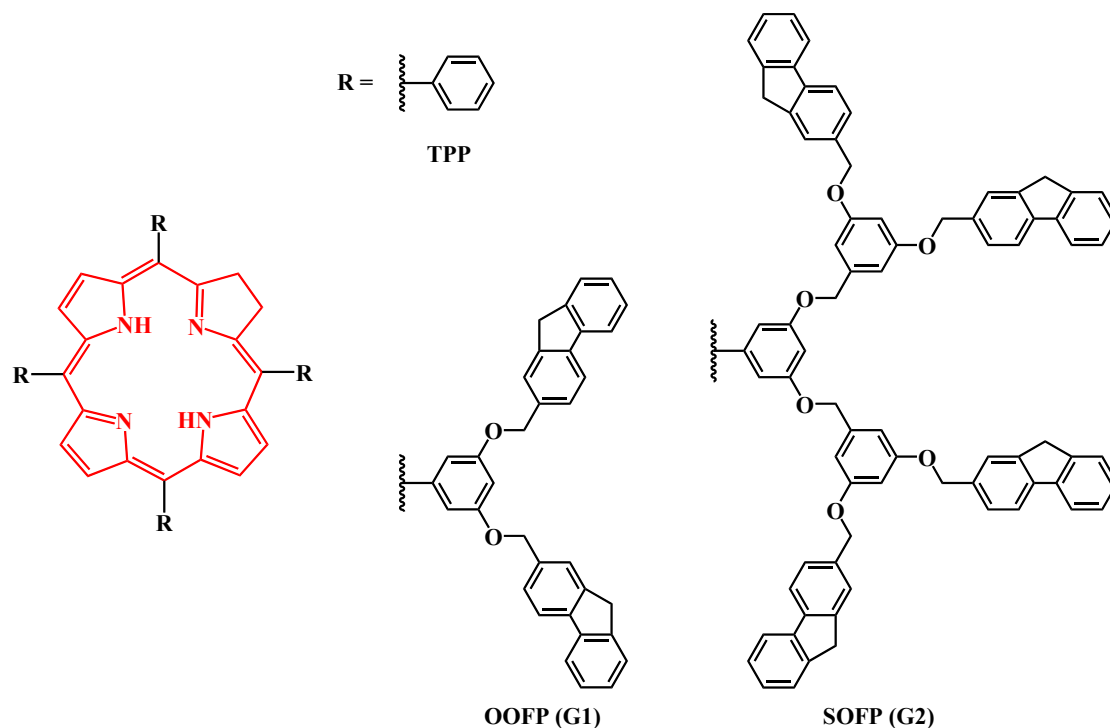


Figure 3.1.1 Structures of the non-conjugated porphyrin dendrimers (OOFP and SOFP) and TPP

Table 3.1.1 Photophysical data in DCM of OOFP, SOFP and reference TPP

	<u>UV-visible absorption</u>			<u>Emission /nm</u>					
	λ_{dendron} /nm	λ_{Soret} /nm	λ_{Qbands} /nm	Excited at λ_{Soret}		Φ_{fl}^a / %	τ /ns	$\lambda_{\text{TPA}}^{\text{max}}$ /nm	σ_2^{max} [GM] ^b
				Q (0,0)	Q (0,1)				
TPP	-	417	513, 548, 589, 646	650	714	11	8,6	790	11 ^c
OOFP	263	423	516, 551, 592, 652	652	718	13	7,5	790	45
SOFP	270	423	517, 552, 590, 647	652	715	14	-	790	75

^a Fluorescence quantum yield determined relative to TPP in toluene, upon excitation at the Soret band.

^b Intrinsic TPA cross-sections measured by TPEF in the femtosecond regime; a fully quadratic dependence of the fluorescence intensity on the excitation power is observed and TPA responses are fully non-resonant.

^c Data from literature [4].

3.1.1.2 Conjugated porphyrin dendrimers

In 2016, our laboratory reported a group of TPP cored porphyrin dendrimers: **TPP1-TPP6**. These were synthesized by a convergent route ^[5] and were intended to show improved optical properties. The entire range of these compounds is shown in Figure 3.1.2.

The *meso*-phenyl units of the TPP core provide two positions, *para* and *meta*, that can easily be modified to carry functionalization. TPP-based porphyrin dendrimers that feature fluorenyl dendrons in these positions were targeted and their optical properties (absorption and emission) were studied. These porphyrin dendrimers could be categorized into *para*-substituted (**TPP1**, **TPP2** and **TPP3**) and *meta*-substituted (**TPP4**, **TPP5** and **TPP6**) classes, whose different dendrons allow the number of attached terminal fluorenyl arms to be varied from four to sixteen.

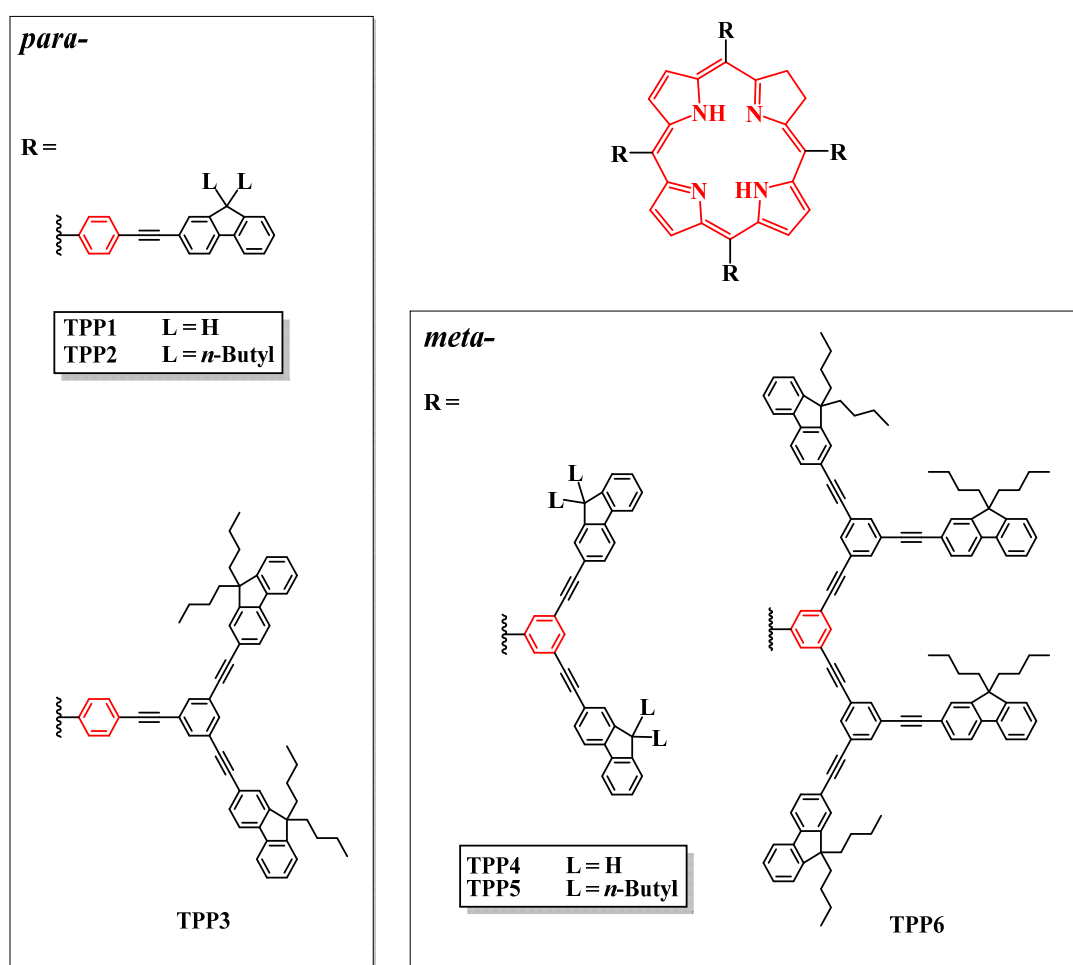


Figure 3.1.2 The entire structures of porphyrin dendrimers: TPP1-TPP6

The photophysical properties of **TPP1-TPP6** are listed in Table 3.1.2. In the UV-Visible spectra, these TPP based porphyrin dendrimers present red shifts for the Soret bands relative to **TFP** (data listed in Table 3.1.1), and also red-shifted Q-bands. The dendron absorption of **TPP1-TPP6** in the UV region also presents red shifts. The quantum yields of these conjugated porphyrin dendrimers are greater than those of **TFP**.

The non-substituted **TPP1** and **TPP4** are not soluble enough to allow TPEF measurements but the σ_2 of the other dendrimers (**TPP2**, **TPP3**, **TPP5** and **TPP6**) were measured using the experimental methods of Xu and Webb [6]. It can be seen that all the σ_2 values are greater than in **TFP**, as well as two to four times larger than the value of 90 GM found in **TFP**.

Table 3.1.2 Photophysical properties of dendrimers TPP1-TPP6 in dilute CH₂Cl₂ at 298K

	UV-visible absorption /nm ^a			Emission /nm ^a		Φ_f^b /%	τ^c /ns	λ_{TPA} /nm	σ_2 [GM]
	$\lambda_{Dendron}$	λ_{Soret}	λ_{Qbands}	Excited at λ_{Soret} Q(0,0)	Q(0,1)				
TFP	-	426	519,557,593,649	663	730	24	-	790	90
TPP1	320	426	518,554,592,650	656	722	20	9.8	-	-
TPP2	324	426	518,555,592,650	657	722	20	9.8	790	380
TPP3	330	425	520,555,592,650	655	721	19	9.7	790	190
TPP4	324	427	517,552,589,646	651	718	13	10.7	-	-
TPP5	326	427	517,552,589,646	650	718	11	10.8	790	200
TPP6	327	427	517,552,590,646	651	716	13	10.7	790	290

^a Experiments were achieved in distilled CH₂Cl₂ with the UV-visible absorption region from 250 to 800 nm and emission region from 300 to 800 nm.

^b Experiments for fluorescence quantum yields were achieved in distilled toluene by Soret band (426 nm) excitation.

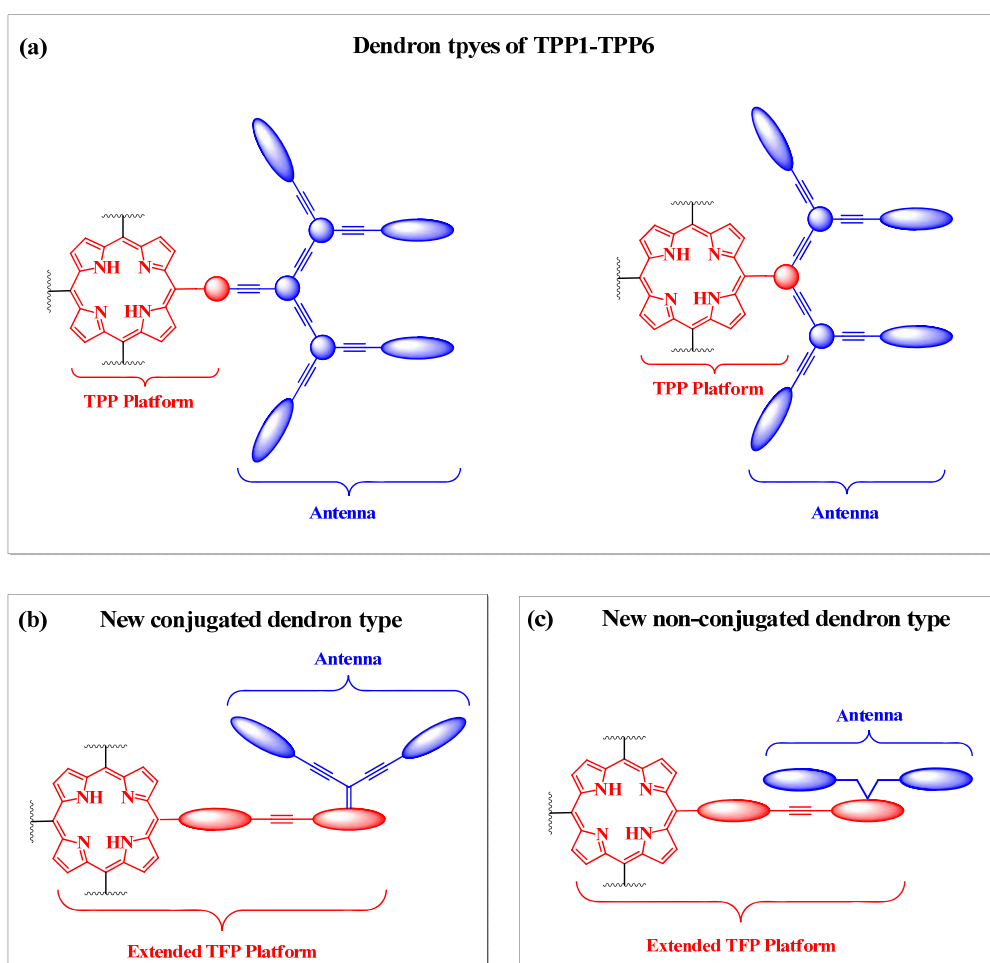
^c Fluorescence lifetime was measured in dilute toluene, using pulsed excitation at 426 nm.

3.1.2 The target porphyrin dendrimers

In this chapter, we will exploit these previous results in the design of two new dendrimer classes that have different substitution patterns (Scheme 3.1.1).

The antennae of new conjugated dendrons are connected to the porphyrin platform as shown in Scheme 3.1.1(b). Their structure means that they are more rigid than the dendrons of the former series of **TPP1-TPP6** (Scheme 3.1.1(a)).

In contrast, the new non-conjugated antennae take the form given in Scheme 3.1.1(c). This type of dendron is more flexible. The elaboration of these two new types of conjugated and non-conjugated dendrons is detailed below, along with two models: **Model 1 (25)** and **Model 2 (29)**. These models assist in the understanding of the photophysical properties of the new series of porphyrin dendrimers.



Scheme 3.1.1 Comparison of TPP1-TPP6 type of dendrons (a) and New conjugated (b) or Non-conjugated (c) types of dendrons

We designed and synthesized two new bromo dendrons **26** and **30**, which provide the new conjugation pathways described in Scheme 3.1.1(b) and (c). Their complete structures are shown in Figure 3.1.4.

It can be seen that the new conjugated dendron **26**, which is substituted in the 9 position by a unique double bond and then connected to two substituted fluorenyl antennae by triple bonds, is totally conjugated. It therefore shows a structure that is entirely planar except for the four butyl chains.

In contrast, the non-conjugated dendron **30** has a tetravalent carbon in the 9 position, so that the antennae present at the methylene groups of (2-methyl)-9,9-dibutyl-fluorene lie on opposite sides of the fluorene plane. As a consequence, the structure of this dendron is flexible about the 9 position.

The two bromo-dendrons **26** and **30** are not adapted to Energy Transfer (ET), so the corresponding **Model 1** and **2** were prepared to provide an understanding of the photophysical behavior of this new series of porphyrin dendrimers, particularly with respect to ET. As shown in Figure 3.1.4, these two models have identical structures except for the bromo and hydrogen substituents in the 2 position.

We performed preliminary studies of ET from donor **Models 1** and **2** toward the acceptor **tetra-alkynyl TFP (17)** core, so as to understand their optical properties and aid in the design of new dendrimers. Figure 3.1.5 shows the UV-visible absorption spectrum **17** and the emission spectra of the **Model 1** and **2**. The corresponding photophysical data are listed in Table 3.1.3.

In the UV-visible absorption spectrum of **Tetra-alkynyl TFP (17)** (solid line), the fluorenyl absorption band appears at 292 nm in UV region; the intense Soret band is at 428 nm, and the four Q-bands range at 500-700 nm. In the emission spectra, the conjugated **Model 1** was excited at 410 nm; after this excitation, **Model 1** exhibits a broad emission band in the region of 410-700 nm (dashed line). This band overlaps with the Soret band and Q-bands absorption of **17** (in red shadow), which suggests that ET from dendron **26** towards the porphyrin core might be efficient.

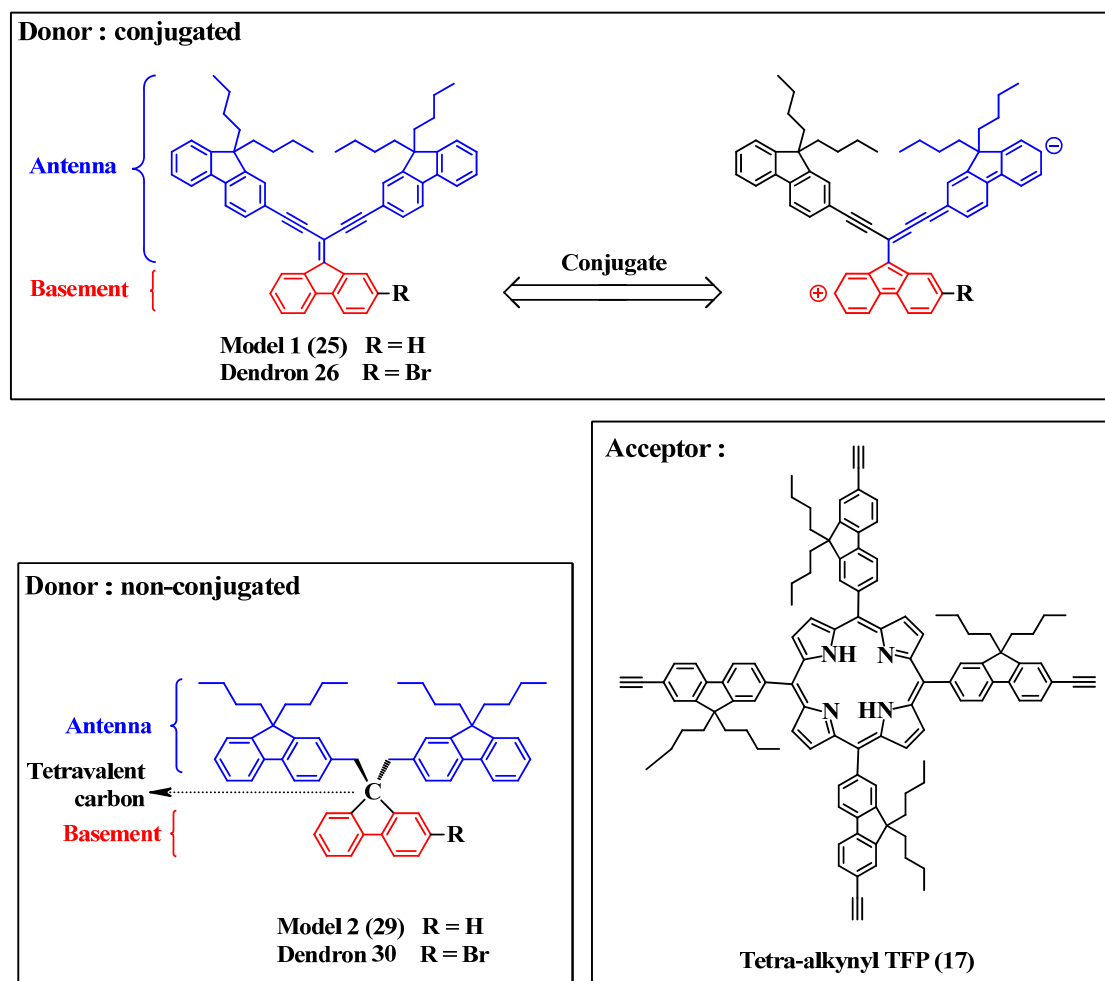


Figure 3.1.4 Molecular structure of two new dendrons (26, 30) and the corresponding Models (1, 2) and tetra-alkynyl TFP (17)

Secondly, we excited **Model 2** at 274 nm under the same conditions as those for the excitation of **Model 1**. The narrow emission band that was obtained (dash dot line) has a partial overlap with the dendron absorption band of **Tetra-alkynyl TFP (17)** (in blue shadow), which means that energy transfer from this dendron to the porphyrin core of **17** is also promising.

Encouraged by these results, the fully elaborated dendrons (**26** and **30**) that correspond to models (**1** and **2**) were connected by ethynyl chains to the high fluorescence core –TFP ($\Phi_{fl} = 24\%$). The optical properties, energy transfer behavior and two photon absorption properties of the products are studied in this chapter.

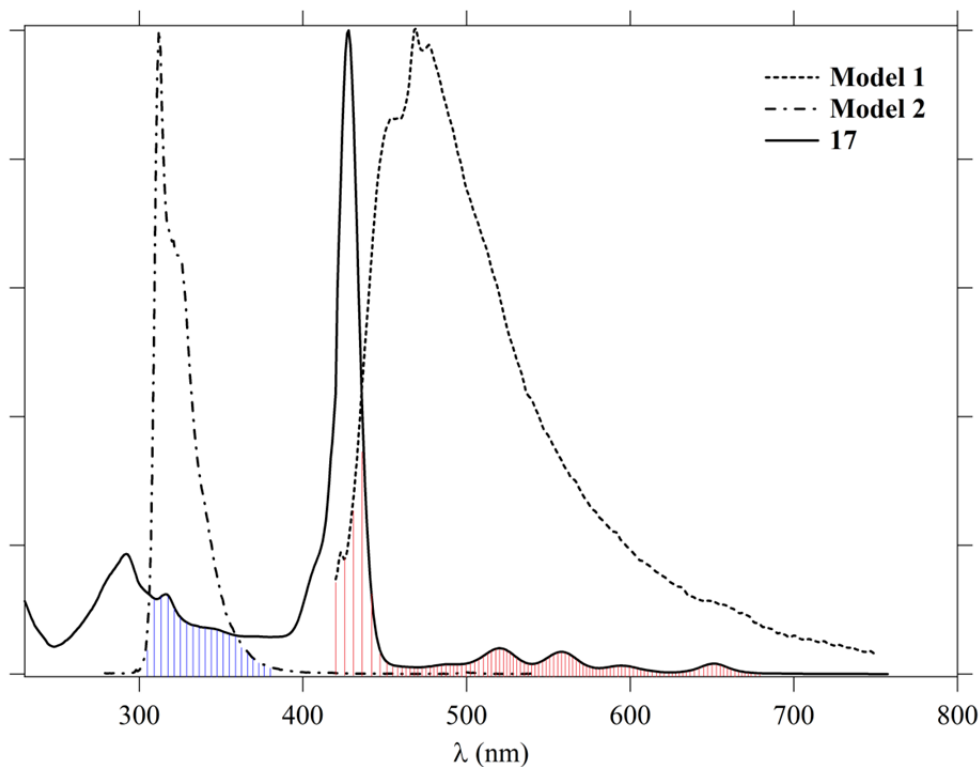


Figure 3.1.5 The UV-visible absorption spectrum of Tetra-alkynyl TFP (17) and the emission spectra of Models 1 and 2

Table 3.1.3 UV-Visible absorption data of Tetra-alkynyl TFP (17), Model 1 and Model 2 in DCM

Tetra-alkynyl TFP (17)	$\lambda_{\text{abs}}^{\text{dendron}}$ /nm	292	Model 1	$\lambda_{\text{max}}^{\text{dendron}}$ /nm	410
	$\lambda_{\text{abs}}^{\text{Soret}}$ /nm	428		λ_{em} /nm	469
	$\lambda_{\text{abs}}^{\text{Q-bands}}$ /nm	520, 558, 694, 651	Model 2	$\lambda_{\text{max}}^{\text{dendron}}$ /nm	274
				λ_{em} /nm	312

3.2 Syntheses of the new series of porphyrins

For synthesizing the new dendrimers, the successful Lindsey Method ^[7,8] and Sonogashira coupling reaction ^[9] strategies were used to form the precursors and models. The syntheses involve two steps.

3.2.1 The precursor formations

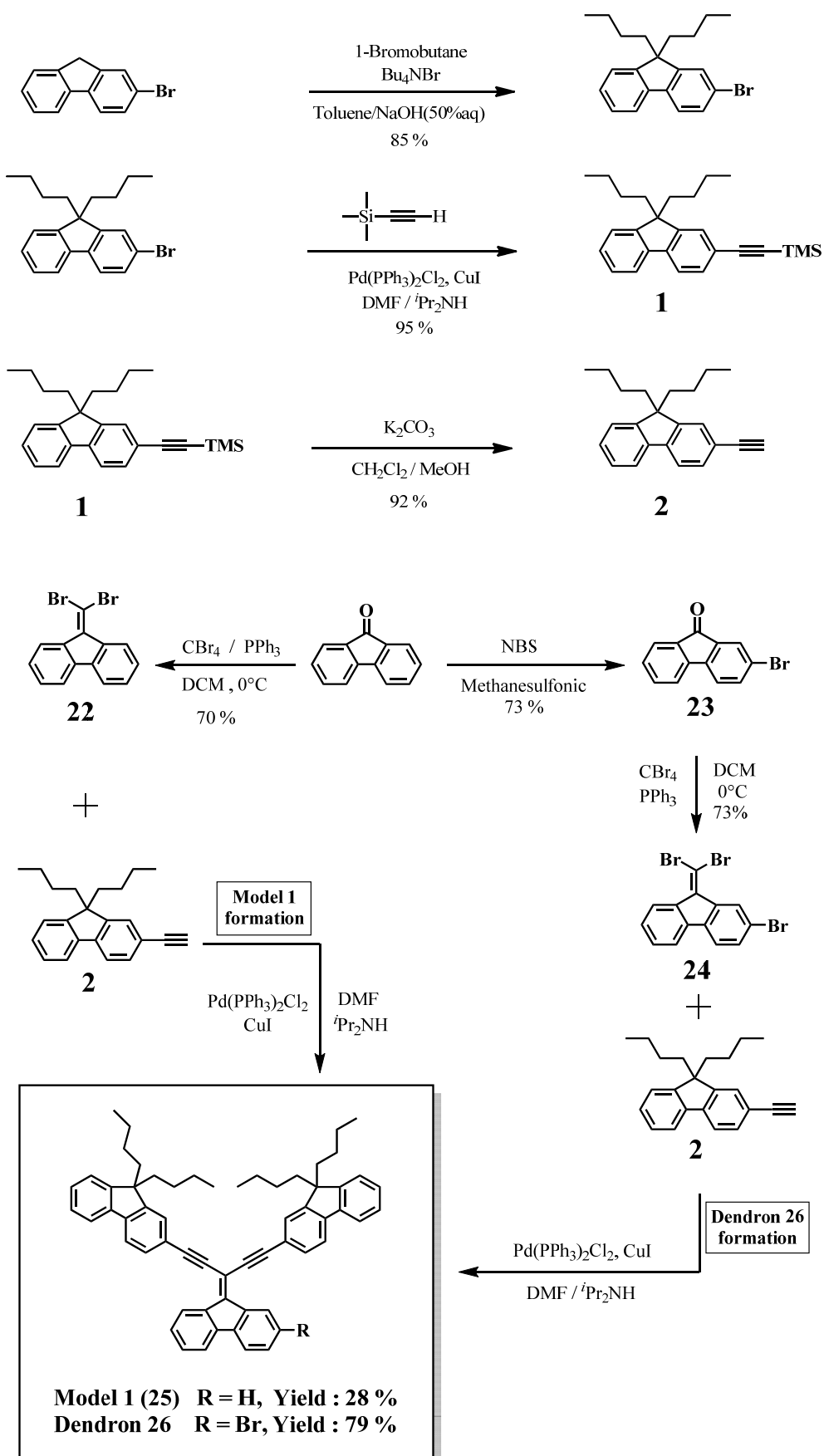
3.2.1.1 Conjugated dendron **26** and corresponding **Model 1**

The detailed syntheses of conjugated **Model 1** and dendron **26** are shown in Scheme 3.2.1. It can be seen that the final conjugated products, which connect two fluorenyl arms to the 9 position of 2-bromofluorene, were formed essentially by repetitive Sonogashira couplings.

Firstly, to improve solubility, *n*-butyl groups were added in 9 position of 2-bromofluorene to provide **2-bromo-9,9-dibutyl-fluorene** in a yield of 85 %. Then we used a Sonogashira coupling with ethynyltrimethylsilane to obtain compound **1**, whose alkyne is protected by a TMS group (yield 95%). Deprotection with K₂CO₃ in a MeOH/CH₂Cl₂ mixture then allowed isolation of the 9,9-dibutyl-2-ethynyl-fluorene (compound **2**) product in a yield of 92%.

Subsequently, commercial fluorenone was treated with N-bromosuccinimide (**NBS**) to form compound **23** in 73% yield, and further reaction with *in situ* formed dibromomethylenephosphorane (CBr₄/PPh₃) allowed **24** to be prepared. In a similar reaction, compound **22** was obtained by direct methylenation of fluorenone. The yields for these reactions were 70% and 73% respectively.

Finally, by connecting two equivalents of alkyne **2** to fluorene **22** and **24**, the **Model 1 (25)** and the new conjugated dendron **26** were synthesized successfully in yields of 28% and 79%, respectively.



Scheme 3.2.1 Syntheses of the new conjugated dendron 26 and corresponding Model 1

3.2.1.2 Non-conjugated dendron **30** and corresponding **Model 2**

The synthetic methods used previously for obtaining compound **28** and dendron **30** were selected from three possibilities.

Each of these different methods have been evaluated for the synthesis of the desired compound **28**, and the results for methods I, II and III are reported in Table 3.2.1. Reagents CBr₄, HBr and NBS are acting as the bromine source respectively, and in method II, HBr (48% aq.) is also the solvent [10-12]. These three reactions are performed at around 0.3 mmol/mL (calculation from reagent **27**, shown in Scheme 3.2.2), and they gave yields of 31%, 60% and 86% respectively. Method **III** was therefore chosen for synthesis of compound **28** because of the high yield of 86%.

Table 3.2.1 Comparison of three synthesis methods of compound 28

Method	Solvent ^a		Equivalent ^b	T / °C	t / min	yield / %	
I	CBr ₄	PPh ₃	THF	1.2 / 1.2	0	195	31
II	HBr		—	1.2	53	180	60
III	NBS	PPh₃	THF	1.1 / 1.1	0	60	86

^a distilled solvent; ^b calculation from reagent **27**

As listed in Table 3.2.2, three paths were also compared to obtain the desired dendron **30**. Method IV constitutes the classical way of connecting the butyl chains to the fluorenyl 9 position for improving the solubility. Unfortunately, this method failed, as did method V. Method VI (stirring under mild conditions) gave a good yield, 77% [5,13,14], so this last method was used to synthesize dendron **30**.

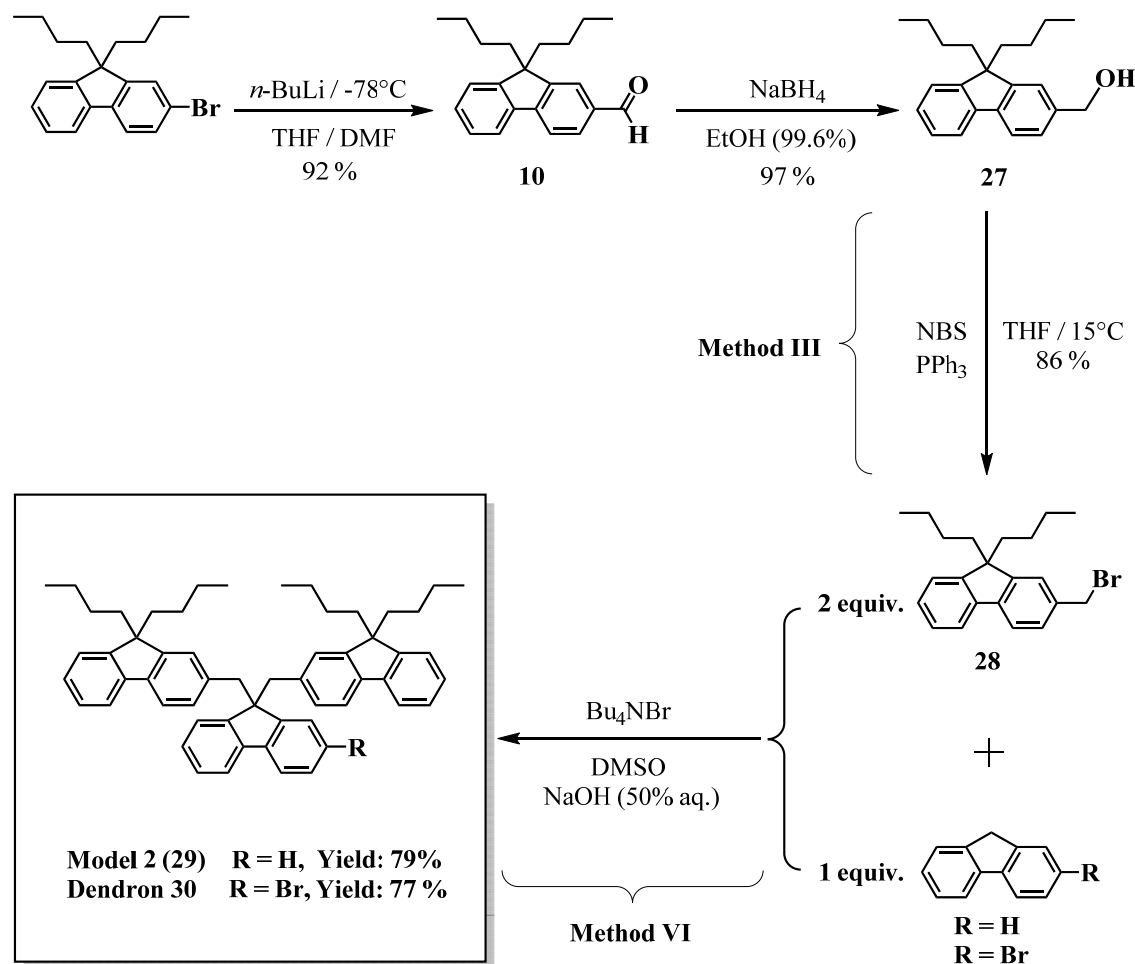
Table 3.2.2 Comparison of three synthesis methods of dendron 30

Method	Solvent ^a	Catalyst	Equivalent ^b	T / °C	t / h	yield / %
IV	Toluene	Bu ₄ NBr	1.6	60	18h	—
V	DMSO	<i>t</i> -BuOK	3	50	12h	—
VI	DMSO	Bu₄NBr	0.1	R.T.	3h	77

^a technical solvents; ^b calculation from 2-bromofluorene

The selected synthesis pathways are summarized in Scheme 3.2.2. In detail, compound **10** is formed from the reaction of **2-bromo-9,9-dibutyl-fluorene** and *n*-BuLi in THF, followed by DMF, the yield is 92%. Then **10** was reduced to obtain **27** and, after bromination, compound **10** is isolated, with the yield for these two steps being 82%.

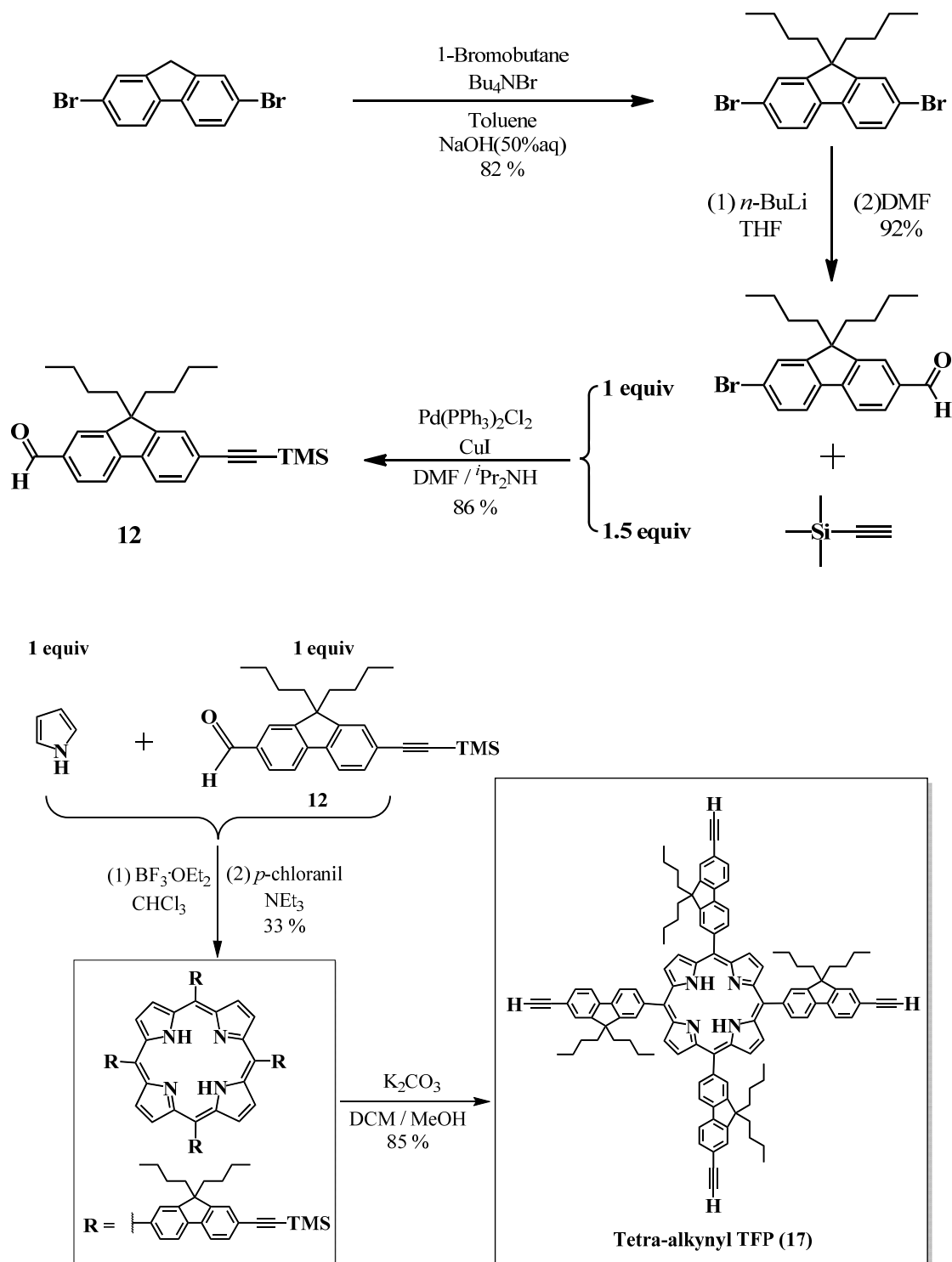
For synthesizing the non-conjugated **Model 2 (29)** and dendron **30**, two fluorenyl units bridged by methylene chains to 9 position of a fluorene are achieved, with the yield of 79% and 77%, respectively.



Scheme 3.2.2 Synthesis of the new non-conjugated dendron **30** and corresponding **Model 2**

3.2.1.3 Tetra-alkynyl TFP (17) formation

For the synthesis of the desired porphyrins, it is clearly necessary to have the required aldehyde, so we prepared compound **12** over three steps in 53% overall yield (as shown in Scheme 3.2.3).

Scheme 3.2.3 Syntheses of Tetra-alkynyl TFP (**17**)

Lindsey conditions for condensation with pyrrole then allowed the TMS protected porphyrin to be isolated by chromatography in 33% yield. After deprotection, the desired **Tetra-alkynyl TFP (17)** is obtained with a yield of 85%.

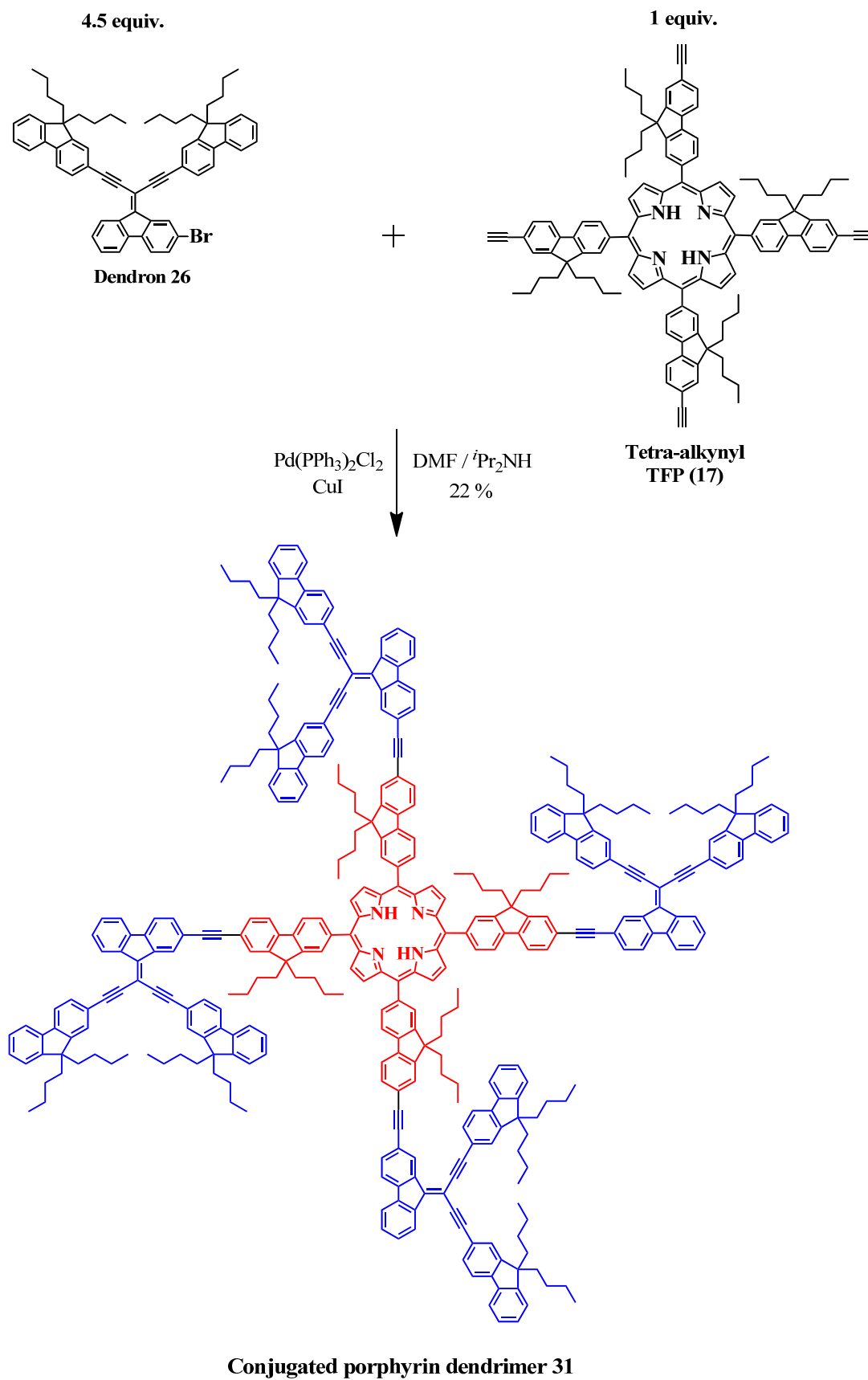
3.2.2 New porphyrin dendrimers formation

Once the new building blocks, having conjugated dendron **26**, the non-conjugated dendron **30** and the **tetra-alkynyl TFP (17)** had been prepared, we could start assembling them to obtain our target porphyrin dendrimers.

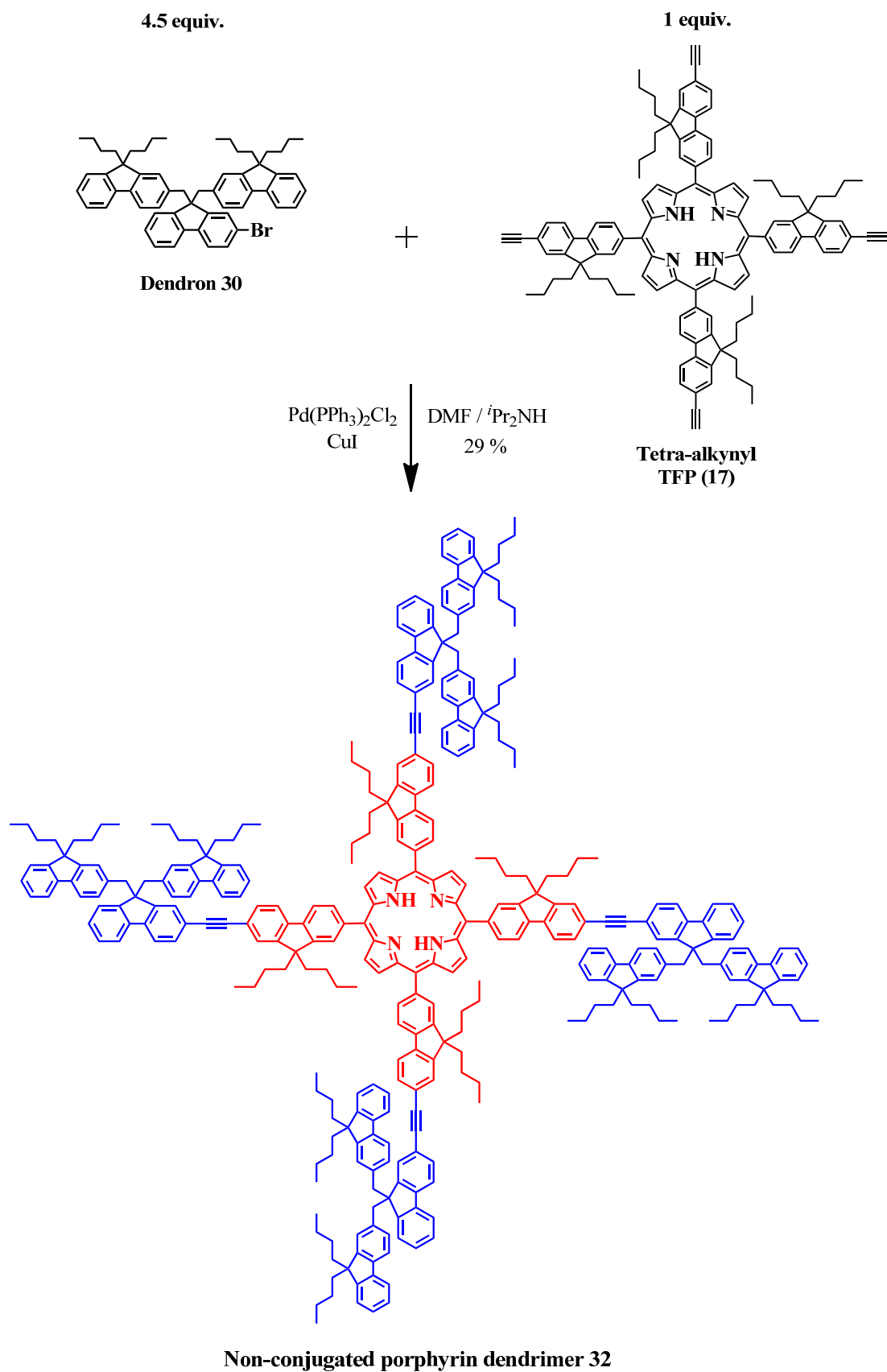
As shown in scheme 3.2.4, the two porphyrin dendrimers **31** and **32** were obtained using similar Sonogashira coupling conditions. In this named reaction, Pd(PPh₃)₂Cl₂ and CuI were chosen as the catalyst system, ⁱPr₂NH as the base and DMF as the solvent.

Then the reacting mixture was degassed by two freeze-pump-thaw cycles. Because CuI is light-sensitive, the system was covered by aluminum foil. Finally, the mixture was heated in an oil bath at 95 °C for at least 72h, with monitoring by TLC until the starting material disappeared.

Under the conditions described above, the conjugated and non-conjugated porphyrin dendrimers **31** and **32** were synthesized in yields of 22% and 29% respectively.



- Assembling of dendron **26** and tetra-alkynyl TFP (**17**) to conjugated porphyrin dendrimer **31**



- Assembling of dendron 30 and tetra-alkynyl TFP (17) to non-conjugated porphyrin dendrimer 32

Scheme 3.2.4 Assembling of new porphyrin dendrimers 31 and 32

3.3 ^1H NMR analyses

3.3.1 The dendrons and the models

As the final substituents, compound **2** is studied by ^1H NMR in CDCl_3 (400MHz) as were its intermediates. On the ring, the two butyl chains that substitute the fluorenyl 9 position to increase solubility (Figure 3.3.1) are well identified by the multiplets from 0 to 2.5 ppm; as can be seen in the magnified section of the alkyl region of **2-bromo-9,9-dibutyl-fluorene** (frame a'). The peaks corresponding to aromatic protons are found between 7.3 to 7.7 ppm. These peaks are all similar to those of compounds **1** and **2**. Compound **1** was formed by substitution of bromo by ethynylTMS, and this last group appears as the anticipated strong singlet around 0 ppm for the nine protons of CH_3 . After deprotection, compound **2** was purified on a short silica column. As anticipated, the TMS singlet completely disappeared, and was replaced by another singlet at 3.2 ppm that corresponds to the terminal H of the triple bond.

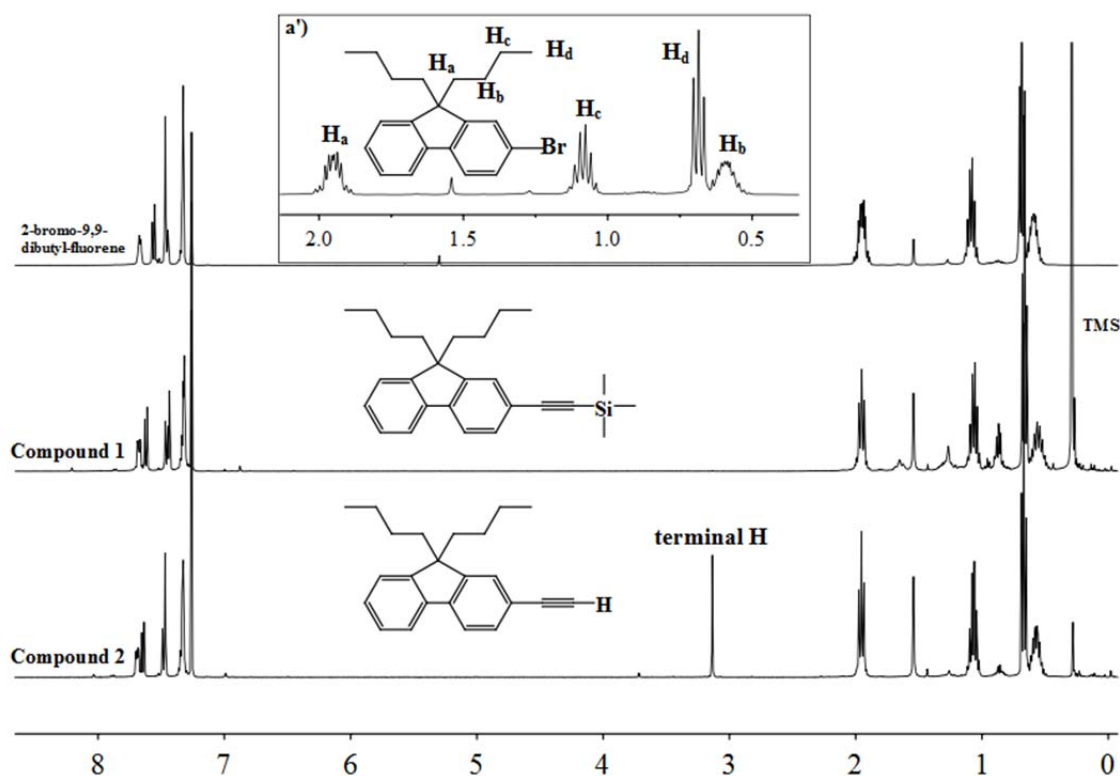


Figure 3.3.1 Complete ^1H NMR spectra of compounds **1** and **2** in CDCl_3

Figure 3.3.2 provides comparative partial ^1H NMR spectra of **9-fluorenone**, compound **22** and **Model 1 (29)**. The **9-fluorenone** starting material is transformed into compound **22** by exchanging oxygen for carbon. The presence of the two bromo atoms in **22** causes a large shift in the peaks of protons 4 and 5 to low field from 7.6 to 8.6 ppm. Two further fluorenyl antennae were then connected to **22**, to provide **Model 1**. For this new compound, only the doublets of protons 4 and 5 could be clearly identified. The other peaks overlap in the 7.3 to 7.5 ppm and 7.6 to 7.9 ppm regions, but can be identified by comparison to the previous spectra.

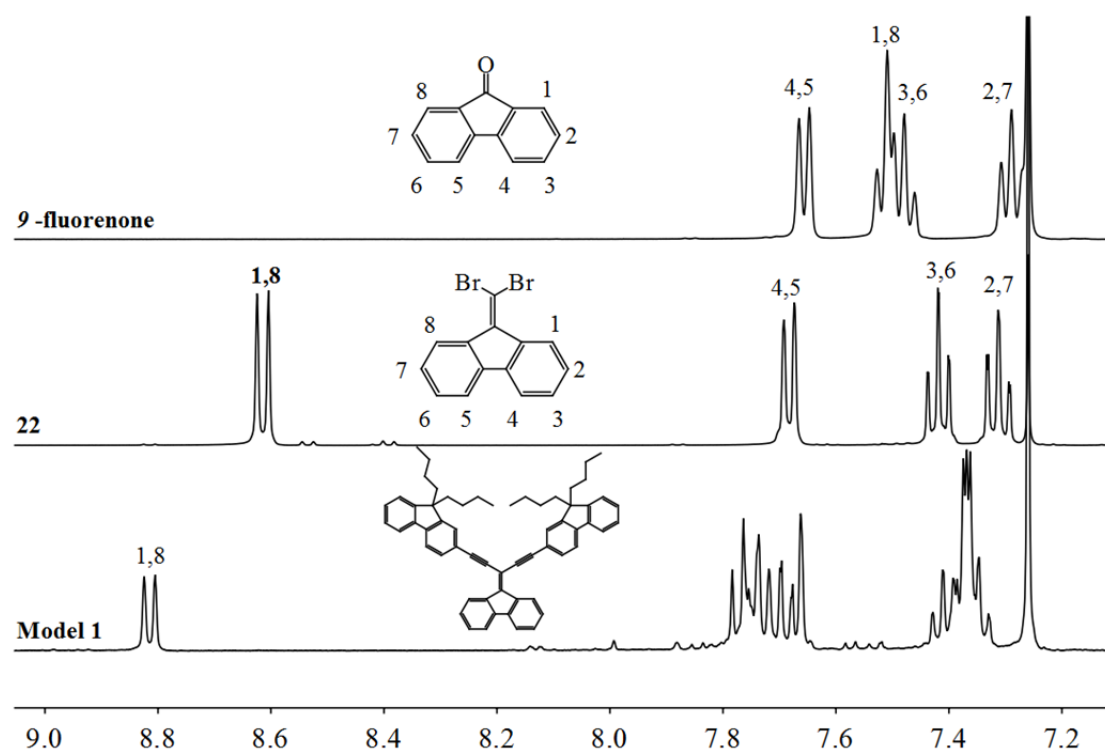


Figure 3.3.2 Partial ^1H NMR spectra of **9-fluorenone**, compound **22** and **Model 1** in CDCl_3

Finally, the corresponding dendron **26** was synthesized in the same way as **Model 1**, and a comparison of partial ^1H NMR spectra for pertinent compounds is shown in Figure 3.3.3. In the first step, the product 2-bromo-fluorenone and 2,7-dibromo-fluorenone have similar polarity and this causes problems during separation (as shown in Figure 3.3.3, TLC in P.E./THF = 100:1). However, a reasonable quantity

of desired product **23**, containing small quantities of impurity, could be obtained after repeated chromatography on fine silica. The spectrum of the product is shown in Figure 3.3.3, with small peaks due to of impurities shown in frames. We also obtained the tribromo compound **24**, which provides the potential for preparing molecules such as those shown in Figure 3.3.4. Fortunately we were able to collect pure dendron **26**.

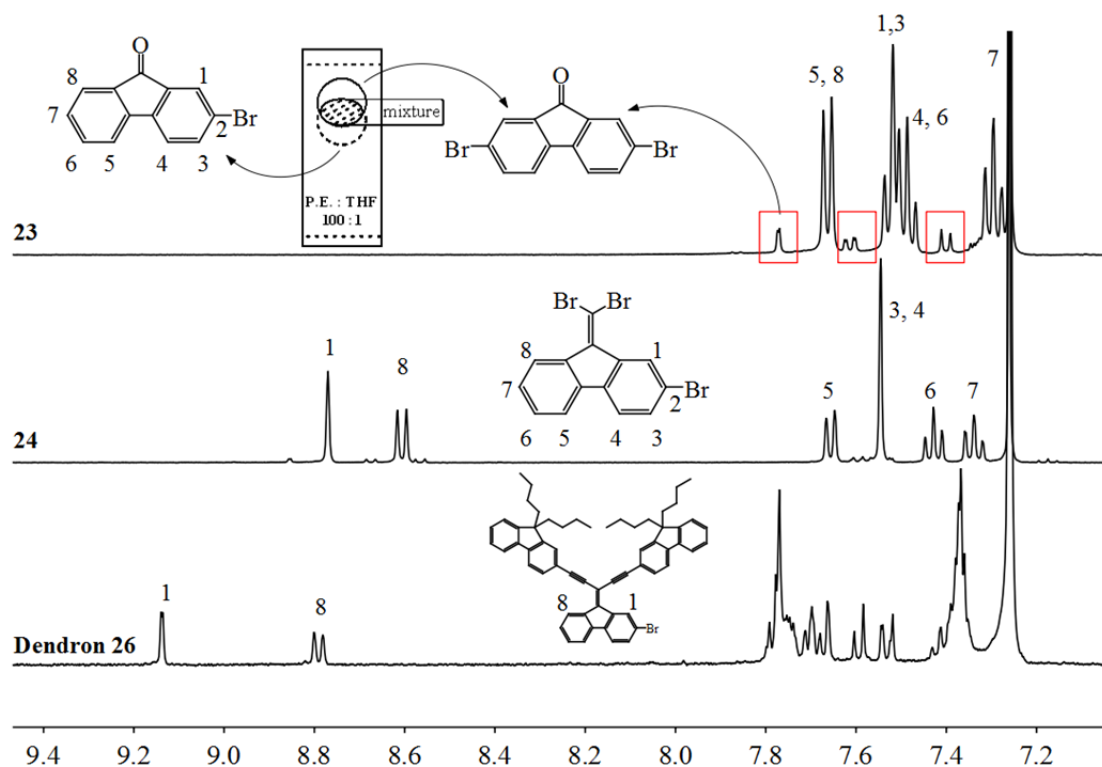


Figure 3.3.3 ^1H NMR spectra of compound **23**, **24** and dendron **26** in CDCl_3

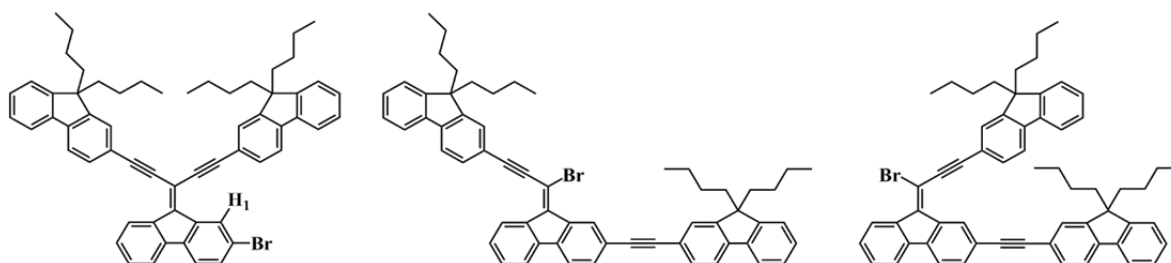


Figure 3.3.4 Three potential molecular structures possibly obtained as side-products during formation of dendron **26**

Figure 3.3.5 shows a comparison of the complete ^1H NMR spectra of compounds **10**, **27** and **28**. Compound **10** contains an aldehyde group which is characterized by a single peak at 10 ppm. This aldehyde was reduced to the corresponding alcohol in **27**, whose methylene group shows a typical triplet (in blue line) at 1.68 ppm. The protons of methylene bridge connecting the fluorenyl and alcohol functionalities appear at 4.8 ppm as a doublet (in red), whereas they appear as a singlet upon transforming the OH functionality to Br in compound **28**. As expected, the typical triplet of OH disappeared in the last NMR spectrum. The aromatic and butyl chains are all well-identified and lie in the range from 7.3-8.0 ppm and 0.5-2.5 ppm respectively.

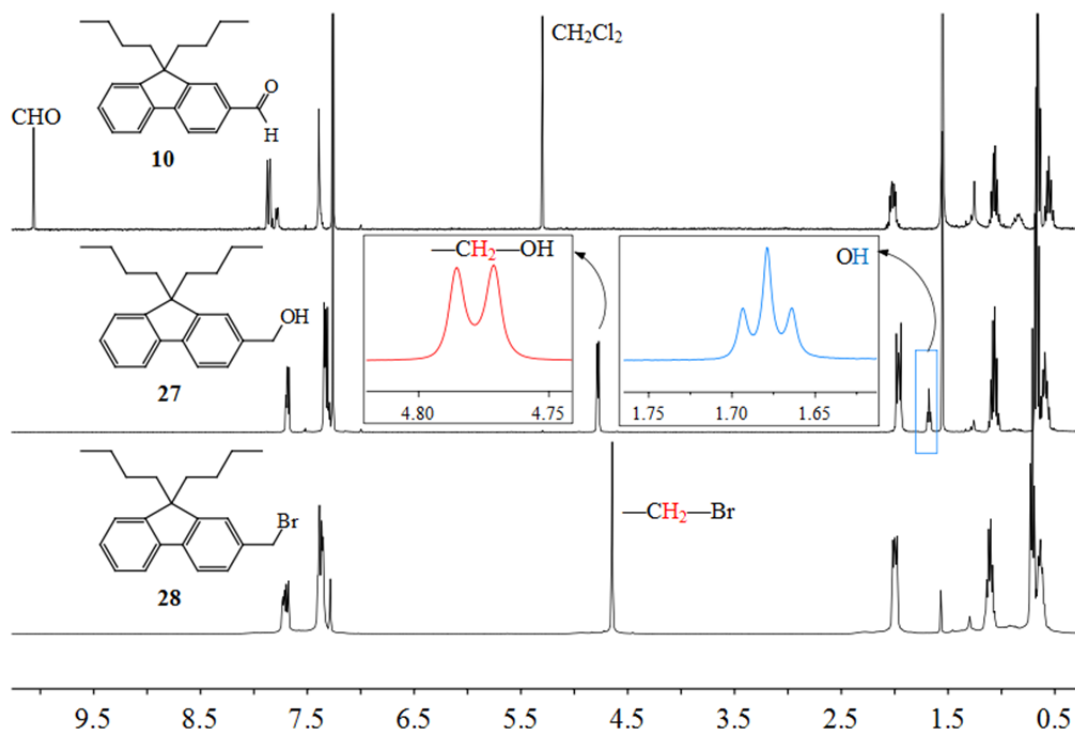
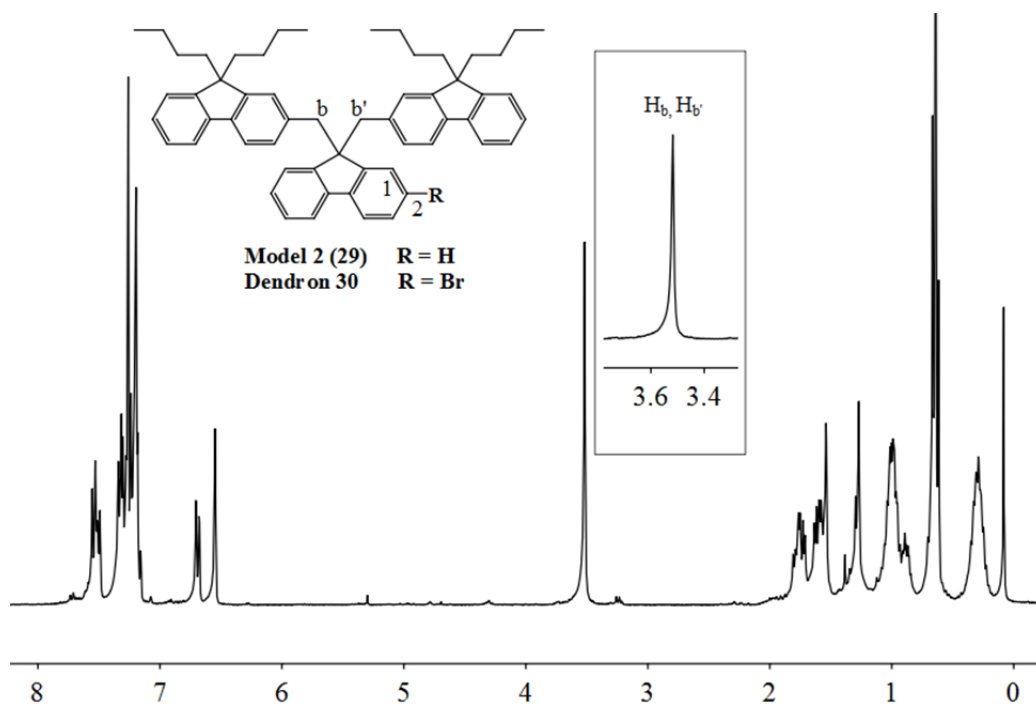


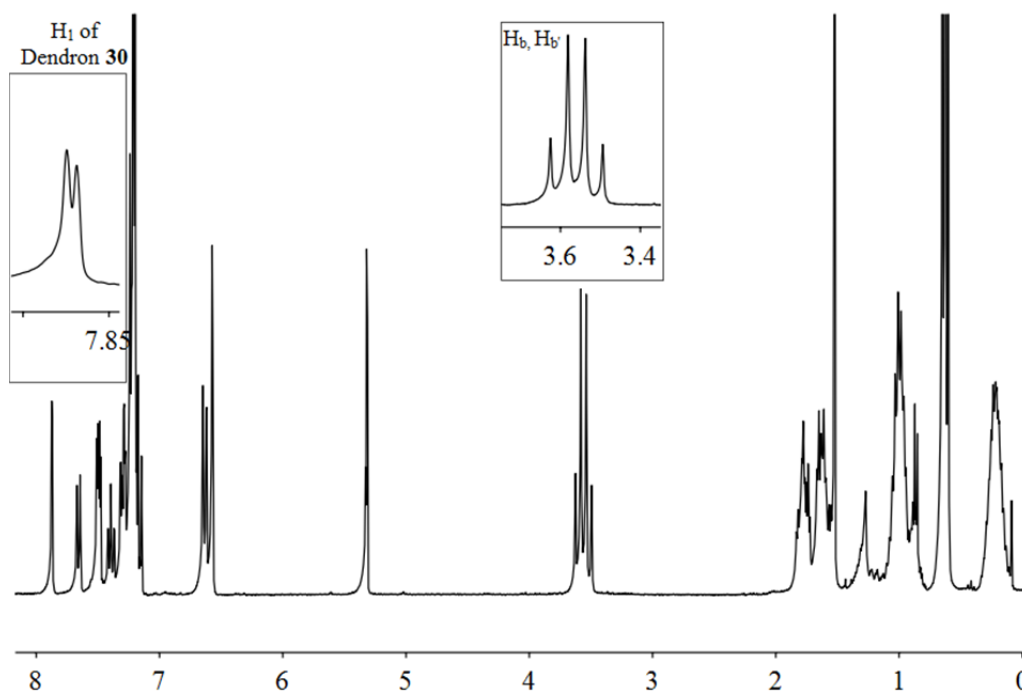
Figure 3.3.5 Complete ^1H NMR spectra of compound **10**, **27** and **28** in CDCl_3

The spectrum of **Model 2** presents a very complex profile in Figure 3.3.6(a), but the two methylene bridges (**Model 2**, $\text{H}_{b,b'}$) appear clearly as a singlet at 3.5 ppm due to their symmetrical structure. After introducing the bromo substituent in the 2 position of fluorenyl (shown in Figure 3.3.6 (b)), the symmetry is modified, so the $\text{H}_{b,b'}$ peaks of dendron **30** present a well-defined multiplet ranging from 3.4 to 3.6 ppm. The protons of the aromatic and butyl chains could be identified; H_1 of the fluorenyl functionality is

notable and appears at 7.9 ppm as a sharp doublet ($^4J = 1.6$ Hz) because of the presence of the bromo substituent.



(a) ^1H NMR spectrum of **Model 2** in CDCl_3



(b) ^1H NMR spectrum of dendron **30** in CD_2Cl_2

Figure 3.3.6 Comparison of ^1H NMR spectra of Model 2 and dendron 30

3.3.2 Porphyrins

3.3.2.1 Tetra-alkynyl TFP precursor

The complete ^1H NMR spectrum of **Tetra-alkynyl TFP (17)** is shown in Figure 3.3.7. As usual, the singlet of eight β -pyrrolic protons appears at 8.9 ppm. The fluorenyl protons are seen clearly between 7.5 and 8.5 ppm, and the protons of the 1, 3, 4, 5, 6 and 8 positions are assigned in Figure 3.3.7. The four terminal H appear as a singlet at 3.2 ppm, the two NH protons are characterized by a singlet at -2.6 ppm, and butyl chains are identified in alkyl region (0.5-2.1 ppm).

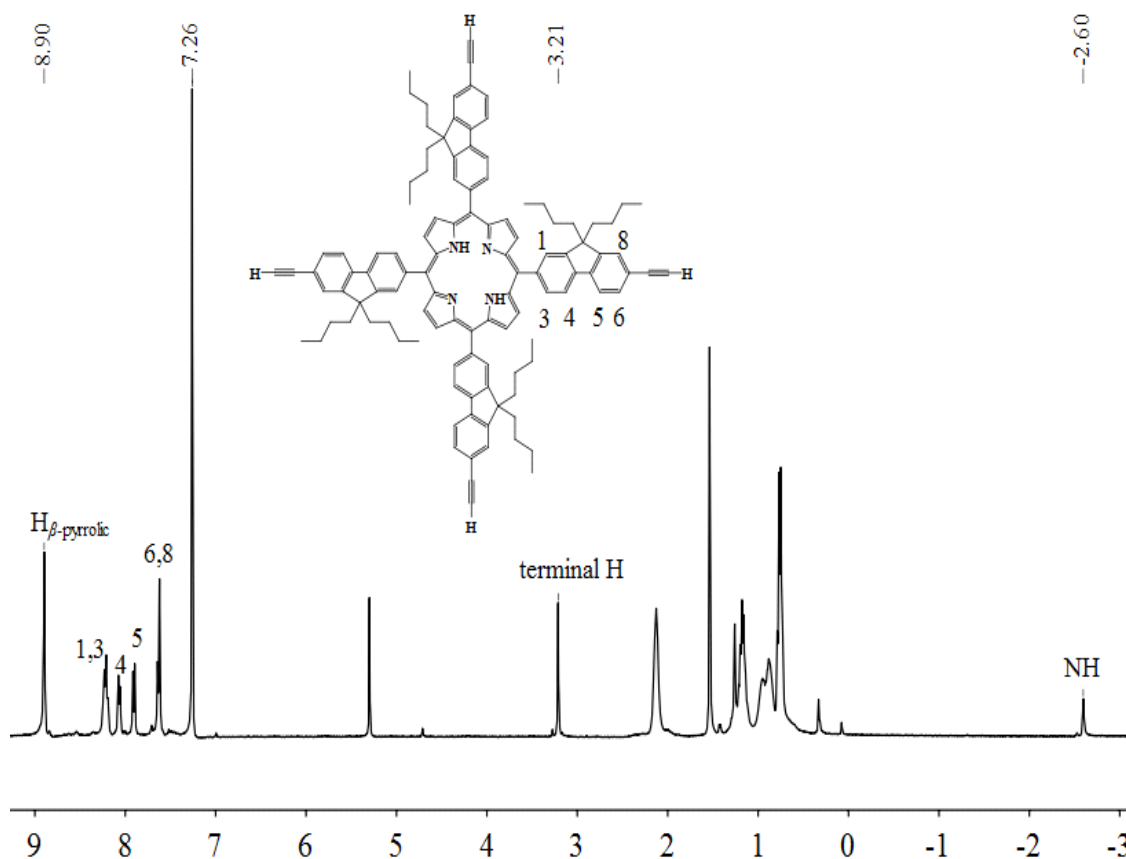


Figure 3.3.7 ^1H NMR spectrum of tetra-alkynyl TFP (17) in CDCl_3

3.3.2.2 New porphyrin dendrimers

The new porphyrin dendrimers **31** and **32** were characterized by ^1H NMR. Firstly: the partial comparative spectra are shown in Figure 3.3.8. The peaks around 9.0 ppm correspond to the eight β -pyrrolic protons of the TFP core. For dendrimer **31**, the four H_1' derived from the dendron **26** (see Figure 3.4.1) are attributed to the singlet at 9.2 ppm. In the aromatic zone, the peaks overlap strongly because of the large number of fluorenyl arms in these Dendrons.

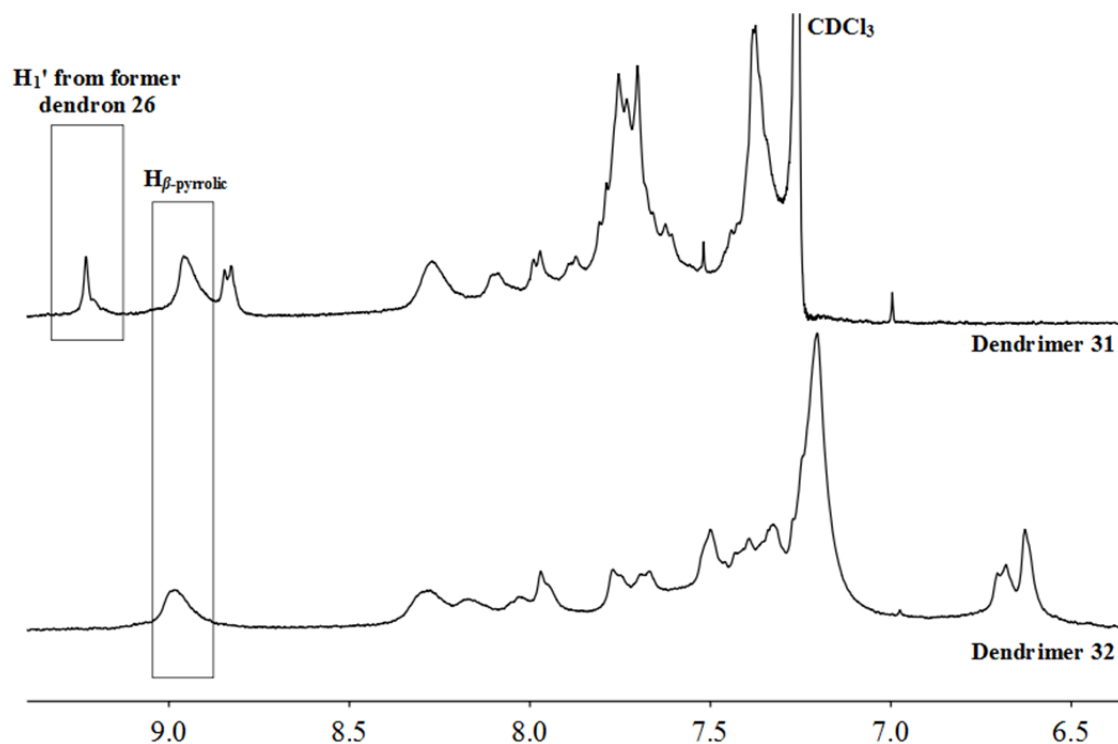
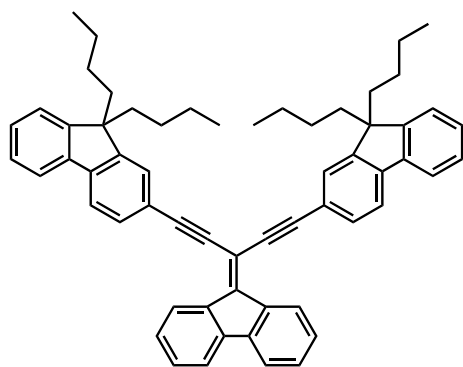


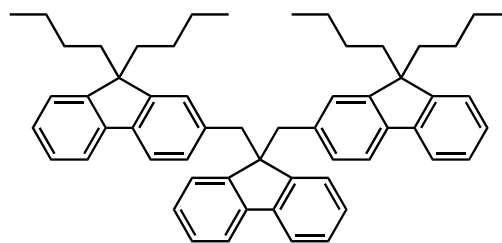
Figure 3.3.8 Partial ^1H NMR spectra of new porphyrin dendrimers **31** and **32**

3.4 Optical properties

To better understand the optical properties, the photophysical spectra of porphyrin dendrimers **31** and **32** are measured, and compared to the reference compounds: **TFP-Bu**, **Model 1** and **Model 2**. The full structures of the porphyrins and the model compounds under study are summarized in Figure 3.4.1 and their optical properties data are listed in Table 3.4.1.



Model 1 (25)



Model 2 (29)

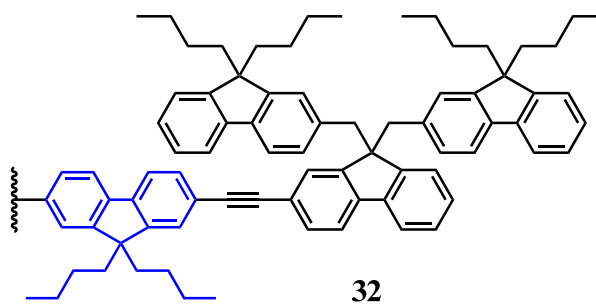
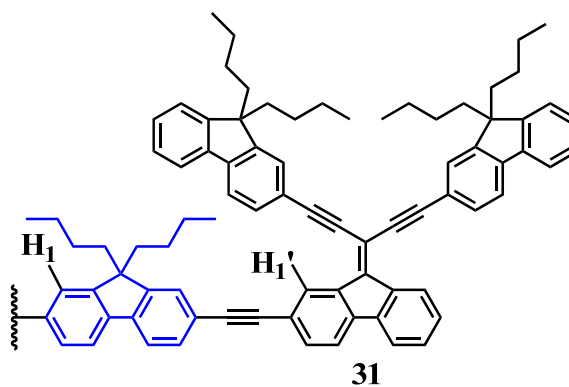
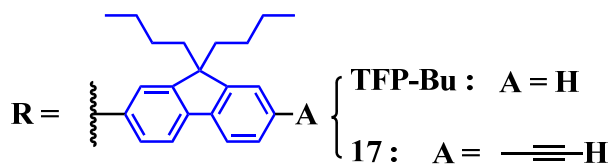
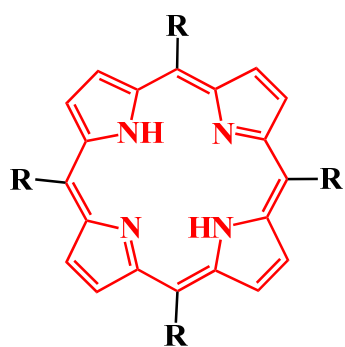


Figure 3.4.1 Structures of Model 1 and 2, TFP-Bu, tetra-alkynyl TFP 17 and new porphyrin dendrimers 31 and 32

Table 3.4.1 Photophysical data of Model 1, Model 2, TFP-Bu, 17 and new dendrimers 31 and 32 in CH₂Cl₂ at R.T.

	UV-visible absorption ^a /nm			Emission /nm		Φ_{fl} / %	τ ^c /ns
	λ_{abs}^{1st}	λ_{abs}^{2nd}	λ_{abs}^{3rd}	excited at λ_{abs}^{1st}			
Model 1	275	410	323	469		-	-
Model 2	274	308	-	312		-	-
	$\lambda_{dendron}$	λ_{Soret}	$\lambda_{Q-bands}$ /nm	excited at λ_{Soret} /nm			
	/nm	/nm		Q (0,0)	Q (0,1)		
TPP	-	417	513, 548, 589, 646	653	721	11 ^b	8,6
TFP-Bu	-	426	519, 555, 592, 652	660	724	18 ^d	8.2
17	292	428	520, 558, 594, 652	660	724	19 ^d	8,2
31	325	430	521, 557, 593, 652	660	726	17 ^d	8.0
32	309	430	524, 555, 591, 652	660	725	12 ^d	7.1

^a Experiments were made in distilled CH₂Cl₂ with the UV-visible absorption region from 230 to 800 nm and emission region from 230 to 800 nm.

^b Experiments for fluorescence quantum yields were made in distilled toluene by Soret band (426 nm) excitation.

^c Fluorescence lifetime was measured in dilute CH₂Cl₂, using pulsed excitation at 375 nm.

^d Fluorescence quantum yield determined relative to TPP in toluene.

3.4.1 Absorption and emission

The UV-Visible spectra of **31** and **32** both have two components:

- Absorptions around 300-400 nm, due to the absorptions of the four dendrons;
- An intense Soret-band at 430 nm and four Q-bands from 520-660 nm, which are typical of free base porphyrin absorptions.

The emission spectra of dendrimers **31** and **32** present the two anticipated Q-bands: Q(0, 0) and Q(0,1) in 600-800 nm region. The normalized UV-visible (abs) and emission (em) spectra of **Model 1** and porphyrins **17**, **31** are measured in CH₂Cl₂ at room temperature (R.T.), as shown in Figure 3.4.2.

In more detail, the blue solid line presents the UV-visible absorption of conjugated porphyrin dendrimer **31**. The maximum dendron absorption appears at 325 nm. An intense Soret band absorption is found at 430 nm; the four Q-bands appear in the typical free base porphyrin region of 500-700 nm. With respect to the absorption of porphyrin

17 (black solid line), the dendron absorption of **31** (blue solid line) shows an obvious red shift also observed for the Soret band, due to the connection with the four conjugated dendrons. We also observe a strong dendron absorption in UV region due to the twelve extra fluorenyl units that are provided by the new conjugated dendrimer **31**.

After exciting **17** and **31** at their λ_{Soret} respectively, the two porphyrins exhibit the expected red emission with two Q-bands: the strong Q(0,0) and a weaker Q(0,1) band. The smaller emission band Q(0,1) of porphyrin **31** (in red solid line) shows a lower intensity by comparison to the emission observed for **17** (black dashed line). The ratio between the Q-bands is slightly different.

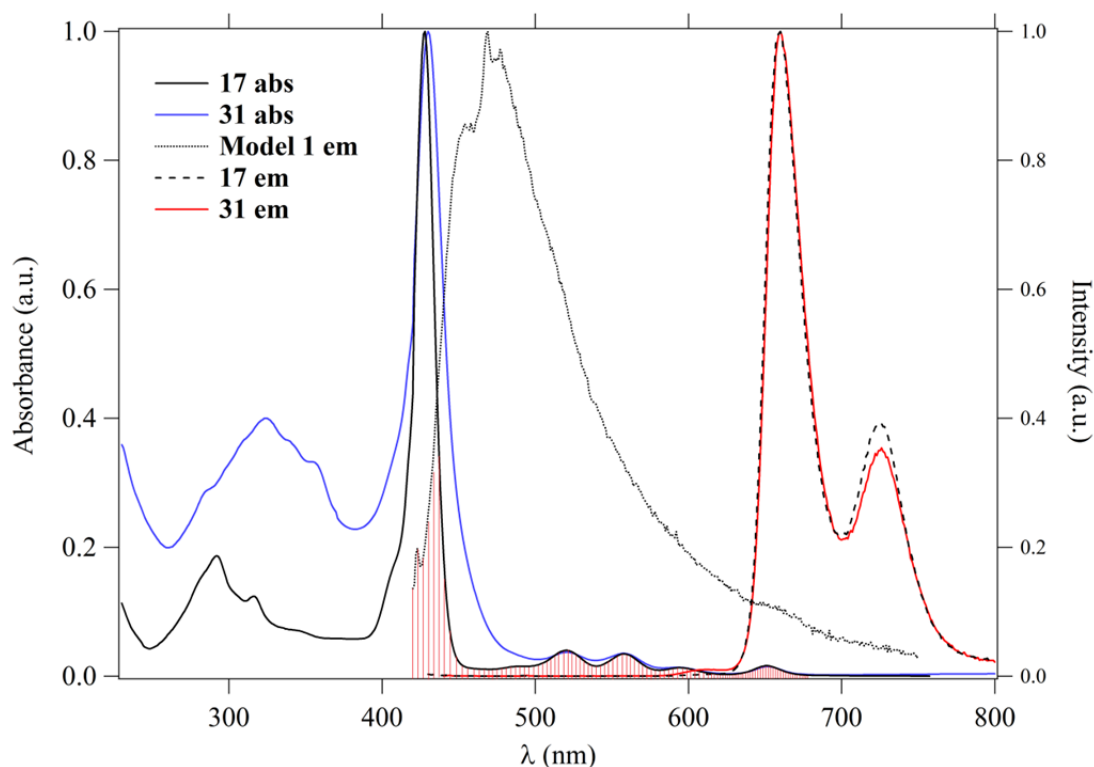


Figure 3.4.2 The normalized UV-visible (abs) and emission (em) spectra of Model 1, **17** and **31**

The normalized UV-visible (abs) and emission (em) spectra of dendron **Model 2** and new dendrimer **32** were obtained under the same conditions and are shown in Figure 3.4.3 along with data for porphyrin **17**.

In Figure 3.4.3, we also report the UV-visible absorption spectrum of non-conjugated dendrimer **32** (as the solid blue line). In the UV region, a broad dendron absorption band appears whose maximum is at 305 nm, which constitutes a weak red shift relative to porphyrin **17**. meaning that the red shift of the dendron absorption in **32** is smaller than in **31**, due to the non-conjugated structure of dendron **30**. The Soret band of dendrimer **32** appears at 430 nm, which is again slightly red shifted relative to precursor **17**; here we notice that the Soret bands of **31** and **32** are at the same wavelength (430 nm); a possible explanation for this effect is that the fluorenyl units (marked blue in Figure 3.4.1) increase the distance between the porphyrin ring and the **Model 2** type dendrons, which reduces the dendron's effect to the porphyrin core. The four Q-bands of **32** appear in the range of 500-700 nm.

When excited at λ_{Soret} , porphyrin dendrimer **32** exhibits strong red emission. The emission band Q(0,1) of porphyrin **32** (in red solid line) shows small decrease for this band with respect to the emission spectrum of **17** (black dashed line), as was also observed for dendrimer **31**.

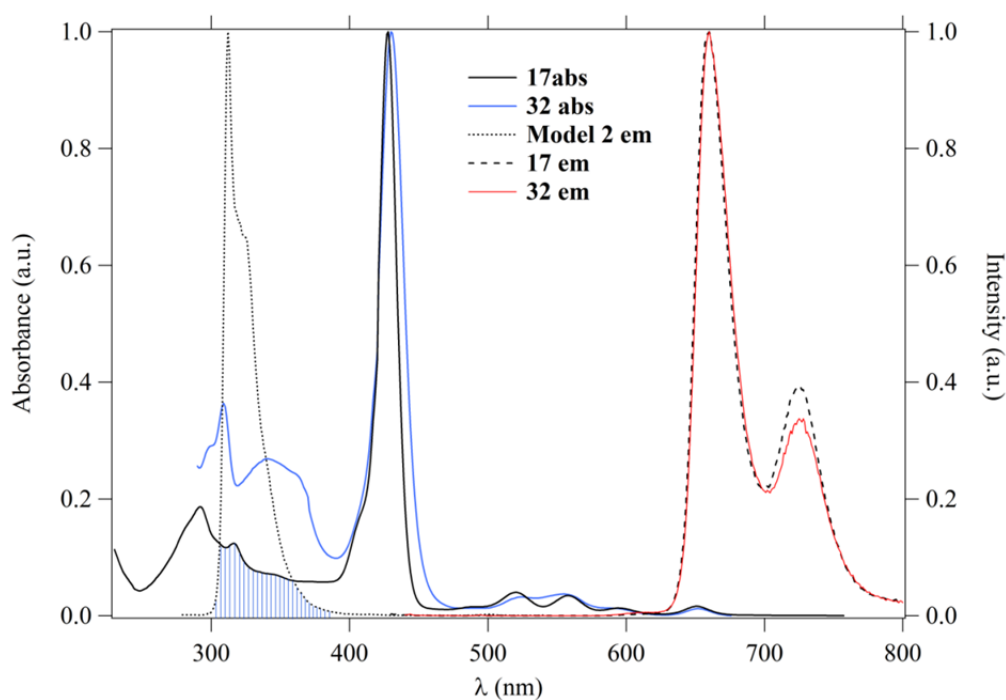


Figure 3.4.3 The normalized UV-visible (abs) and emission (em) spectra of Model 2, 17 and 32

3.4.2 Energy transfer behaviors

The energy transfer behavior (ET) of porphyrin dendrimers **31** and **32** are expected to be promising, as was discussed in the introduction of this chapter with respect to **Models 1** and **2**. The normalized emission spectra are shown in Figure 3.4.4.

After excitation in the dendron absorption region (300 nm), the conjugated dendrimer **31** exhibits only red emission from porphyrin core. The large emission from conjugated **Model 1** type dendrons is completely quenched in the ET process and so that red emission from the porphyrin is exclusively seen.

For the dendrimer **32**, which has non-conjugated **Model 2** type dendrons, the strong blue dendron emission is not totally quenched, and a very weak dendron emission band appears at 322 nm. This suggests the ET from dendrons to TFP core is less efficient than for **31**, but the energy transfer efficiency of **32** is still near 100%.

To conclude, the ET is efficient in both situations, in relation with a good overlap between the donor emission spectrum of the large dendrons and the absorption spectrum of the TFP core (see hatched areas in figures 3.4.2 and 3.4.3).

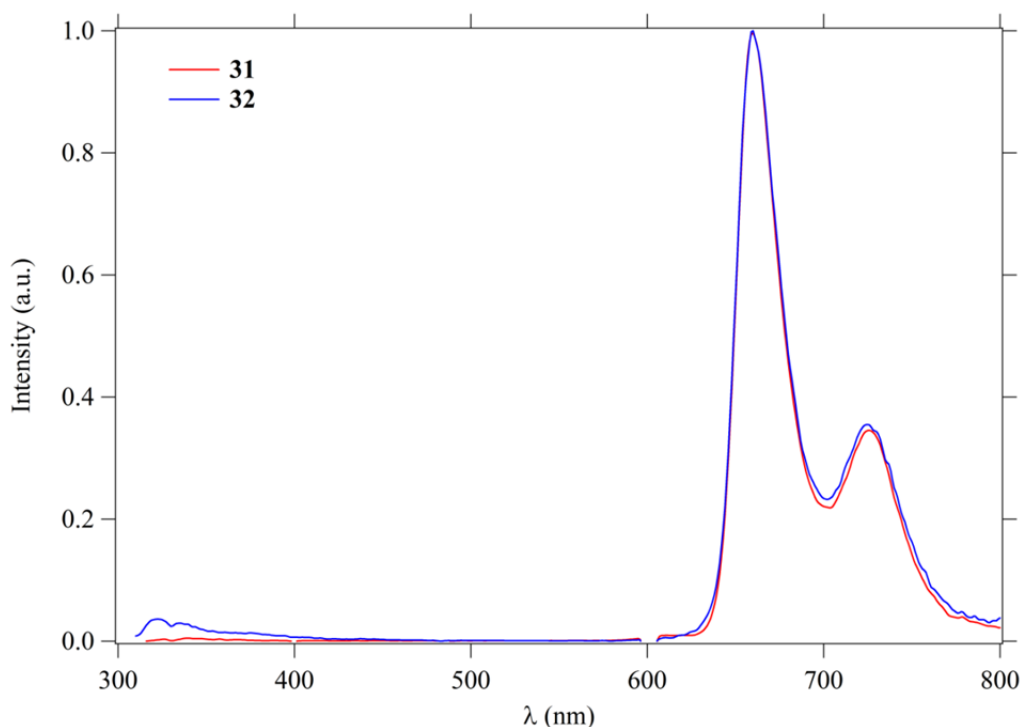


Figure 3.4.4 The normalized emission spectra of **31** and **32** excited at 300 nm

3.5 Two-photon absorption (TPA)

The two-photon absorption (TPA) cross-sections (σ_2) of new porphyrin dendrimers **31** and **32** were determined by investigating their two-photon excited fluorescence in dichloromethane, following the experimental protocol described by Xu and Webb^[15]. A quadratic dependence of the fluorescence intensity on the excitation power was observed for each sample at all the wavelengths of the spectra shown in Figure 3.5.1, indicating that the cross-sections determined are only due to TPA.

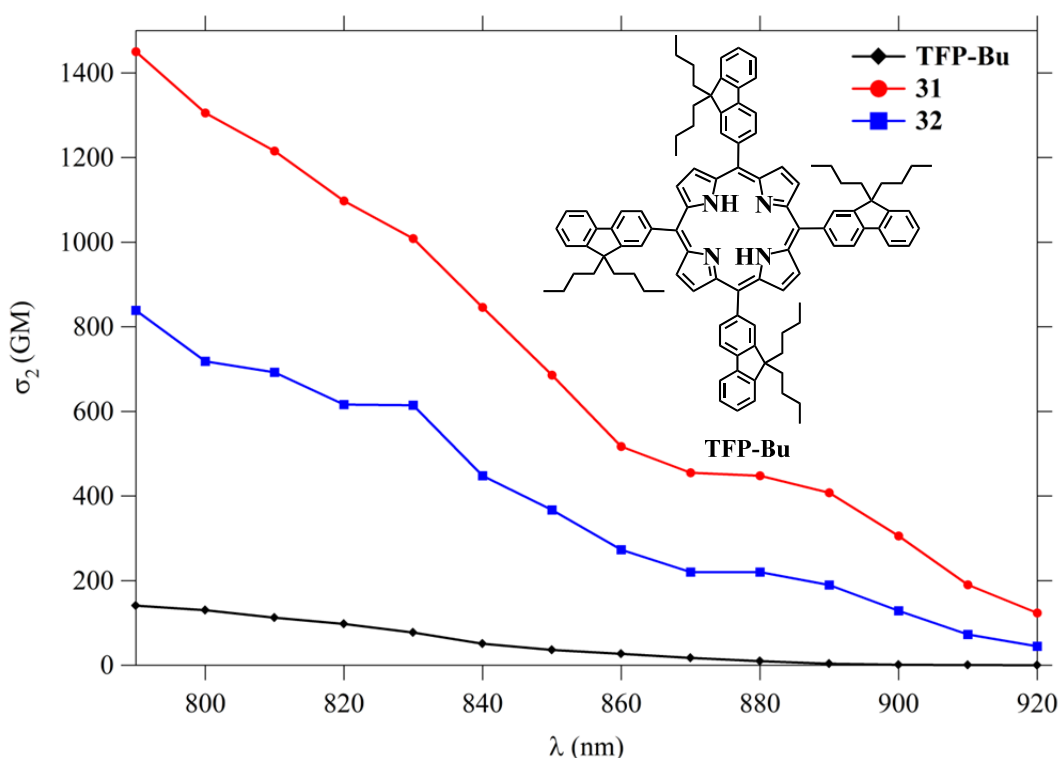


Figure 3.5.1 Two-photon absorption cross-section spectra of TFP-Bu, 31 and 32

Compared to σ_2 of TFP-Bu (140 GM at 790 nm), an obvious increased σ_2 was observed for both new porphyrin dendrimers: **31** and **32**. Comparison between these two porphyrins reveals that the addition of dendrons (**26** and **30**) result a clear improvement of the TPA properties: as an impact factor, the cross-sections are up to ten times increased when these two dendrons were coupled with the TFP core.

The connection of dendrons on TFP core also enhanced the two-photon brightness ($\Phi_{\text{fl}} \cdot \sigma_2^{\text{max}}$), from 25 GM to 247 and 101 GM, respectively.

Table 1.5.1 Two-Photon Absorption and Brightness Properties of TPP, TFP-Bu and porphyrin dendrimers 31 and 32

	Φ_{fl} / %	$\lambda_{\text{TPA}}^{\text{max}}$ /nm	σ_2^{max} /GM ^c	$\Phi_{\text{fl}} \cdot \sigma_2^{\text{max}}$ /GM ^d	Two-photon brightness enhancement factor ^e
TPP	11 ^a	790	11	1.3	1
TFP-Bu	18 ^b	790	140	25	19
31	17 ^b	790	1450	247	190
32	12 ^b	790	840	101	78

^a Data from lit.[14];

^b Fluorescence quantum yields were measured in toluene (HPLC grade) using TPP ($\Phi_{\text{fl}} = 11\%$) as standard, upon excitation at Soret band (errors are around $\pm 10\%$);

^c Intrinsic TPA cross-sections measured in 10^{-4} M dichloromethane solutions by TPEF in the femtosecond regime;

^d Maximum two-photon brightness in dichloromethane;

^e Enhancement factor: $\Phi_{\text{fl}} \cdot \sigma_2^{\text{max}}$ of the compounds normalized to that of TPP.

3.6 Conclusions

1. Two new porphyrin dendrimers **31** and **32** were designed and synthesized successfully based on a new platform, by coupling the new conjugated dendron **26** and the new non-conjugated dendron **30**, respectively.

2. For the non-conjugated dendron **30**, the synthesis strategies were selected from six paths, finally the dendron formation methods were optimized to obtain the maximum yield of each component.

3. The new types of dendrons (**26** and **30**), as well as their corresponding models (Model **1** and Model **2**), and the new porphyrin dendrimers (**31** and **32**) were characterized and analyzed by ^1H NMR.

4. The linear optical properties of porphyrins **17**, **31** and **32** were studied through UV-visible and emission spectra, compared with the emission spectra of Model **1** and **2**:

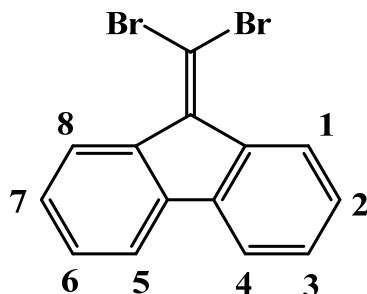
(i) Compared to porphyrin **17**, the Soret band of **31** and **32** present slightly red shifts:

(ii) In emission spectra, excited at Soret band, dendrimers **31** and **32** exhibit typical red emissions and almost without red shifts compared to **17**;

(iii) To study the energy transfer (**ET**) behaviors, the emission band of porphyrin **17** overlaps with the Model **1** in Soret band absorption and Q-bands area, so the ET from the corresponding conjugated dendron **26** to porphyrin core is efficient. While for the Model **2**, its emission overlapped with UV absorption of **17** in UV region, resulting in the ET from the related non-conjugated dendron **30** to the porphyrin core is slightly less efficient.

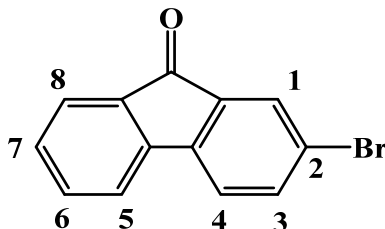
5. The two-photon absorption cross-sections of **31** and **32** were largely enhanced compared to the reference **TFP-Bu**, as well as their two-photon brightness.

Experimental Section

9-(dibromomethylene)fluorene (22)

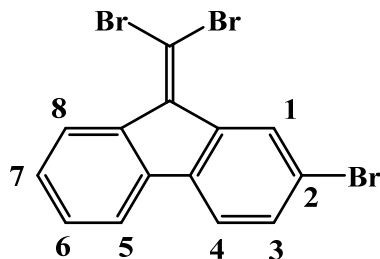
In a Schlenk tube, a mixture of commercial CBr_4 (368.0 mg, 1.1 mmol, 2 equiv.) and PPh_3 (291.0 mg, 1.1 mmol, 2 equiv.) were stirred in distilled and degassed DCM (2 mL) at 35 °C under argon until the color turn to orange. Then, in another Schlenk tube, commercial **9-fluorenone** (100 mg, 0.55 mmol, 1 equiv.) dissolved in DCM (3 mL) was transferred into the former Schlenk tube dropwise. The mixture was stirred at 35 °C for 5 h under argon. After evaporation of the volatiles, residue was purified by silica chromatography using heptane as eluent, **9-(dibromomethylene)fluorene (22)** was isolated as a white powder (130 mg, 70% yield).

$^1\text{H NMR}$ (400 MHz, CDCl_3 , ppm): δ = 8.61 (d, J = 8.0 Hz, 2H, $\text{H}_{4,5}$), 7.68 (d, J = 8.0 Hz, 2H, $\text{H}_{1,8}$), 7.42 (t, J = 8.0 Hz, 2H, $\text{H}_{2,7}$), 7.31 (t, J = 8.0 Hz, 2H, $\text{H}_{3,6}$).

2-bromo-fluoren-9-one (23)

In a two-neck bottle, the commercial **9-fluorenone** (2 g, 11.11 mmol, 1 equiv.) was stirred in methanesulfonic acid (100 mL) at R.T. Then the commercial **NBS** (2.97 g, 16.7 mmol, 1.5 equiv.) was added into the system in small portions over 30 min. The reaction was monitored by TLC until the starting material had disappeared. The mixture was poured into ice-water mixture for quenching terminating the reaction. The yellow precipitate was collected by filtration and washed by saturated NaHCO_3 (aq.). At last, residue was further purified by fine silica chromatography using heptane as eluent. The **2-bromo-fluoren-9-one (23)** was isolated as the yellow powder (2.09 g, 73% yield).

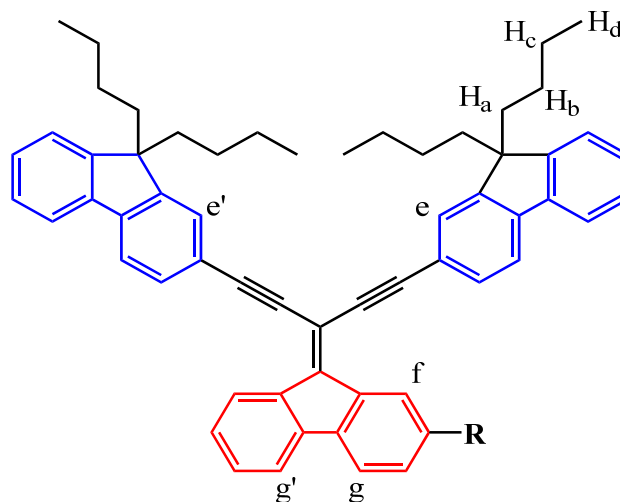
$^1\text{H NMR}$ (400 MHz, CDCl_3 , ppm): δ = 7.66 (d, 2H, J = 8.0 Hz, $\text{H}_{5,8}$), 7.54-7.47 (m, 4H, $\text{H}_{1,3,4,6}$), 7.30 (t, 1H, J = 6.0 Hz, H_7).

2-bromo-9-(dibromomethylene)-fluorene (24)

In a Schlenk tube, the **2-bromo-fluoren-9-one (23)** (1 g, 3.9 mmol, 1 equiv.) and **PPh₃** (4.05 g, 15.4 mmol, 4 equiv.) were dissolved in distilled and degassed DCM under argon. The ice-water bath was fixed for cooling the system to 0 °C. Then, **CBr₄** (5.12 g, 15.4 mmol, 4 equiv.) was added into the system under argon. The mixture was stirred overnight at R.T. After evaporation of the volatiles, residue was further purified by silica chromatography using petroleum ether as eluent. The **2-bromo-9-(dibromo-methylene)fluorene (23)** was isolated as the yellow powder (1.17 g, 73% yield).

¹H NMR (400 MHz, CDCl₃, ppm): δ = 8.77 (s, 1H, H₁), 8.61 (d, 1H, *J* = 8.0 Hz, H₅), 7.66 (d, 1H, *J* = 8.0 Hz, H₄), 7.55 (s, 2H, H₃, H₈), 7.43 (t, 1H, *J* = 8.0 Hz, H₇), 7.34 (t, 1H, *J* = 8.0 Hz, H₆).

¹³C NMR (100 MHz, CDCl₃, ppm): δ = 139.6, 139.4, 138.5, 137.8, 132.2, 129.6, 129.0, 127.7, 126.0, 121.0, 120.7, 119.6, 93.0, 92.3.

Model 1 (25) and Dendron 26

Model 1 (25): R = H

Dendron 26: R = Br

To synthesize **Model 1**, in a Schlenk tube, a mixture of **9,9-dibutyl-2-ethynyl-fluorene (2)** (113 mg, 0.4 mmol, 2.5 equiv.), **9-(dibromomethylene)fluorene (22)** (50 mg, 0.15 mmol, 1 equiv.), Pd(PPh₃)₂Cl₂ (excess) and CuI (excess) were stirred in DMF (1 mL) and ⁱPr₂NH (1 mL) was added under argon. The reaction medium was degassed by freeze-pump-thaw twice and heated for 48 h at 95 °C. After evaporation of the volatiles, residue was further purified by silica chromatography using pentane as eluent. Orange crystals (33 mg, 28% yield) were obtained.

¹H NMR (400 MHz, CDCl₃, ppm): δ = 8.81 (d, *J* = 4.0 Hz, 2H, H_{g, g'}), 7.78-7.66 (m, 10H, H_{fluorenyl}), 7.43-7.33 (m, 10H, H_{fluorenyl-blue}, H_{fluorenyl-red}), 2.08-1.98 (m, 8H, H_a), 1.16-1.07 (m, 8H, H_c), 0.74-0.59 (m, 24H, *J* = 8.0 Hz, H_d, H_b).

To synthesize **Dendron 26**, in a Schlenk tube, a mixture of **9,9-dibutyl-2-ethynyl-fluorene (2)** (300 mg, 1.0 mmol, 2 equiv.), **2-bromo-9-(dibromomethylene)-fluorene (24)** (206 mg, 0.5 mmol, 1 equiv.), Pd(PPh₃)₂Cl₂ (4.2 mg, 0.01 mmol, 0.6% equiv.) and CuI (excess) were stirred in DMF (2 mL) and ⁱPr₂NH (2 mL) was added under argon. The reaction medium was degassed by freeze-pump-thaw twice and heated for 48 h at 95 °C. After evaporation of the

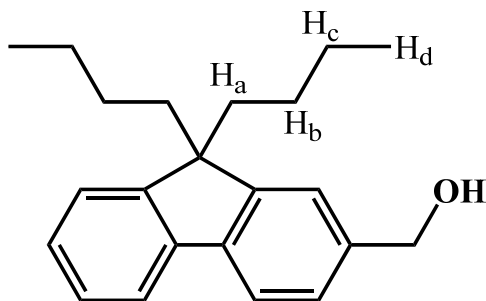
volatiles, residue was further purified by silica chromatography using pentane as eluent. The title product (340 mg, 79% yield) was obtained as an orange powder.

¹H NMR (400 MHz, CDCl₃, ppm): δ = 9.14 (d, J = 1.6 Hz, 1H, H_f), 8.79 (d, J = 8.0 Hz, 1H, H_g), 7.79-7.66 (m, 8H, H_{fluorenyl}, H_{g'}), 7.60-7.52 (m, 3H, H_{fluorenyl}), 7.43-7.35 (m, 8H, H_{fluorenyl}), 2.13-1.96 (m, 8H, H_a), 0.90-0.83 (m, 8H, H_c), 0.73-0.54 (m, 20H, H_b, H_d).

¹³C NMR (100 MHz, CDCl₃, ppm): δ = 151.4, 151.2, 143.3, 142.8, 142.7, 140.4, 140.3, 139.5, 139.3, 139.0, 137.6, 131.9, 131.2, 131.1, 129.6, 128.9, 128.1, 128.0, 127.9, 127.2, 127.1, 126.5, 126.3, 125.7, 123.1, 123.0, 121.3, 120.9, 120.8, 120.7, 120.4, 120.1, 120.0, 119.9, 103.3, 100.2, 100.1, 89.2, 89.1, 59.7, 55.5, 55.3, 53.6, 40.4, 40.3, 38.3, 32.1, 32.0, 31.4, 29.9, 29.8, 29.5, 26.1, 23.3, 23.2, 22.9, 22.8, 14.3, 14.0.

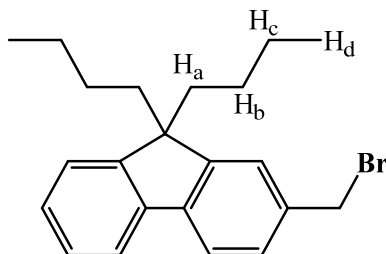
HRMS-ESI for C₆₀H₅₇Br: m/z = 856.3636 [M+H]⁺ (calcd: 856.3638).

Anal. Calcd. (%) for C₆₀H₅₇Br: C 83.99; H 7.44. **Found:** C 83.28; H 8.27.

2-methanol-9, 9-dibutyl-fluorene (27)

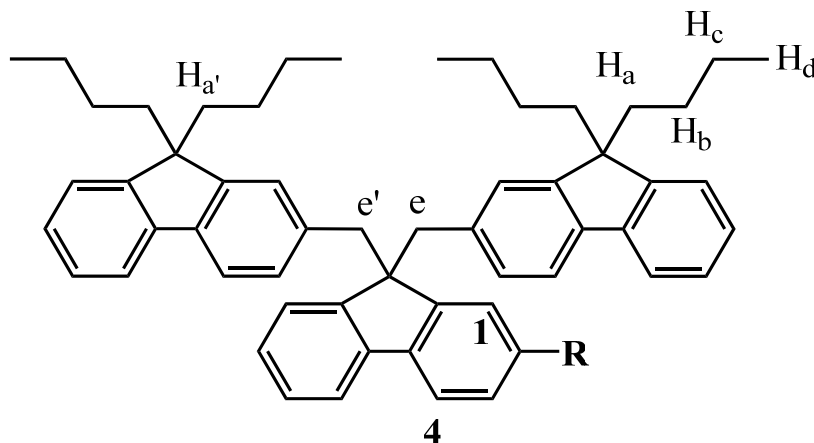
In a Schlenk tube, the **9, 9-dibutyl-fluorene-2-carbaldehyde (10)** (3.0 g, 9.8 mmol, 1 equiv.) was dissolved in EtOH (99.6%) under argon. The ice-water bath was fixed for cooling the system to 0 °C. Then NaBH₄ (444.0 mg, 11.8 mmol, 1.2 equiv.) was added under argon. The system was firstly stirred at 0 °C for 1 h, followed another 2 h at R.T. The mixture was extracted with ethyl acetate/water for 3 times and washed by saturated NaCl. After evaporation of the volatiles, the residue was further purified by silica chromatography using DCM/heptane (1:1) as eluent. The **2-methanol-9, 9-dibutyl-fluorene (27)** was isolated as white crystals (2.94 g, 97% yield).

¹H NMR (400 MHz, CDCl₃, ppm): δ = 7.70-7.67 (m, 2H, H_{fluorenyl}), 7.34-7.29 (m, 5H, H_{fluorenyl}), 4.78 (d, *J* = 5.64 Hz, 2H, H_{CH₂-methylene}), 1.98-1.94 (m, 4H, H_a), 1.68 (t, *J* = 5.84 Hz, 1H, H_{OH}), 1.12-1.03 (m, 4H, H_c), 0.67 (t, *J* = 8.0 Hz, 6H, H_d), 0.63-0.55 (m, 4H, H_b).

2-(bromomethyl)-9, 9-dibutyl-fluorene (28)

In a two-neck bottle, a mixture of **2-methanol-9, 9-dibutyl-fluorene (27)** (1.13 g, 3.7 mmol, 1 equiv.) and PPh_3 (1.06 g, 4.0 mmol, 1.1 equiv.) was dissolved in THF (20 mL) and cooled to 15 °C. Then NBS (717 mg, 4.0 mmol, 1.1 equiv.) was added at once. The reaction was stirred for additional 1 h and immediately quenched by cold water. The precipitates were extracted into DCM. The organic extracts were collected, washed with saturated NaCl (aq.) and dried over anhydrous MgSO_4 . After evaporation of the volatiles, residue was further purified by silica chromatography using DCM/hexane (1:5) as eluent. The **2-(bromomethyl)-9, 9-dibutyl-fluorene (28)** was isolated as white crystals (639 mg, 86% yield).

$^1\text{H NMR}$ (400 MHz, CDCl_3 , ppm): $\delta = 7.71\text{-}7.65$ (m, 2H, $\text{H}_{\text{fluorenyl}}$), $7.38\text{-}7.28$ (m, 5H, $\text{H}_{\text{fluorenyl}}$), 4.62 (s, 2H, $\text{H}_{\text{CH}_2\text{-methylene}}$), 1.99-1.95 (m, 4H, H_a), 1.13-1.04 (m, 4H, H_c), 0.68 (t, $J = 8.0$ Hz, 6H, H_d), 0.64-0.67 (m, 4H, H_b).

Model 2 (29) and Dendron 30

Model 2 (29): R = H
Dendron 30: R = Br

To synthesize **Model 2**, the commercial fluorene (26 mg, 0.16 mmol, 1 equiv.), Bu₄NBr (5.0 mg, 0.02 mmol, 10% equiv.) were dissolved in DMSO (2 mL) and NaOH (50% aq., 0.02 mL) was injected into the mixture. After the colour turning to orange, **2-(bromomethyl)-9,9-dibutyl-fluorene (28)** (127.0 mg, 0.35 mmol, 2.2 equiv.) was added and stirred at R.T. for 2 h. The mixture was extracted by DCM/saturated NaCl for 3 times and dried over anhydrous MgSO₄. After evaporation of the volatiles, residue was further purified by silica chromatography using heptane as eluent. **Model 2** was isolated as yellow crystals (88 mg, 79% yield).

¹H NMR (300 MHz, CDCl₃, ppm): δ = 7.55-7.49 (m, 4H, H_{fluorenyl}), 7.34-7.28 (m, 6H, H_{fluorenyl}), 7.24-7.16 (m, 8H, H_{fluorenyl}), 6.70 (d, *J* = 9.0 Hz, 2H, H_{fluorenyl}), 6.55 (s, 2H, fluorenyl), 3.52 (s, 4H, H_{CH₂-methylene}), 1.81-1.58 (m, 8H, H_a), 1.06-0.93 (m, 8H, H_c), 0.70-0.62 (m, 12H, H_d), 0.42-0.17 (m, 8H, H_b).

To synthesize **Dendron 30**, the commercial 2-bromofluorene (186 mg, 0.76 mmol, 1 equiv.), Bu₄NBr (24.4 mg, 0.076 mmol, 10% equiv.) were dissolved in DMSO (6 mL) and NaOH (50% aq., 0.05 mL) was injected into the system. After the color turning to orange, **2-(bromomethyl)-9,9-dibutyl-fluorene (28)** (619 mg, 1.67 mmol, 2.2 equiv.)

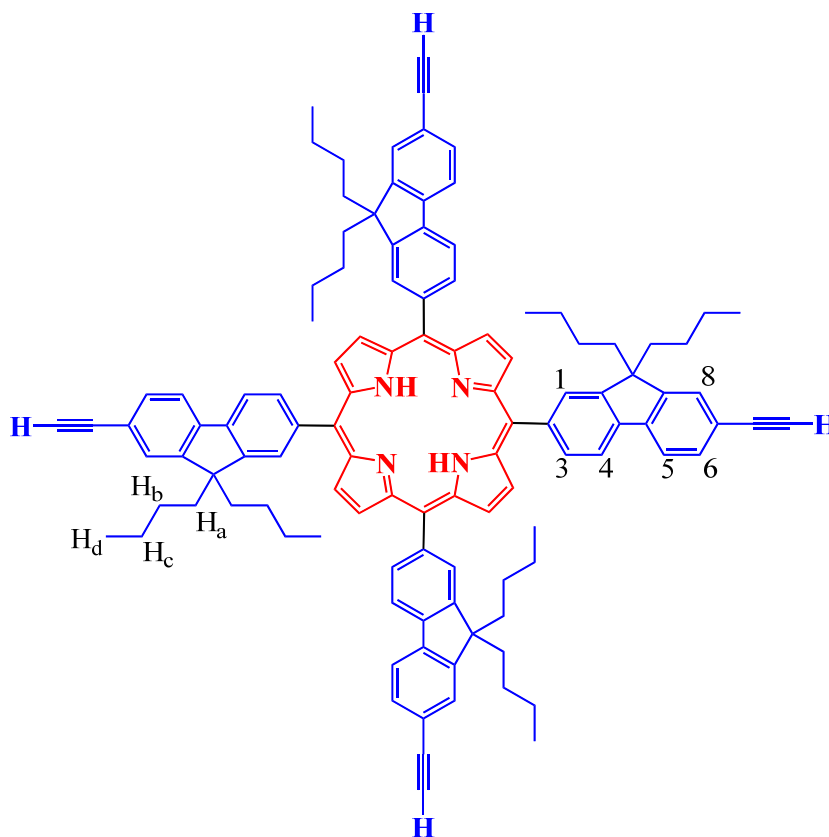
was added and stirred at R.T. for 1 h. The mixture was extracted by DCM/saturated NaCl for 3 times and dried over anhydrous MgSO₄. After evaporation of the volatiles, the residue was further purified by silica chromatography using heptane as eluent. The desired products were isolated (480 mg, 77% yield).

¹H NMR (400 MHz, CD₂Cl₂, ppm): δ = 7.88 (d, $J^A = 1.64$ Hz, 1H, H₁), 7.67 (d, $J = 7.56$ Hz, 1H, H₄), 7.51-7.49 (m, 2H, H_{fluorenyl}), 7.40 (t, $J = 8.0$ Hz, 1H, H_{fluorenyl}), 7.32-7.29 (m, 2H, H_{fluorenyl}), 7.24-7.16 (m, 10H, H_{fluorenyl}), 6.64 (d, $J = 5.76$ Hz, 2H, H_{fluorenyl}), 6.58 (s, 2H, H_{fluorenyl}), 3.62-3.51 (q, 4H, H_{e, e'}),), 1.83-1.74 (m, 4H, H_{a'}), 1.66-1.5 (m, 4H, H_a), 1.09-0.93 (m, 8H, H_c), 0.63 (t, $J = 7.32$ Hz, 12H, H_d), 0.31-0.11 (m, 8H, H_b).

¹³C NMR (100 MHz, CD₂Cl₂, ppm): δ = 151.2, 151.1, 150.1, 148.4, 141.5, 140.8, 140.7, 139.5, 136.3, 130.7, 129.3, 128.5, 127.9, 127.3, 127.1, 127.0, 125.4, 125.0, 121.3, 120.6, 120.1, 119.7, 118.7, 58.6, 55.0, 46.5, 40.7, 40.6, 30.3, 26.4, 26.3, 14.3, 14.2.

HRMS-ESI for C₅₇H₆₁Br: $m/z = 847.3849$ [M+Na]⁺ (calcd: 847.3850).

Anal. Calcd. (%) for C₅₇H₆₁Br: C 82.88; H 7.44. **Found:** C 82.71; H 7.66.

Tetra-alkynyl TFP (17)

In a two-neck flask, a mixture of **9,9-dibutyl-7-((trimethylsilyl)ethynyl)-fluorene-2-carboxaldehyde (12)** (689 mg, 1.7 mmol, 1 equiv.) and pyrrole (0.17 mL, 1.7 mmol, 1 equiv.) were dissolved in dried chloroform (200 mL) under argon. After degassing the mixture with argon bubbling for 30 min, $\text{BF}_3 \cdot \text{OEt}_2$ (0.05 mL, 0.4 mmol, 0.25 equiv.) was injected and the reaction was stirred in dark for 3 h under argon at room temperature. Then oxidant *p*-chloranil (315 mg, 1.28 mmol, 0.75 equiv.) was added, and the reaction was heated at 60 °C for another 2 h without any protection. After cooling the reaction to room temperature, NEt_3 (2 mL) was injected, and then stirring was kept for several minutes. After evaporation of the volatiles, purification was done by silica chromatography using $[\text{CH}_2\text{Cl}_2/\text{heptane} (1:4)]$ mixture as eluents; the porphyrin was collected as red powder. The crude porphyrin was firstly deprotected by K_2CO_3 (470 mg, 3.4 mmol, 8 equiv.) in a mixed solvents $\text{CH}_2\text{Cl}_2/\text{THF}/\text{MeOH} (3:1:1)$ at 60 °C, overnight. At last, the **tetra-alkynyl TFP (17)** was isolated by silica

chromatography using a CH₂Cl₂/ heptane (1:4) mixture as eluent. The yield is 28% for these two steps.

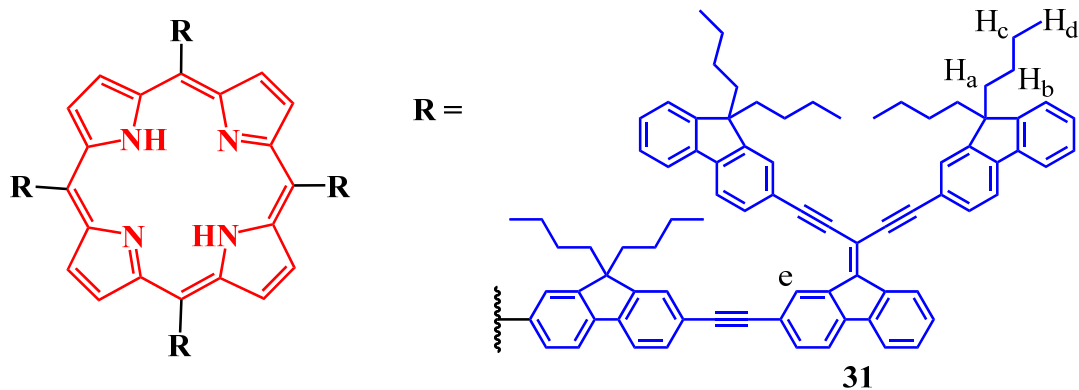
¹H NMR (400 MHz, CDCl₃, ppm): δ = 8.90 (s, 8H, H_{β-pyrrolic}), 8.25-8.19 (m, 8H, H_{1'}, H_{3'}), 8.07 (d, 4H, *J* = 7.3 Hz, H_{4'}), 7.91 (d, 4H, *J* = 7.8 Hz, H_{5'}), 7.63 (d, 8H, *J* = 8.0 Hz, H_{6'}, H_{7'}, H_{8'}), 3.21 (s, 4H, H_{7'}), 2.13 (t, 16H, *J* = 6.9 Hz, H_a), 1.21-1.14 (m, 16H, H_c), 0.92-0.83 (m, 16H, H_b), 0.79-0.73 (m, 24H, H_d), -2.60 (s, 2H, NH).

¹³C NMR (100 MHz, CDCl₃, ppm): δ = 151.4, 149.7, 141.9, 141.7, 140.1, 133.9, 131.6, 129.5, 126.9, 120.8, 120.2, 118.4, 88.6, 84.9, 77.4, 59.7, 55.5, 40.4, 38.3, 31.4, 29.7, 26.5, 23.3, 14.1, 14.0.

UV-vis (λ_{max}, CH₂Cl₂, nm): 428, 520, 558, 592, 650.

MS (Maldi-DCTB) for C₁₁₂H₁₁₀N₄: *m/z* = 1510.869 [M⁺⁺] (calcd: 1510.8725).

Anal. Calcd. (%) for C₁₁₂H₁₁₀N₄·EtOH: C, 87.87; H, 7.50; N, 3.60. **Found:** C, 87.89; H, 7.59; N, 3.49.

Conjugated porphyrin dendrimer (**31**)

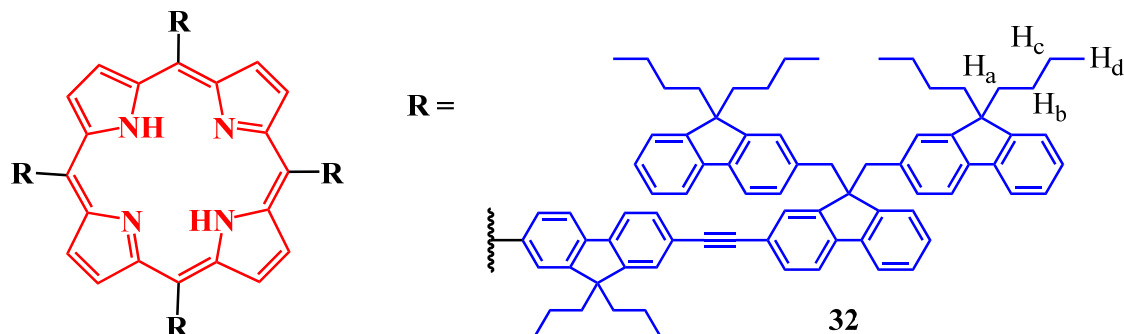
In a Schlenk tube, dendron **26** (100 mg, 0.12 mmol, 4.5 equiv.) and **Tetra-alkynyl TFP (17)** (39.0 mg, 0.03 mmol, 1 equiv.), Pd(PPh₃)₂Cl₂ (excess) and CuI (excess) were stirred in DMF (2 mL) and ⁴Pr₂NH (2 mL) was added under argon. The reaction medium was degassed by freeze-pump-thaw twice and heated for 72 h at 95 °C. After evaporation of the volatiles, residue was purified by silica chromatography using petroleum/THF (30:1) as eluent. The desired porphyrin dendrimer **31** was isolated as a dark violet powder (26 mg, 22% yield).

¹H NMR (400 MHz, CDCl₃, ppm): δ = 9.23 (t, *J* = 8.8 Hz, 4H, H_e), 8.97 (s, 8H, H_β-pyrrolic), 8.87-8.83 (m, 4H, H_{fluorenyl}), 8.67-8.50 (m, 4H, H_{fluorenyl}), 8.28 (s, 8H, H_{fluorenyl}), 8.11-8.09 (m, 4H, H_{fluorenyl}), 7.99-7.88 (m, 10H, H_{fluorenyl}), 7.79-7.61 (m, 38H, H_{fluorenyl}), 7.44-7.34 (m, 28H, H_{fluorenyl}), 2.19-2.04 (m, 48H, H_a), 1.19-1.06 (m, 48H, H_c), 0.78-0.58 (m, 110H, H_b, H_d), -2.53 (s, 2H, NH).

¹³C NMR (100 MHz, CDCl₃, ppm): δ = 151.5, 151.4, 151.3, 151.2, 140.4, 140.3, 131.2, 131.1, 129.7, 129.4, 128.0, 127.2, 126.5, 123.1, 121.1, 121.0, 120.5, 120.4, 120.2, 120.1, 120.0, 55.4, 55.3, 40.4, 26.1, 23.2, 14.0.

UV-vis (λ_{max}, CH₂Cl₂, nm): 325, 430, 521, 557, 593, 652.

Anal. Calcd. (%) for C₃₅₂H₃₃₆N₄·4CH₂Cl₂: C, 86.14; H, 6.98; N, 1.14. **Found:** C, 86.39; H, 7.09; N, 1.26.

Non-conjugated porphyrin dendrimer (32)

In a Schlenk tube, dendron **30** (100 mg, 0.14 mmol, 4.5 equiv.) and **Tetra-alkynyl TFP (17)** (45.0 mg, 0.03 mmol, 1 equiv.), Pd(PPh₃)₂Cl₂ (excess) and CuI (excess) were stirred in DMF (2 mL) and ⁱPr₂NH (2 mL) was added under argon. The reaction medium was degassed by freeze-pump-thaw twice and heated for 114 h at 95 °C. After evaporation of the volatiles, residue was purified by silica chromatography using petroleum/THF (30:1) as eluent. The desired porphyrin dendrimer **32** was isolated as a dark violet powder (38 mg, 29% yield).

¹H NMR (400 MHz, CD₂Cl₂, ppm): δ = 9.00 (s, 8H, H_β-pyrrolic), 8.31-7.96 (m, 22H, H_{fluorenyl}), 7.77-7.68 (m, 12H, H_{fluorenyl}), 7.50-6.97 (m, 60H, H_{fluorenyl}), 6.71-6.63 (m, 14H, H_{fluorenyl}), 3.63 (s, 16H, H_{CH2-methyl}), 2.24-1.64 (m, 48H, H_a), 1.09-0.75 (m, 72H, H_d), 0.64-0.23 (m, 96H, H_{b,c}), -2.59 (s, 2H, NH).

¹³C NMR (100 MHz, CD₂Cl₂, ppm): δ = 150.6, 149.5, 141.0, 138.8, 136.0, 124.9, 124.5, 119.2, 118.1, 54.5, 45.9, 40.3, 40.1, 29.7, 25.8, 25.7, 23.1, 23.0, 22.7, 0.7.

UV-vis (λ_{max}, CH₂Cl₂, nm): 309, 430, 524, 555, 591, 652.

Anal. Calcd. (%) for C₃₄₀H₃₅₀N₄·3CH₂Cl₂: C, 86.78; H, 7.54; N, 1.18. **Found:** C, 87.39; H, 7.90; N, 1.01.

References

- [1] S. Drouet, C. O. Paul-Roth, *Tetrahedron*, **2009**, *65*, 10693.
- [2] C. O. Paul-Roth, A. Merhi, D. Yao, O. Mongin, *J. Photochem. Photobiol. A*, **2014**, *288*, 23.
- [3] O. Mongin, V. Hugues, M. Blanchard-Desce, A. Merhi, S. Drouet, D. Yao, C. O. Paul-Roth, *Chem. Phys. Lett.* **2015**, *625*, 151.
- [4] N. S. Makarov, M. Drobizhev, A. Rebane, *Opt. Express*, **2008**, *16*, 4029.
- [5] D. Yao, X. Zhang, O. Mongin, F. Paul, C. O. Paul-Roth, *Chem. Eur. J.* **2016**, *22*, 5583.
- [6] C. Xu, W. W. Webb, *J. Opt. Soc. Am. B*, **1996**, *13*, 481.
- [7] J. S. Lindsey, K. A. Maccrum, J. S. Tyhonas, Y. Y. Chuang, *J. Org. Chem.*, **1994**, *59*, 579.
- [8] F. R. Li, K. X. Yang, J. S. Tyhonas, K. A. Maccrum, J. S. Lindsey, *Tetrahedron*, **1997**, *53*, 12339.
- [9] K. Sonogashira, Y. Tohda, N. Hagihara, *Tetrahedron Lett.*, **1975**, *50*, 4467.
- [10] S. Drouet, C. O. Paul-Roth, G. Simonneaux, *Tetrahedron*, **2009**, *65*, 2975.
- [11] S. E. Kiruthika, P. T. Perumal, *Org. Lett.*, **2014**, *16*, 484.
- [12] C. Adachi, M. A. Baldo, M. E. Thompson, S. R. Forrest. *J. Appl. Phys.* **2001**, *90*, 5048.
- [13] K. R. J. Thomas, J. T. Lin, C. Tsai, H. Lin, *Tetrahedron*, **2006**, *62*, 3517.
- [14] S. Abraham, G. P. T. Ganesh, S. Varughese, B. Deb, J. Joseph, *ACS Appl. Mater. Interfaces*, **2015**, *7*, 25424.
- [15] C. Xu, W. W. Webb, *J. Opt. Soc. Am. B*, **1996**, *13*, 481.

Chapter 4

Syntheses of *para*-Fluorenone TFP Cored Porphyrins and Photophysical Properties

4.1 The targets of the project

4.1.1 *Meso*-fluorenone porphyrin

For full-color applications, a full set of red, green, and blue emitters with sufficiently high luminous efficiency and proper chromaticity are necessary. Nowadays, satisfactory organic materials for green and blue emitter have largely been developed^[1]. Polyfluorenes are leading candidates for blue color and are expected to be a part of the full-color polymer displays^[2]. The red electroluminescence (EL) organic materials are still relatively poorly developed^[3]. Red dyes, such as porphyrins, are organic molecules with reasonable fluorescence efficiency and good thermal stability.

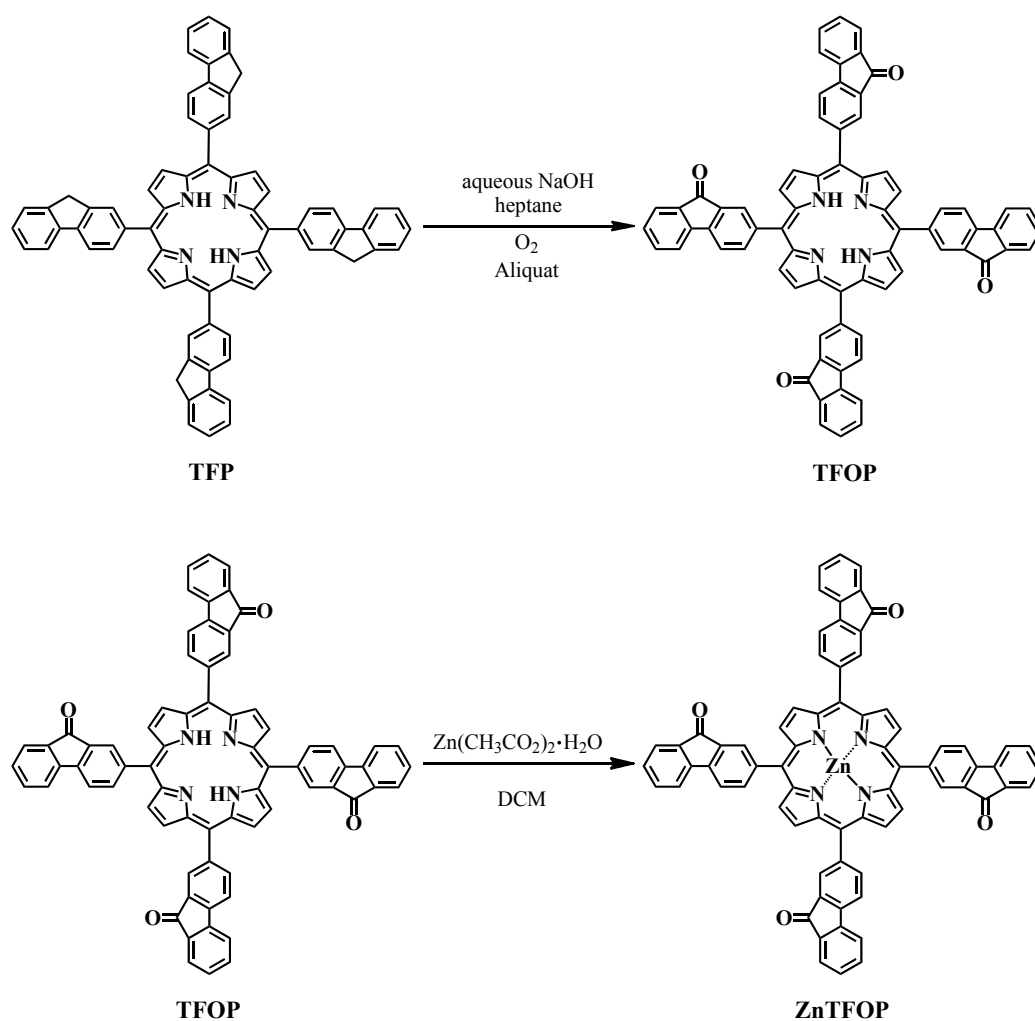


Figure 4.1.1 Syntheses of tetra-fluorenone porphyrin (TFOP) and its corresponding Zinc complex (ZnTFOP)

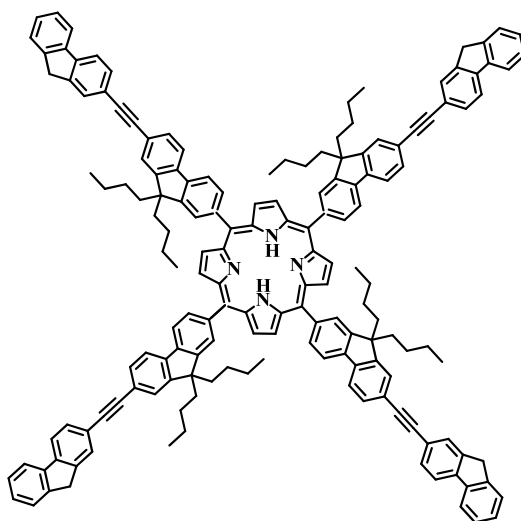
For these reasons, the group of Christine PAUL-ROTH reported a porphyrin with four fluorenone arms in 2006, named **TFOP**, as well as the corresponding zinc complex (**ZnTFOP**). Their synthetic processes are shown in Figure 4.1.1. The extensions of π -electron conjugation into the oxygen atoms slightly enhance the luminescence properties ($\Phi_{fl} = 25\%$)^[4-6]. In their UV-visible absorptions, the organic porphyrin **TFOP** has the intense Soret band at 431 nm, as well as the four Q-bands. Emission spectra were also obtained after excitation at UV-visible region: fluorenone arms (258 nm), Soret band (427 nm) and the highest Qy(0,1) transition (519 nm) were observed. This compound was found to deliver good red chromaticity by exhibiting Q(0,0) and Q(0,1) in the red luminescence zone, and a quantum yield of 25% which is higher than for many other porphyrins^[7].

In part **3.1.1.2** of **Chapter 3**, we have also introduced the **TPP1-TPP6** family and shown that the *para*-substituted TPP-cored porphyrins series (**TPP1-TPP3**) have higher quantum yields ($\Phi_{fl} \approx 20\%$) than the parent molecule **TPP** ($\Phi_{fl} = 11\%$), whereas the *meta*-substituted group (**TPP4-TPP6**) have similar Φ_{fl} ($\approx 13\%$) to **TPP**. Relevant photophysical properties are listed in Table **3.1.2** (**Chapter 3**). For these reasons, we will now be interested exclusively in the *para*-type porphyrins combined with fluorenone^[5].

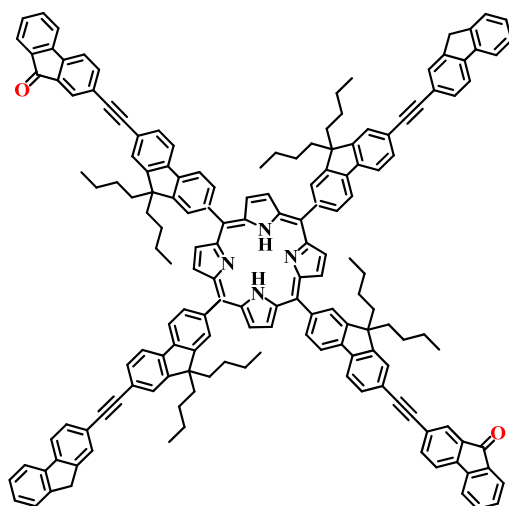
4. 1. 2 Target porphyrin dendrimers

To resume the data above, the *para*-substituted porphyrins (**TPP1-TPP3**) and the fluorenone units both present good optical properties. So now we will concentrate on a new series of porphyrins combining the TFP core and the fluorenone units. The outline structure of these desired *para*-porphyrins is summarized in Figure 4.1.2.

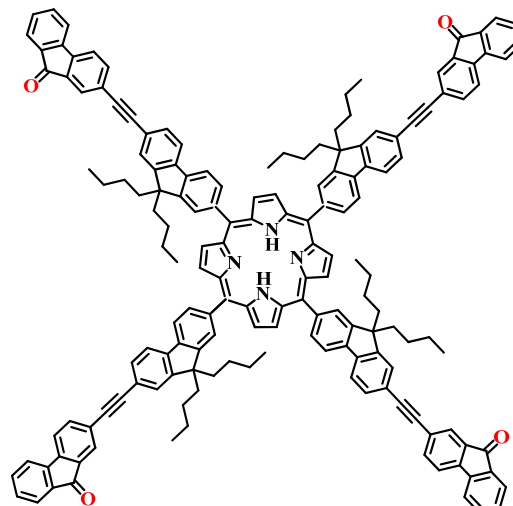
As shown in Figure 4.1.2, the parent porphyrin **TFOP 1 (36)** possesses four linear conjugated difluorenyl arms. In two derivatives the CH₂ group in the 9 position of terminal fluorenyl units will be substituted by oxygen atoms to obtain fluorenone units. This gives rise **TFOP 2 (37)**, which has two oxygen substituted dendrons in *trans*-position and another two difluorenyl dendrons without oxygen atoms, and **TFOP 3 (38)** which is the symmetrical porphyrin having full oxygen substituted dendrons. Their syntheses will be detailed in the following part.



TFOP 1 (36)



TFOP 2 (37)



TFOP 3 (38)

Figure 4.1.2 The entire structures of TFOP 1-3 (36-38)

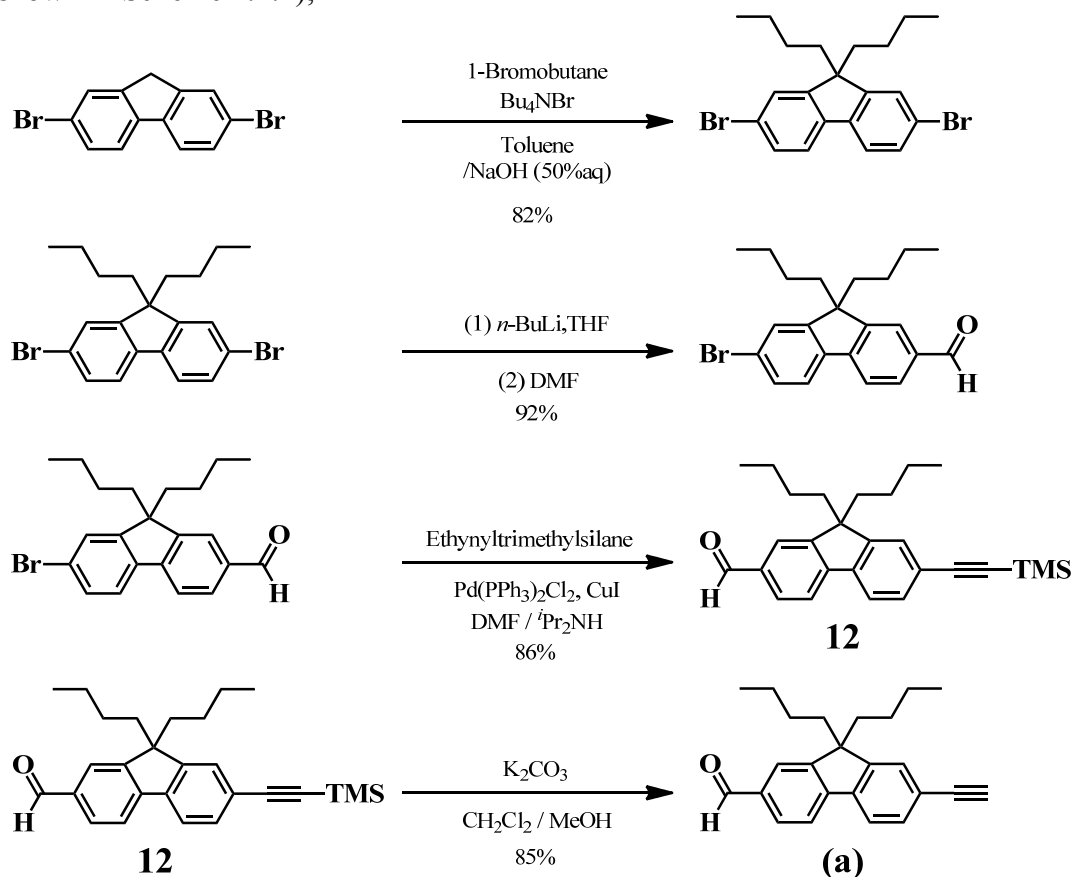
4.2 Syntheses of the new series of fluorenone porphyrins

To prepare this new family of fluorenone porphyrins, the Lindsey Method ^[8,9] followed by Sonogashira coupling ^[10] were used to achieve the target molecules: **TFOP 1, 2** and **3**.

4.2.1 Difluorenyl aldehyde **35** formation

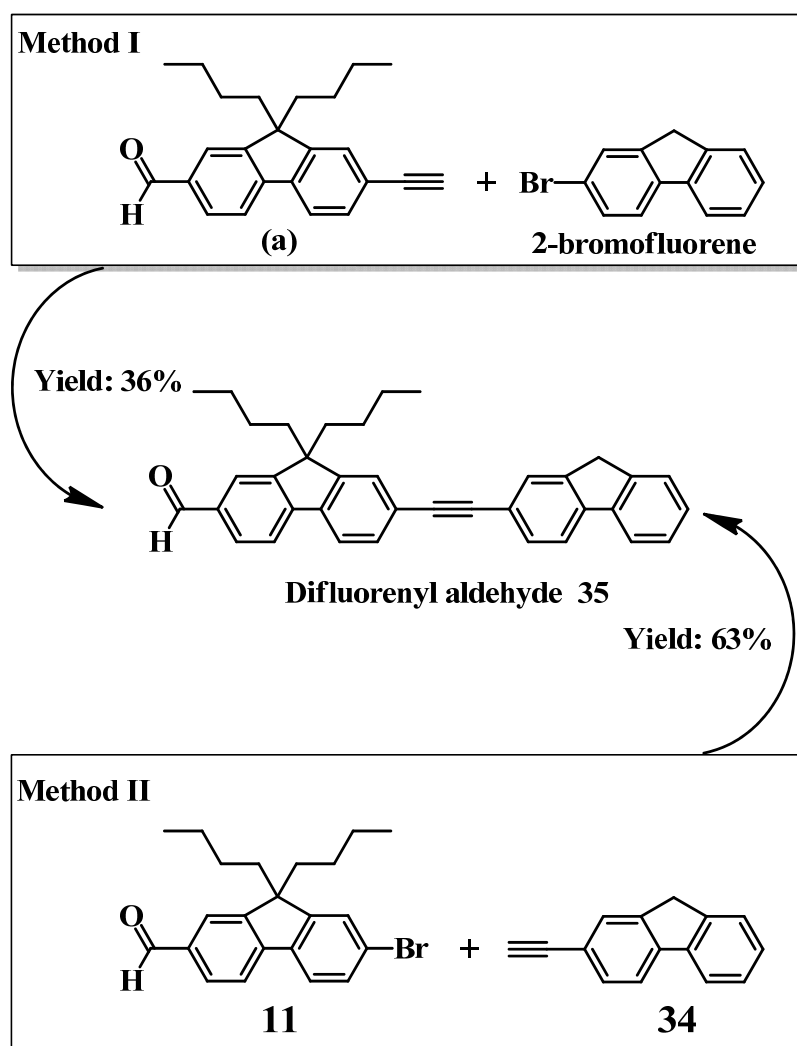
To synthesize these porphyrins, the difluorenyl aldehyde **35** was initially prepared. As illustrated, there are two paths to achieve this linear molecule, both were evaluated.

(1) **Method I**: starting from the commercial 2,7-dibromofluorene, difluorenyl aldehyde (**a**) was obtained in four steps in an overall yield of 41% (shown in Scheme 4.2.1). Then in the final step: difluorenyl aldehyde **35** was formed upon connecting (**a**) to the commercial 2-bromofluorene by Sonogashira coupling, in a yield of 36% (shown in Scheme 4.2.2);



Scheme 4.2.1 Syntheses of 9,9-dibutyl-7-ethynyl-fluorene-2-carbaldehyde (**a**)

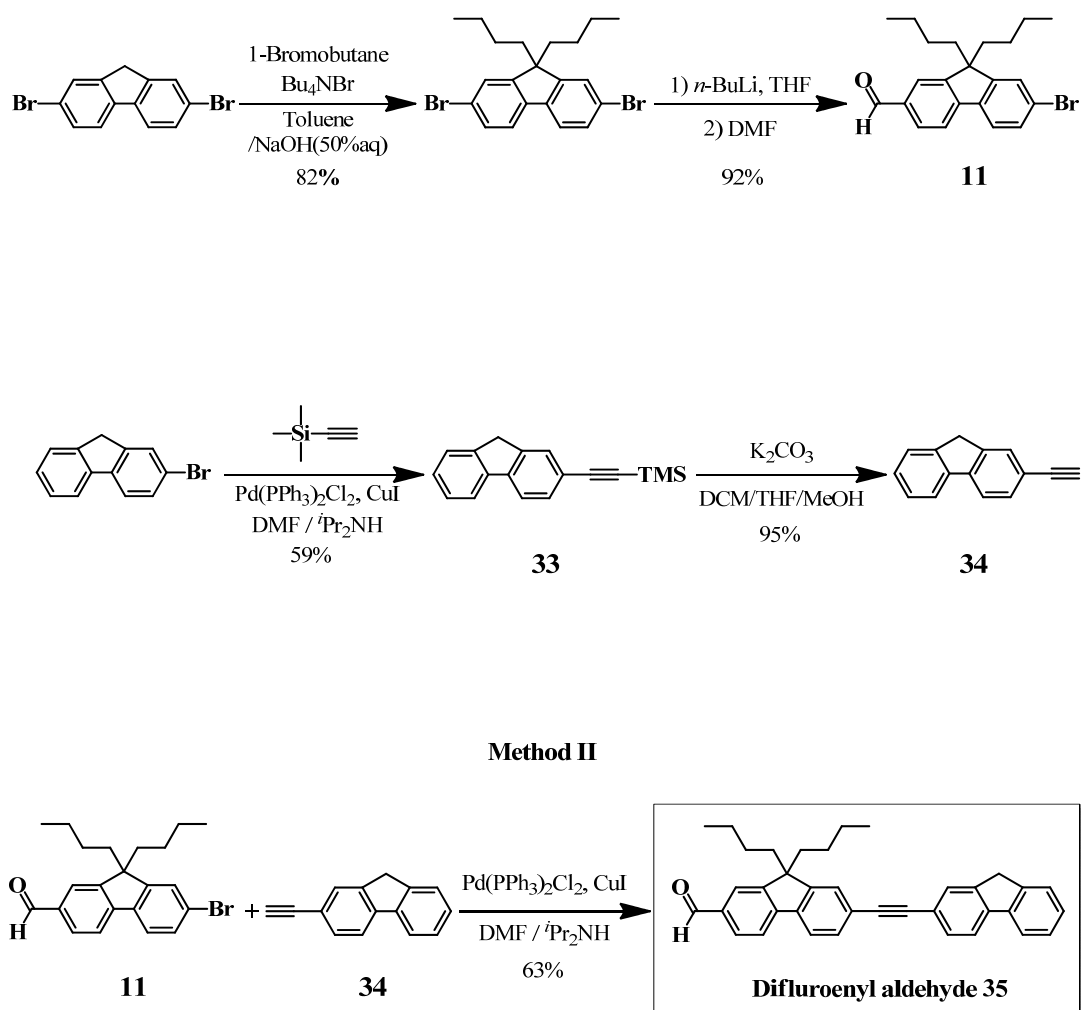
(2) **Method II**: the commercial 2,7-dibromofluorene and 2-bromofluorene were used as starting materials for two steps syntheses of the compounds **11** and **34** respectively. The overall yields were 88% and 55% as described above (Scheme 4.2.3). For the last step, Sonogashira coupling of **11** and **34**, gave the difluorenyl aldehyde **35** in an isolated yield of 63%.



Scheme 4.2.2 Two synthetic paths of difluorenyl aldehyde **35**

Method II was chosen as the most efficient synthetic process to obtain difluorenyl aldehyde **35**. For this method, the full processes shown in Scheme 4.2.3. Firstly one equivalent of 2,7-dibromofluorene was allowed to react with three

equivalent of 1-bromobutane so as to provide *n*-butyl-substituents that increase the solubility of the product compounds; subsequently, compound **11** was formed by exchanging one of the bromines to aldehyde in a yield of 92%. The second reagent, compound **34**, was obtained in two steps starting from 2-bromofluorene in the yield of 56% overall. Finally the difluorenyl aldehyde **35** was obtained by assembling **11** and **34** by the chosen **Method II** affording the yield of 63%.

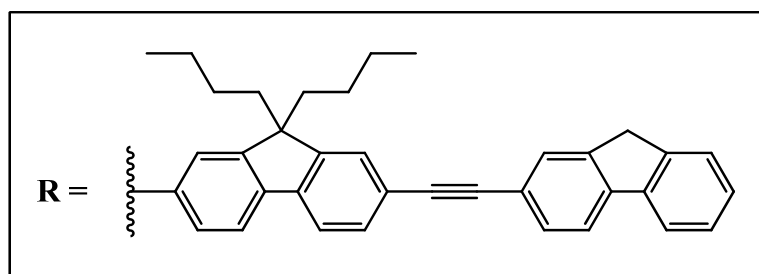
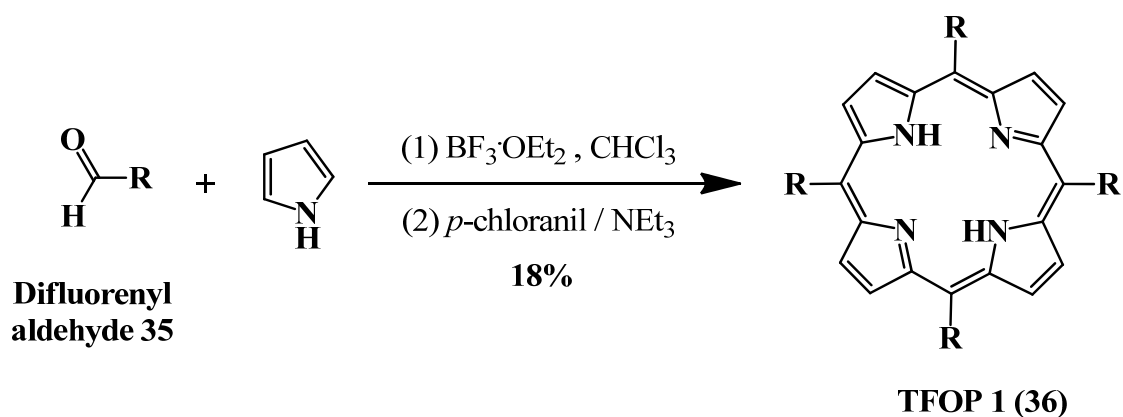


Scheme 4.2.3 Synthetic processes of difluorenyl aldehyde **35**

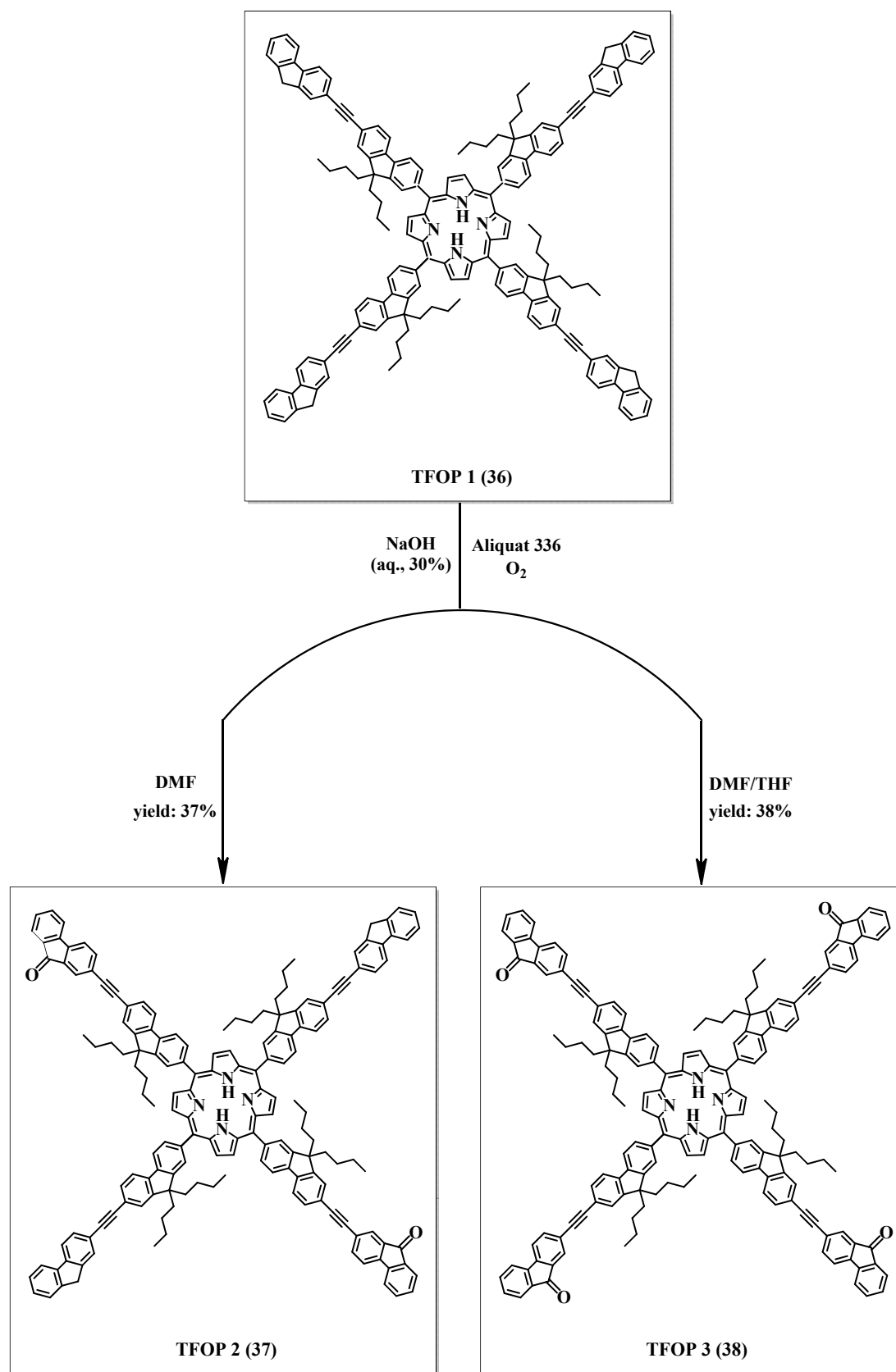
4.2.2 TFOP 1, 2 and 3 formations

Once the precursor aldehyde **35** has been prepared, we can synthesize the three target porphyrins: **TFOP 1-3**.

TFOP 1 (36) was firstly obtained under the classic Lindsey conditions that were described in the **Introduction** chapter. As shown in Scheme 4.2.3, one equivalent of aldehyde **35** and pyrrole were dissolved in distilled CHCl_3 ; the mixture was degassed by argon bubbling for 30 min. Then the system was covered by aluminium foil and $\text{BF}_3 \cdot \text{OEt}_2$ was injected to start the reaction. The mixture was stirred in the dark for 3h under argon protection, and, secondly, *p*-chloranil was added without and protection to convert the product (porphyrinogen) into the aromatic porphyrin, for 1h. Finally, NEt_3 was injected to neutralize the excess acid. The volatiles were evaporated and **TFOP 1 (36)** was isolated by silica gel chromatography in the yield of 18%.



Scheme 4.2.3 Synthesis process of TFOP 1 (36) under Lindsey conditions



Scheme 4.2.4 Synthetic process of TFOP 2 and TFOP 3 from TFOP 1

In 2006, we have already reported the syntheses of **TFOP** by oxidation of **TFP** in our laboratory ^[4] (see Scheme 4.1.1), so here, **TFOP 2 (37)** and **TFOP 3 (38)** were synthesized in the same path from **TFOP 1 (36)**, as described in Scheme 4.2.4.

TFOP 1 (36) was dissolved in DMF, and then aqueous NaOH (30%, aq.) was carefully added, followed by addition of Aliquat 336 (tricaprylmethylammonium chloride). The mixture was stirred vigorously for 59 h, with monitoring by TLC until the starting material disappeared. The pure product was collected by silica gel chromatography; **TFOP 2 (37)** was finally obtained with the yield of 37%.

During the formation of **TFOP 2 (37)**, we noticed that the reaction medium contained many insoluble compounds, meaning the DMF could not dissolve all the **TFOP 1 (36)**. This might be why only two CH₂ groups in 9 position of fluorenyl were oxidized. We tried to synthesize the totally oxidized **TFOP 3 (38)**: the same volume of THF was combined with DMF to help dissolution of the starting materials. In this case, the four terminal fluorenyls of **TFOP 1 (36)** were completely oxidized and symmetrical **TFOP 3 (38)** was obtained in the yield of 38%.

4.3 ¹H NMR analyses

All the new obtained compounds: **11**, **364**, difluorenyl aldehyde **35** and **TFOP 1-3 (36-38)** have been characterized by ¹H NMR spectra.

4.3.1 Compound **11**, **34** and difluorenyl aldehyde **35**

The complete ¹H NMR spectrum of compound **11** in CDCl₃ is shown in Figure 4.3.1. The aldehyde proton is characterized by the singlet at 10.0 ppm. The first following multiplet corresponds to the protons 1, 3. The next two doublets are identified as proton 4 and 5. And the protons 6 and 8 are presented as the second multiplet in aromatic zone.

The peaks of butyl chain protons: H_a, H_b, H_c and H_d lie in the region of 0.5-2.5 ppm as usual.

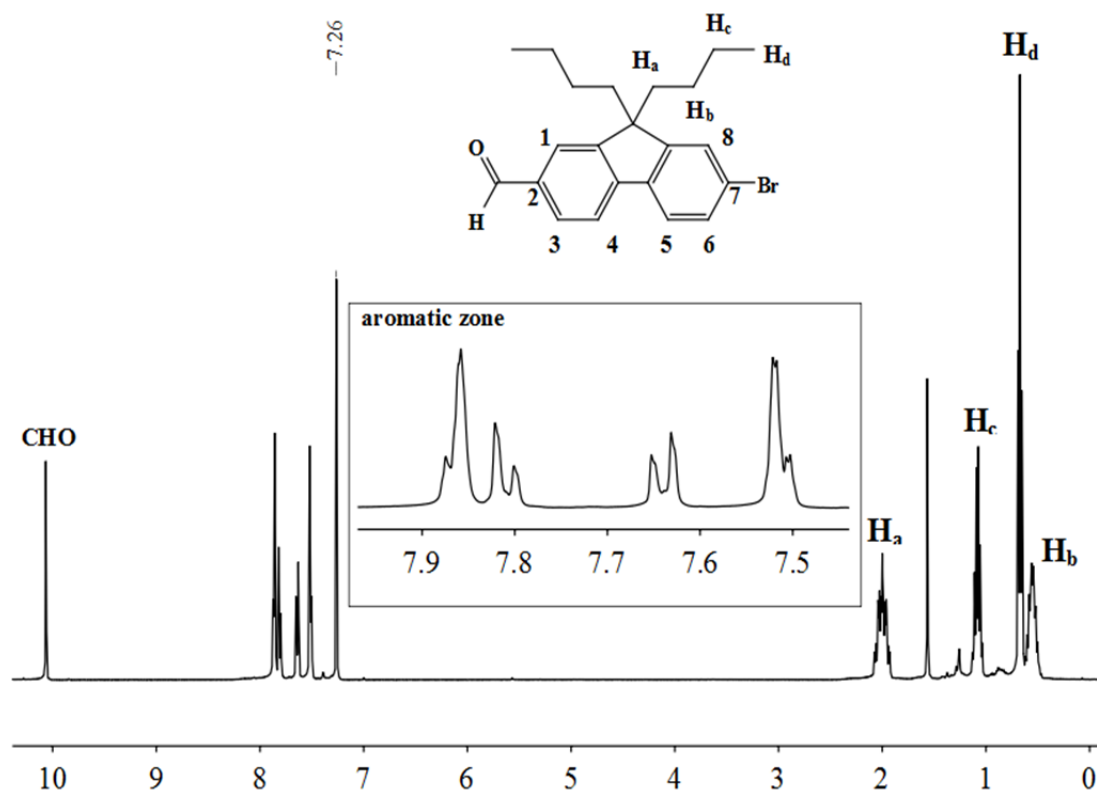


Figure 4.3.1 Complete ^1H NMR spectrum of compound 11

Figure 4.3.2 shows the complete ^1H NMR spectrum of compound 34, all the peaks can be clearly identified. As presented, protons 4 and 5 are identified by the two adjoining doublets between 7.7-7.8 ppm; the following singlet at 7.67 ppm corresponds to proton 1; the two overlapped doublets in range of 7.5-7.6 ppm are recognized as the protons 3 and 8; the next multiplet comprises two overlapped triplets corresponding to protons 6 and 7 between 7.3-7.4 ppm; the two protons 9 of methylene are clearly identified by the singlet at 3.9 ppm, and the terminal proton 10 of alkynyl appears as a singlet at 3.1 ppm.

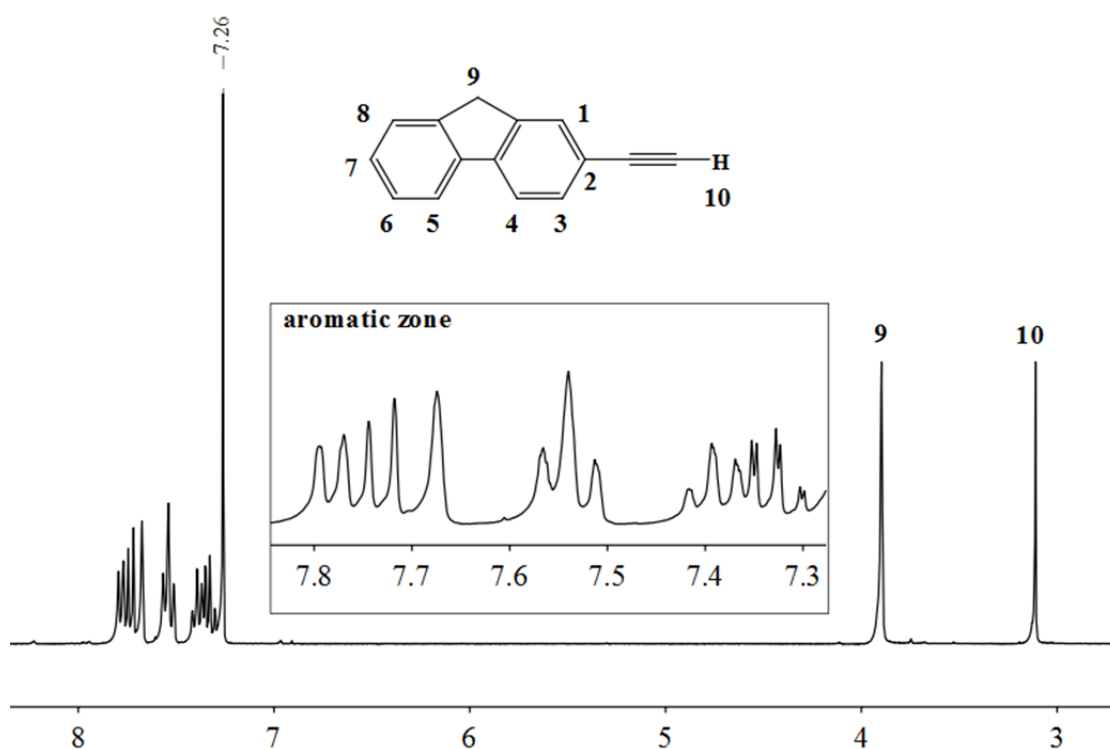


Figure 4.3.2 Complete ^1H NMR spectrum of compound **34**

The complete ^1H NMR spectrum of difluorenyl aldehyde **35** is shown in Figure 4.3.3. The aldehyde proton, as for compound **11**, is presented as a singlet at 10.0 ppm. The aromatic protons of **35** are identified by three multiplets in region of 7.3-8.0 ppm. The singlet at 4.1 ppm corresponds to the two methylene protons H_e of non-substituted fluorenyl, and the *n*-butyl chains protons: H_a , H_b , H_c and H_d are characterized in the normal alkyl zone.

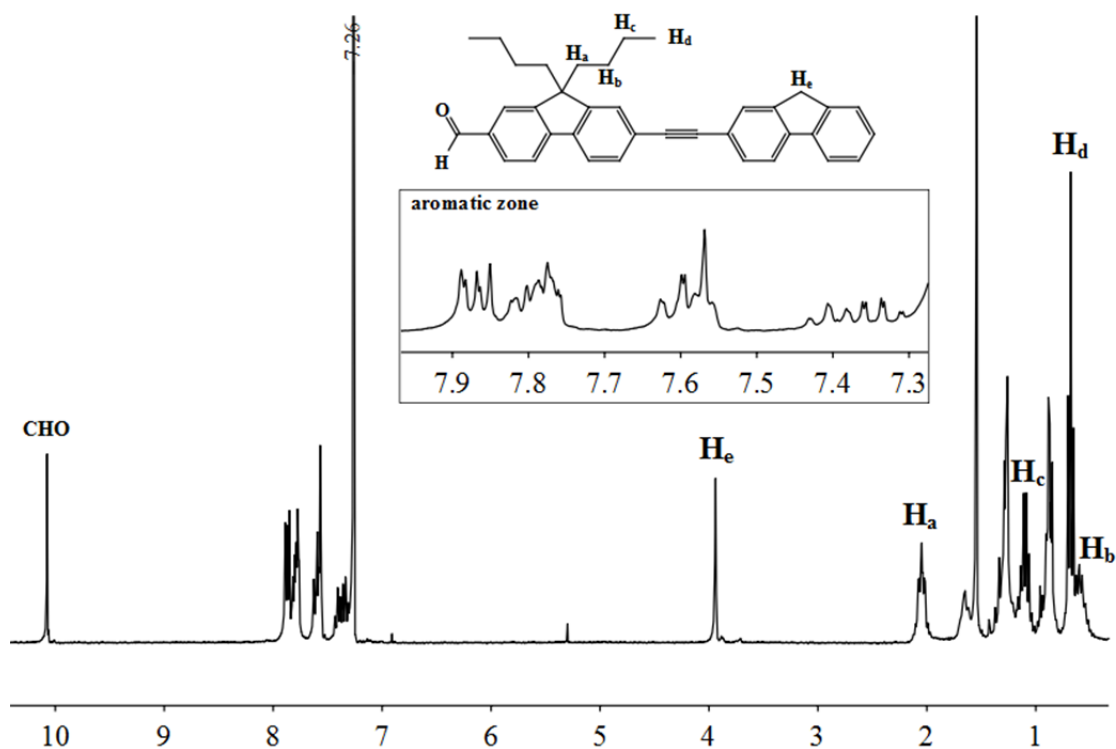


Figure 4.3.3 Complete ^1H NMR spectrum of difluorenyl aldehyde **35**

4.3.2 Porphyrins: **TFOP 1**, **2** and **3**

These desired products: **TFOP 1**, **2** and **3** were characterized by ^1H NMR in THF-d^8 (shown in Figure 4.3.5). Their structures and labels are described in Figure 4.3.4. As expected, the spectra of symmetrical **TFOP 1** and **TFOP 3** are well defined whereas **TFOP 2** resembles a superposition of the two previous spectra. In the comparative partial spectra of aromatic zone, the protons of red colored fluorenyl units, near the porphyrin shielding cone, are clearly recognized by the peaks ranged in 8.0-8.4 ppm region. The peaks, strongly overlapped in 7.5-7.9 region, correspond to blue and orange colored fluorenyl units, including the doublets identifying H_6 and H_8 , but H_{15} , $\text{H}_{15'}$, H_{16} and $\text{H}_{16'}$ are identified by the triplets ranged from 7.2 to 7.6 ppm, particularly the H_{15} and H_{16} of fluorenone units of **TFOP 3**, the last two protons are characterized by two isolated triplets at 7.56 and 7.36 ppm.

In addition, for these three porphyrins, the β -pyrrolic protons are identified as the lowest field singlet, around 8.9 ppm. Because of the long distance from the oxygen atoms to porphyrin core, we cannot judge these two oxygen atoms are in *trans* or *cis* position, so we drew it as *trans* porphyrin. Correspondingly, the singlets, present at 3.9 ppm that relate to H₁₈ for **TFOP 1** and **2**, progressively disappear upon increasing substitution of oxygen atoms.

The *n*-butyl chains are easily recognized in alkyl region and the two NH protons of all of these three porphyrins are found as singlets at the highest field, around -2.5 ppm.

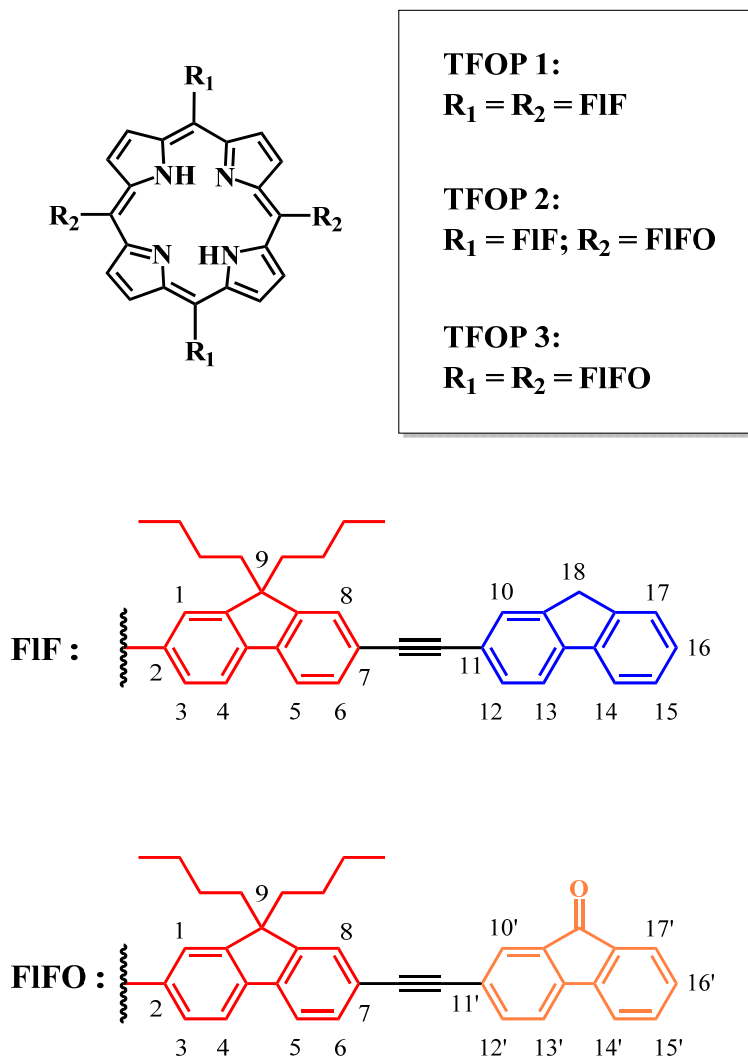


Figure 4.3.4 Molecular structure of porphyrin dendrimers **TFOP 1, 2 and 3**

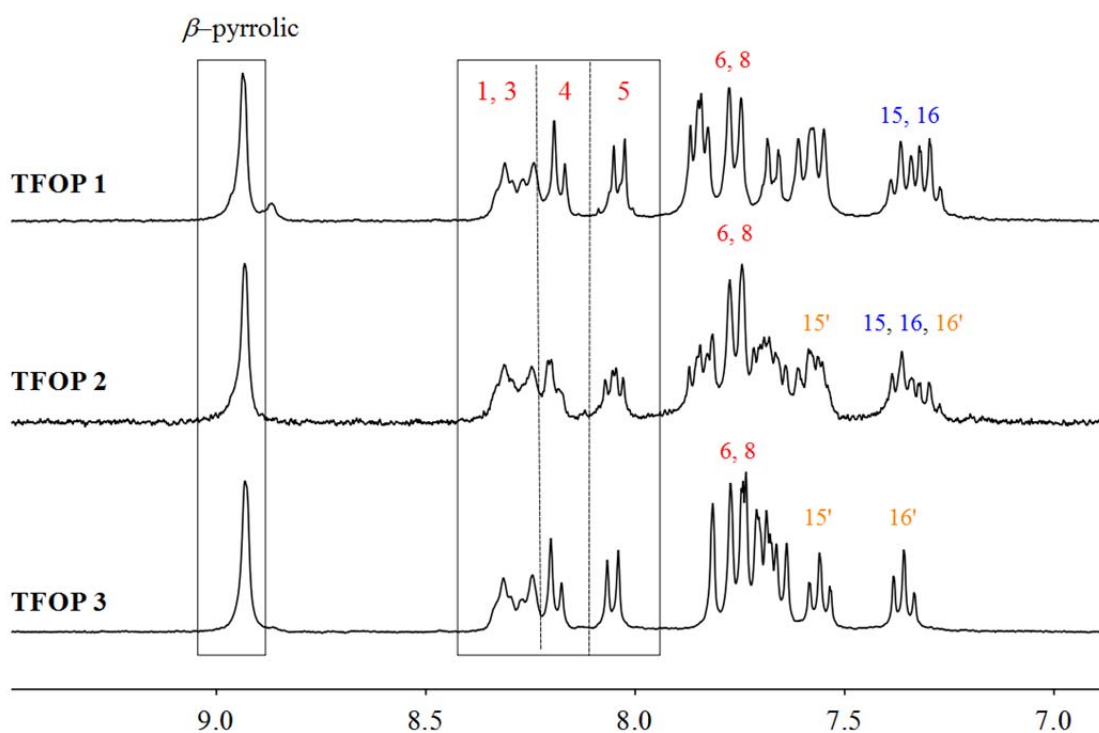


Figure 4.3.5 Partial comparative ^1H NMR spectra of TFOP 1, 2 and 3

4.4 Optical properties

The UV-visible absorption and photoluminescence spectra measurements for new porphyrins **TFOP 1**, **TFOP 2** and **TFOP 3** were performed in CH_2Cl_2 (HPLC level) at room temperature, as well as the reference *tetra*-alkynyl porphyrin **17**. Their detailed structures are shown in Figure 4.4.1.

To investigate the effect on the optical behavior that arises from the presence of the fluorenone units on porphyrin ring, energy transfer was studied. This new family of porphyrins was also excited in the region corresponding to dendron absorption. The detailed optical properties will be described in this section, and the corresponding data are listed in Table 4.4.1.

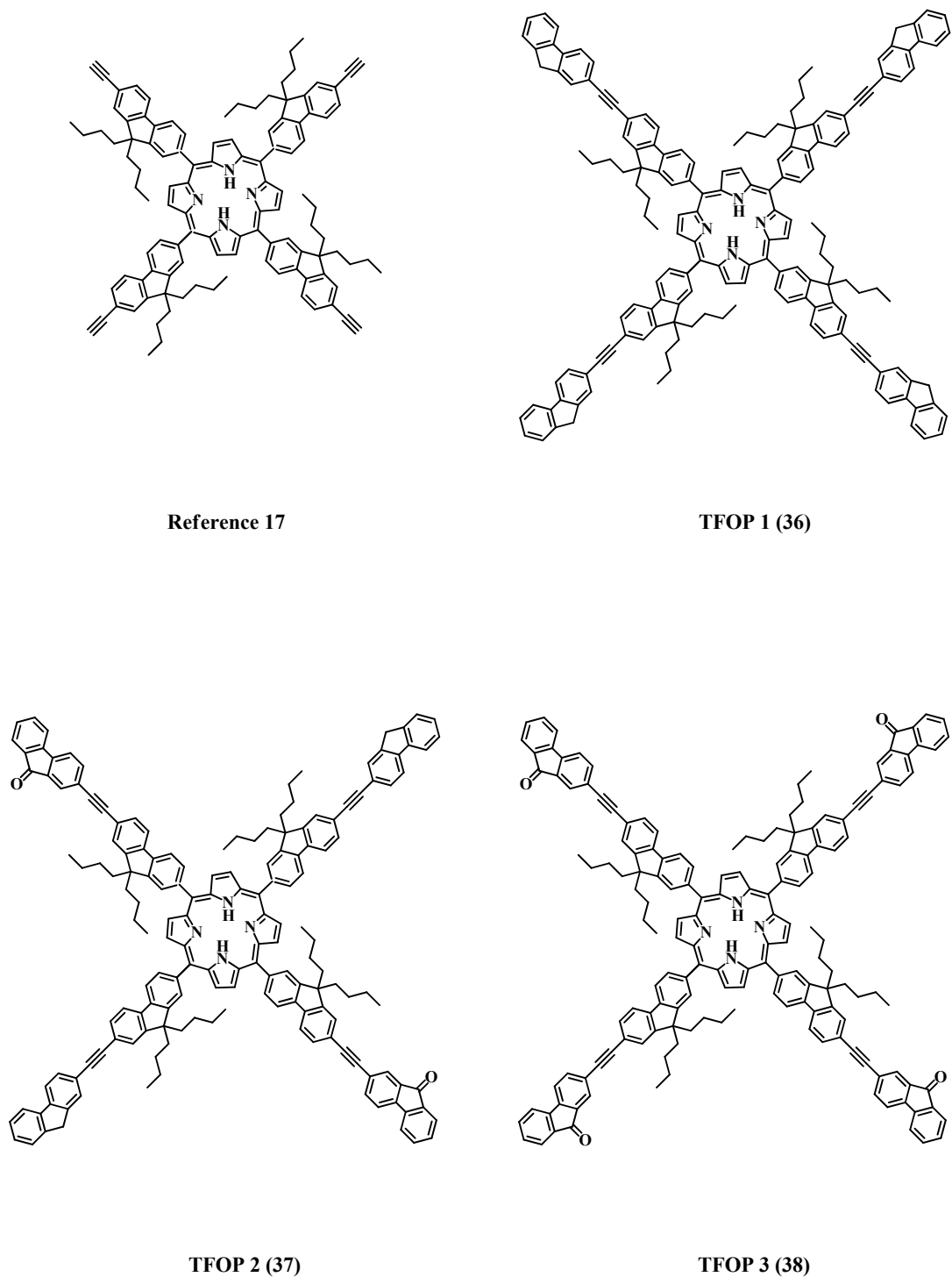


Figure 4.4.1 The entire structure of TFOP 1-3 (36-38) and reference 17

Table 4.4.1 Photophysical properties data of the new series of fluorenone porphyrins: TFOP 1-3 (36-38) and reference 17 in CH₂Cl₂ (HPLC quality) at R.T.

	λ_{dendron} / nm	λ_{Soret} / nm	$\lambda_{\text{Q-bands}}$ / nm	λ_{em} / nm	Φ_{fl}^a / %	τ / ns
17	292	428	520, 558, 594, 652	660, 724	15	8.2
TFOP 1	340	431	521, 559, 596, 652	660, 725	22	8.0
TFOP 2	315, 346	431	521, 558, 596, 652	660, 725	21	8.0
TFOP 3	310, 352	431	521, 560, 596, 652	660, 724	22	8.0

^a Fluorescence quantum yield determined relative to TPP in toluene.

4.4.1 Absorption spectra of TFOP 1, 2 and 3

The *para*-substituted porphyrins **TFOP 1-3**, as well as the reference **17**, have three components in their normalized UV-visible absorption spectra (Figure 4.4.2):

(1) Dendron absorption in 250-400 nm region: these absorption bands are due to the fluorenyl alkynyl units for **17**, and to fluorenyl and fluorenone units for **TFOP 1-3**;

(2) Intense Soret band at 431 nm is a typical porphyrin absorption;

(3) Four Q-bands in 500-700 nm region: these bands characterize **TFOP 1, 2** and **3** as free base porphyrins, that do not have metal atoms in the center of porphyrin ring.

After normalizing the intensity of Soret bands, by comparing to the reference porphyrin **17** in Figure 4.4.2, these three new porphyrins **TFOP 1-3** present the following differences:

(i) The intensity of their dendron absorptions decrease regularly following the increasing fluorenone units and present red shifts, because the fluorenyl-fluorenone arms are stronger conjugated than fluorenyl-alkynyl units; the dendron absorption bands are divided to two peaks regularly following the increasing number of oxygen. Probably the higher energy band at 310 nm corresponds to the oxidized fluorenone units and the lower one at 352 nm is to the fluorenyl units. As expected, these dendron

absorption bands are all stronger than that of reference **17** containing only four fluorenyls;

(ii) Their normalized porphyrin core absorption (Soret band and Q-bands) present slight red shifts compared to **17**, but shows no shifts when compare among **TFOP 1, 2** and **3**.

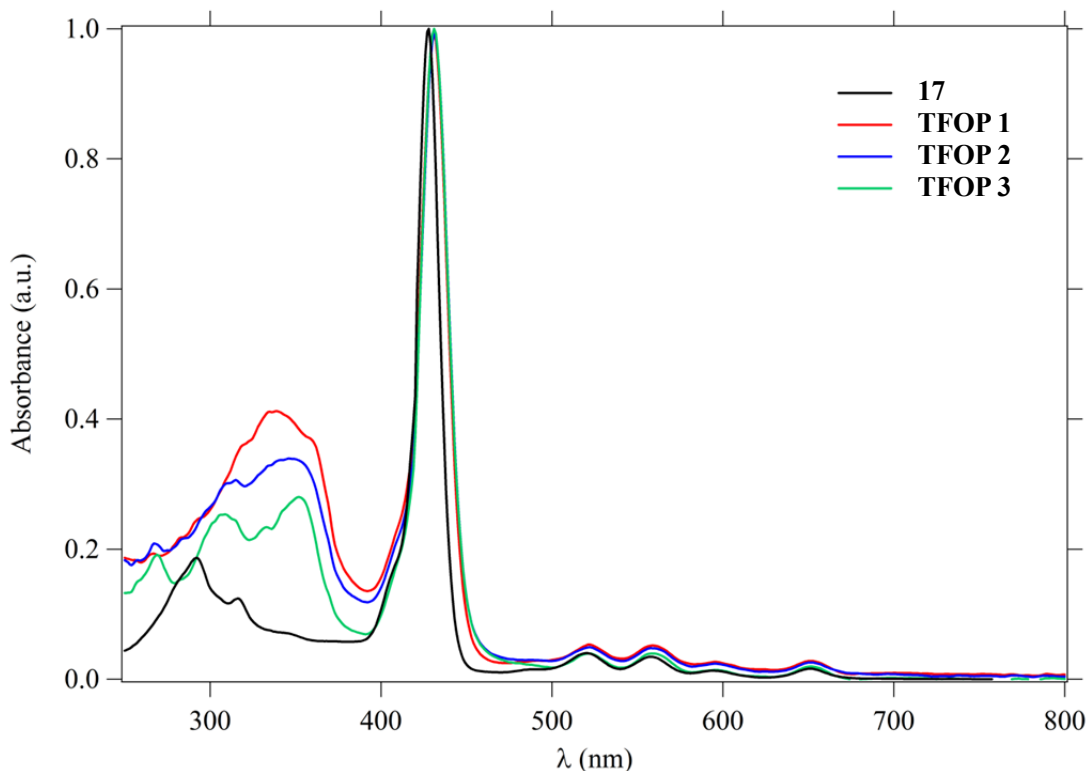


Figure 4.4.2 UV-visible spectra of TFOP 1-3 and reference **17**

4.4.2 Emission spectra of TFOP 1, 2 and 3

After Soret band excitation, porphyrins **17**, **TFOP 1, 2** and **3** all exhibit red fluorescence. The normalized emission spectra are shown in Figure 4.4.3. By comparing to **17**, we can notice that the intense Q(0,0) bands of new porphyrins present no shifts. Their weaker bands Q(0,1) are in the same intensity for **TFOP 1-3**, but slightly lower than the corresponding band of **17**.

Generally, as with **17**, the porphyrin presents only two Q-bands in the emission spectrum, but in the normalized spectra for these new fluorenone porphyrins, their weak emission bands Q_x are supplementary observed in 580-630 nm region, probably

due to the oxygen atoms, shown in Figure 4.4.4. The smallest emission belongs to **TFOP 1** where no oxygen is present; the complete oxidized **TFOP 3** with four oxygen atoms presents a slightly stronger Q_x band, but the most intense emission is from **TFOP 2**, which has only two oxygens substituting at 9 position of terminal fluorenyl unit in *trans*-position. Investigations on the origin of this unexpected extra band Q_x are in progress.

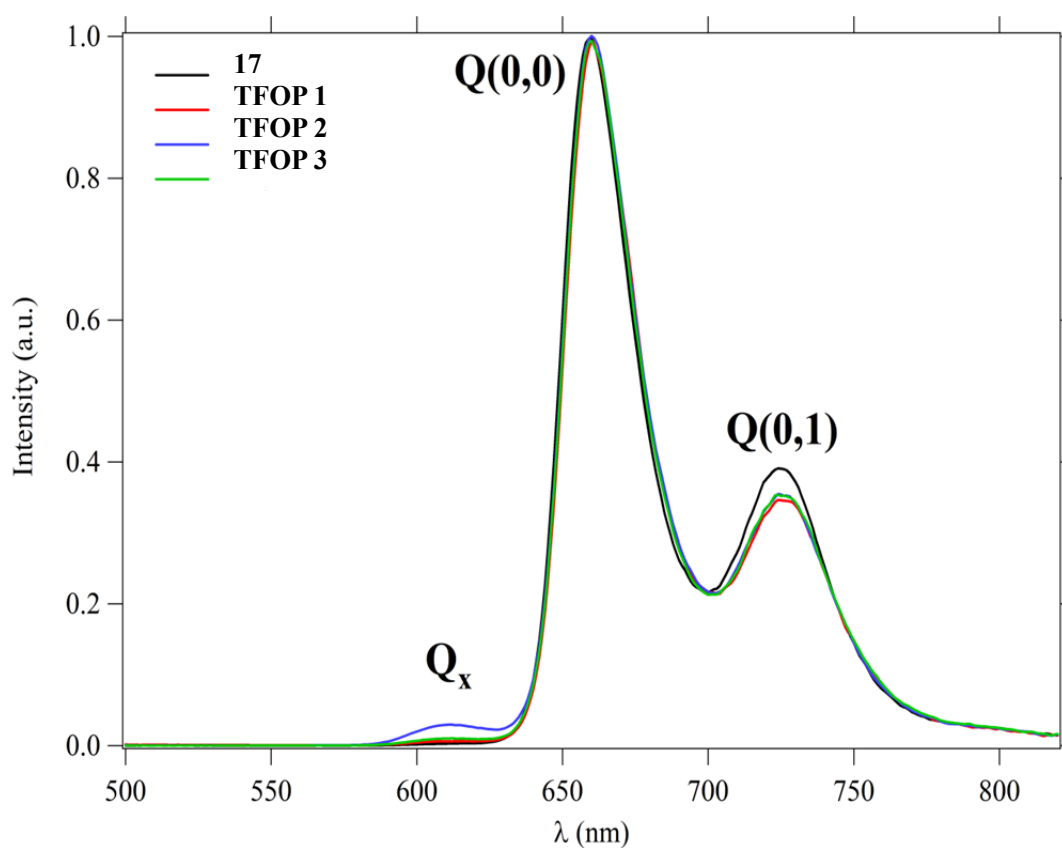


Figure 4.4.3 Normalized emission spectra of 17, TFOP1-3 in 500-820 nm

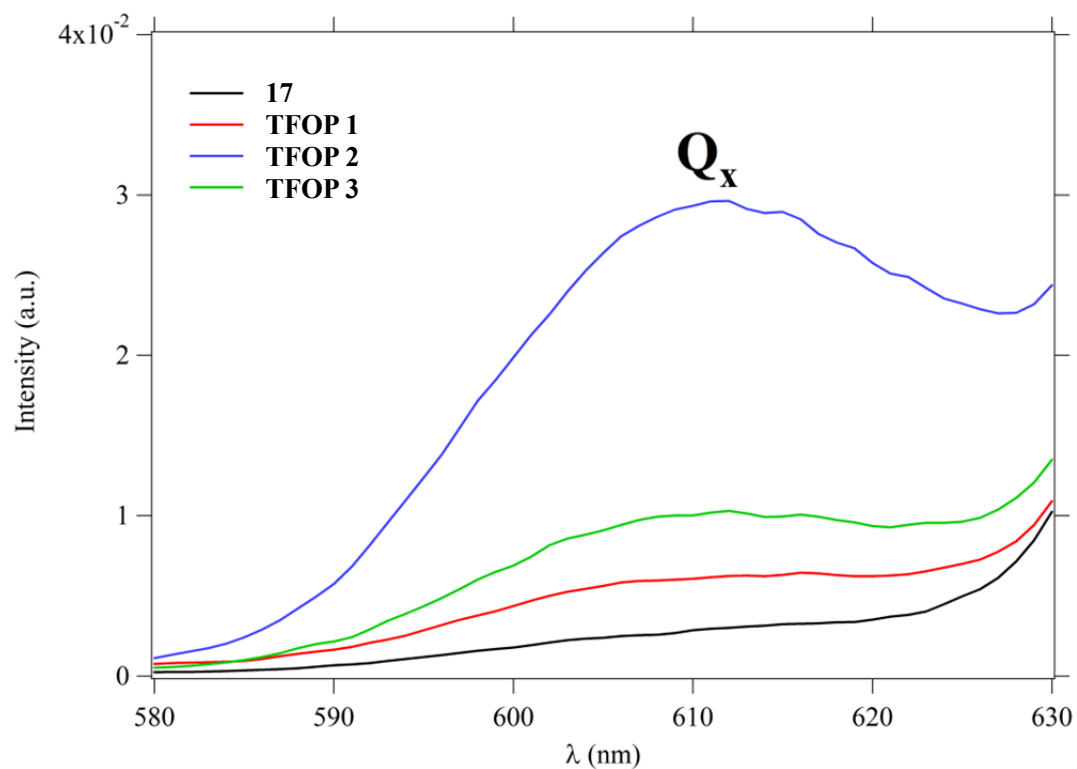


Figure 4.4.4 Partial emission spectra of 17, TFOP 1-3 from 580 to 630 nm

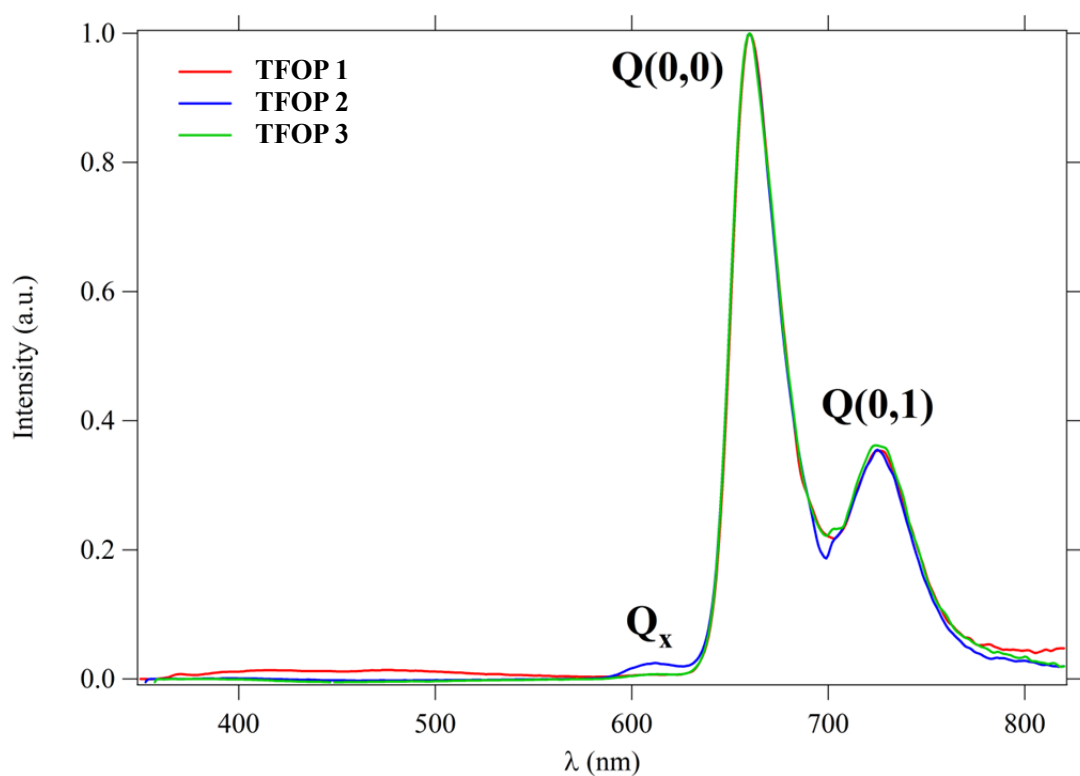


Figure 4.4.5 Normalized emission spectra of TFOP 1-3 excited in dendron absorption (380 nm)

To study the **ET behavior**, all these *para*-fluorenone porphyrins were excited at their dendron absorption region and the obtained normalized spectra are shown in Figure 4.4.5. After excitation, the intense Q(0,0) band, as well as the Q(0,1) band, are observed. The same spectra are obtained in Figure 4.4.4, the weak emission band Q_x of **TFOP 2** is observed again in 580-630 nm region as observed before by Soret excitation.

As shown in Figure 4.4.5, these three porphyrins present almost no residual emission bands in the dendron emission zone, suggesting that the energy transfer is very efficient from the dendrons to the central porphyrin core.

In addition, the quantum yield and the lifetime were also measured in the same conditions as the previous ones. The quantum yields (Φ_f %) are not modified by the substitution of oxygen atoms, they are very similar for **TFOP 1-3**: 22%, 21% and 22% respectively.

In consequence, these new porphyrins have the same lifetime due to the similar quantum yields.

4.5 Conclusions

1. A new group of fluorenone porphyrin dendrimers: **TFOP 1-3** have been designed and synthesized successfully. Starting from **TFOP 1**, its 9H of terminal fluorenyl units were oxidized partially to isolate the **TFOP 2** and completely to obtain **TFOP 3**.

2. These new dendrimers **TFOP1-3** were characterized and analyzed by ^1H NMR.

3. The linear optical properties of **TFOP 1-3** were studied by measuring their UV-visible absorption and photo luminescence spectra:

(i) For their dendron absorption: the absorption bands appeared at UV region and were divided to two parts following the increasing substitution of oxygen atoms in the 9H of terminal fluorenyl units. Compared to the reference **17**, the typical Soret band absorption of **TFOP 1-3** all present slightly red shifts, with the same phenomenon being observed in their Q-bands;

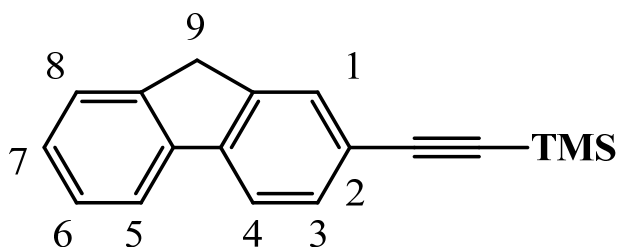
(ii) These new dendrimers all exhibit red luminescence after excitation at their Soret bands. To study their energy transfer (**ET**) behaviors, they also were excited at the dendron absorption bands. The results suggest that their ET from the linear dendrons to porphyrin core is efficient.

(iii) After excitation at Soret band or dendron absorption band, an extra emission band Q_x appeared, especially for the *trans*-fluorenone dendrimer **TFOP 2**, where Q_x band were clearly presented. The studies of this Q_x band are in progress.

4. The nonlinear optical properties of **TFOP 1-3** will be studied. The two-photon absorption cross-sections of these new porphyrin dendrimers **TFOP 1-3** are studied in progress.

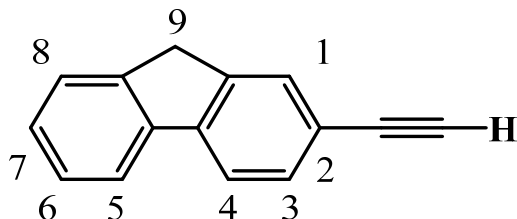
Experimental Section

2-(trimethylsilyl)ethynyl-fluorene (**33**)



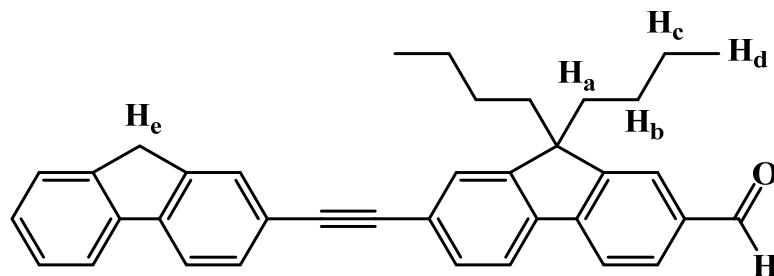
In a Schlenk tube, a mixture of commercial 2-bromofluorene (5.0 g, 20.4 mmol, 1 equiv.), ethynyltrimethylsilane (4.4 mL, 30.6 mmol, 1.5 equiv.), Pd(PPh₃)₂Cl₂ (85.9 mg, 0.12 mmol, 0.6% equiv.) and CuI (11.7 mg, 0.06 mmol, 0.3% equiv.) were dissolved in DMF (12 mL) and ^{*i*}Pr₂NH (12 mL) was added under argon. The reaction medium was degassed by freeze-pump-thaw twice and heated for 48h at 95 °C. After evaporation of the volatiles, residue was further purified by silica chromatography using heptane as eluent; the yellow crude powder **33** (3.17 g, 59% yield) was obtained.

¹H NMR (400 MHz, CDCl₃, ppm): δ = 7.77 (d, *J* = 7.6 Hz, 1H, H₅), 7.71 (d, *J* = 8.0 Hz, 1H, H₄), 7.66 (s, 1H, H₁), 7.54 (d, *J* = 7.6 Hz, 1H, H₈), 7.50 (d, *J* = 8.4 Hz, 1H, H₃), 7.38 (t, *J* = 7.2 Hz, 1H, H₇), 7.32 (t, *J* = 7.6 Hz, 1H, H₆), 3.88 (s, 2H, H₉), 0.27 (s, 9H, H_{TMS}).

2-ethynyl-fluorene (34)

The former crude product **33** (1.88 g, 7.15 mmol, 1 equiv.) was dissolved in a mixture of CH_2Cl_2 (90 mL), THF (30 mL) and MeOH (30 mL), together with K_2CO_3 (3.0 g, 21.5 mmol, 3 equiv.). Then this mixture was stirred at 40 °C overnight. After evaporation of the volatiles, residue was purified by silica gel chromatography using heptane as eluent; **2-ethynyl-fluorene (34)** was isolated as white powder (1.29 g, 95% yield).

$^1\text{H NMR}$ (300 MHz, CDCl_3 , ppm): $\delta = 7.78$ (d, $J = 7.5$ Hz, 1H, H_5), 7.73 (d, $J = 7.8$ Hz, 1H, H_4), 7.67 (s, 1H, H_1), 7.54 (t, $J = 8.4$ Hz, 2H, $\text{H}_{8,3}$), 7.42-7.30 (m, 2H, $\text{H}_{6,7}$), 3.90 (s, 2H, H_9), 3.11 (s, 1H, $\text{H}_{\text{alkynyl}}$).

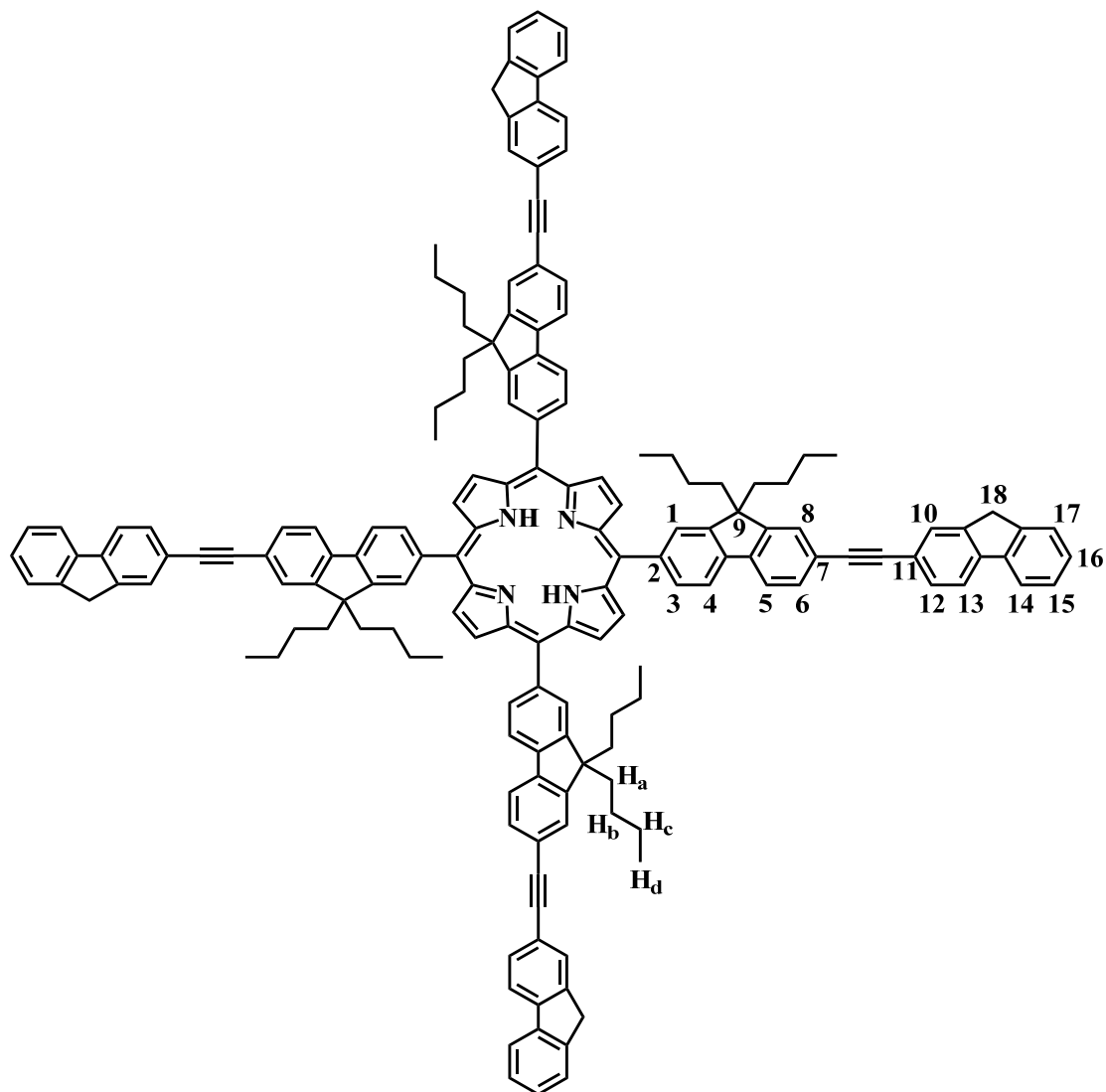
Difluorenyl aldehyde (35)

In a Schlenk tube, a mixture of **7-bromo-9,9-dibutyl-fluorene-2-carboxaldehyde (11)** (492 mg, 1.28 mmol, 1 equiv.), **2-ethynyl-fluorene (34)** (365 mg, 1.92 mmol, 1.5 equiv.), Pd (PPh₃)₂Cl₂ (5.4 mg, 0.008 mmol, 0.6% equiv.) and CuI (excess) were dissolved in DMF (5 mL) and then ⁱPr₂NH (5 mL) was added under argon. The reaction medium was degassed by freeze-pump-thaw twice and heated for 48h at 95 °C. After evaporation of the volatiles, residue was further purified by silica chromatography using heptane as eluent; the compound **35** (398 mg, 63% yield) was obtained as a yellow powder.

¹H NMR (400 MHz, CDCl₃, ppm): δ = 10.07 (s, 1H, H_{CHO}), 7.89-7.76 (m, 7H, H_{fluorenyl}), 7.63-7.57 (m, 3H, H_{fluorenyl}), 7.43-7.31 (m, 3H, H_{fluorenyl}), 3.94 (s, 2H, H_e), 2.10-1.99 (m, 4H, H_a), 1.16-1.04 (m, 4H, H_c), 0.70-0.44 (m, 10H, H_b, H_d).

¹³C NMR (100 MHz, CDCl₃, ppm): δ = 186.6, 186.5, 177.7, 162.2, 161.9, 161.7, 161.0, 157.6, 156.2, 155.2, 150.9, 150.6, 149.0, 143.1, 139.1, 138.3, 137.8, 133.6, 131.2, 130.7, 128.3, 105.1, 99.5, 65.8, 65.6, 50.7, 50.6, 50.5, 48.8, 45.4, 44.9, 42.6, 41.5, 40.4, 40.0, 35.2, 33.6, 33.3, 23.9, 11.1.

TFOP 1 (36)



In a two-neck flask, a mixture of **difluorenyl aldehyde 35** (564 mg, 1.14 mmol, 1 equiv.) and pyrrole (0.08 mL, 1.14 mmol, 1 equiv.) were dissolved in distilled chloroform (250 mL) under argon. After degassing the mixture with argon bubbling for 30 min, $\text{BF}_3 \cdot \text{OEt}_2$ (0.04 mL, 0.29 mmol, 0.25 equiv.) was injected and the reaction

was stirred in dark for 3 h under argon at room temperature. Then oxidant *p*-chloranil (210 mg, 0.86 mmol, 0.75 equiv.) was added, and the reaction was heated at 45 °C for another 1 h without any protection. After cooling the reaction to room temperature, NEt₃ (2 mL) was injected, and then keep stirring for several minutes. After evaporation of the volatiles, purification was done by silica gel chromatography using THF/heptane (1:4) mixture as eluents, the porphyrin **36** was collected as violet powder (110 mg, 18% yield).

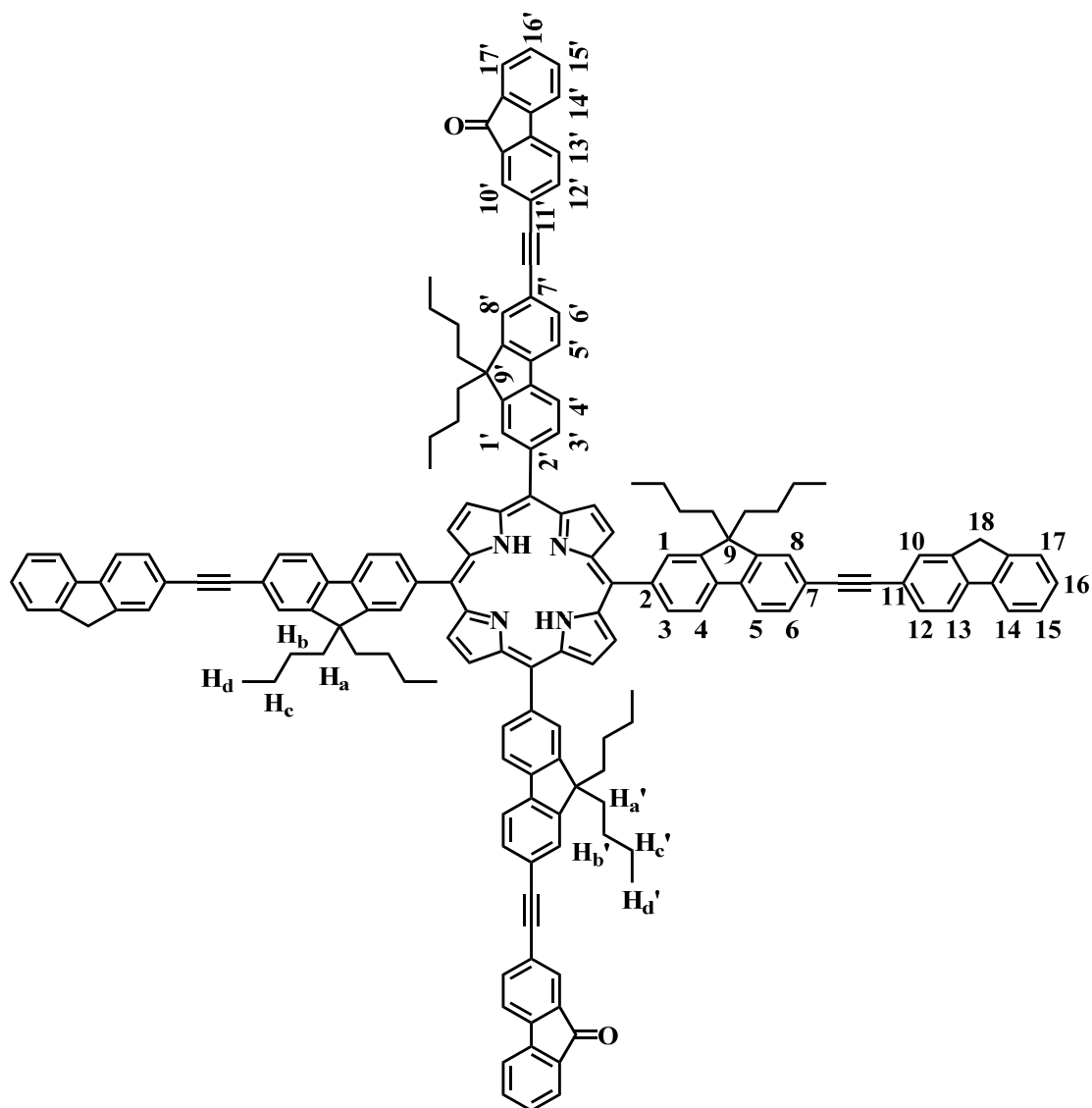
¹H NMR (300 MHz, THF-d₈, ppm): δ = 8.94 (s, 8H, H_{β-pyrrolic}), 8.31-8.24 (m, 8H, H_{1,3}), 8.18 (d, 4H, *J* = 7.8 Hz, H₄), 8.04 (d, 4H, *J* = 8.1 Hz, H₅), 7.87-7.83 (m, 8H, H_{10,12}), 7.76 (d, 4H, *J* = 8.4 Hz, H_{6,8}), 7.67 (d, 4H, *J* = 7.8 Hz, H₁₃), 7.61-7.55 (m, 8H, H_{14,17}), 7.39-7.27 (m, 8H, H_{15,16}), 3.95 (s, 8H, H₁₈), 2.25 (s, 16H, H_a), 1.28-1.19 (m, 16H, H_c), 1.10-0.94 (m, 16H, H_b), 0.83-0.77 (m, 24H, H_d), -2.50 (s, 2H, NH).

¹³C NMR (100 MHz, CDCl₃, ppm): δ = 143.7, 143.4, 141.9, 141.5, 141.3, 141.0, 140.4, 133.5, 130.7, 130.2, 129.3, 128.6, 127.9, 127.0, 126.7, 125.9, 124.8, 122.5, 121.6, 120.6, 120.1, 119.7, 118.2, 90.4, 90.2, 65.9, 55.3, 40.1, 36.4, 29.6, 26.4, 23.1, 13.4.

UV-vis (λ_{max}, CH₂Cl₂, nm): 340, 431, 521, 559, 596, 652.

HRMS-ESI for C₁₆₄H₁₄₂N₄: *m/z* = 2168.1231 [M+H]⁺ (calcd: 2168.13073).

Anal. Calcd. (%) for C₁₆₄H₁₄₂N₄·3THF: C 88.62; H 7.01; N 2.35. **Found:** C 88.71; H 7.15; N, 2.32.

TFOP 2 (37)

TFOP 2 (37) is synthesized by oxidizing **TFOP 1 (36)**, as described below. In a two-neck flask, **TFOP 1 (36)** (50 mg, 0.02 mmol, 1 equiv.) is dissolved in 1 mL of DMF. Aqueous NaOH (30%, 4.6 mL) is carefully added, followed by addition of Aliquat 336 (tricaprylmethylammonium chloride). The mixture is stirred for 59 h. Reaction progress is monitored by TLC, spotting directly from the organic layer. Then, the dark violet solution is separated and concentrated. The crude is chromatographed

on silica gel column with THF/heptane (1:4) as eluent, the **TFOP 2 (37)** is obtained as dark violet powder (19 mg, 37% yield).

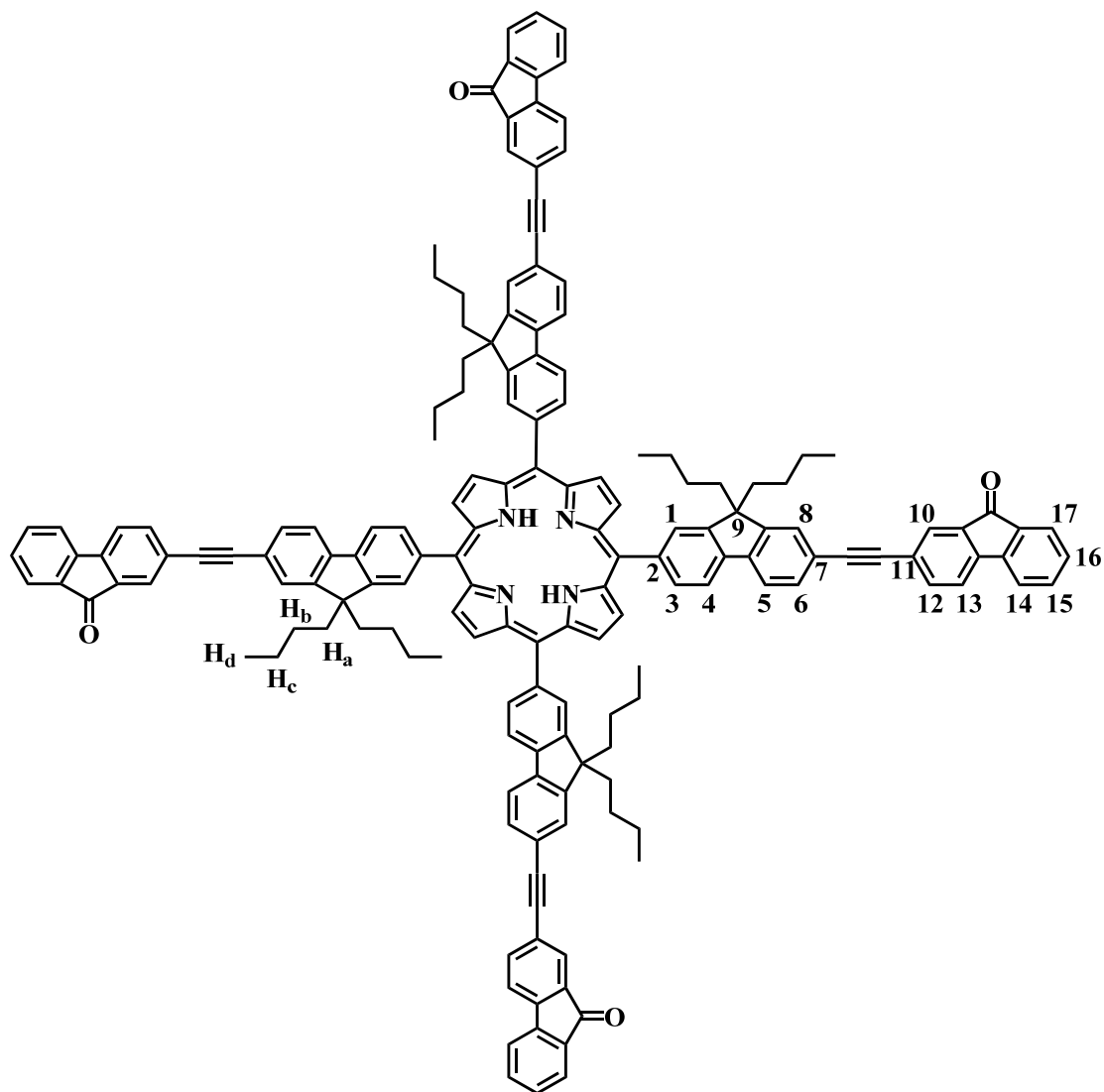
¹H NMR (300 MHz, THF-d₈, ppm): δ = 8.93 (s, 8H, H _{β} -pyrrolic), 8.34-8.18 (m, 12H, H_{1,3,4}, H_{1',3',4'}), 8.07-8.03 (m, 4H, H₅, H_{5'}), 7.87-7.82 (m, 6H, H_{fluorenyl, fluorenone}), 7.76 (d, 8H, J = 8.7 Hz, H_{6,8}, H_{6',8'}), 7.72-7.64 (m, 8H, H_{fluorenyl, fluorenone}), 7.61-7.54 (m, 8H, H_{fluorenyl, fluorenone}), 7.39-7.27 (m, 8H, H_{15,16}, H_{15',16'}), 3.96 (s, 8H, H₁₈), 2.25 (s, 16H, H_a, H_{a'}), 1.25-1.16 (m, 16H, H_c, H_{c'}), 1.10-0.93 (m, 16H, H_b, H_{b'}), 0.87-0.77 (m, 24H, H_d, H_{d'}), -2.50 (s, 2H, NH).

¹³C NMR (100 MHz, CDCl₃, ppm): δ = 143.7, 137.2, 134.8, 130.2, 129.3, 127.9, 126.7, 126.4, 124.8, 124.3, 123.8, 121.8, 120.8, 120.6, 120.0, 119.7, 90.4, 88.8, 40.0, 36.4, 29.6, 26.4, 23.1, 13.4.

UV-vis (λ_{max} , CH₂Cl₂, nm): 351, 431, 521, 560, 596, 652.

HRMS-ESI for C₁₆₄H₁₃₈N₄O₂: m/z = 2196.0847 [M+H]⁺ (calcd: 2196.08926).

Anal. Calcd. (%) for C₁₆₄H₁₃₈N₄O₂·3THF: C 87.60; H 6.77; N 2.32. **Found**: C 87.98; H 6.52; N, 2.25.

TFOP 3 (38)

TFOP 3 (38) is synthesized by completely oxidizing 9H on terminal fluorenyl arms of **TFOP 1 (36)**, as described below. In a two-neck flask, **TFOP 1 (36)** (36 mg, 0.02 mmol, 1 equiv.) is dissolved in DMF (1 mL) and THF (1 mL). Aqueous NaOH (30%, 4.6 ml) is carefully added, followed by addition of Aliquat 336 (tricaprylmethylammonium chloride). The mixture is stirred for 72 h. Reaction progress is monitored by TLC, spotting directly from the organic layer. Then, the dark violet solution is separated and concentrated. The crude is chromatographed on silica

gel column with THF/heptane (1:1) as eluent, the **TFOP 3 (38)** is obtained as dark violet powder (14 mg, 38% yield).

¹H NMR (300 MHz, THF-d₈, ppm): δ = 8.93 (s, 8H, H _{β} -pyrrolic), 8.32-8.25 (m, 8H, H_{1,3}), 8.19 (d, 4H, J = 7.8 Hz, H₄), 8.05 (d, 4H, J = 7.8 Hz, H₅), 7.82-7.64 (m, 28H, H_{fluorenyl, fluorenone}), 7.77-7.74 (m, 12H, H_{6,8,12}), 7.71-7.64 (m, 8H, H_{13,14,17}), 7.56 (t, 4H, J = 8.0 Hz, H₁₅), 7.36 (t, 4H, J = 7.4 Hz, H₁₆), 2.25 (t, J = 7.8 Hz, 16H, H_a), 1.26-1.16 (m, 16H, H_c), 1.11-0.93 (m, 16H, H_b), 0.82-0.77 (m, 24H, H_d), -2.50 (s, 2H, NH).

¹³C NMR (500 MHz, CDCl₃, ppm): δ = 193.5, 174.2, 153.2, 151.4, 145.8, 145.6, 143.6, 143.5, 142.1, 139.1, 136.6, 136.2, 135.3, 132.8, 131.2, 128.2, 128.0, 126.2, 125.7, 123.6, 122.6, 122.5, 122.4, 122.0, 120.2, 93.8, 90.6, 68.9, 68.8, 68.7, 68.6, 61.4, 57.2, 41.9, 39.9, 38.6, 33.7, 32.7, 31.5, 28.3, 26.7, 26.4, 26.2, 24.9, 15.3, 7.5.

UV-vis (λ_{max} , CH₂Cl₂, nm): 346, 431, 521, 558, 596, 652.

HRMS-ESI for C₁₆₄H₁₃₄N₄O₄: m/z = 2224.0442 [M+H]⁺ (calcd: 2224.04778).

Anal. Calcd. (%) for C₁₆₄H₁₃₄N₄O₄·3THF: C 86.59; H 6.52; N 2.30. **Found**: C 86.56; H 6.57; N, 2.07.

References

- [1] H. Nakamura, C. Hosokawa, T. Kusumoto, in: R.H. Mauch, H.E. Gumlich (Eds.), *Inorganic and Organic Electroluminescence/ EL 96*, Wissenschaft und Technik, Berlin, **1996**, 65.
- [2] J. Rault-Berthelot, E. Raoult, F. L. Floch, *J. Electroanal. Chem.*, **2003**, 546, 29.
- [3] X. H. Zang, Z. Y. Xie, F. P. Wu, L. L. Zhou, O. Y. Wong, C. S. Lee, H. L. Kwong, S. T. Lee, S. K. Wu, *Chem. Phys. Lett.*, **2003**, 382, 561.
- [4] C. O. Paul-Roth, G. Simonneaux, *Tetrahedron Lett.*, **2006**, 47, 3275.
- [5] D. Yao, X. Zhang, O. Mongin, F. Paul, C. O. Paul-Roth, *Chem. Eur. J.*, **2016**, 22, 5583.
- [6] C. O. Paul-Roth, G. Simonneaux, *C. R. Chimie*, **2006**, 9, 1277.
- [7] R.G. George, M. Padmanabhan, *Polyhedron*, **2003**, 22, 3145.
- [8] J. S. Lindsey, H. C. Hsu, I. C. Schreiman, *Tetrahedron Lett.*, **1986**, 27, 4969.
- [9] J. S. Lindsey, I. C. Schreiman, H. C. Hsu, P. C. Kearney, A. M. Marguerettaz, *J. Org. Chem.*, **1987**, 52, 827.
- [10] K. Sonogashira, Y. Tohda, N. Hagihara, *Tetrahedron Lett.*, **1975**, 50, 4467.

Perspectives

A different type of *meso* substituted porphyrin, like **ethynyl moieties substituted porphyrins**, leads to new materials for various potential applications, such as precursors for new conducting polymers ^[1-3], non-linear optical materials ^[4,5], photosynthetic models ^[6,7] and enzyme mimics ^[8-10]. Most of these kinds of porphyrin only contain one or two ethynyl moieties. However macrocycles that are fully *meso*-substituted by arylethynyl fragments have proved to generate an effect on the UV-visible absorption of porphyrins ^[11-15]. The net effect is to turn the typical red color of porphyrin solution to a brilliant green: hence the trivial name **Chlorophyrin** was given for such arylethynyl-*meso*-substituted porphyrins ^[12-15].

In this series, Anderson reported a new porphyrin class named *meso*-alkynyl porphyrins – **H₂1** in 1992 ^[11]. Subsequently, the related porphyrins **H₂2** and **H₂3** were synthesized successfully by the others ^[12,16]. For this kind of porphyrin, the terminal groups are linked to the porphyrin ring by alkynyl bridges, with the aim of developing highly conjugated porphyrin polymers and nets by using these building blocks. Their structures are compared to reference **TFP-Bu**, these porphyrin **H₂1** and the developed **H₂2** and **H₂3** have the same structural feature: *meso*-substituted groups all bridged to the porphyrin core by alkynyl units. We are particularly interested in symmetrical porphyrins with four alkynyl groups, one reason is that the Soret band appears around 460 nm. This strong red shift indicates better conjugation compared to **TFP-Bu** (426 nm) having four fluorenyl arms directly connected to *meso* positions.

For these reasons, we designed and synthesized the new porphyrin shown in Figure 1.2. This porphyrin has four fluorenyl units bridged by alkynes to the core, which allow better π conjugation due to higher planarity. Effectively, this new molecule shows less steric hindrance between H₁ and H₃ of fluorenyl units and the β -pyrrolic protons H β (see Figure 5.2).

As usual, the butyl chains are connected to the fluorenyl units in the 9 position to improve the solubility of the final architecture.

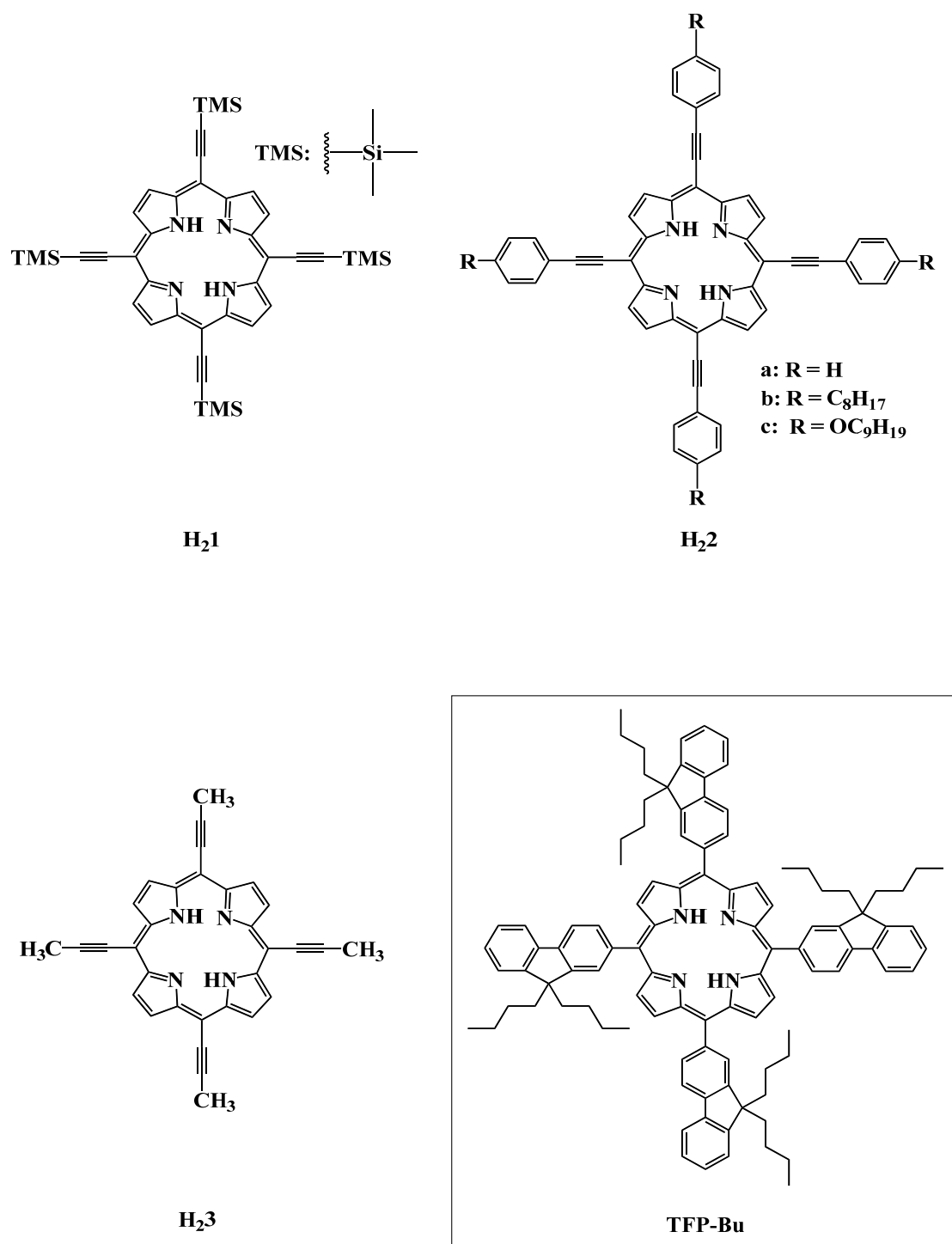


Figure 5.1 Molecular structures of reported *meso*-alkynyl porphyrins (H₂₁, H₂₂, H₂₃) and reference TFP-Bu

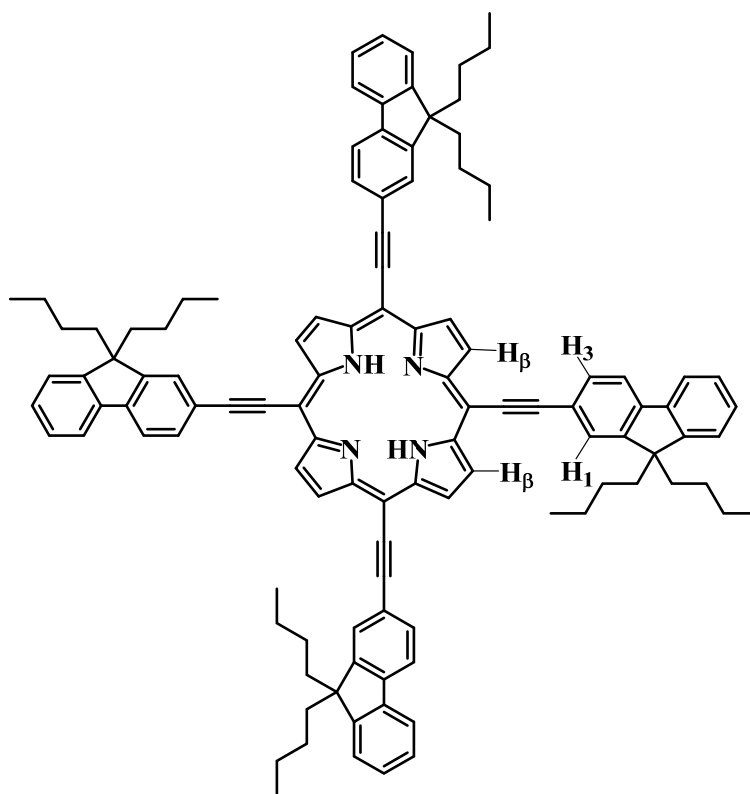
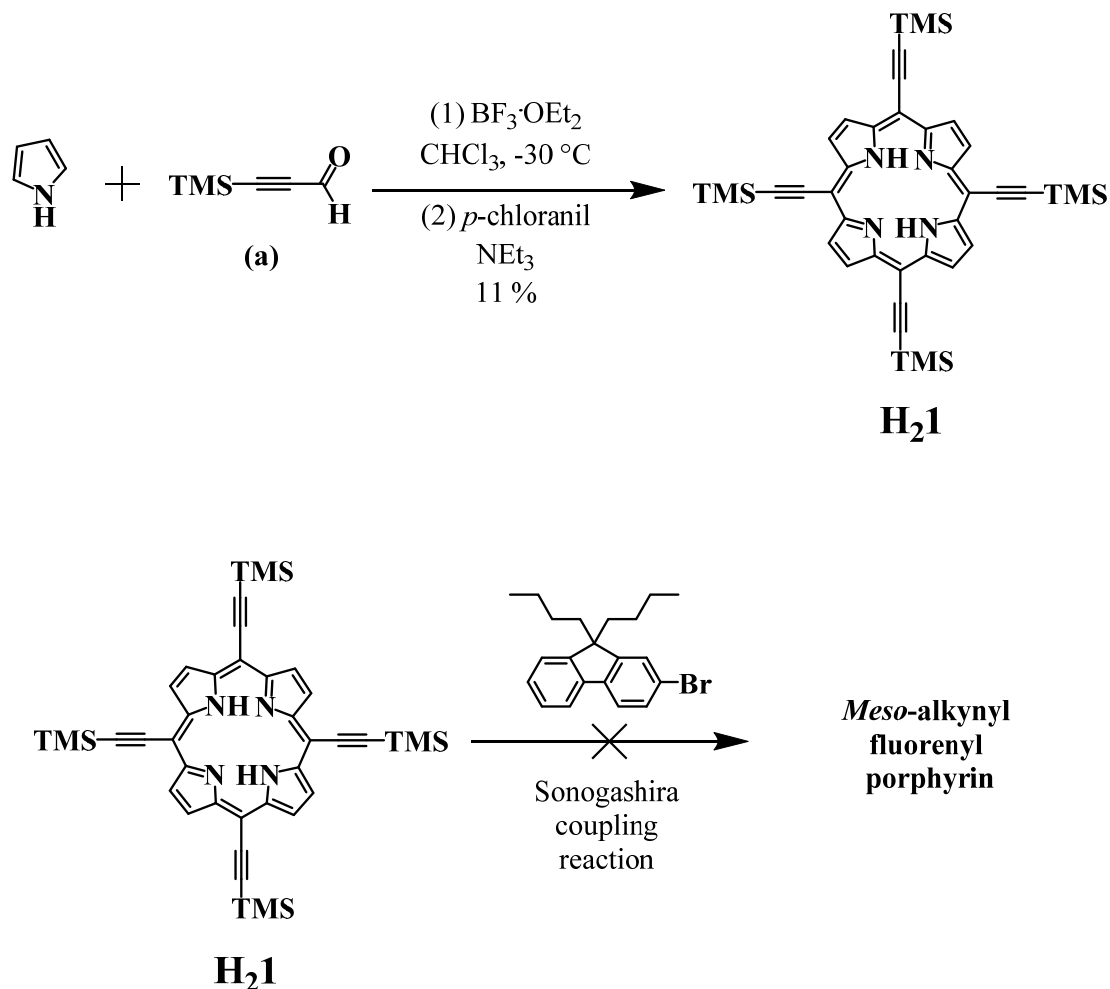


Figure 5.2 Structure of new *meso*-alkynyl fluorenyl porphyrin (**40**)

Synthetic Processes-To synthesize this desired porphyrin **40**, two strategies were explored at the same time:

(I) **Strategy 1:** As shown in Scheme 5.1, under Lindsey' conditions, one equivalent of the commercial 3-(trimethylsilyl)-2-propynal (**a**) and pyrrole were dissolved in distilled CH_3Cl under argon. This reaction was conducted using the process given by Anderson in the literature [1], which allowed the isolation of porphyrin **H₂1**.

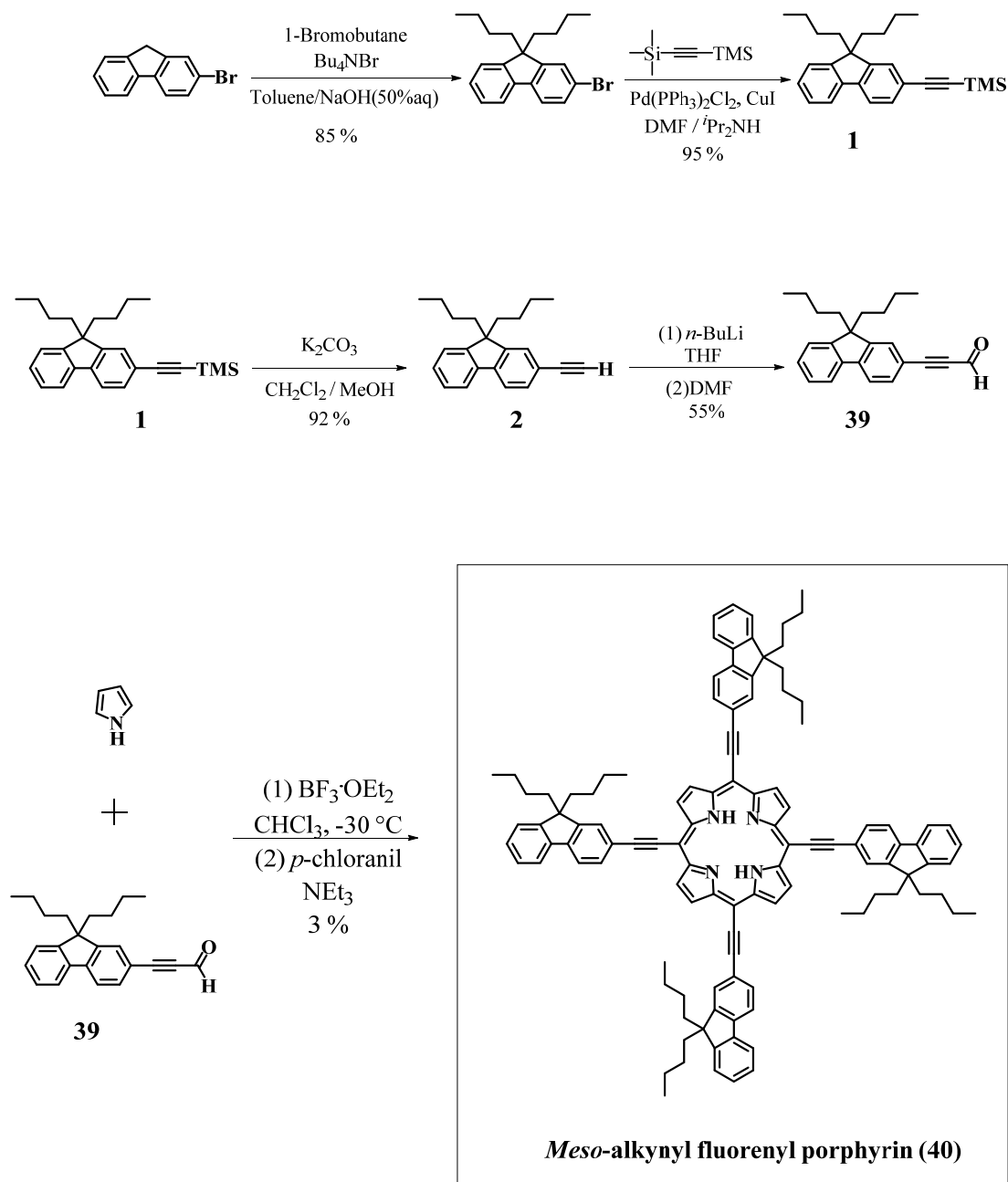
Considering the certain quantity of **H₂1** required for the next coupling step and the high price of 3-(trimethylsilyl)-2-propynal (**a**), we did not explore this strategy further.

Strategy 1:

Scheme 5.1 Syntheses path of Strategy 1

(II) **Strategy 2:** In this path, as shown in Scheme 5.2, the intermediate alkyne **2** was prepared in three steps as described in **Chapter 1**. Then by exchanging the terminal proton of compound **2**, we obtain aldehyde **39** ^[17]. Finally, the desired porphyrin **40** was synthesized successfully under Lindsey's conditions by using aldehyde **39**, but unfortunately only in a low yield of 3%.

Strategy 2:

Scheme 5.2 Synthetic designs of the target molecule: *meso*-alkynyl fluorenyl porphyrin (40)

Finally we chose this last **Strategy 2** as the basis for the syntheses (Scheme 5.2), the reasons being that each step is well known and they can be operated easily with good yields (except the last step: **39** \rightarrow **40**).

^1H NMR-All the compounds are characterized step by step. Comparison of the spectra of classic aldehyde **9**, 9-dibutyl-fluorene-2-carboxaldehyde and new (9,9-dibutyl-fluorenyl)-2-propiolaldehyde (**39**) are shown in Figure 5.3. As shown, all the peaks of protons of aldehyde **39** move to higher field in ^1H NMR spectra upon the introduction of alkynyl units. The two singlets at 9.46 ppm (for **39**) and 10.08 ppm (for **10**) correspond to the aldehyde protons. Compared to the singlet of H_{CHO} of **10**, the former presents a very clear 0.60 ppm shift. The multiplets corresponding to aromatic and *n*-butyl protons present shifts similar to those observed before.

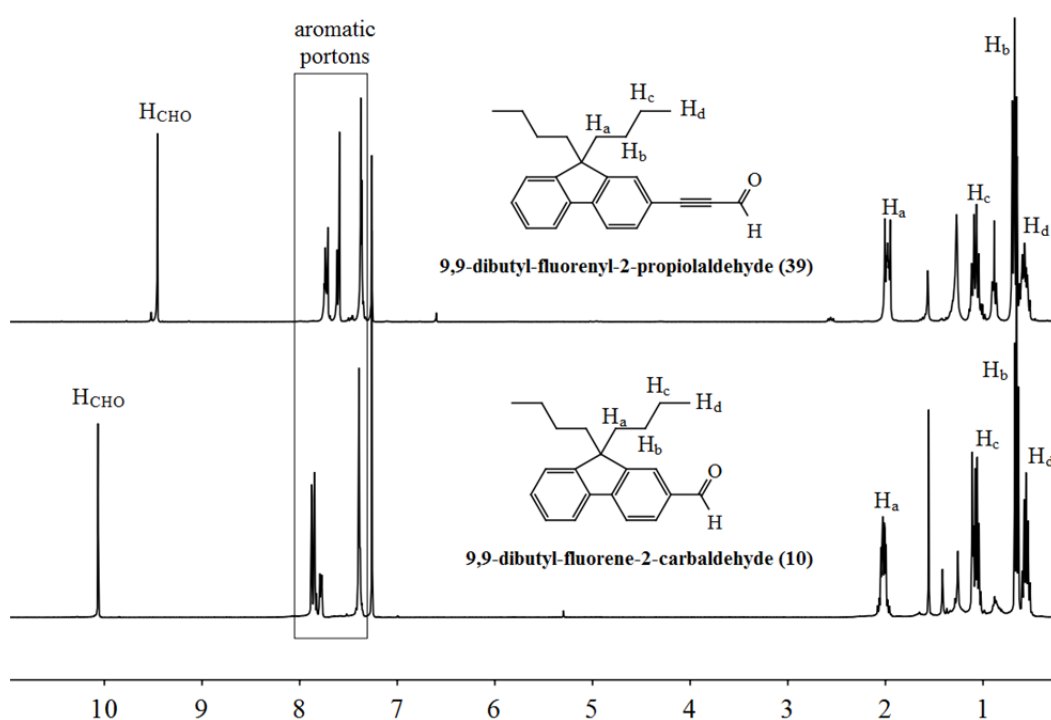


Figure 5.3 Comparison of complete ^1H NMR spectra of 9,9-dibutyl-fluorene-2-carbaldehyde **10** and **39**

The new *meso*-alkynyl fluorenyl porphyrin (**40**) was characterized by ^1H NMR in CD_2Cl_2 . The partial spectrum is compared in Figure 1.4 to **TFP-Bu** (**13**). As shown, the singlet at 9.69 ppm, corresponding to eight β -pyrrolic protons of the new porphyrin **40**, is shifted to lower field compared to that at 8.92 ppm of **TFP-Bu** (**13**). The combination of the alkynyl bridges and fluorenyl units causes decreased electron density at the porphyrin ring, so the singlet at -1.36 ppm of NH protons is strongly

shifted to lower field compared to that at -2.57 ppm of **TFP-Bu (13)**. We observe the same phenomenon for the β -pyrrolic protons. On the contrary, the electron density of fluorenyl arms was increased, leading to higher field aromatic peaks in the ^1H NMR.

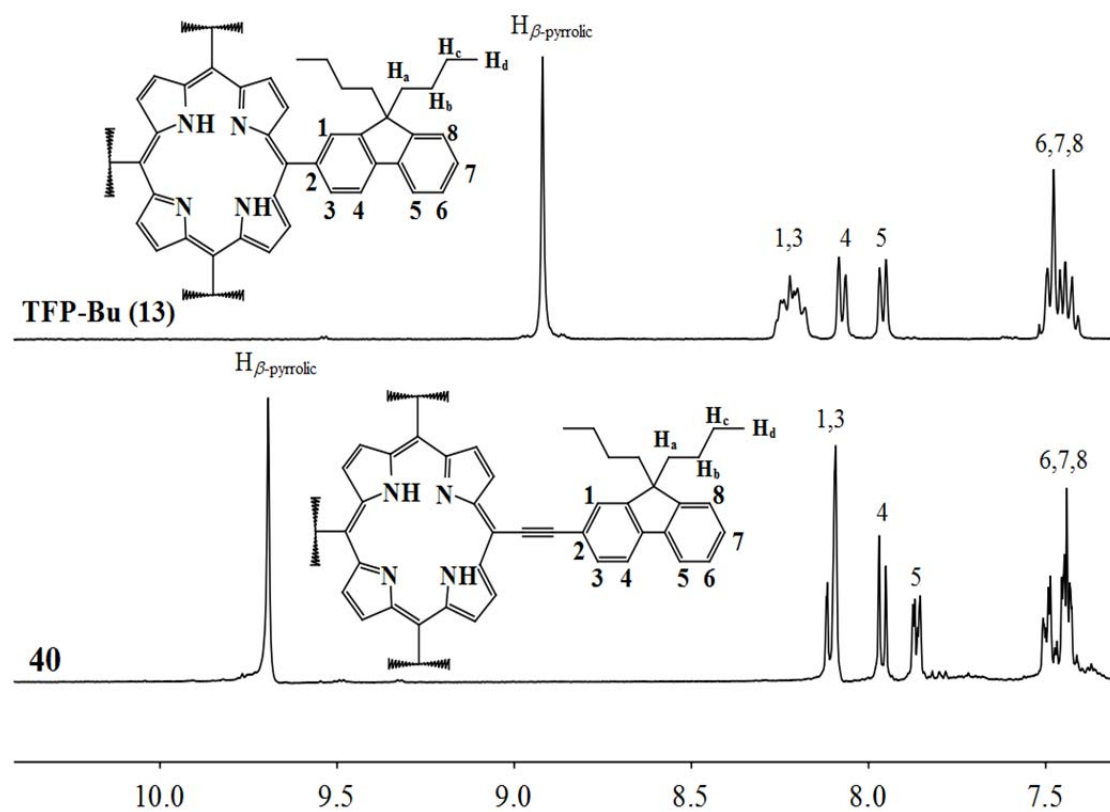


Figure 5.4 The partial ^1H NMR spectra of *meso*-alkynyl fluorenyl porphyrin **40**
And reference **TFP-Bu**

Photophysical properties - The UV-visible absorption spectra and emission spectra of new porphyrin **40** and reference **TFP-Bu** were measured in CH₂Cl₂ (HPLC level) at room temperature. Their photophysical data are listed in Table 1.1.

Table 1.1 Photophysical data of new *meso*-alkynyl fluorenyl porphyrin **40 And **H₂1**, **H₂2** (a,b,c) **H₂3** and **TFP-Bu**, **TPP****

	UV-visible absorption / nm		Emission /nm				
	λ_{Soret}	$\lambda_{\text{Q-bands}}$	excited at λ_{Soret}		$\Phi_{\text{fl}} / \%$	τ / ns	
			Q (0,0)	Q (0,1)			
TFP-Bu	426	520, 557, 593, 650	TPP	653	721	11	8,6
H₂1^a	451	567, 606, 646, 710	TFP	663	730	24	8,0
H₂2a^a	463	621, 717	TFP-Bu	660	724	18	8.2
H₂2b^a	466	599, 642, 673, 737	40	760	-	-	-
H₂2c^a	472	712, 795					
H₂3^a	446	517, 563, 602, 647, 708					
40	479 (486)	661, 748					

^a data from lit. [1-3].

In Figure 5.5, the normalized UV-visible absorption spectrum of **40** is mainly made up of two parts:

(1) The dendron absorption band, which appears in UV region, with $\lambda_{\text{max}}^{\text{Dendron}} = 319$ nm;

(2) The porphyrin absorption: the Soret band is at 479 nm, and only two Q-bands, at 661 and 748 nm respectively, are observed in visible region.

Compared to the reference **TFP-Bu**, which does not have alkynyl bridges, the Soret band of **40** presents a large red shift ($\Delta = 53$ nm) due to the alkynyl bridges, which increase the π conjugation to the porphyrin.

Generally, the free based porphyrins have four obvious Q-bands, but for this new porphyrin **40**, only two Q-bands are observed in visible region, with maximum absorptions at 661 and 748 nm respectively. Whilst, compound **H₂1**, synthesized by Anderson, has four classic Q-bands at 567, 606, 696 and 710 nm. In the series of **H₂2**, which has the similar structures to our new porphyrin **40**, **H₂2a** and **H₂2c** have the

same profile and show two Q-band absorptions; we can notice that **H₂2b** has four Q-bands as **H₂1** [3]. Surprisingly, the porphyrin **H₂3** has more Q-bands in the visible region [2]. Further investigations on these surprising results are in progress.

The emission spectrum of **40** was measured in CH₂Cl₂ (HPLC grade) at room temperature. These spectra, normalized by comparison with **TFP-Bu**, are shown in Figure 5.6. Reference **TFP-Bu** emits a typical red luminescence, the strong band Q(0,0) and weaker band Q(0,1) are both in the red zone of the visible region. For the new *meso*-alkynyl fluorenyl porphyrin **40**, only one emission band can be detected in the measurable window (until 900 nm), and this presents a large red shift of 100 nm compared to **TFP-Bu**; the maximum emission occurs at 760 nm in red zone. This intense band has a part of its emission in near infrared zone (starting from 780 nm, in dark red shadow, Figure 5.6). The detector of the Edinburgh FS920 Fluorimeter (Xe900) can only collect the signal at the maximum wavelength of 900 nm, so for the moment the quantum yield and lifetime of this new porphyrin **40** could not be calculated. A further investigation in the greater wavelength region (from UV to infrared region) will have to be made.

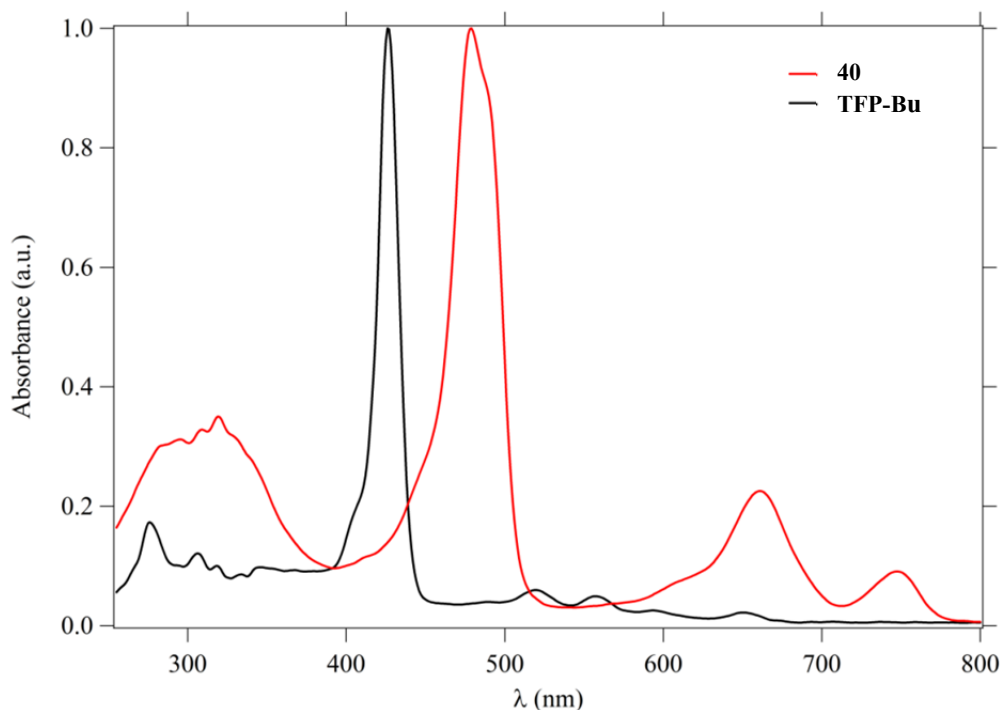


Figure 5.5 Comparison UV-visible absorption spectra of **40** and **TFP-Bu**

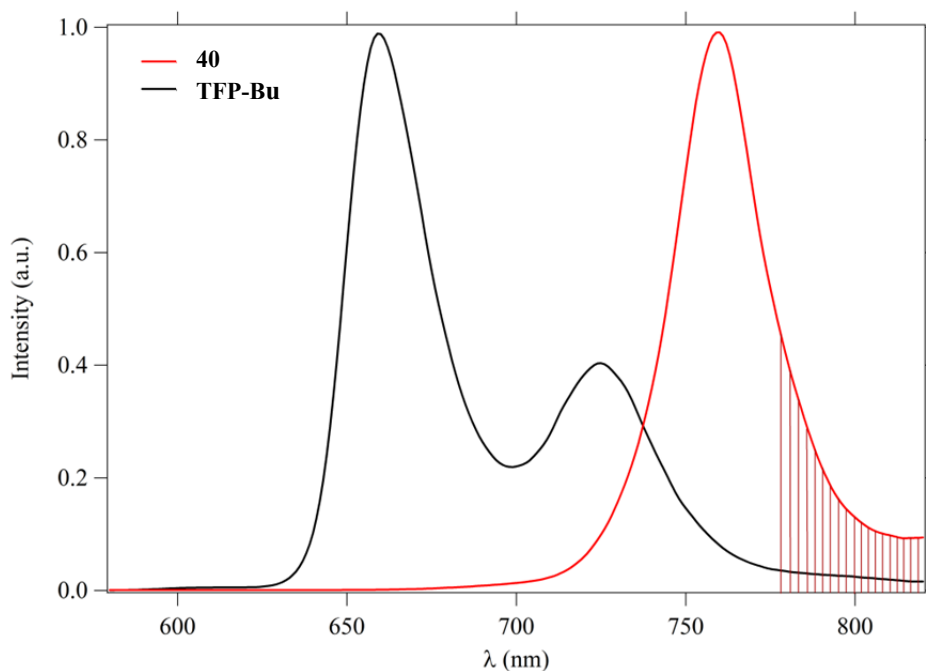
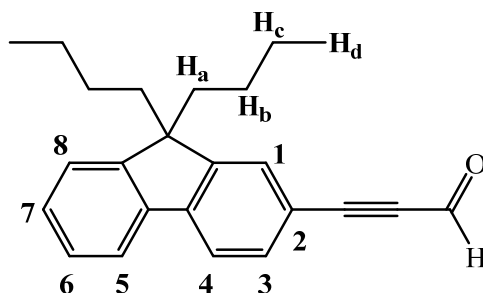


Figure 5.6 Comparison emission spectra of 40 and TFP-Bu

Conclusion - In this last chapter, presented as perspectives, we could only synthesize the generation 0 of a new family of promising dendrimers. In future, the new *meso*-alkynyl fluorenyl porphyrin **40** should provide an efficient platform for elaborating conjugated dendrimers of higher generation 1, 2, etc...

For the moment, studies of the promising NLO properties of this generation 0 compound are in progress.

Experimental section

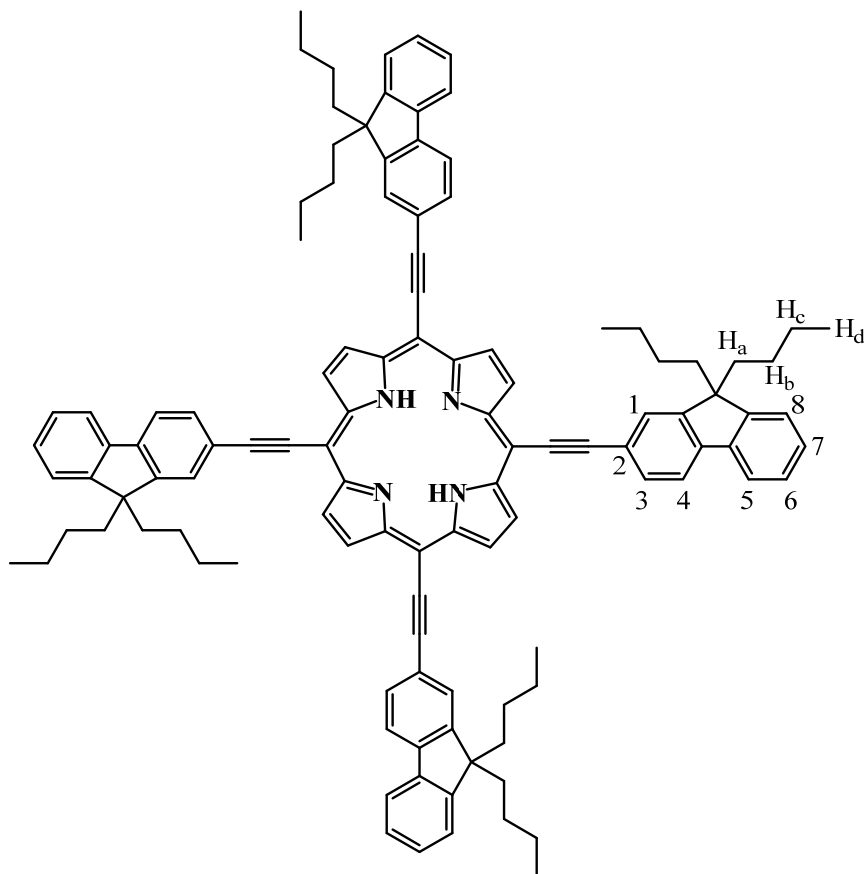
9,9-dibutyl-fluorenyl-2-propargylaldehyde (39)

In a Schlenk tube, a mixture of **9, 9-dibutyl-2-ethynyl-fluorene (2)** (synthesized in **Chapter 1**) (1.03 g, 3.41 mmol, 1 equiv) was dissolved in dried THF (10 mL). The reaction medium was degassed by freeze-pump-thaw for three times and cooled to $-78\text{ }^{\circ}\text{C}$ in liquid nitrogen-acetone bath. Under low temperature, *n*-BuLi (2.60 mL, 4.09 mmol, 1.2 equiv) was injected dropwise to the mixture over 30 min. The system was kept stirring at $-78\text{ }^{\circ}\text{C}$ for 3 h. Then dried DMF (0.53 mL) was injected and the reaction went on stirring at $-78\text{ }^{\circ}\text{C}$ for another 1h. The reaction was stirred overnight at room temperature. At last saturated NH_4Cl (aq.) was injected for quenching the reaction. The mixture was extracted with ethyl acetate/water. After evaporation of the volatiles, residue was purified by silica chromatography using heptane/ CH_2Cl_2 (5:1) as eluent, **9,9-dibutyl-fluorenyl-2-propiolaldehyde (39)** was isolated as a white powder (623 mg, 55% yield).

^1H NMR (400 MHz, CDCl_3 , ppm): $\delta = 9.44$ (s, 1H, H_{CHO}), 7.77-7.75 (m, 2H, $\text{H}_{1,3}$), 7.64-7.62 (m, 2H, $\text{H}_{4,5}$), 7.41-7.35 (m, 3H, $\text{H}_{6,7,8}$), 2.03-1.99 (m, 4H, H_a), 1.13-1.04 (m, 4H, H_c), 0.67 (t, $J = 7.2$ Hz, 6H, H_d), 0.60-0.52 (m, 4H, H_b).

^{13}C NMR (100 MHz, CD_2Cl_2 , ppm): $\delta = 176.6, 151.5, 151.1, 144.6, 139.7, 132.5, 128.5, 127.9, 127.1, 123.1, 120.5, 119.9, 117.2, 96.3, 88.8, 55.2, 39.9, 25.9, 23.0, 13.5$.

HRMS-ESI: $m/z = 330.1990$ [M] $^+$ (calcd: 330.19837).

Meso-alkynyl fluorenyl porphyrin (40)

In a two-neck flask, a mixture of **9,9-dibutyl-fluorenyl-2-propionaldehyde (39)** (300 mg, 0.91 mmol, 1 equiv) and distilled pyrrole (0.06 mL, 0.91 mmol, 1 equiv) were dissolved in dried chloroform (60 mL) under argon. After degassing the mixture with argon bubbling for 30 min, $\text{BF}_3 \cdot \text{OEt}_2$ (0.02 mL, 0.16 mmol, 0.25 equiv) was injected and the reaction was stirred in dark for 1 h under argon at $-30\text{ }^\circ\text{C}$. Then oxidant *p*-chloranil (315 mg, 1.28 mmol, 0.75 equiv) was added, and the reaction was continued at R.T. for another 1h without any protection. At last, NEt_3 (2 mL) was injected, and then keep stirring for several minutes. After evaporation of the volatiles, purification was done by silica chromatography using THF/heptane (1:10) mixture as eluents, and the porphyrin **40** was collected as green powder (10 mg, 3% yield).

¹H NMR (400 MHz, CD₂Cl₂, ppm): δ = 9.69 (s, 8H, H_β-pyrrolic), 8.11 (d, 8H, *J* = 10.5 Hz, H_{1,3}), 7.96 (d, 4H, *J* = 7.6 Hz, H₄), 7.88-7.85 (m, 4H, H₅), 7.51-7.43 (m, 12H, H_{6,7,8}), 2.30-2.15 (m, 16H, H_a), 1.25-1.17 (m, 16H, H_c), 0.78 (t, 24H, *J* = 7.3 Hz H_d), 0.75-0.62 (m, 16H, H_b), -1.36 (s, 2H, NH).

¹³C NMR (400 MHz, CD₂Cl₂, ppm): δ = 151.3, 151.2, 142.4, 140.5, 131.1, 127.9, 127.0, 126.1, 123.1, 121.7, 120.1, 103.1, 55.4, 40.3, 29.7, 26.2, 23.2, 13.7.

UV-vis (λ_{max}, CH₂Cl₂, nm): 319, 479, 661, 748.

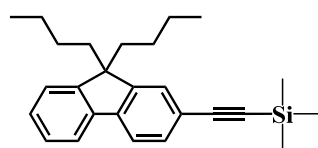
HRMS-ESI: *m/z* = 1511.8797 [M+H]⁺ (calcd: 1511.88033).

References

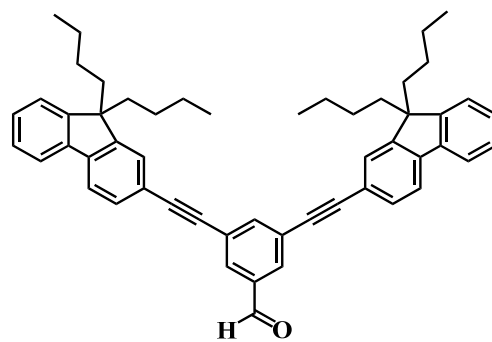
- [1] R. W. Wagner, J. S. Lindsey, *J. Am. Chem. Soc.*, **1994**, *116*, 9759.
- [2] H. L. Anderson, *Inorg. Chem.*, **1994**, *33*, 972.
- [3] D. P. Arnold, L. J. Nitschinsk, *Tetrahedron*, **1992**, *48*, 8781.
- [4] S. M. LeCours, H. W. Guan, S. G. DiMagno, C. H. Wang, M. J. Therien, *J. Am. Chem. Soc.*, **1996**, *118*, 1497.
- [5] H. L. Anderson, , S. J. Martin, D. D. C. Bradley, *Angew. Chem. Int. Ed. Engl.*, **1994**, *33*, 655.
- [6] R. W. Wagner, , T. E. Johnson, F. Li, I. S. Lindsey, *J. Org. Chem.*, **1995**, *60*, 5266.
- [7] V. S. Y. Lin, , S. G. DiMagno, M. J. Therien, *Science*, **1994**, *264*, 1105.
- [8] H. L. Anderson, J. K. M. Sanders, *Angew. Chem. Int. Ed. Engl.*, **1990**, *29*, 1400.
- [9] H. L. Anderson, J. K. M. Sanders, *J. Chem. Soc. Chem. Commun.*, **1992**, 946.
- [10] L. G. Mackay, H. L. Anderson, J. K. M. Sanders, *J. Chem. Soc. Chem. Commun.*, **1992**, 4344.
- [11] H. L. Anderson, *Tetrahedron Lett.*, **1992**, *33*, 1101.
- [12] L. R. Milgrom, G. Yahiolgla, *Tetrahedron Lett.*, **1995**, *36*, 9061.
- [13] L. R. Milgrom, G. Yahiolgla, *Tetrahedron Lett.*, **1996**, *37*, 4069.
- [14] L. R. Milgrom, G. Yahiolgla, *Adv. Mater.*, **1997**, *9*, 313.
- [15] F. Z. Henari, W. J. Blau, L. R. Milgrom. G. Yahiolglu, D. Phillips, J. A. Lacey, *Chem. Phys. Lett.*, **1997**, *267*, 229.
- [16] G. Proess, D. Pankert, L. Hevesi, *Tetrahedron Lett.*, **1992**, *33*, 269.
- [17] A. Bugarin, B. T. Connell, *Tetrahedron Lett.*, **2015**, *23*, 3285.

Appendix

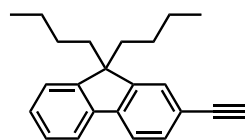
Chapter 1 :



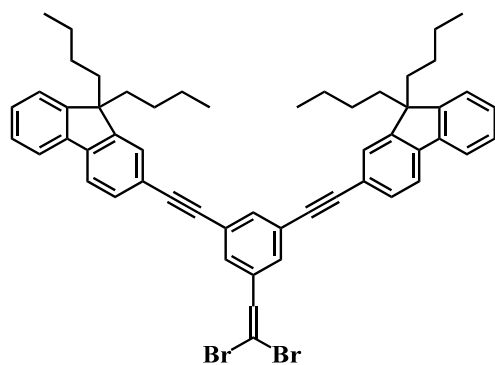
(1)



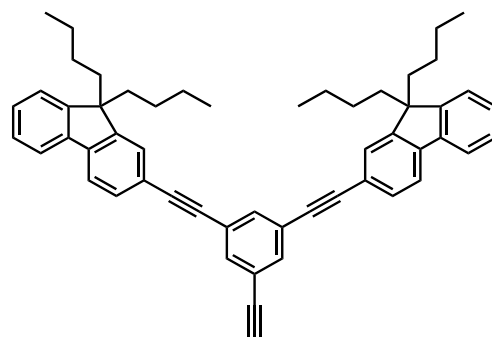
(3)



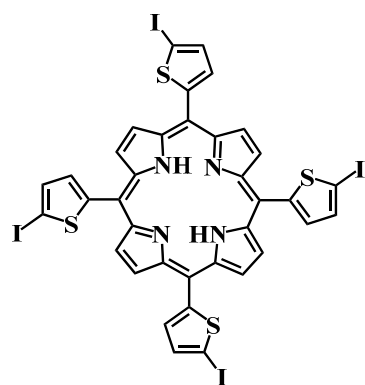
(2)



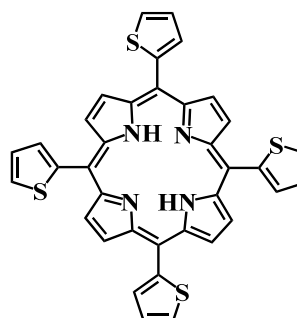
(4)



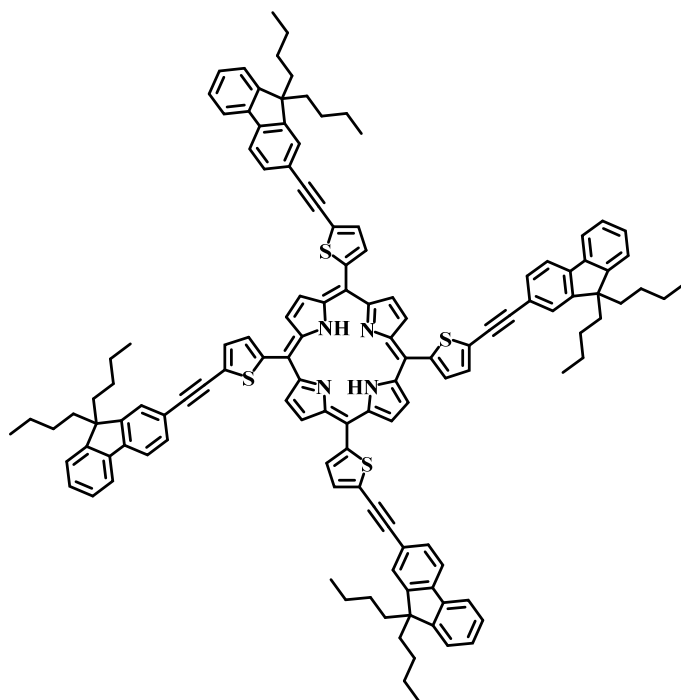
(5)



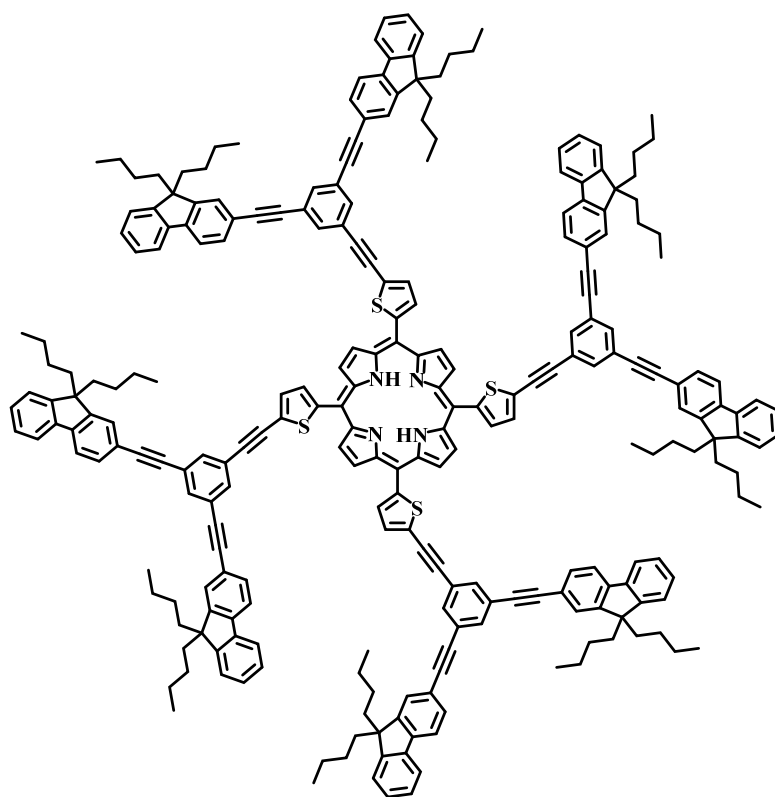
(6)



TThP (7)

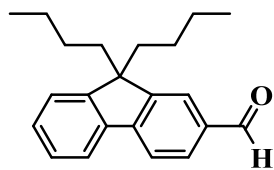


Meso-(2-((9,9-dibutyl-fluoren-2-yl)ethynyl)thienyl)porphyrin (8)

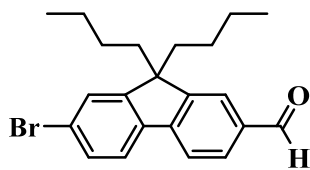


Meso-(2-((3,5-bis((9,9-dibutyl-fluoren-2-yl)ethynyl)phenyl)ethynyl)thienyl)porphyrin (9)

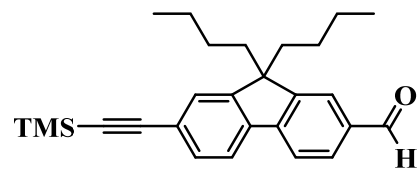
Chapter 2 :



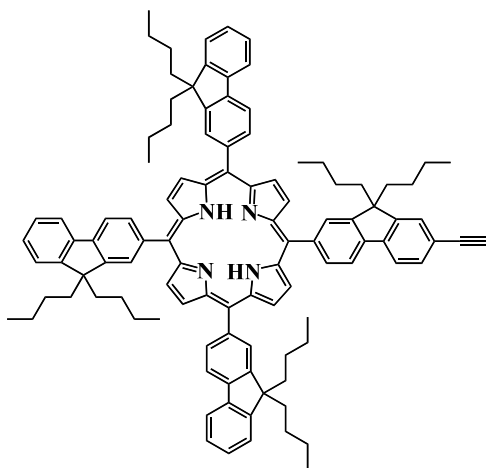
(10)



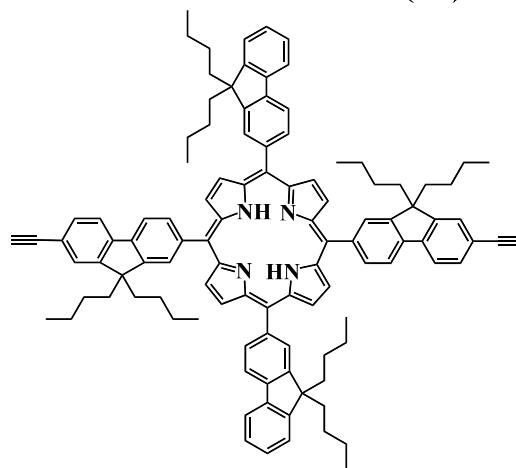
(11)



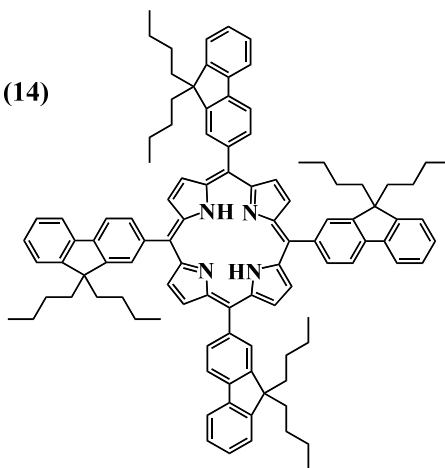
(12)



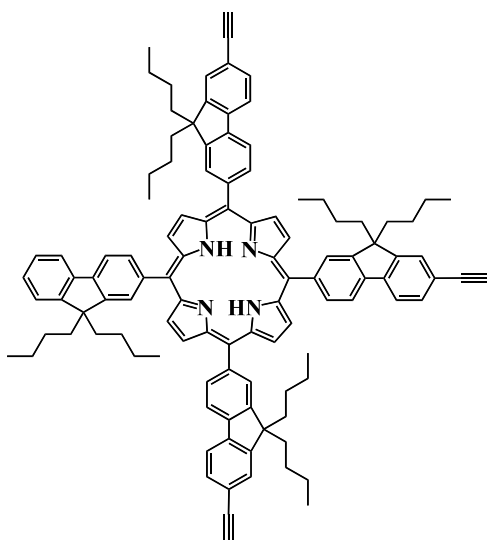
Mono-alkynyl TFP (14)



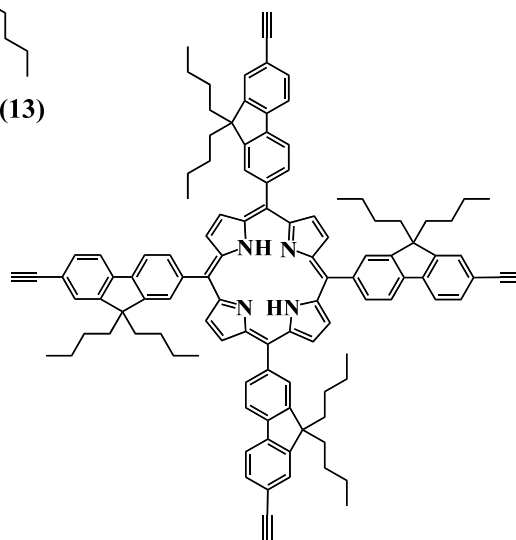
Bis-alkynyl TFP (15)



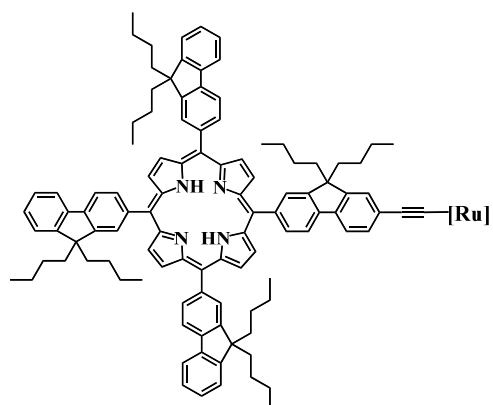
TFP-Bu (13)



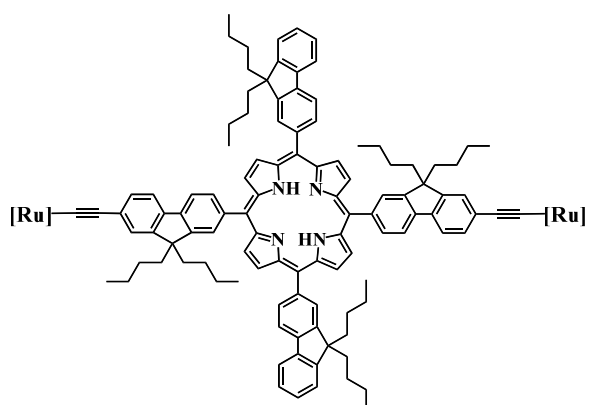
Tri-alkynylTFP (16)



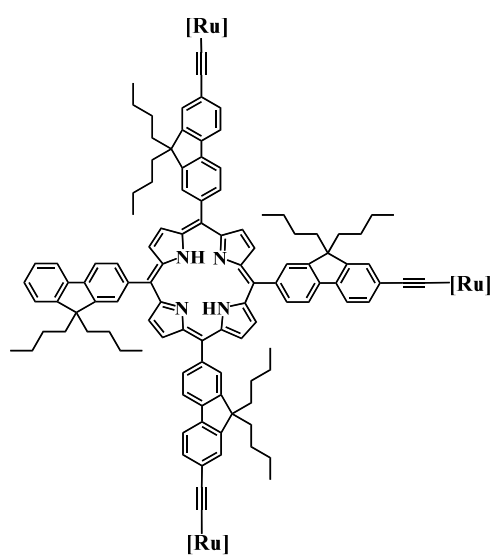
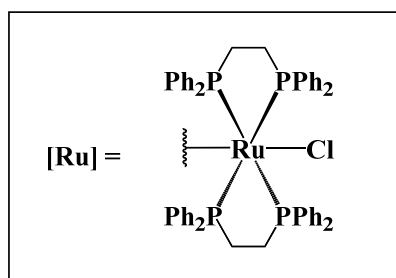
Tetra-alkynylTFP (17)



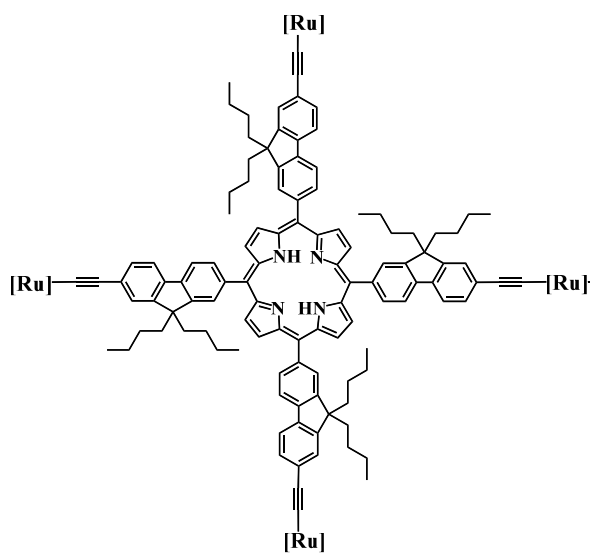
Mono-Ru TFP (18)



Bis-Ru TFP (19)

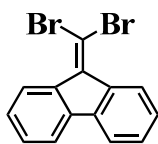


Tri-Ru TFP (20)

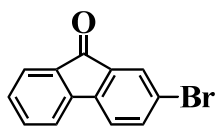


Tetra-Ru TFP (21)

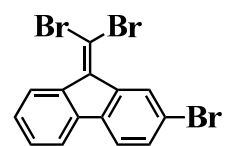
Chapter 3 :



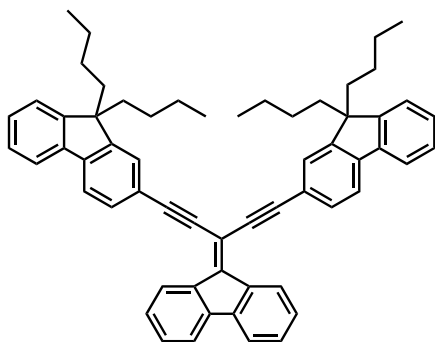
(22)



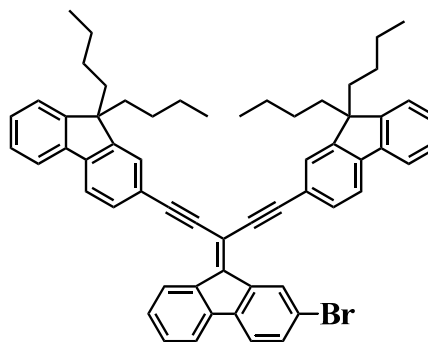
(23)



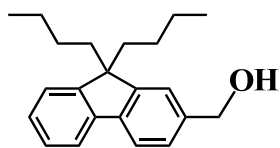
(24)



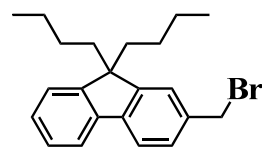
Model 1 (25)



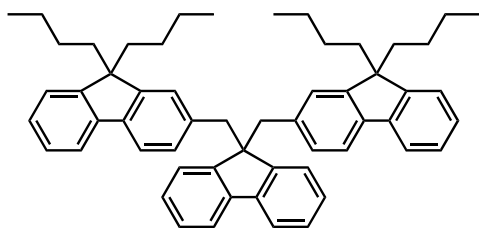
Dendron 26



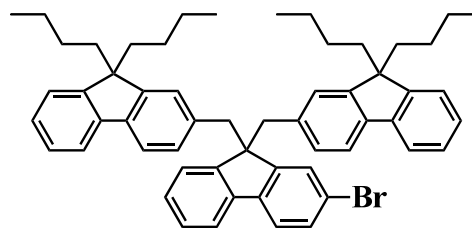
(27)



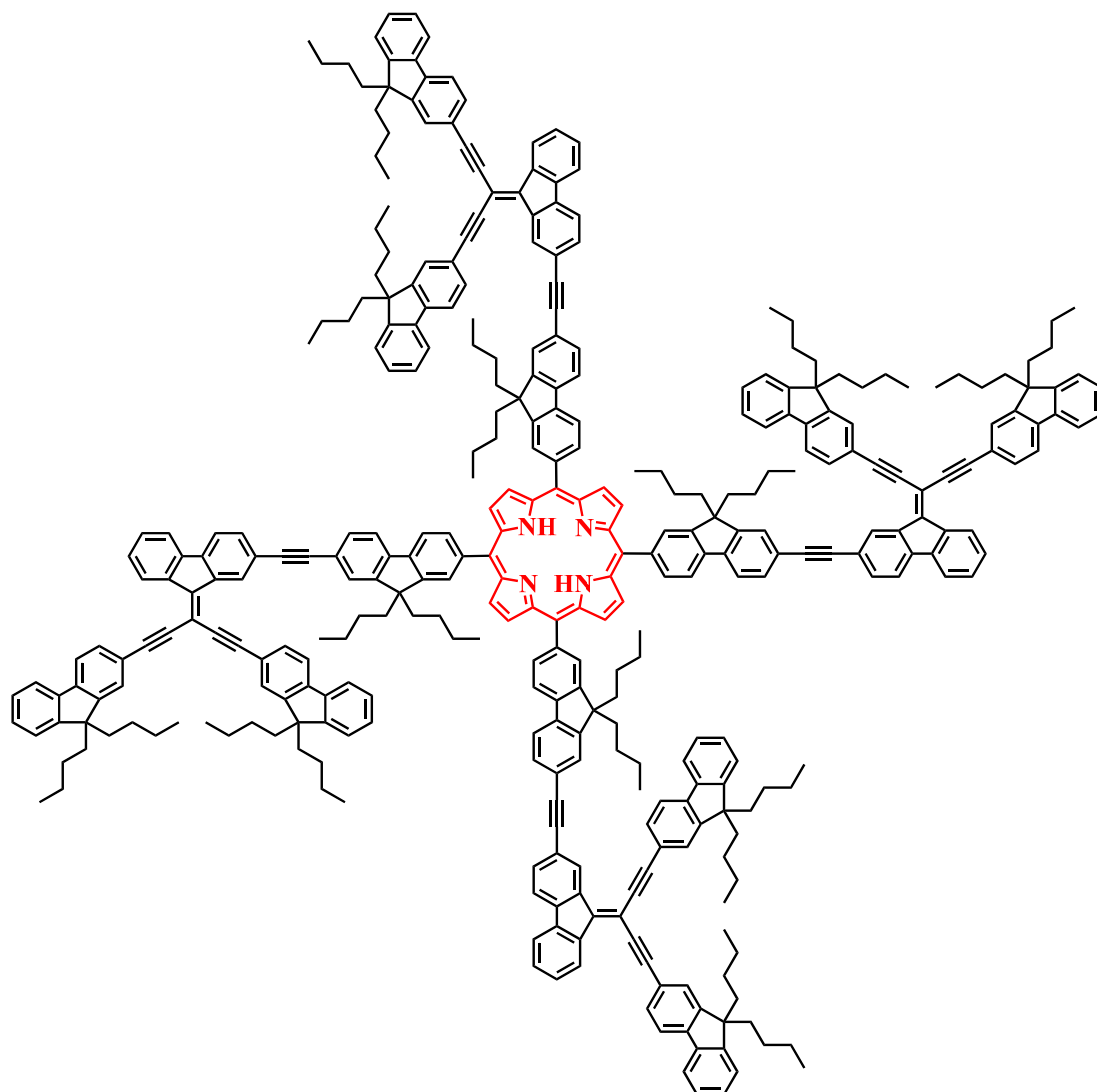
(28)



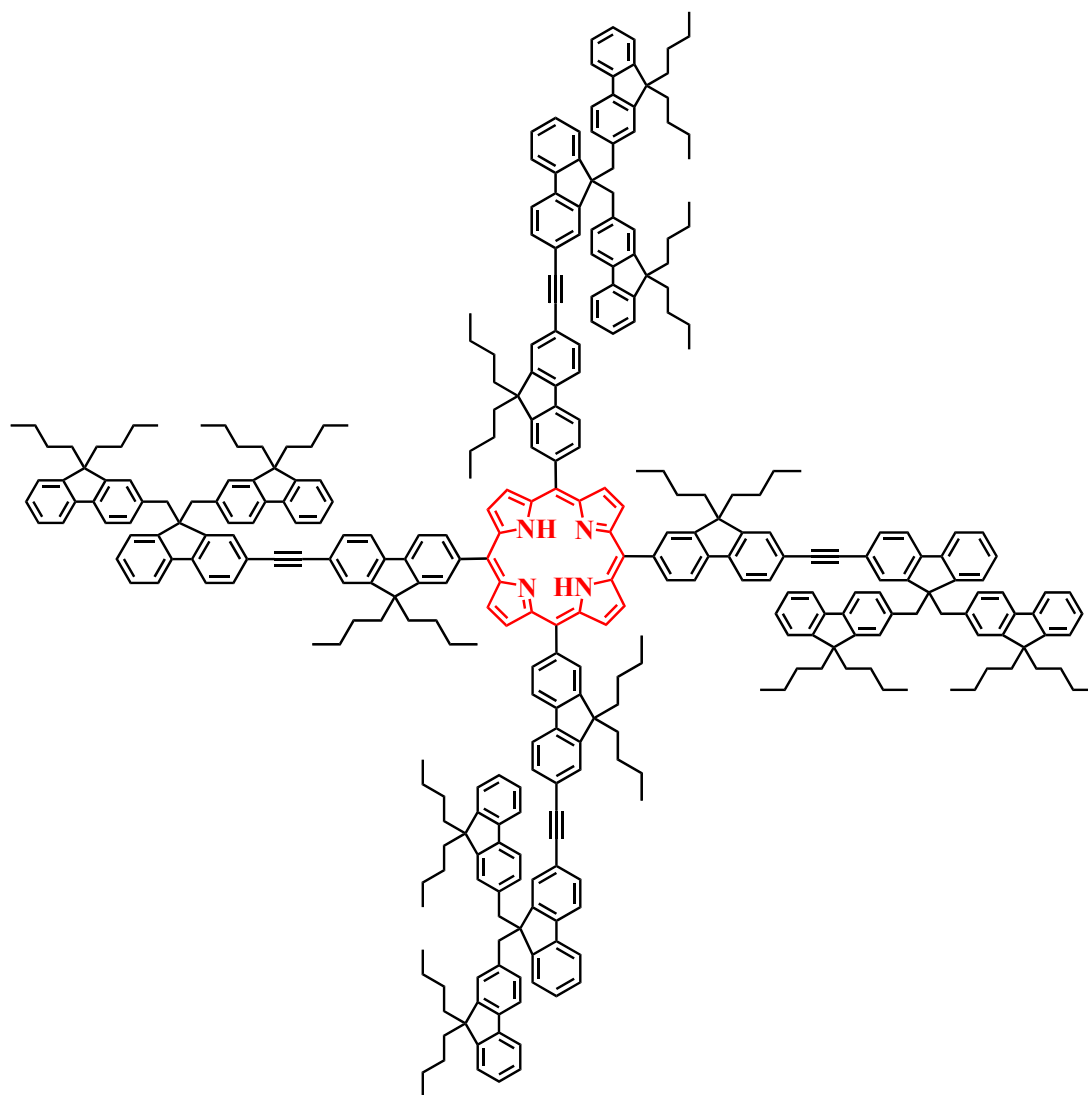
Model 2 (29)



Dendron 30

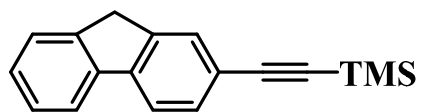


Conjugated porphyrin dendrimer (31)

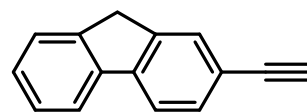


Non-conjugated porphyrin dendrimer (32)

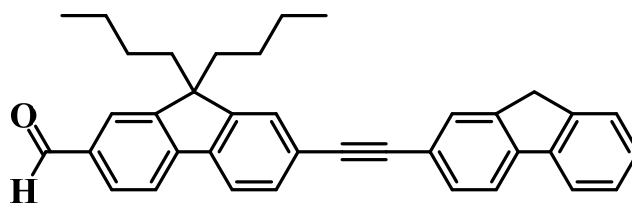
Chapter 4 :



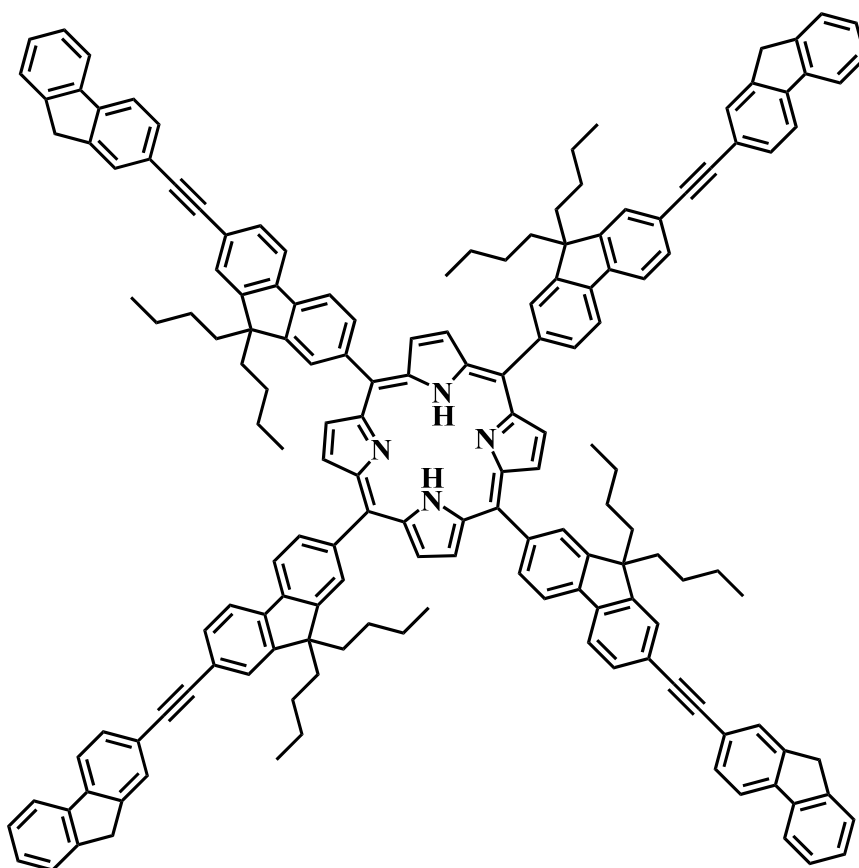
(33)



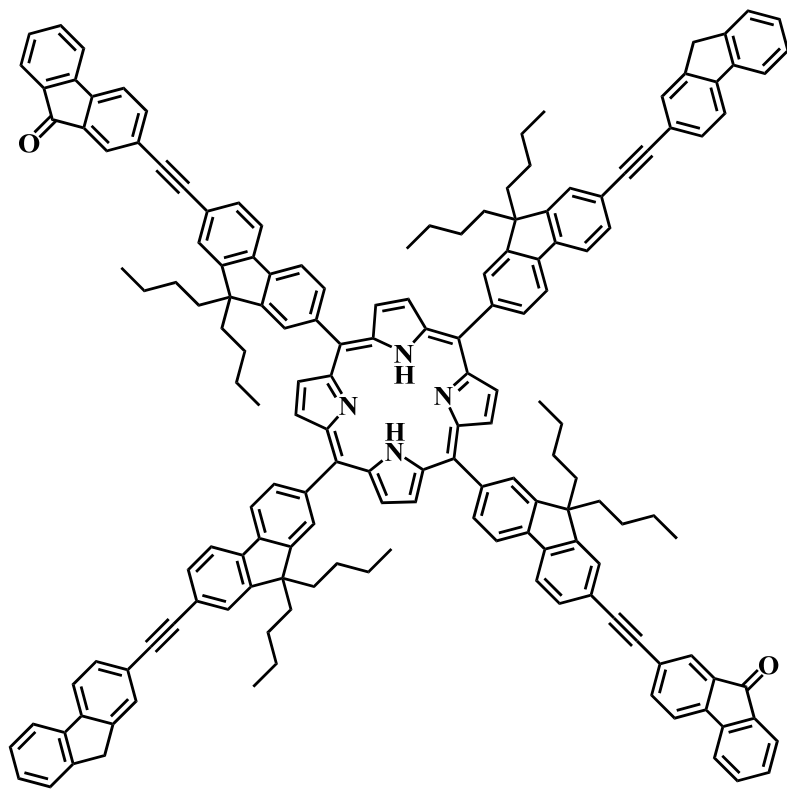
(34)



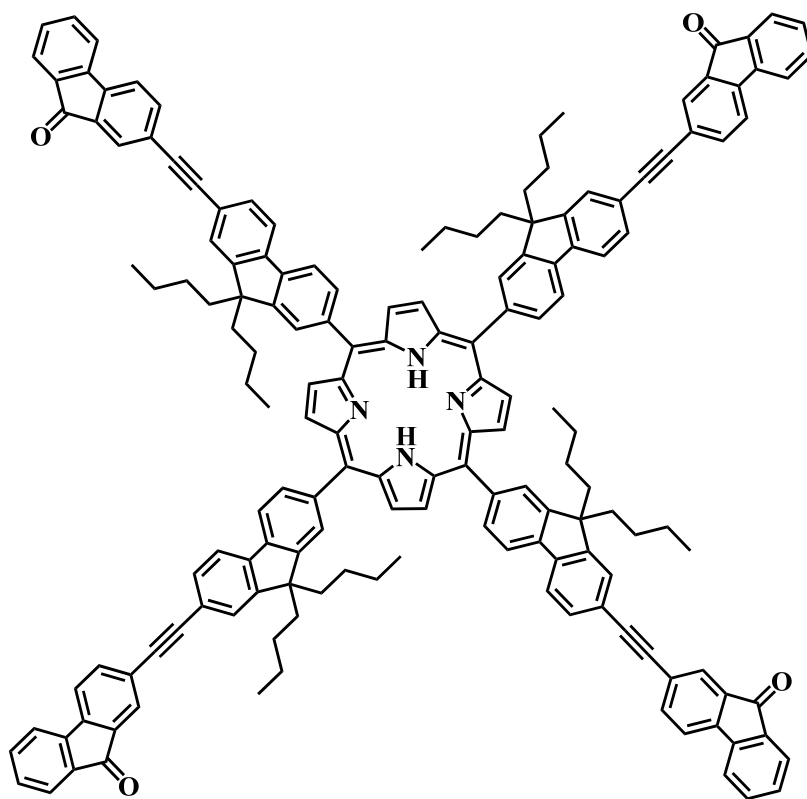
Difluorenyl aldehyde (35)



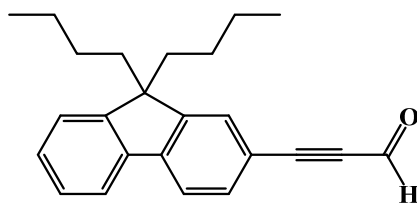
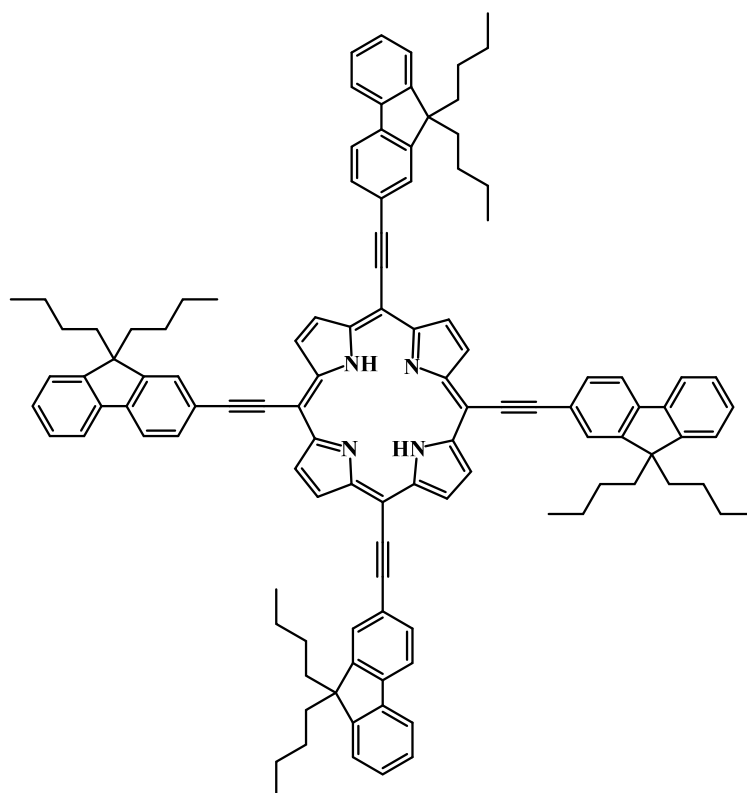
TFOP 1 (36)



TFOP 2 (37)

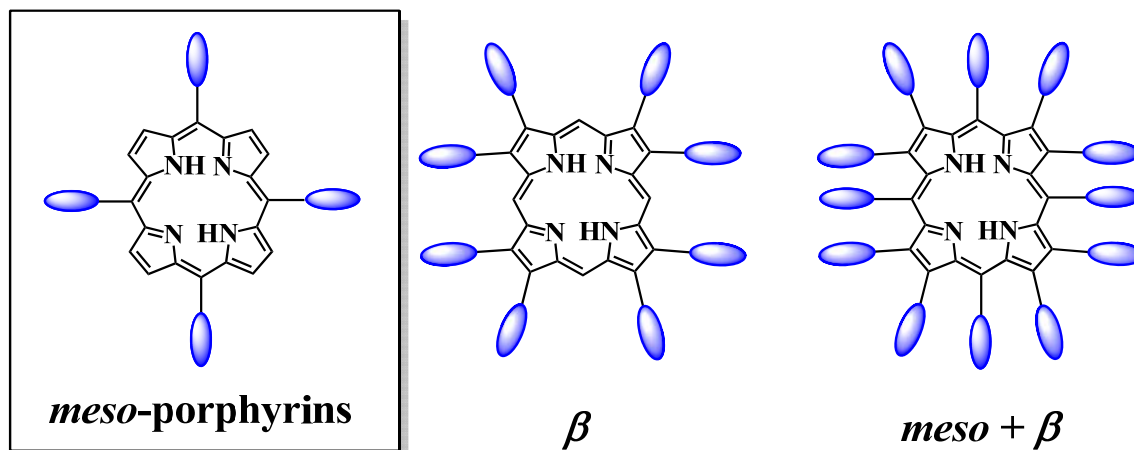
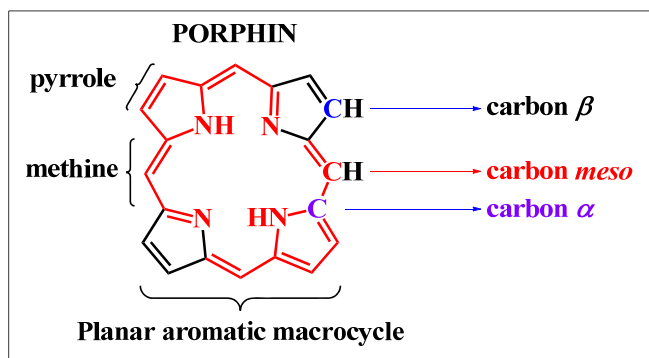


TFOP 3 (38)

Perspectives :**(39)*****Meso*-alkynyl fluorenyl porphyrin (40)**

Résumé étendu

Les porphyrines sont des **macrocycles aromatiques à 18 électrons π** conjugués, constitués de quatre unités pyrroliques liées entre elles par des ponts méthynes. Cette forte conjugaison implique une bonne stabilité et une forte absorption dans le domaine du visible de ces composés.



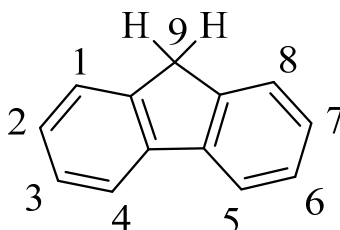
*Structure de la **porphine** proposée par Kuster et numérotation IUPAC*

Les porphyrines peuvent aussi se comporter comme des diacides ou des dibases et elles peuvent par conséquent, être métallées par presque tous les métaux de la classification périodique. Dans le premier cas, la porphyrine est dite “base libre”, dans le second cas, elle est dite “métallée”.

Le but de ce travail est d'utiliser la porphyrine comme brique moléculaire pour l'élaboration de composés ayant des activités optiques linéaires et non linéaires intéressantes.

Dans le chapitre d'Introduction, dans un premier temps nous avons détaillé les méthodes de synthèse et de caractérisation de **porphyrines** décrites dans la littérature.

Nous allons également introduire l'unité **fluorène** qui possède des propriétés photophysiques très intéressantes comme antenne collectrice de lumière. Cette unité fluorène permet l'élaboration de modèles artificiels du système photosynthétique de type dendrimère.



Structure de l'unité fluorène

Récemment au laboratoire, une nouvelle famille de composés porphyriniques a été synthétisée. Une porphyrine tétra substituée en position *meso* par des groupements fluorényles, la **tétrafluorénylporphyrine (TFP)**, a été obtenue. Des études ont montré qu'après une excitation sélective des antennes fluorényles par lumière UV ou de la bande de Soret, le cœur de la porphyrine émettait une forte lumière rouge.

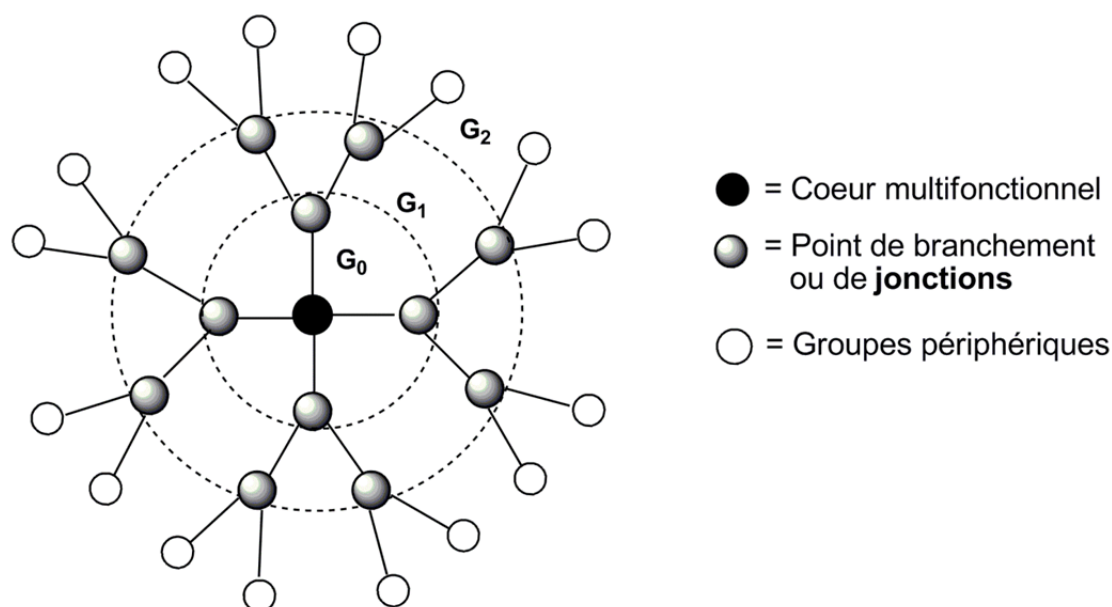
De plus, le rendement quantique de luminescence est considérablement amélioré pour ce composé **TFP** comparé à la **tétraphénylporphyrine (TPP)**. En effet, le rendement quantique passe de 13% à 22%, où le fort intérêt pour les **dendrimères et les oligomères**, possédant un nombre plus élevé d'antenne fluorène, puis d'étudier les propriétés photophysiques pour tester cet effet d'augmentation du nombre des bras fluorényles et comparer leurs rendement quantique avec la référence du laboratoire : **TFP**.

Les **dendrimères** forment une famille de molécules possédant une structure arborescente. Ils présentent des propriétés variables qui peuvent être adaptées et contrôlées telles que la taille, la forme de la molécule et la position des groupements fonctionnels.

Ces macromolécules sont constituées d'unité de base, qui s'associent selon un processus arborescent autour d'un cœur polyfonctionnel. Leur architecture rappelle

celle des complexes collecteurs de lumière dans les photosystèmes.

Leur construction arborescente s'effectue par la répétition d'une même séquence de réactions qui permet l'obtention à la fin du cycle réactionnel, d'une nouvelle génération appelée **G** et d'un nombre croissant de branches identiques. Ce sont des molécules tridimensionnelles, de taille et de structure bien définies, hautement symétriques, généralement de hauts poids moléculaire, possédant un grand nombre de chaînes terminales afin d'assurer leur solubilité.



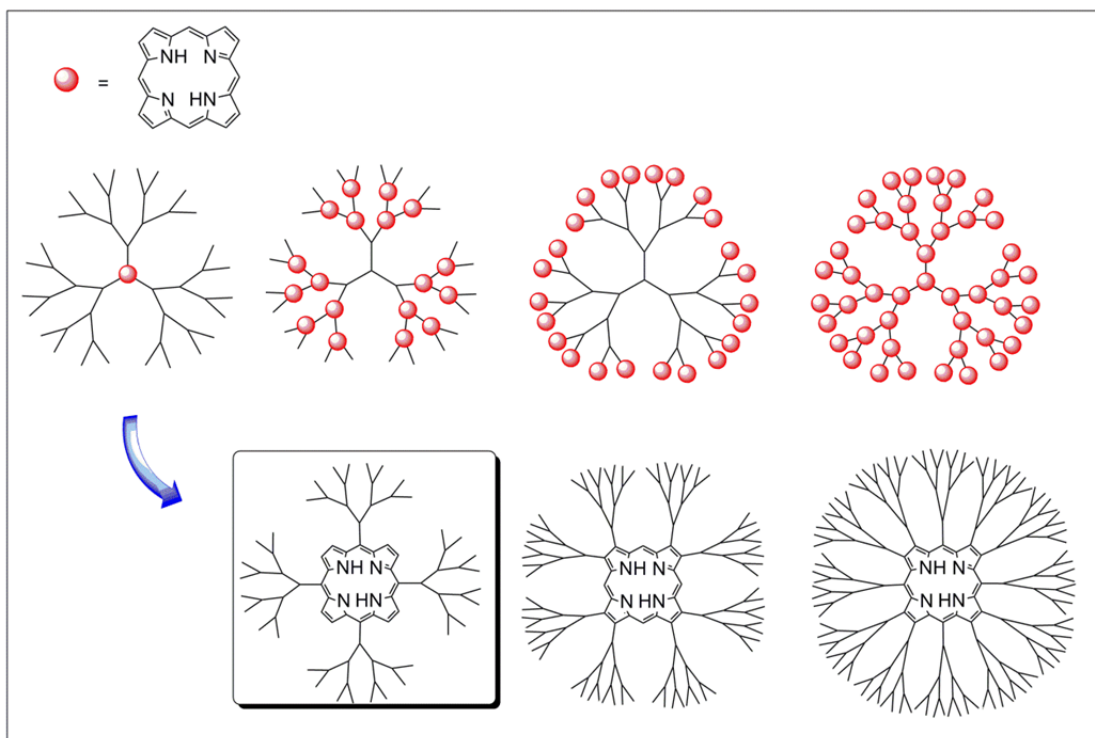
Représentation schématique d'un dendrimère

Il existe deux voies de synthèse principales pour la préparation des dendrimères. La première utilisée fut la synthèse dite **divergente** utilisée par les groupes de Vögtle, Newkome et Tomalia.

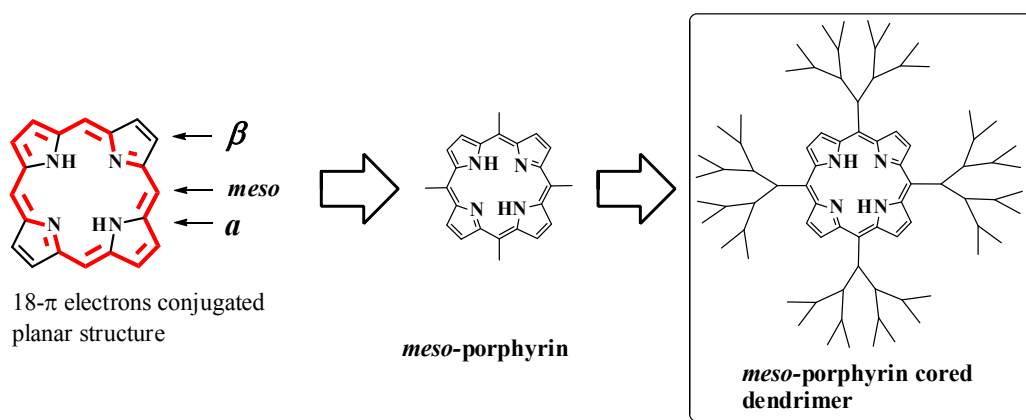
Ce n'est que plus tard que la synthèse **convergente** fut introduite par Fréchet et Miller au début des années 90. Elle permet un meilleur contrôle de l'architecture et du placement des groupes fonctionnels.

Nous présentons également les différents dendrimères reportés dans la littérature, notamment les différentes positions de fixations des porphyrines (**boule rouge**) dans ces structures :

- Centrale
- Pontée
- Terminale

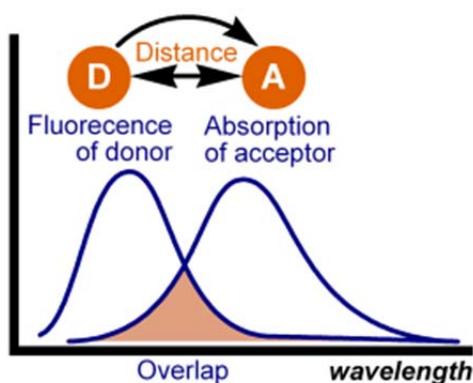


Porphyrin dendrimers with different structures



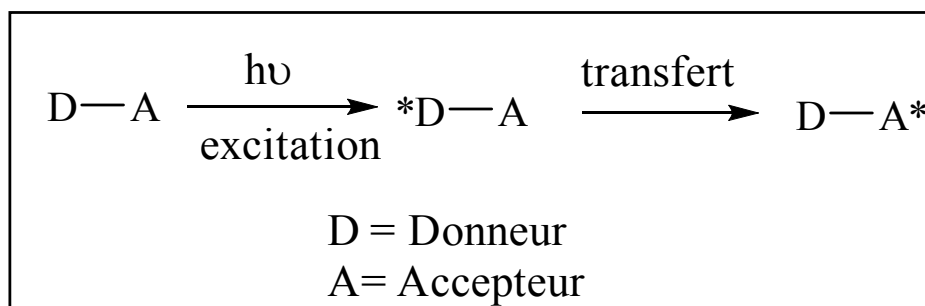
La structure de la porphyrine dendrimère étudiée

Ensuite, nous présenterons les caractérisations classiques de la porphyrine comme la spectroscopie UV-visible, et la luminescence, et dans un deuxième temps, le **transfert d'énergie** est détaillé:



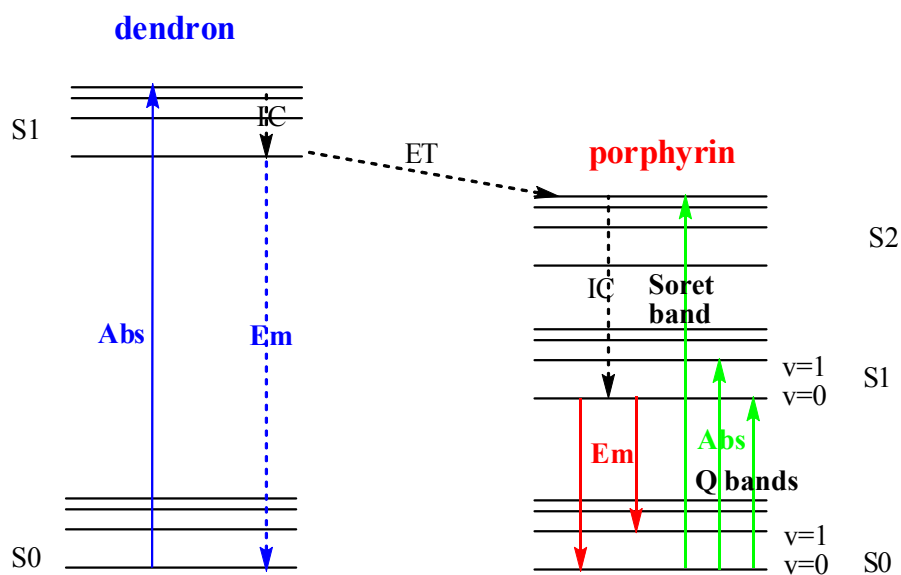
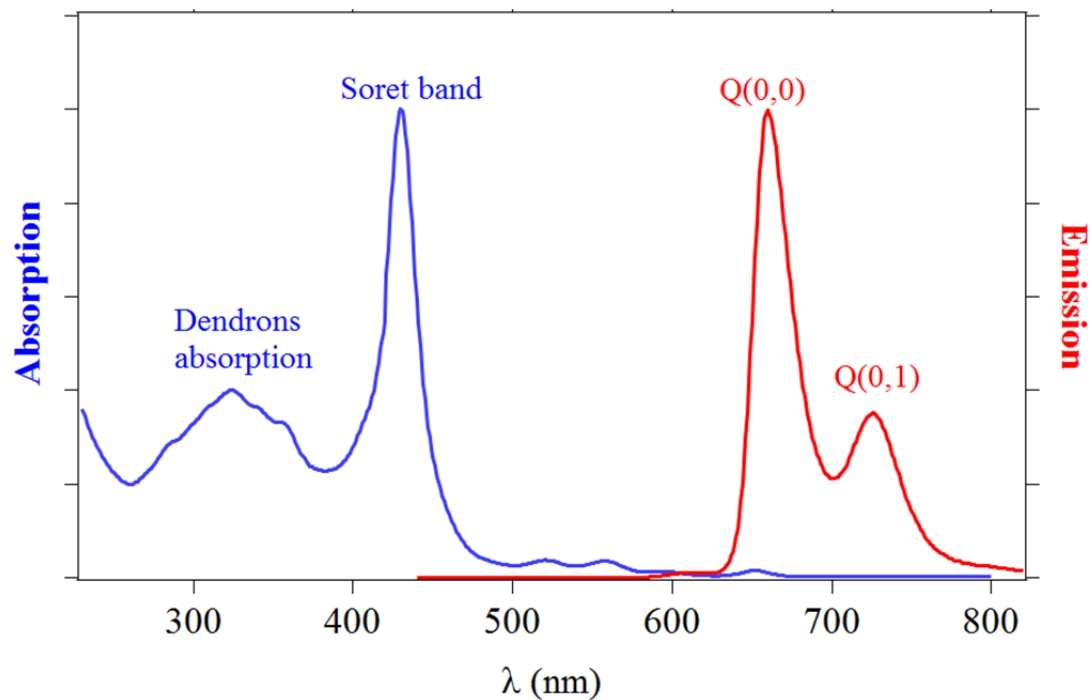
Spectral overlap between donor emission and acceptor absorption

Il existe deux types de transfert d'énergie : le transfert d'énergie de **type Dexter** privilégié dans le cas d'interactions à courte distance et le transfert d'énergie de **type Förster** dans les autres cas. Le transfert d'énergie singulet-singulet, entre deux chromophores maintenus à une certaine distance, peut se représenter de la manière suivante.



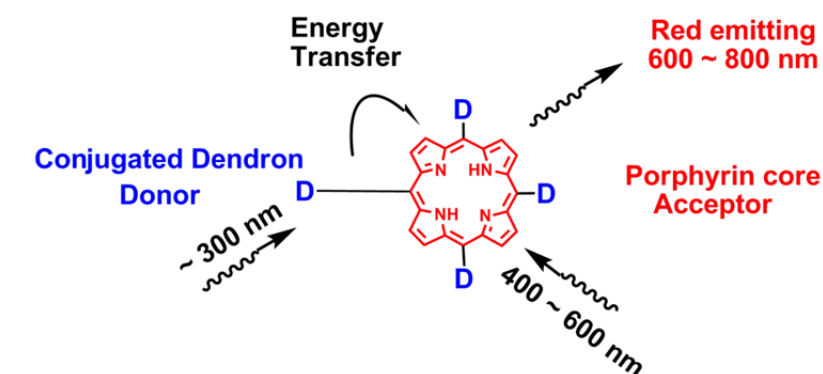
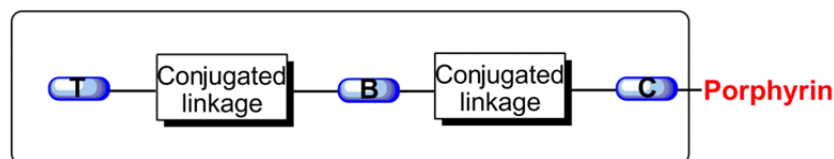
Transfert d'énergie entre deux chromophores D et A

Comme exemple, ci-dessous sont reportés les spectres d'absorption et d'émission d'un dendrimère de porphyrine méso (base libre) et de son diagramme de niveau d'énergie:

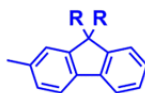


*Spectres d'absorption et d'émission d'un dendrimère de porphyrine meso (base libre)
son diagramme de niveau d'énergie*

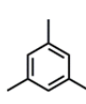
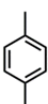
Au cours de cette thèse, nous avons synthétisé et caractérisé trois groupes de dendrimères fluorényle-porphyrine avec des structures conjuguées :

Meso-porphyrin cored dendrimer:**Conjugated Dendron D :****Terminated group**

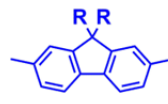
:

**Bridged group**

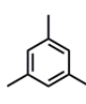
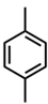
:



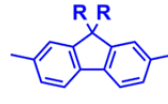
or

**Cored group**

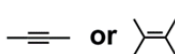
:



or

**Conjugated linkage**

:

*Structures de meso-porphyrine dendrimères*

Puis leurs propriétés optiques liées à la structure ont été discutées en détail, ainsi que les comportements de transfert d'énergie à partir du dendron donneur conjugué vers le groupement porphyrine accepteur.

Dans ce chapitre d'introduction, nous avons présenté le contexte général de la chimie de porphyrine en considérant trois aspects: la structure, les propriétés optiques et la méthode synthétique.

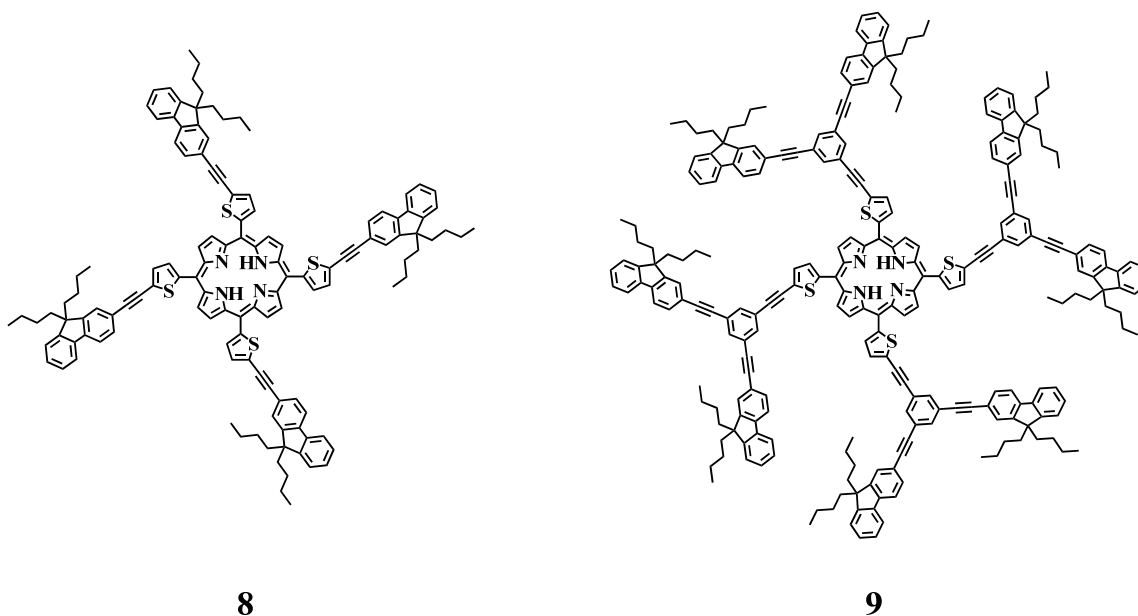
Nous avons également présenté les porphyrines étudiées préalablement dans notre groupe de recherche et proposé des nouveaux modèles dans cette thèse. Pour étudier la

corrélation sur la propriété optique structure pour ces nouveaux dendrimères porphyrine, nous avons considéré leur structure de deux parties: porphyrine comme base et dendron conjugué.

Nous avons donc décidé d'utiliser le dendron de quatre façons:

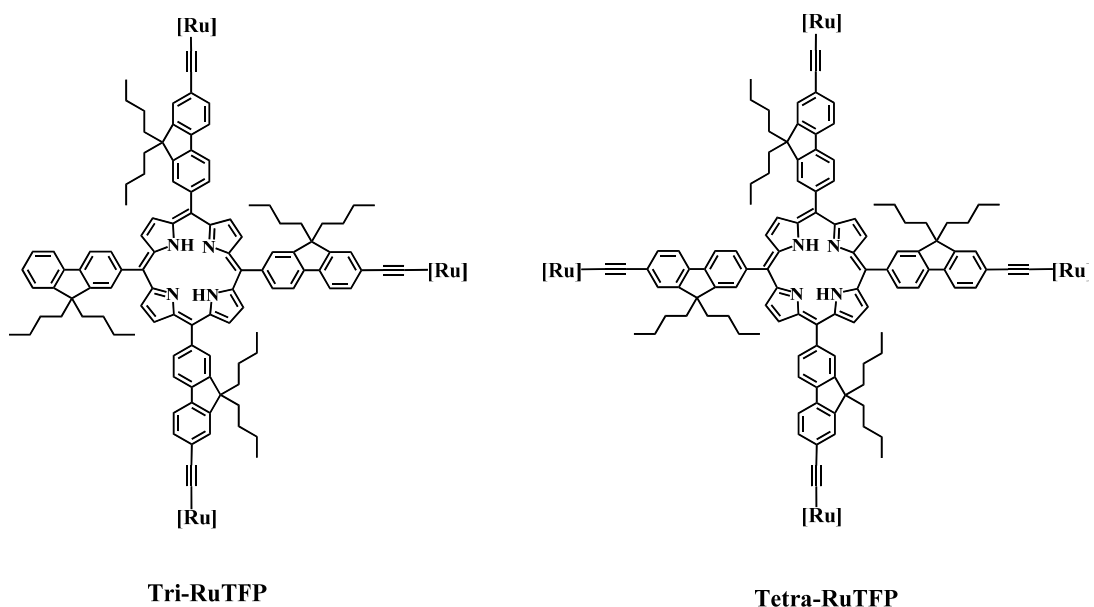
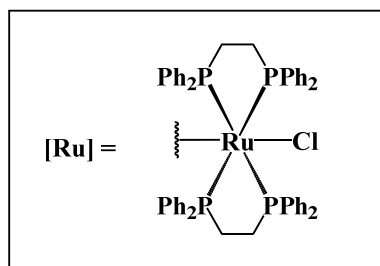
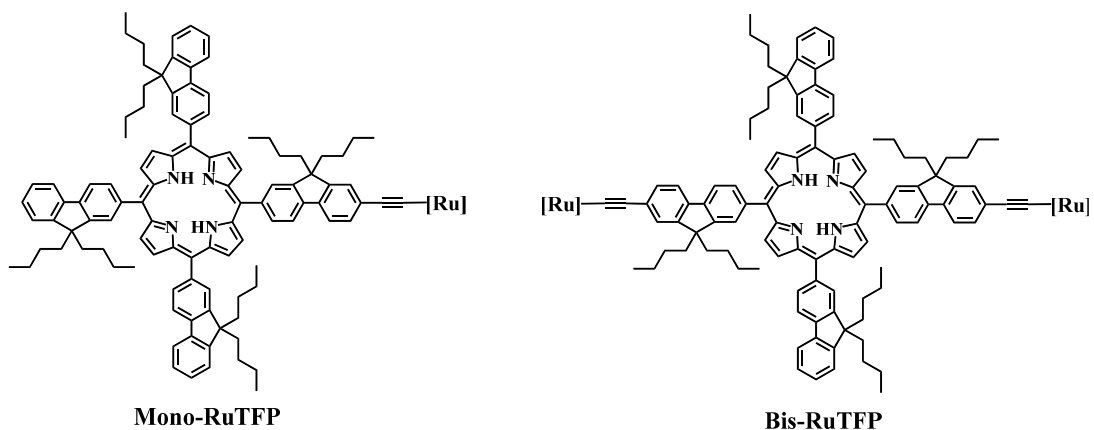
- groupe Central
- groupe Ponté,
- groupe Terminale
- assemblage Conjugué

Dans le premier chapitre, nous présentons la synthèse d'un groupe de dendrimères dérivés de thiényl-porphyrines. Les unités thiényles font le pont entre les dendrons conjugués de type fluorényle et le cœur de la porphyrine. Le transfert d'énergie pour ces molécules est efficace et ces dernières présentent des propriétés en optique non linéaire qui sont intéressantes avec une amélioration de l'absorption à deux photons (ADP).



Structures moléculaires de dendrimères de porphyrine avec un cœur thiényl-porphyrine central

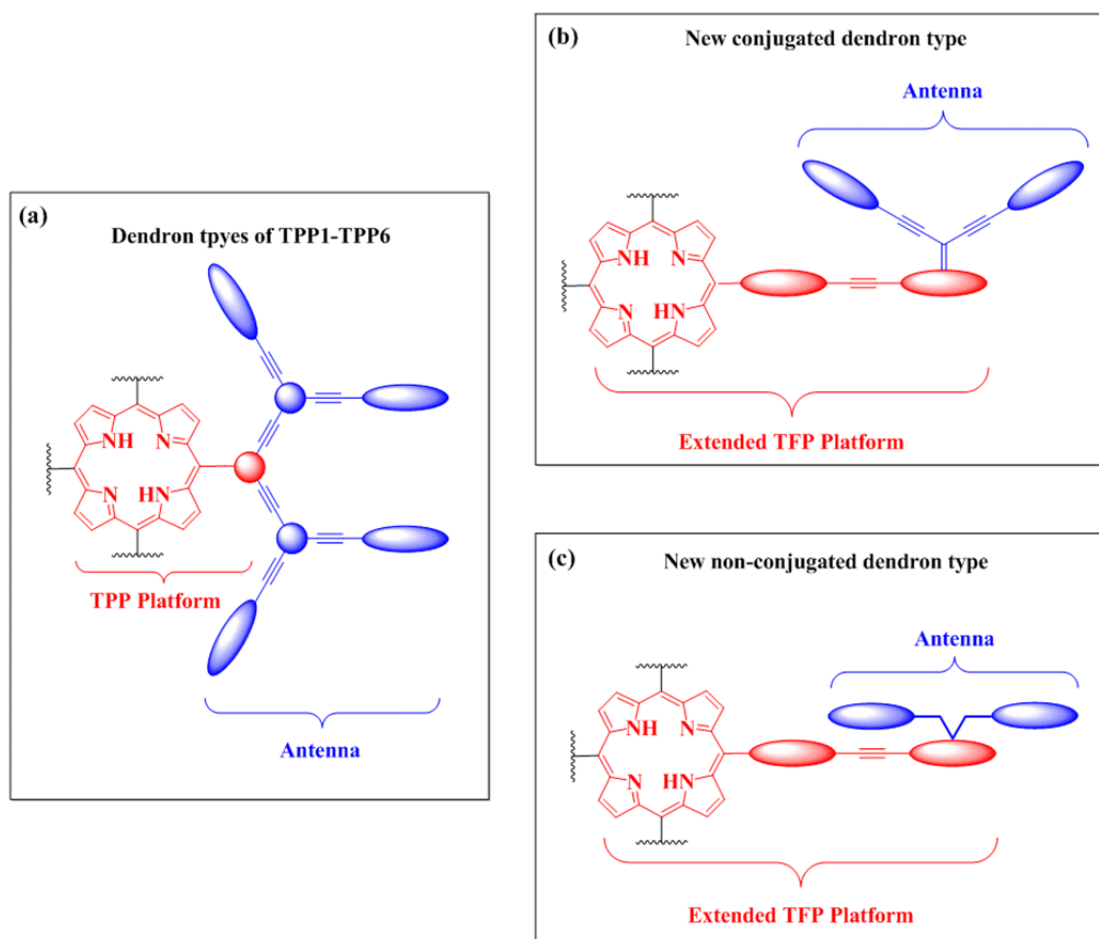
Dans le deuxième chapitre, nous présentons la synthèse d'une série de composés à base de ruthénium, dérivés de la tétra-fluorényl-porphyrine (TFP), pour des applications en optique non linéaire (ONL).



Mono-, Bis-, Tri- and Tetra-ruthenium tetra-fluorenyl porphyrins

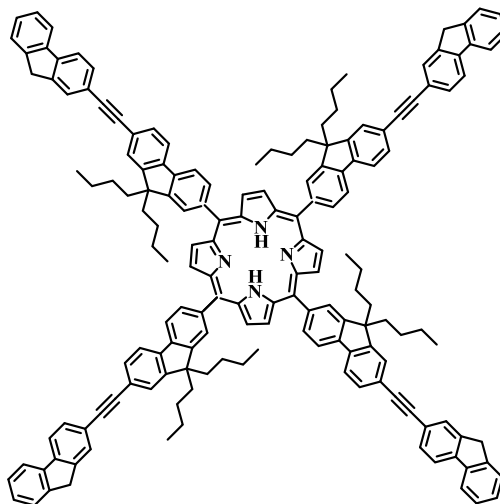
Dans le troisième chapitre, nous présentons la synthèse de deux nouveaux dendrons avec des antennes fluorényles terminales greffées en position 9 d'un troisième fluorényle, respectivement par un sont conjugués ou non conjugués.

Puis deux nouveaux dendrimères ont été obtenus par couplage de Sonogashira à partir de ces dendrons sur le cœur porphyrine TFP. Le transfert d'énergie de ces dendrons vers la porphyrine est efficace. Ces molécules présentent des propriétés en optique non linéaire qui sont très intéressantes et les résultats en ADP sont également très prometteurs.

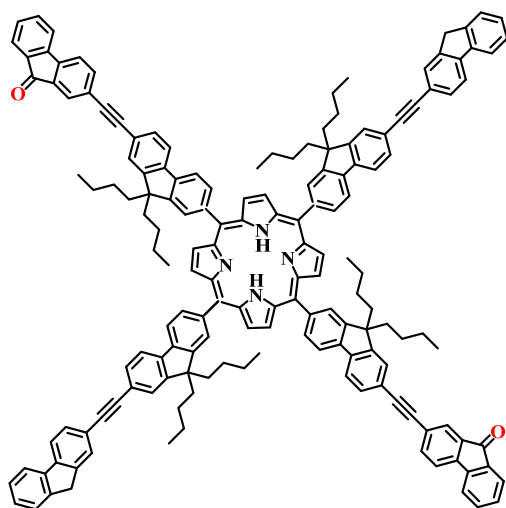


New conjugated (b) or Non-conjugated (c) types of dendrons

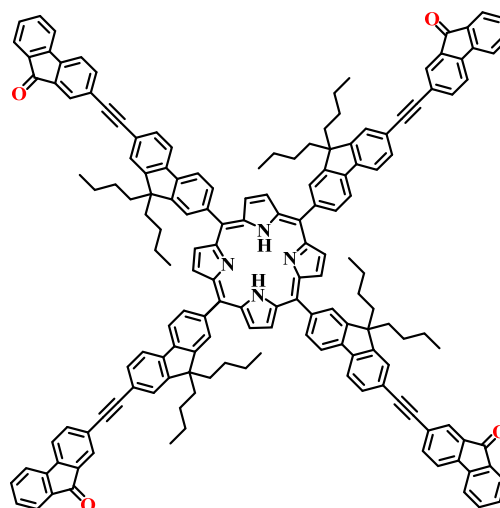
Dans le quatrième chapitre, nous présentons la synthèse de porphyrines avec des **bras fluorénones** terminales. Ces porphyrines émettent également une luminescence rouge et le transfert d'énergie est très efficace.



TFOP 1



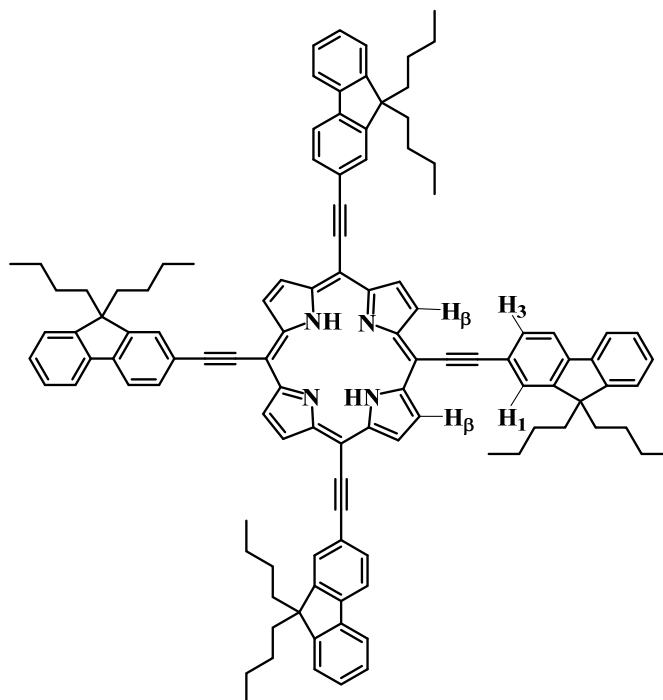
TFOP 2



TFOP 3

The entire structures of TFOP 1, TFOP 2 and TFOP 3

Dans le dernier chapitre, comme Perspectives, un nouveau type de porphyrine *meso*-alkynyle est envisagé. Pour l'instant nous avons juste synthétisé la **génération 0** de cette série de dendrimères : Les quatre bras fluorényles sont pontés au cœur de la porphyrine avec des liens alkynes, et les études optiques de ces prototypes sont en cours. Par la suite nous allons synthétiser la génération suivante G1, voire la génération G2.



Structure of new meso-alkynyl fluorenyl porphyrin

Les caractérisations de toutes ces nouvelles molécules synthétiques : dendrimères et oligomères cibles, ont été faites par les mesures RMN ^1H et ^{13}C , masse à haute résolution et microanalyse.

Service de la Recherche

Affaire suivie par :
Service Recherche
Tél : +33 (0)2 23 23 84 87
recherche@insa-rennes.fr

Demande de confidentialité de mémoire de thèse

Une thèse soumise à une clause de confidentialité ne pourra être diffusée, reproduite, communiquée pendant la durée de confidentialité définie, quand bien même le docteur le souhaiterait.

Je soussigné(e), Qualité¹ : *du directeur de thèse*

NOM : PAUL-ROTH

Prénom : Christine

Je soussigné(e), Qualité¹ : *du doctorant*

NOM : ZHANG

Prénom : Xu

Sollicite, de Monsieur le Directeur de l'INSA de Rennes

la confidentialité du mémoire de thèse² jusqu'au³ : 01/03/2019

Une soutenance à huis-clos : OUI

NON x

Sujet de la thèse : **Organic and Organometallic Fluorenyl-Porphyrins for Optics**

Motif(s) de la demande : Lors de cette thèse, nous avons abordé une nouvelle approche de formations de dendrimères très prometteuse, ces nouveaux composés **Fluorenyl-Porphyrins** vont faire l'objet **de dépôt de brevets** donc pour cela il est nécessaire de pouvoir bénéficier de la **confidentialité de mémoire de thèse.**

Les applications thérapeutiques et en imagerie sont très innovantes, pour les molécules déjà publiées nous venons de bénéficier du soutien de « **La Ligue nationale contre le cancer** ».

A Rennes , le 23/01/2017

Signature du doctorant


Xu ZHANG

INSA RENNES

20, Avenue des Buttes de Cœsmes
CS 70839 - 35 708 Rennes Cedex 7
Tél. + 33 (0)2 23 23 82 00 - Fax + 33 (0)2 23 23 83 96
www.insa-rennes.fr

Signature du Directeur de thèse




UNIVERSITÉ
EUROPÉENNE
DE BRETAGNE


L'Union fait la France
RÉPUBLIQUE FRANÇAISE

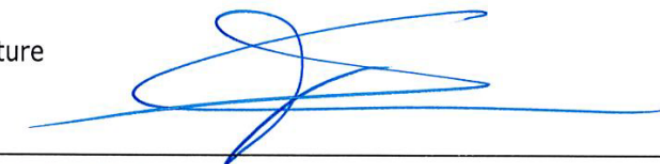
MINISTÈRE
DE L'ÉDUCATION NATIONALE,
DE L'ENSEIGNEMENT SUPÉRIEUR
ET DE LA RECHERCHE

1. La demande de confidentialité peut émaner du doctorant lui-même, d'un membre du jury, de l'organisme financeur, ou du directeur de thèse.
2. Conformément à l'arrêté du 25 Mai 2016 relatif aux modalités de dépôt : Article 25 : « Sauf si la thèse présente un caractère de confidentialité avéré, sa diffusion est assurée dans l'établissement de soutenance et au sein de l'ensemble de la communauté universitaire. La diffusion en ligne de la thèse au-delà de ce périmètre est subordonnée à l'autorisation de son auteur, sous réserve de l'absence de clause de confidentialité»
3. Durées conseillées : 2 ans maximum après la soutenance pour le dépôt de brevets ou la rédaction de publications, 5 ans maximum s'il s'agit de résultats permettant un avantage concurrentiel pour un industriel.

Le directeur de l'INSA :

- autorise la confidentialité du mémoire jusqu'au : 1/03/2019
- n'autorise pas la confidentialité du mémoire
- autorise la soutenance à huis-clos
- n'autorise pas la soutenance à huis-clos

Signature



INSA
RENNES
M'hamed DRISSI
Directeur

INSA RENNES

20, Avenue des Buttes de Cœsmes
CS 70839 - 35 708 Rennes Cedex 7
Tél. + 33 (0)2 23 23 82 00 - Fax + 33 (0)2 23 23 83 96
www.insa-rennes.fr



MINISTÈRE
DE L'ÉDUCATION NATIONALE,
DE L'ENSEIGNEMENT SUPÉRIEUR
ET DE LA RECHERCHE

ENGAGEMENT de CONFIDENTIALITE

Je, soussigné, _____, domicilié(e), _____. agissant en qualité de _____
(Rapporteur, Examineur, Membre Invité/Professeur, Maitres de Conférence, Ingénieur de
Recherche, etc.) à _____ dans le jury de thèse de **Xu ZHANG**, doctorant(e) à l'INSA de
Rennes, m'engage à tenir pour confidentielles toutes les informations recueillies dans le cadre
de la soutenance de thèse intitulée « **Organic and Organometallic Fluorenyl-Porphyrins for
Optics** » qui sera défendue le **17/03/2017** prochain.

Ces informations seront tenues confidentielles du **17/03/2017** jusqu'au **01/03/2019** (soit deux
ans après la soutenance).

Ne seront pas considérées comme confidentielles les informations :

- que je détenais auparavant, preuve pouvant être faite par des documents écrits et datés
de façon indiscutable,
- qui font partie du domaine public sous forme de documents écrits, et sous réserve que
ces derniers ne résultent pas d'une divulgation abusive de ma part,
- qui me sont communiquées par un tiers non tenu au secret et ayant la capacité de me
les communiquer.

Je m'engage à ne pas utiliser le savoir-faire lié aux informations confidentielles dans le but
d'une exploitation directe ou indirecte.

Ces informations seront maintenues secrètes jusqu'à ce que ces informations tombent dans le
domaine public.

Je m'abstiendrai durant ce délai de les divulguer sous quelque forme que ce soit à des tiers, y
compris à une société, un établissement, sauf accord préalable de l'INSA de Rennes.

Fait à.....
le.....
en deux exemplaires originaux.

Je soussigné

AVIS DU JURY SUR LA REPRODUCTION DE LA THESE SOUTENUE

Titre de la thèse:

Organic and Organometallic Fluorenyl-Porphyrins for Optics

Nom Prénom de l'auteur : ZHANG XU

Membres du jury :

- Monsieur BLANCHARD Philippe
- Madame LEDOUX Isabelle
- Monsieur MONGIN Olivier
- Madame PAUL-ROTH Christine
- Monsieur PAUL Frédéric
- Monsieur CARMICHAEL Duncan

Président du jury :

Isabelle LEDOUX

Date de la soutenance : 17 Mars 2017

Reproduction de la these soutenue

Thèse pouvant être reproduite en l'état

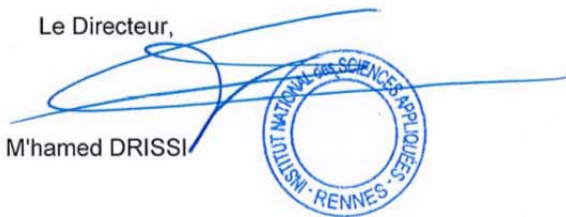
~~Thèse pouvant être reproduite après corrections suggérées~~

Fait à Rennes, le 17 Mars 2017

Signature du président de jury

Le Directeur,

M'hamed DRISSI



Isabelle LEDOUX

A handwritten signature in blue ink, appearing to be "Isabelle LEDOUX", written over a horizontal line.

Résumé

Au cours de cette thèse, nous avons synthétisé de nouveaux composés en utilisant des macrocycles de porphyrines comme socle pour nos architectures. L'objectif était d'étudier leurs propriétés en optique linéaire et non linéaire. Plus précisément, nous avons synthétisé et caractérisé trois groupes de dendrimères de type fluorényl-porphyrine, une série de porphyrines organométalliques dérivés du ruthénium, et commencé une dernière série de nouvelles porphyrines. Les corrélations entre les propriétés et la structure ont été étudiées, le processus de transfert d'énergie du donneur vers la porphyrine a aussi été évalué.

En introduction, nous avons présenté le contexte général de la chimie des porphyrines basé sur quatre aspects: (1) la structure chimique, (2) les voies de synthèse, (3) les propriétés en optique linéaire (4) et en optique non linéaire. Nous avons ensuite présenté les différents travaux qui ont été effectués dans notre groupe, et conclut en proposant de nouvelles structures basées sur ces résultats.

Dans le premier chapitre, nous présentons la synthèse d'un groupe de dendrimères dérivés de thiényl-porphyrines. Les unités thiényles font le pont entre les dendrons conjugués de type fluorényle et le cœur de la porphyrine. Le transfert d'énergie pour ces molécules est efficace et ces dernières présentent des propriétés en optique non linéaire qui sont intéressantes avec une amélioration de l'absorption à deux photons (ADP).

Dans le deuxième chapitre, nous présentons la synthèse d'une série de composés à base de ruthénium dérivés de la Tétra-fluorényl-porphyrine (TFP), pour des applications en optique non linéaire (ONL). Dans le troisième chapitre, nous présentons la synthèse de deux nouveaux dendrons avec des antennes fluorényles terminales greffées en position 9 d'un troisième fluorényle, respectivement par voie conjuguées ou non conjuguées. Puis deux nouveaux dendrimères ont été obtenus par couplage de Sonogashira à partir de ces dendrons sur le cœur porphyrine TFP. Le transfert d'énergie de ces dendrons vers la porphyrine est efficace. Ces molécules présentent des propriétés en optique non linéaire qui sont intéressantes et les résultats en ADP sont très prometteurs.

Dans le quatrième chapitre, nous présentons la synthèse de porphyrines avec des bras fluorénones terminales. Ces porphyrines émettent également une luminescence rouge et le transfert d'énergie est très efficace.

Comme perspectives, un nouveau type de porphyrine méso-alcynyle est envisagé, pour l'instant nous avons juste synthétisé la génération 0 de cette série de dendrimères: Les quatre bras fluorényles sont pontés au cœur de la porphyrine avec des liens alcynyles, et les études optiques de ces prototypes sont en cours.

Abstract

During this thesis, we have elaborated new compounds using the porphyrin macrocycle as the basic platform of our architectures. The aim, after their syntheses, was to study the linear optical (LO) and non-linear optical (NLO) properties of these new molecules. More precisely, we have synthesized and characterized three groups of fluorenyl-porphyrin dendrimers, a series of ruthenium organometallic porphyrins, and started a series of new type of porphyrin. Their correlations on optical property-structure have been discussed, as well as the energy transfer processes from the donor fragments to porphyrin core acceptor.

In the introduction, we presented the general background of the porphyrin chemistry based on four aspects: (1) structure, (2) synthetic methods, (3) LO properties and (4) NLO properties. We further reviewed prior porphyrin studies done in our group and proposed new molecular designs based on these results.

In the first chapter, we synthesized a group of thienyl porphyrin cored dendrimers. The thienyl units connect the conjugated fluorenyl dendrons to porphyrin ring by alkynyl bridges. The energy transfer (ET) of these porphyrins is very efficient and they present interesting NLO properties with enhanced Two-photon absorption (TPA).

In the second chapter, we synthesized a series of ruthenium compounds based on Tetra-fluorenyl porphyrin core (TFP) for NLO applications.

In the third chapter, we synthesized two new dendrons with two terminal fluorenyl antennae fixed on the 9 position of the fluorenyl units in conjugated or non-conjugated way respectively. Then two new porphyrin dendrimers were obtained by Sonogashira coupling reaction of these dendrons on TFP porphyrin core. Their ET from dendrons to porphyrin core is very efficient. They present interesting LO properties and the TPA results are very promising.

In the fourth chapter, we synthesized a group of TFP cored porphyrins with terminal fluorenone arms. These porphyrins emit red luminescence and the ET is very efficient from the linear arms toward their cores.

As perspective, a new type of meso-alkynyl porphyrin series is considered, for the moment we synthesized only the generation 0 of the dendrimers: the four fluorenyl arms of this porphyrin are bridged to the centre ring by alkynyl chains, and the optical studies of this prototype are in progress.